ELECTROCHEMICAL INVESTIGATION OF POLYPYRROLE AND POLYPYRROLE/HYDROGEL HYBRID MATERIALS FOR SENSING AND SUPERCAPACITOR APPLICATIONS

Thesis Submitted
to the University of Calicut
for the Award of

DOCTOR OF PHILOSOPHY IN CHEMISTRY

By
SHABEEBA.A.K

Under the Supervision of
Dr. YAHYA A.I.

DEPARTMENT OF CHEMISTRY
UNIVERSITY OF CALICUT
KERALA-673 635
OCTOBER 2023

DEPARTMENT OF CHEMISTRY

UNIVERSITY OF CALICUT

Calicut University (P.O), Kerala
Tel: 0494 2407414 Email: chemistryhead@gmail.com

CERTIFICATE

This is to certify that the thesis entitled "**Electrochemical Investigation of Polypyrrole and Polypyrrole/Hydrogel Hybrid Materials for Sensing and Supercapacitor Applications**" is an authentic record of precise research work carried out by **Shabeeba.A.K** at the Department of Chemistry, University of Calicut under my guidance and supervision for the award of the degree of Doctor of Philosophy in Chemistry. The contents of the thesis have been checked for plagiarism using the software 'DrillBit' and the similarity index falls under permissible limit, and I further certify that the thesis or part has not previously formed the basis for the award of any degree, diploma or associate ship of any other University or Institute. I also certify that the adjudicators have not suggested any major changes or corrections in the scientific content, results and interpretations of the thesis. However, the minor suggestions recommended by the examiners are incorporated in the revised thesis.

Dr. Yahya A.I.
Associate Professor
Department of Chemistry
University of Calicut

Calicut University

DECLARATION

I, **Shabeeba.A.K**, hereby declare that the thesis entitled "**Electrochemical Investigation of Polypyrrole and Polypyrrole/Hydrogel Hybrid Materials for Sensing and Supercapacitor Applications**" submitted to the University of Calicut is the bonafide report of the original research work carried out by me under the supervision and guidance of **Dr. Yahya A. I.**, Associate Professor, Department of Chemistry, University of Calicut, in partial fulfillment of the requirements for the award of the degree of Doctor of Philosophy in Chemistry under the Faculty of Sciences, University of Calicut, Kerala. The contents of this thesis have not been presented previously for the award of any degree, diploma or associate ship in any other University or Institution.

University of Calicut **Shabeeba.A.K**

ACKNOWLEDGEMENTS

*It gives me an immense pleasure to write this note of thanks as a finishing touch to my thesis, a gateway to express my gratitude to everyone who has supported me throughout the journey of my Ph. D. program. First of all I would like to thank the Almighty "**ALLAH**" for always being with me, showing me the right path and giving me the self-confidence, self-belief, strength and the ability to carry out this research work.*

*At this moment of accomplishment, it is definitely a pleasing privilege for me to express my deep and sincere gratitude to my research supervisor **Dr. Yahya A.I.**, Associate Professor, Department of chemistry, University of Calicut, for giving me the opportunity to do research, providing invaluable guidance, supervision, constant encouragement and patience at all stages of the research work. It was great privilege and honor to work and study under his guidance. I am short of words to express my feelings for the consistent moral support and freedom he has given me to carry out this research work.*

*I wish to extent my sincere gratitude to our present Head of the Department, **Dr. Rajeev S. Menon**, and the former HODs of the department for providing me the necessary facilities for the successful completion of the research work in the department. I am deeply grateful to all other teachers and non-teaching staff (present and former) of the department of chemistry for their valuable support and encouragement. It is a great pleasure to acknowledge the expeditious service received from the librarian and instrument technician of our department. I am extremely grateful to all my teachers who taught me*

in my academic period, as they motivated me and built the foundation for this achievement.

I express my genuine gratitude to Dr. Mohamed Shahin Thayyil, Associate Professor, Department of Physics, University of Calicut and his research group for helping me to conduct electrical characterization. I gratefully acknowledge UGC-India for providing JRF and SRF fellowships for the successful completion of my Ph.D. work. I acknowledge CSIF University of Calicut, STIC Cochin University of Science and Technology and NIT Calicut for providing the necessary characterization facilities for my work.

I would fail in my duty, if I don't express my deep sense of gratitude to my research group members, Sidheekha M P, Lijin Rajan, Sivakrishna Prakash, Roopasri R and Razana P K. Everybody in the group was treated like members of a family and enjoyed every bit of research life by sharing our feelings and emotions in addition to stimulating thoughts and interesting research ideas. Words fall too short when it comes to mention Sidheekha and Lijin, my best friends and critic ever since we began our Ph.D. journey together. They were always there for the useful scientific discussions and helping me out in moments of struggle and different situations. I extent my hearty thanks to our former M. Phil scholars Anjali C, Geethu E R, Thasneem C and Athira A for their valuable support.

It is also a pleasure to acknowledge present research scholars especially Deepak Joshy and former research scholars in my department for giving the friendly atmosphere, enthusiastic support and helping me in every possible way with their advices to make my Ph. D.

a memorable experience. They make my research life more enjoyable in between the stress.

Finally, my family deserves a special mention for their unflagging love and unconditional support throughout my research work. I find no words to express my feelings towards my mother Shahina K and father Mayinkutty A K, the main driving force for all my achievements, who have given me the freedom to choose my path. Their prayer, patience and sacrifices for me were what sustained me thus far. I would also like to thank my brothers Shafeeq Niyas A K and Nasrul Ameen A K for their unconditional support and encouragement. For the sake of formality, I express my gratitude to my dear husband, Shabeer C for being my power and his whole hearted support made me to realize my dream. I would like to express my thanks to my beloved daughter Sheza Zahan C and my beloved son Shezin Aizam, for cheering me up to tunnel the work pressure during the course. I consider myself the luckiest in the world to have such a lovely, affectionate and understanding family and without them this venture would not have been possible. I like to dedicate this thesis to my family-My parents, brothers, husband, daughter and son.

My thanks are also extended to each and every personality, who directly and indirectly assisted me for the successful completion of the research work. Though many have not been mentioned, none is forgotten.

Shabeeba.A.K

Dedicated to

My Family

TABLE OF CONTENTS

PREFACE

In the dynamic landscape of the 21st century, the pursuit of multifunctional materials has become paramount in meeting the escalating demands of a progressively sophisticated and discerning society. The modern era has borne witness to an unprecedented diversification and intensification of demands for materials with versatile functionalities. As we project into the future, the impetus for intelligent materials and smart systems with integrated functions will only intensify. The advancement of science and technology has catapulted a new class of organic materials, particularly conducting polymers, to the forefront, poised to supplant traditional metal-based counterparts in step with the needs of our modern society. This thesis embarks on a journey to explore the pivotal role that can be played by conducting polymers (polypyrrole here) in the design of reactive sensors and self-sensing macromolecular devices and in shaping a more affluent and enlightened world.

For decades, scientific community had been trying to fabricate multi-sensing intelligent motors integrated into a single reactive device capable of sensing the surrounding variables at any instant through the same two connecting wires. Present day technology integrates individual specific functionalities in series, each requiring a couple of connecting wires and demanding complex software to take autonomous decisions. Consequently, one of the major challenges in materials science is the realization of a single device with multiple functionalities.

Conducting polymers, the Nobel Prize-winning materials are multifunctional polymers that find widespread application in a variety of fields, ranging from electrochemical sensors, biosensors, supercapacitors, actuators, batteries, solar cells, electrochromic devices, etc. because of their unique electrical, electrochemical and optical properties. Furthermore, their composition-dependent properties including conductivity, stored charge, stored conformational energy, stored counterions, porosity, volume, color, and wettability can be tuned under electrochemical reaction control by several orders of magnitude. Despite their significant interest in the above mentioned fields, their composition-dependent properties and applications have not been explored properly till date.

Among the various conducting polymers, Polypyrrole stands out as a research hotspot. Its outstanding features ranging from superior electrochemical activity, high electrical conductivity, lightweight, ease of synthesis, and excellent environmental stability render it both scientifically and commercially interesting. Yet, inherent to polypyrrole, as in other conducting polymers, there are some significant challenges: its poor mechanical strength, limited elongation at break, brittleness, and consequently, its low solubility and processability. One of the promising solutions for improving the processability lies in the combination of polypyrrole with hydrogels. By incorporating a conducting polymer into a hydrogel matrix, the resultant hybrid material combines the best of the properties of both materials: the electrical conductivity and electroactivity of the conducting polymers with the processability and mechanical robustness of hydrogels. This thesis is focused on the fundamental electrochemistry of polypyrrole

and the development of self-sensing macromolecular motors based on polypyrrole/hydrogel hybrid films that can self-sense the working energetic conditions using the same two connectivities.

The thesis consists of seven chapters.

Chapter 1 furnishes an overall introduction to conducting polymers, focusing particularly on polypyrrole. This chapter encompasses various facets of polypyrrole and polypyrrole/hydrogel hybrid films. Topics covered include general synthetic methods of conducting polymers, their structures, properties and potential applications in various fields. Further, the chapter briefly elucidates the electrochemistry of conducting polymers and their biomimetic characteristics. The chapter also discusses the aim and objectives of the current study.

Chapter 2 provides a comprehensive overview of the experimental framework of the study. It details the materials employed, outlines the synthesis protocols followed, describes the characterization methods used especially the methods employed for electrochemical studies. Additionally, this chapter elucidates the fundamental principles underpinning each characterization method.

Chapter 3 ***'Characterizations of polypyrrole with a special emphasis on electrochemical characterization'*** This chapter deals with the results of characterizations of synthesized polypyrrole, and discusses its electrochemical analysis in detail. It meticulously examines the structural faradaic processes of polypyrrole and employs coulovoltammetry to quantify the charge consumed during the processes. Furthermore, the chapter investigates the impact of both cathodic and anodic potential limits on voltammetric and

coulovoltammetric responses. Overall, this chapter furnishes a deep insight into the electrochemical behavior of polypyrrole.

Chapter 4 ***'Polypyrrole as reactive sensors of working ambient: chronopotentiometric and voltammetric investigations'*** This chapter focuses on a comprehensive exploration of reaction-driven sensing characteristics of polypyrrole under various working energetic conditions, including electrical, thermal, and chemical conditions. Chronopotentiometry is used to monitor the consumed electrical energy, while cyclic voltammetry is employed to track the electrical charge consumed during reactions. In addition, this chapter delves into the theoretical explanations that support the unique reaction-driven sensing abilities of polypyrrole, offering a comprehensive understanding of the principles behind its sensing behavior.

Chapter 5 ***'Polypyrrole/Chitosan hybrid films for reactive sensing and supercapacitor applications'*** This chapter confronts the fundamental challenges with polypyrrole: its poor mechanical strength and limited processability which traditionally makes it unfit for device applications. The primary objective is the design of a free standing electrode material based on polypyrrole, capable for both sensing and energy storage applications. Towards this goal, polypyrrole/chitosan hybrid films are synthesized through a facile and cost-effective method. The chapter offers a thorough characterization of these films, investigates their innate reaction-driven sensing capabilities, and assesses their performance as a freestanding electrode material for supercapacitors.

Chapter 6 ***'Polypyrrole/PVA hybrid films as self sensing macromolecular motors: application as sensing supercapacitor'*** This chapter centers on fabricating highly mechanically stable, flexible and electroactive polypyrrole/PVA hybrid films for device fabrications. In-depth electrochemical studies have been carried out for the comprehensive characterization of these films, along with their reaction-driven sensing capabilities. The study examines how anions of varying sizes affect the reaction-driven sensing characteristics of the hybrid film. A significant section is dedicated to understanding how different reaction conditions including chemical, thermal, and electrical energetic variables affect the cooperative actuation due to conformational movements of multistep molecular motors of PPy. Additionally, attention is turned towards the fabrication of a sensing supercapacitor device based on polypyrrole/PVA hybrid films which remarkably senses the working energetic conditions without external connections. Overall, this chapter paves the way for the innovative prospect of fabricating user-friendly, smart, multi-sensing macromolecular devices that can self-sense and adapt to varying working energetic conditions through the same two connectivities.

Chapter 7 summarizes the major findings and standout moments from the current research. Additionally, this chapter sheds light on the biological and technological perspectives of the present investigation with a particular focus on the future prospects of developing various biomimetic devices.

LIST OF TABLES

LIST OF FIGURES

LIST OF ABBREVIATIONS

ATR	*Attenuated total reflection*
BDS	*Broadband dielectric spectrometer*
CE	*Counter electrode*
CP(s)	*Conducting polymer(s)*
CPH(s)	*Conducting polymer/hydrogel system(s)*
Cs	*Chitosan*
CuPcTs	*copper phthalocyanine-3,4',4", 4‴-tetra sulphonic acid tetrasodium salt*
CV(s)	*Cyclic voltammogram(s)*
EDLC	*Electrical double layer capacitor*
EDX	*Energy dispersive X-ray spectroscopy*
EIS	*Electrochemical impedance spectroscopy*
EMI	*Electromagnetic interferences*
ESCR	*Electrochemically stimulated conformational relaxation model*
ESR	*Equivalent series resistance*
FESEM	*Field emission scanning electron microscope*
FTIR	*Fourier transform infrared, Spectroscopy*
GCD	*Galvanostatic charge discharge*
GCE	*Glassy carbon electrode*
HOMO	*Highest occupied molecular orbital*
ICM	*Intracellular matrix*
ICP	*Intrinsically conducting polymer*
LiTFMSI	*lithium bis(trifluoromethanesulfonyl)imide*

LUMO	*Lowest unoccupied molecular orbital*
PA	*Polyacetylene*
PANI	*Polyaniline*
PCF1	*Single coated Polypyrrole/chitosan hybrid film*
PCF2	*Second coated Polypyrrole/chitosan hybrid film*
PCF3	*Third coated Polypyrrole/chitosan hybrid film*
PCF4	*Fourth coated Polypyrrole/chitosan hybrid film*
PEDOT	*Poly(3,4-ethelenedioxythiophene*
PIN	*Polyindole*
PP	*Poly(para-phenylene)*
PPF1	*Single coated Polypyrrole/PVA hybrid film*
PPF2	*Second coated Polypyrrole/PVA hybrid film*
PPF3	*Third coated Polypyrrole/PVA hybrid film*
PPF4	*Fourth coated Polypyrrole/PVA hybrid film*
PPV	*Poly(para-phenylenevinylene)*
PPy	*Polypyrrole*
PQ	*Polyquilonine*
PTh	*Polythiophene*
PVA	*Polyvinyl alcohol*
QV	*Coulovoltammogram*
RE	*Reference electrode*
TGA	*Thermogravimetric analysis*
UTM	*Universal test frame machine*
WE	*Working electrode*

Chapter 1

INTRODUCTION

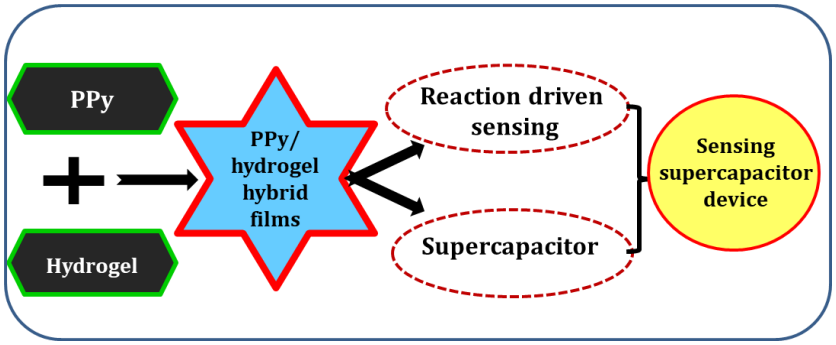

Conducting polymers offer tremendous opportunities in the discovery of new multifunctional materials due to their unique electrical and electrochemical properties. Novel hybrid materials using conducting polymers with enhanced properties and superior performances have been synthesized during the last two decades. Among various conducting polymers, polypyrrole has emerged as a prolific candidate for various potential applications as it is endowed with interesting material properties such as tunable electrical conductivity, excellent electrochemical activity over a wide range of pH, ease of synthesis and environmental stability. Conducting polymer/hydrogel hybrid systems combine the gel properties with electrical properties of conducting polymers and offer unique opportunities for the development of next generation materials with outstanding features. This chapter presents a general introduction to conducting polymers and conducting polymer/hydrogel systems. This chapter also explores the electrochemical and biomimetic properties of conducting polymers.

Twenty first century is witnessing an exponential advancement in the field of science and technology, and scientists are relentlessly trying to develop new functional materials with superior properties which can trigger new avenues in the field of materials research. Many innovative materials have been synthesized/fabricated during the last two years. Polymer science is one of the advancing fields of materials research because of their impressive and inherent physico-chemical properties and diverse applications in science and technology. Among these, conducting polymers (CPs) with designed properties have emerged as an attractive material for the researchers by virtue of their capability to tune their electrical and electrochemical properties.

1.1. Conducting polymers

Polymeric materials have been greatly contributed for the comfort of human life due to their outstanding inherent physical properties and it is thought-provoking to imagine human advancement without polymers. The perception that polymeric materials are traditional electrical insulators has been challenged with the discovery of electrically conducting polymers. These novel materials combine the electrical characteristics of both semiconductors and metals with the familiar properties of conventional polymers. The era of intrinsically conducting polymers (ICPs) started by the discovery of electrically conducting trans-polyacetylene by Alan MacDiarmid, Hideki Shirakawa, and Alan Heeger in 1977 (Figure 1.1). The Nobel Prize in Chemistry was jointly awarded for them in the year 2000 “for the discovery and development of electronically conductive polymers” [1, 2]. After their discovery, the CPs have emerged as a prolific

multifunctional material due of their tunable electrical conductivity leading to potential applications. Further a large number of fundamental investigations are carried out to understand their electronic, electrical and thermal properties.

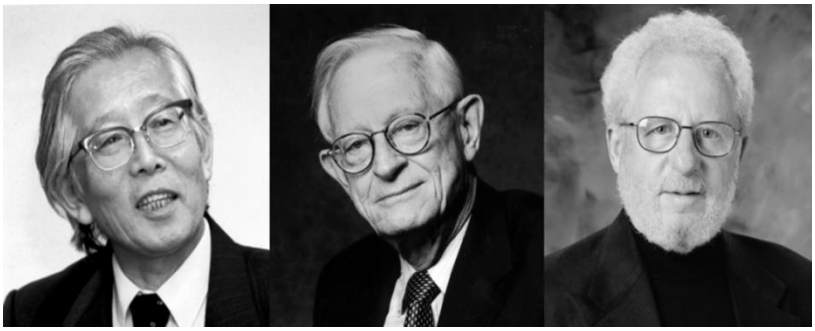

Figure 1.1 *Hideki Shirakawa, Alan MacDiarmid and Alan Heeger*

The ICPs, more commonly known as “synthetic metals”, are carbon-based multifunctional polymers having spatially extended π-electron conjugation that confers unique electrical, electrochemical and optical properties. These polymers are the "Materials of twenty first century" [3] that orchestrate the positive properties of conductors (electrical and optical properties) and conventional polymers (mechanical flexibility, ease of synthesis and thermal stability). The CP backbones are made up of sp^2 hybridized carbon atoms with a half filled pz orbital orthogonal to it. The fundamental characteristic of CPs are the presence of conjugated double bonds along the polymer back bone which acquire the positive or negative charges by oxidation or reduction process. Due to this extended π-electron conjugation, they exhibit unique electrical, optical and electrochemical properties. CPs are insulators in the undoped state. They gain high electrical conductivity through a process named “doping” [4]. Thus the

conductivity of CPs can be tuned anywhere between insulators and semiconductors or even between insulators and metals by varying the type and extent of doping. Through doping the conductivity of CPs can reach upto 10^3 S cm^{-1}. Conductivity of polyacetylene increases by 10 million-fold when it was oxidized by iodine vapor [5-7]. The conductivity range CPs is shown in figure 1.2.

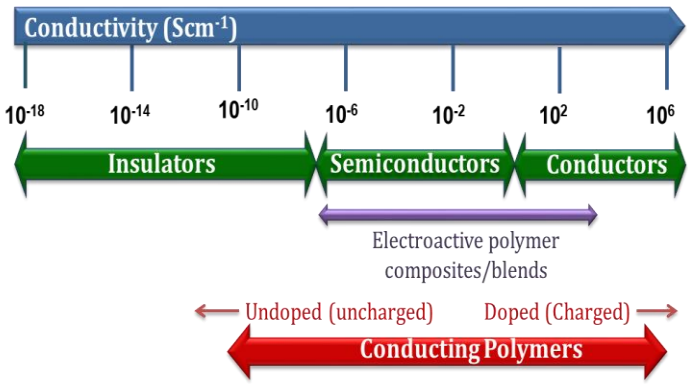

Figure 1.2 *Conductivity range of CPs with respect to insulators, semiconductor and conductors*

CPs have received immense attention in both the academic and industrial communities for more than three decades owing to their potential electrical, electronic and electrochemical applications such as actuators [8, 9], chemical or biological sensors [10, 11], electrochromic windows [12], supercapacitors [13], batteries [14, 15], microelectronics [16], light-emitting diodes [17, 18], desalination [19], etc. They offer outstanding features such as lightweight, interesting electroactive properties, ease of synthesis, low operational voltage, excellent doping-dedoping properties, high theoretical capacitance and tunable conductivities. The various properties of CPs (electrical, chemical, electrochemical, morphological, dielectric etc.) can be tuned by

adjusting the synthetic parameters like type and extent of doping, monomer concentration, nature of solvents, polymerization time, pH and temperature. The CPs are inherently intractable (i.e. brittle, insoluble and infusible) due to the backbone rigidity associated with the conjugated π-electron system. Many attempts have been made by researchers to improve the properties and performances of CPs like co-polymerization, use of substituted monomers [20, 21], use of surfactants [22, 23], the formation of blends, composites, use of various templates, fabrication of hybrid systems with mechanically strong polymers [24, 25] and so on.

1.1.1. Examples of conducting polymers

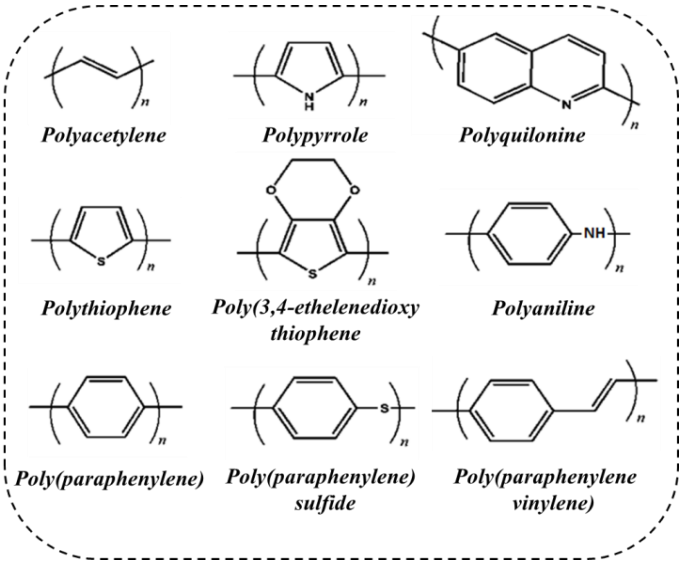

Figure 1.3 *Chemical structures of some electrically conductive polymers*

The early work on conductive polymers was started by the discovery polyacetylene (PA) [1], a polymer that is normally only semiconducting and conductivity increased by 10 million-fold of

magnitude when doped with iodine. The infusibility, insolubility and instability of polyacetylene in air has led to the discovery of vast variety of CPs, including polypyrrole (PPy), polyaniline (PANI), polyindole (PIN), polythiophene (PTh), poly(para-phenylene) (PP), polyquilonine (PQ), poly(3,4-ethelenedioxythiophene) (PEDOT), poly(para-phenylenevinylene) (PPV), etc. for both research and industrial applications. The structures of some of the important electrically CPs are given in Figure 1.3.

1.1.2. Doping of conducting polymers

CPs are insulators or semiconductors in the pristine state and do not contain any intrinsic charge-carriers. The charge carriers must be provided extrinsically through 'doping' with a suitable oxidizing or reducing agent. The ultimate conductivity of CPs depends on several factors such as type of dopant, concentration of dopant, mobility of charge carriers, homogeneity of doping, morphology etc. The doping in CPs differs from that of the conventional inorganic semiconductors which generates either holes in the valence band or electrons in the conduction band. In CPs, doping results in the generation of conjugational defects in the polymer chain viz. solitons, polarons and bipolarons. Some of the commonly used doping methods are given below:

(a) Redox doping: It is the most widely used technique which includes chemical and electrochemical doping. The chemical doping is attained through either p-type doping (oxidation with electron acceptors) or n-type doping (reduction with electron donors) [26]. The commonly

used p-type dopants include $FeCl_3$, $HClO_4$, HNO_3, H_2SO_4, AsF_5, HCl, CH_3COOH, H_3PO_4, NH_4BF_4, SO_3CF_3, $NOPF_6$, etc. and n-type dopants include Na, K, Li etc. For example, oxidation of polyacetylene with iodine increases the conductivity from 10^{-5} S cm^{-1} to 10^2 S cm^{-1}.

$$trans(CH)_n + \frac{3x}{2} I_2 \rightarrow (CH)_n^{x+} + xI_3^- \quad (1.1)$$

Similarly, polyacetylene can be doped with electron donors like alkali metal to attain high conductivities [27].

$$trans(CH)_n + xNa \rightarrow (CH)_n^{x-} + xNa^+ \quad (1.2)$$

The n-doping and p-doping can also be achieved electrochemically with the CP either acting as an electron source or as an electron sink. Compared to chemical, in electrochemical the doping de-doping process is highly reversible and the doping level can be achieved by simply monitoring the current passed. CPs can be doped without the incorporation of counterions by 'photo-doping' (by irradiating with photons having energy higher than the CP band gap and when the irradiation ceases, the photo-generated charge carriers disappears.

(b) Non-redox doping: In non-redox doping, the energy levels of the CPs get rearranged and no changes occur in the number of electrons associated to the polymer chain. A typical example for non-redox doping is the protonic acid doping in PANI (emeraldine base form) to produce conducting polysemiquinone radical cations [28].

(c) Doping by ion implantation: Here, the dopant atoms first ionize to form positive charged ions and focused on the surface of the substrate.

With high acceleration voltage, the ions gain enough energy to penetrate into the polymer matrix, and collide with the lattice atoms or their electrons. The implantation by I^+ ion increases the electrical conductivity of PANI by10-15 orders of magnitude [29].

(d) Self-doping: The ionizable groups attached to the polymer backbone act as dopant and hence no external doping agent is required [30]. A typical example is the self doping of poly(anthranilic acid) [31].

(e) Doping by heat treatment: It is a rarely used technique for doping CPs with ladder like structure [32]. The conductivity increases from 10^{-8} S cm^{-1} to 10^{-4} S cm^{-1} by heat treatment. [33].

1.1.3. Electronic conduction in conducting polymers

1.1.3.1. Charge carriers in conducting polymers

CPs can undergo redox reaction more easily because of the π-electron conjugation and the charge carrier, i.e., quasi-particles such as solitons, polarons and bipolarons are generated as a result of doping of CPs. [34]. These defects (charge carriers) are delocalized along the polymer chains, and are mobile in nature resulting in improved conduction [35]. As a result of doping the electrons are extracted from the highest occupied molecular orbital (HOMO) of the valence band or transferred to the lowest unoccupied molecular orbital (LUMO) of the conduction band. The conductivity is affected by the alignment of the polymer chains, the mobility of the charge carrier, the charge density and the charge carried by each carrier. Based on the native bond structure, CPs can exist in degenerate and non-degenerate states. Degenerate CPs have two identical geometric structures in the ground

state and non-degenerate CPs possess two non-identical structures in the ground state with different energies (e.g., benzenoid and quinoid structures). In degenerate CPs, solitons are the charge carriers and in non-degenerate CPs polarons and bipolarons carry the charge [36]. p-doping of CPs are generally more preferred method of doping because the positively charged carriers are more stable [37].

(a) Solitons: A solitons has a ± ½ spin with zero charge, which is formed when a single carbon atom in a conjugated polymer chain does not share its electron with either of its adjacent atoms [38]. In this state, one of the neighbouring atoms can change from its π-bonded state with the tertiary atom to a state of π-bonding with the primary atom in question. That is, a new π -bond is formed and the radical moves to the tertiary carbon atom. As both the states are degenerate, the process occurs both naturally and spontaneously. The solitons are the basic charge carriers in a conjugated systems and are delocalized throughout the polymer chain [38]. A neutral soliton is created when cis-PA chains undergo "thermal" isomerization to the trans structure [39]. A neutral soliton on oxidation gives positive soliton by losing an electron and on reduction gives negative soliton by gaining an electron. Both positive and negative soliton have zero spin.

(b) Polarons: The π-conjugated systems with aromatic rings such as PPy, PANI, PTh, PIN and PEDOT have non-degenerate ground states and possess different energies on either sides of the defect [40]. Thus, a single bond alternation defect in such a chain cannot behave as solitons. In such polymers, the removal of an electron from the π system produces a positive charge and a free radical. Thus a polaron

is defined as the combination of a charged site coupled with the free radical via a local lattice distortion due to polarization of the surrounding medium [41]. They have a spin of ± ½ with an electric charge of ± *e*. That is a polaron is either a radical cation (doped with electron accepter) or a radical anion (doped with electron donor) and its formation creates new localized electronic states in the bandgap. Unlike solitons, polarons possess a definite length (the distance between the coupled electron and hole) and it decreases as the dopant ion concentration increases. In PPy, this lattice distortion is extended over about four pyrrole rings, while in CPs like PIN and PANI, this may restrict to two rings only.

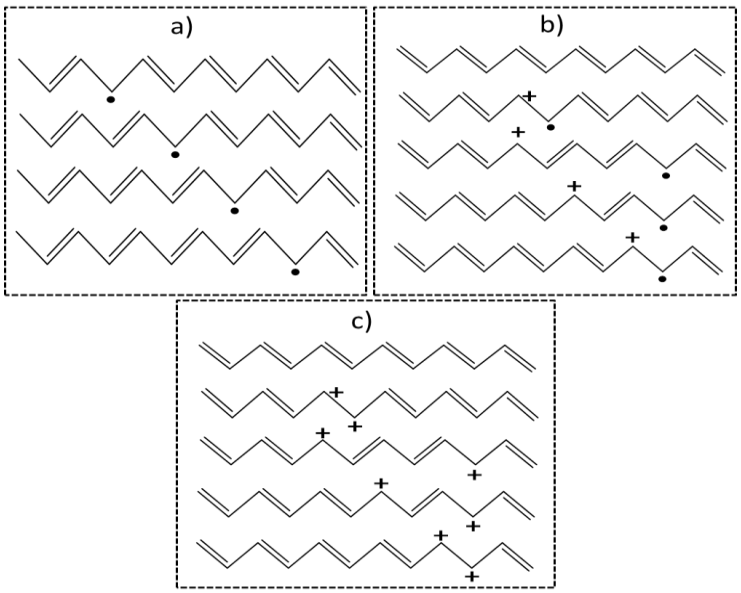

Figure 1.4 *(a) Charge transport in trans-polyacetylene as the soliton hops along the polymer chain. Mechanism of transportation of (b) a polaron and (c) a bipolaron in trans-polyacetylene*

(c) Bipolarons: In most of the non-degenerate CPs, the electrical conductivity of the system is found to be spinless, suggesting the

presence of a new charge carrier called bipolarons generated through the polaron interactions. When the concentration of dopant ion increases above certain limits, two polarons couple to form another characteristic self-localized particle-like defects in the polymer backbone called bipolarons (dication or dianion) [42]. The distance between two of the positively charged atoms is considered as the length of a bipolaron [43]. When a polymer chain containing a polaron is further oxidized, an electron can be removed either from the rest of the chain or from the polaron [44]. In the former case, two polarons are generated and in the latter case, two new positive charges (bipolaron) are formed by removing the polaron radical. Like bosons, they possess quantum spin values of 0 or 1, but have a charge of ± 2*e*. Compared to two polarons, the generation of a bipolaron leads to a decrease in ionization, making it thermodynamically more favorable. The formation of a soliton, a polaron and a bipolaron along the polymer chains of PA are represented in Figure 1.4.

1.1.3.2. Band Theory

The electrical conductivity of a material is a function of the number or concentration of charges carriers (n), the mobility of the charge carriers (μ) and the charge on each carrier (ε). The electrical conductivity (σ) can be given as:

$$\sigma = n \varepsilon \mu \tag{1.3}$$

Electronic conduction in CPs can be described in terms of the band theory. According to this theory, the outer atomic orbitals containing the valence electrons in solids split into bonding and

antibonding orbitals and undergoes mixing to form two series of closely-spaced energy bands called the valence band and conduction bands respectively. The interactions of the conjugated π-orbitals in the repeating units of the polymer chain are accountable for the band structure in CPs. As the energy gap between the valence band and conduction band in CPs is in the range 1.5-3.0 eV, they are considered as semiconductors in the undoped state (defect-free state). The electrons can be excited from the HOMO to the LUMO [41]. As mentioned earlier, the doping generates polarons or bipolarons along the chains. The presence of the polarons in conjugated polymer generates two new polaron energy levels in the band gap, where the energy of HOMO is increased and that of LUMO is decreased by a value corresponding to the binding energy of the polaron as shown in Figure 1.5. Thus the energy gap decreases.

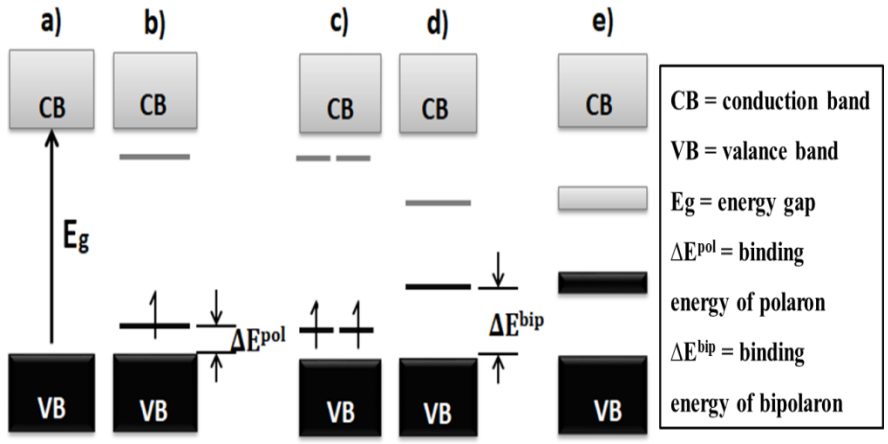

Figure 1.5 *Energy profile diagram of CPs: (a) undoped state, (b) with a polaron, (c) with two polarons, (d) a bipolaron with further reduced energy gap due to coupling of polarons and (e) bipolaron band at highly doped state*

In the case of a bipolaron, the energy gap is further decreased by a value corresponding to the coupling energy of two polarons as shown in Figure 1.5. As the concentration of the dopant increases, there occurs a subsequent increase in the number of polarons and they couple to form bipolarons. In highly doped systems, these bipolaron states overlap to form two wide bipolaron bands in the energy gap. This allows greater number of electrons to carry charge and contributing to the enhanced electrical conductivity.

1.1.3.3. Hopping and tunnelling

The electronic conduction in CPs occurs not only through the movement of charge carriers along the chains but also from one chain to another through hopping or tunneling, and hence the band theory alone is not sufficient to explain the electronic conduction in CPs. The charge transport can be explained by phonon-assisted hopping or tunnelling mechanism also [38]. The CPs are characterized by a high degree of disorder and are primarily a mixture of crystalline or amorphous regions. Therefore, it is necessary to consider the transport of charge carriers along and in between the chains, and at the complex boundaries. As mentioned earlier, the electrical conductivity depends on concentration of charge carriers and their mobility. Due to low degree of crystallinity and many other defects, the CPs may possess low mobility of charge carriers. The mobility of charge carriers here means both intrachain mobility and interchain mobility. The interchain mobility requires more energy than that required for intrachain mobility as it involves the hopping or tunneling of the charge from one chain to another. When they reach at the end of a chain or meet an insulating

barrier between two conducting regions or approach any kind of defect, they jump across or hop or tunnel from one site to the next within energy band gap and deliver the charges [45]. At low non-zero temperature, the energy for hopping is given by the phonons. The electrons absorb phonons and start hopping from one energy state to another. The conductivity is zero at zero temperature in such CPs [46].

1.1.4. Properties of Conducting Polymers

(a) Tunable electrical conductivity: The conductivity of CPs depends on the type and concentration of the dopant, structure, morphology and temperature. By changing any of these parameters, the conductivity can be further tuned. Usually the conductivity of CPs ranges from 10^{-3} S cm^{-1} to 10^{3} S cm^{-1}. In the de-doped state, they behave as insulators with a conductivity range of 10^{-9} S cm^{-1} to 10^{-6} S cm^{-1}.

***(b) Swelling and de-swelling*:** During redox reactions, the dimension of the CPs changes due to the entrance/expulsion of the ions/solvents to the polymer matrix. There are two components for the swelling/de-swelling processes: an intrinsic part related to bond length and conformational changes and secondly the osmotic expansion of the polymer phase [47]. In the case of anion driven actuation, the polymer swells by oxidation and shrinks by reduction. For cation driven actuation (when large anions are incorporated during polymerization), the reverse processes occur [48].

(c) Wettability: Wettability is an important feature of solid surfaces for applications like bioseperations, microfluidics, drug delivery and

self-cleaning surfaces. Generally CPs are hydrophilic in nature, but hydrophobic character can be imparted through doping with hydrophobic acids [49]. Thus they exhibit reversible switching from superhydrophobic and superhydrophilic surface by controlling their chemical compositions.

(d) Porous nature: In the neutral state, CPs have compact porous structure with short average chain distances. During oxidation, positive charges are generated and the coulombic repulsions between the newly formed positive charges increase the average distance between chains. This allows the counter ions to enter into the polymer matrix.

(e) Electrochemical properties: Due to the faradaic reversible doping/de-doping behavior, CPs exhibit interesting electrochemical properties. The typical electrochemical behavior and the redox states of CPs can be analyzed by cyclic voltammetric studies. The doping of the polymer leads to the generation of charge carriers accompanied by changes in structure from benzenoid to quinoid forms. On reduction or de-doping, it recovers back to the pristine structure. The electrochemical reactions of CPs are discussed detail in section 1.1.5.

(f) Pseudocapacitance: The charge storage mechanism of CPs originates from the faradaic reversible doping/dedoping reactions of the ions in the polymer backbone and exhibits a typical peak-shaped cyclic voltammogram [50]. The charging process proceeds through oxidation reaction, where electrons are released and anions are inserted to polymer matrix. Conversely, the discharging process is accompanied by reduction reaction. However, they exhibit poor cycling stability as a

consequence of the structural instability due to large swelling, shrinkage, and cracking of CPs during charge/discharge processes leading to deterioration of mechanical properties and degradation of electrochemical performance.

(g) Electrochromism: Some of the CPs undergoes distinct color changes during the reversible oxidation and reduction processes. This is called electrochromism. The doping/de-doping processes in CPs are accompanied by the insertion/de-insertion of dopant ions. The switching of color depends on the energy gap of the CPs and the dopants. The color varies with various redox states. For example, PANI changes color from transparent yellow to green, blue and violet. The electrochromism of CPs depend on the temperature, pH of electrolyte, chemical structures, speed of migration of dopants and redox capability of the polymer.

1.1.5. Electrochemical reactions of conducting polymers

CPs follows reversible oxidation/reduction processes in suitable electrolytes during which ions and solvent molecules are exchanged between polymer chain and electrolyte. Two basic types of electrochemical reactions can be envisaged for CPs.

1.1.5.1. p-doping (oxidation)

The most common type of doping in CP is p-doping. It involves the generation of positive charges, or holes, on the polymer chains by the extraction of electrons when submitted to anodic potential. The generated charge is compensated by the ions penetrated into the

polymer from the electrolyte solution. Here, the transformation from a neutral state into an oxidized state occurs through two different ways:

(a) prevailing anion exchange

The positive charges generated on the polymer chains by oxidation are balanced through the penetration of anions from the solution. The osmotic balance is maintained by the entrance of solvent from the solution. During reduction, the anions inside the polymer chains are released. Thus the polymer swells by oxidation and shrinks by reduction as observed in reaction 1.4.

$$(Pol^0)_s + n(A^-)_{aq} + m(Solv) \rightleftharpoons [(Pol^{n+})_s(A^-)_n(Solv)_m]_{gel} + n(e^-)_{metal} \qquad (1.4)$$

where the different sub-indexes mean: *s*, solid and *aq*, aqueous solution, Pol^0 represents the reactive centres on the polymer chains and A- represents the anions. Figure 1.6 represents the volume change from a compact state (packed solid state) to a gel state by the reaction 1.4.

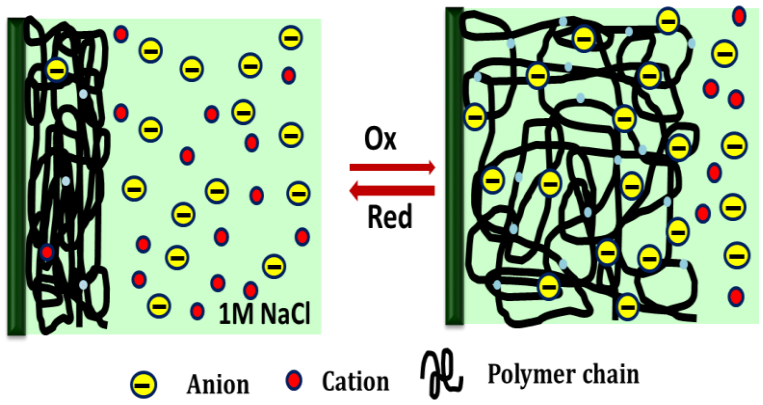

Figure 1.6 *Schematic representation of polymer showing volume changes (swelling/ shrinking) produced during p-doping by anion exchange*

(b) prevailing cation exchange

If the polymer is generated in presence of a large macro anion, it remains inside the polymer matrix regardless of the oxidation state of the CPs. In such case, during reduction, the cations penetrate into the polymer matrix for charge balance and during oxidation these cations are expelled as shown in reaction 1.5. Thus the polymer swells by reduction and shrinks by oxidation as can be observed in Figure 1.7.

$$[(Pol^0)(MA^-)_n(C^+)_n]_s \rightleftharpoons [(Pol^{n+})(MA^-)_n]_s + n(C^+)_{aq} + n(e^-)_{metal} \quad (1.5)$$

where MA^- is the large macro anion trapped inside the polymer matrix during polymerization and C^+ is the cation balancing the charge.

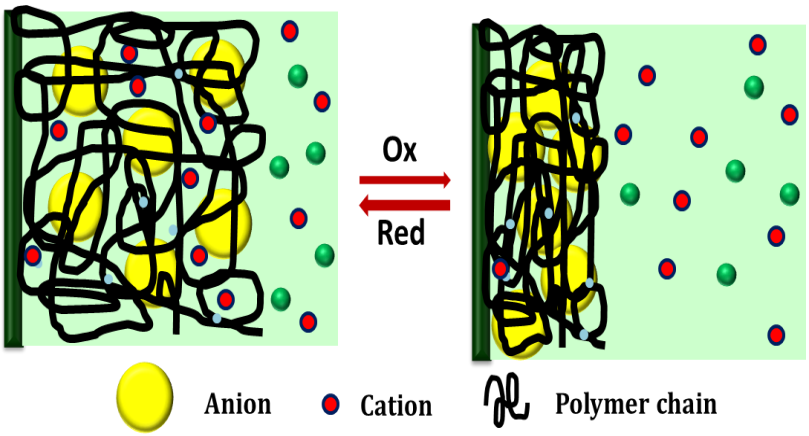

Figure 1.7 *Schematic representation of polymer showing volume changes (swelling/ shrinking) produced during p-doping by cation exchange*

In both reaction 1.4 and 1.5, the polymeric chains hold positive charges and thus the name is p-doping.

1.1.5.2. n-doping (reduction)

In CPs with high electronic affinity, n-doping typically happens, facilitating transitions from a neutral state to a reduced one. The negative charges produced by electron injection are stored on the chains under high cathodic potentials. Examples of CPs that undergo n-doping include PEDOT, PTh, and polyfluorenes. To execute the reaction (1.6), highly stable solvents and salts are required. Notably, the material swells during reduction and shrinks upon neutralization.

$$(Pol^0)_s + n(C^+)_{aq} + n(e^-)_{metal} \rightleftharpoons [(Pol^{n-})_s(C^+)_n(Solv)_m]_{gel} \quad (1.6)$$

1.1.6. Conducting polymers as multistep molecular motors

CPs are unique reactive materials capable of undergoing electrochemically-driven oxidation/reduction reactions with associated exchange of ions and solvent molecules. The insertion of ions and solvent molecules to into the CP chains occurs only when there is enough free volume available for their accommodation. Therefore the electrochemical reaction induces structural changes, particularly accompanied by volume changes in CPs. During oxidation, when the electrons are extracted, there occurs a redistribution of σ and π bonds along the polymer chain due to the formation of radical cations or bications (Figure 1.8a). As a result, the polymer chain uncoils and expands by the insertion of counterions and solvent molecules for charge and osmotic pressure balance. This results in a rod-like structure (Figure 1.8b). All the processes are reversed during reduction. These intra and intermolecular interactions can lead the CPs to act as

reversible molecular motors in solution. The *n* electron extraction occurs through *n* consecutive chemical equilibrium steps or *n* consecutive fundamental conformational energetic states in a reversible manner. As a result, they can act as multi-step macromolecular motors.

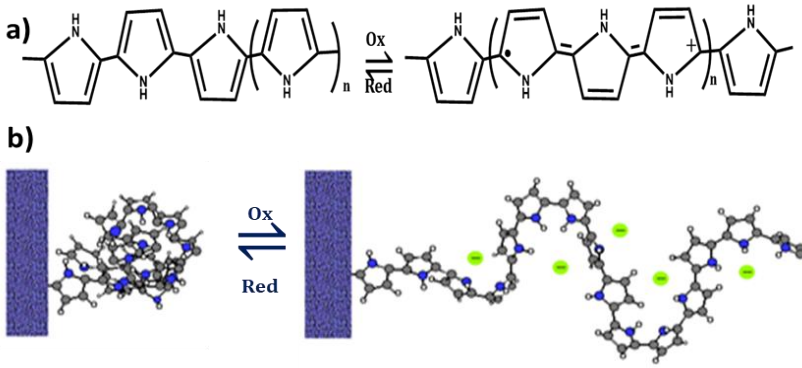

Figure 1.8 *(a) Formation/destruction of π bonds by oxidation/reduction of PPy chains and (b) Schematic representation of reversible conformational movements of PPy*

1.1.7. Biomimetic properties of conducting polymers

A series of polymer-based sensors are involved in the interaction of biological systems with their surrounding environment. These sensors convert chemical or physical stimuli into electrical impulses and transmit them to the brain through nerves. During electrochemical reactions, CPs drive the exchange of ions and solvent with the electrolyte to become dense and reactive gels. CPs can be visualized as the model materials that can mimic the intracellular matrix (ICM) of the living cell in its most elemental expression (one reactive macromolecule, one anion, and one solvent) during electrochemical

reactions through the same two connecting wires. The composition-dependent properties (conductivity, stored charge, stored chemicals, volume, porosity, wettability, color, etc.) of CPs can be tuned under electrochemical control by several orders of magnitude and envisages the development of biomimetic (electrochemical) devices and products. The reactive nature of the CPs mimics functions and properties of specialized living cells as shown in Figure 1.9.

Figure 1.9 *Biomimetic properties of CPs driven by the electrochemical reaction, the mimicked biological functions and the related organs*

1.1.8. Applications of conducting polymers

The CPs find applications in diverse fields due to their fascinating electrochemical, electronic and optical properties.

(a) Artificial muscles: One of the important applications of CPs that are receiving considerable attention recently includes actuators or artificial muscles due to their ability to change their physical dimensions when stimulated by an electrical signal. The dimensional variation of CPs occurs as a result of the unique electrochemical

reactions based on the ionic and aqueous exchanges of the polymer with the electrolyte. The performance of CP actuators is comparable with natural muscles (10% stroke and 0.3 MPa stress) and piezoelectric polymers (0.1% stroke and 6 MPa).

(b) Sensors: Due to the tunable electronic, optoelectronic, or electromechanical properties, CPs are widely used for developing various sensors including biosensors [51]. Here, the measured signals can be current flow, change in potential, change in resistance etc. The CP based sensors shows various advantages, such as lightweight, adjustable sensing performance, corrosion resistance and ease of processing when compared to conventional sensors made up of metals or ceramic materials. Due to their stimuli responsive behavior, they are employed as strain sensor [52], vapor sensor [53], pressure sensor [54], tactile sensor [55], liquid sensor [56] and temperature sensor [57].

(c) Supercapacitors: Among many candidates, CPs are widely used for supercapacitor applications owing to their low cost, lightweight, excellent doping-dedoping properties, high theoretical capacitance and tunable electrical conductivity [58, 59]. CPs are pseudocapacitors and their charge storage mechanism originates from the faradaic reversible doping/dedoping reactions in the polymer backbone [50].

(d) EMI shielding and Microwave absorbing materials: To shield the lower power frequencies in electromagnetic waves shielding of electromagnetic interferences (EMI) is necessary. PANI or PPy has been used as an excellent EMI shielding material due to its high conductivity [60-62].

(e) Rechargeable batteries: CPs are widely used in batteries owing to their high energy density, good portability high flexibility, high electrical conductivity, low-cost and ease of synthesis [63].

(f) Electronic devices: CPs act as promising materials to fabricate electronic devices like light emitting diodes [64], solar cells [65], field effect transistor [66], photovoltaic devices [67], Schottky diodes [68], etc.

(g) Biomedical applications: The CPs are efficient candidates for biomedical applications due to their low cost, redox properties, ease of synthesis, high porosity, large surface area, biodegradability and biocompatibility [69, 70]. The better bioactivity, adhesion and proliferation at low potential current make them suitable for tissue engineering applications. The CPs like PPy and PEDOT can act as neural interface material as they shows better adherence to the surface of the electrodes [71].

***(h) Electrochromic windows*:** The CPs, like PANI and PTh which can undergo distinct color changes under an applied potential are employed in electrochromic devices [72]. PANI transcends a number of colors with different potentials and PTh switches from red (oxidized) to blue (reduced) during their electrochemical reaction [73].

(i) Corrosion protection: The CP based new-generation corrosion protection coatings involves controlled release of corrosion inhibitors and provide beneficial protection to many metals [74, 75].

1.2. Polypyrrole

Polypyrrole, PPy, a classical nitrogen-based CP, is formed by the polymerization of pyrrole. It is predominantly a p-type electronic conductor and can be polymerized chemically as well as electrochemically. Tunable electrical conductivity, fascinating electrochemical activity over a wide range of pH, lightweight, ease of synthesis, stability towards repeated oxidation/reduction cycles and excellent environmental stability make PPy as a potential CP for its application in sensors, actuators, supercapacitors, batteries, solar cells, corrosion-protecting materials, electromagnetic shielding, fuel cells and electrochromic devices. During the synthesis, the color of PPy varies gradually from yellow to black with increase in degree of oxidation. They are highly stable at room temperature and the conductivity ranges from 10-1000 S cm^{-1} depending on the counterions [76].

1.2.1. Polypyrrole: A brief history

In 1888, oligomers of pyrrole were first synthesized by Dennsted and Zimmermann through chemical oxidative polymerization [77]. PPy was first synthesized by Angelo Angeli as an amorphous black powder called "pyrrole black" using pyrrole monomer and an oxidizing agent (hydrogen peroxide/acetic acid) in 1916 [78]. Many years later, the conducting nature of PPy was reported in 1963 by Weiss, McNeill and Bolto, where PPy was synthesized from tetraiodopyrrole by pyrolysis [79]. In 1968, Dall'Ollio and others obtained a powdery precipitate of PPy for the first time through electrochemical polymerization in 0.1 N H_2SO_4, that had an electrical conductivity of

8 S cm^{-1} [80]. In 1979, Diaz et.al produced coherent flexible films of PPy (5-50 mm) with a conductivity of 100 S cm^{-1}, leading to the proliferation of electrochemical method as the major route for CP synthesis. Later He et al. synthesized PPy by the chemical oxidative polymerization of pyrrole in an aqueous solution using $FeCl_3$ as oxidant [81].

1.2.2. Structure of Polypyrrole

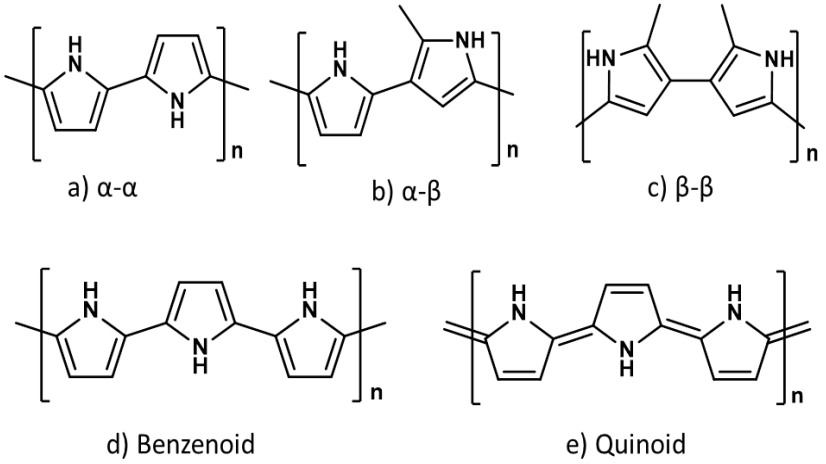

Figure 1.10 *(a-c) The possible bonding between the monomer units of PPy, (d) benzenoid and (e) quinoid forms of PPy*

In PPy chains, the bonding between monomer units is primarily via α-α carbons atoms (Figure 1.10a); however a minimum number of monomer is bonded at α-β and β-β positions also (Figure 1.10) [82, 83]. Due to the presence of conjugated double bonds, PPy is electrically conducting and there is delocalization of electron density in the molecule. Generally the de-doped (neutral) state of PPy corresponds to the benzenoid form (aromatic), which is insulator with a large band gap of approximately 3.16 eV. The conductivity is achieved through

doping, by removing a π-electron from the neutral chain. The doping changes its structure from the benzenoid to a quinoid form [84]. The structure of de-doped and doped PPy is shown in Figure 1.10.

1.2.3. Doping in Polypyrrole

The extended π-conjugated network structure of PPy ensures the electrical conductivity, but is not sufficient to produce appreciable conductivity. Doping is essential to show a marked increase in conductivity. Upon doping, usually carried out by oxidation (more common) or reduction, the polymer changes from an insulating regime to a metallic one. Neutral PPy consists of benzenoid rings, that could lose an electron from the valence band during the oxidation process and generates a positive charge and a free radical connected by local charge resonance which is called a polaron (Figure 1.11b). As the oxidation progresses, a second electron is eliminated from the PPy chain that results in the formation of a doubly positive charged bipolaron (Figure 1.11c) which is energetically preferred as it possesses energy lower than two separate polarons [41]. Both the polaron and bipolaron are extended over four pyrrole units. Due to the presence of conjugated system, the polarons and bipolarons formed are mobile and their movement is responsible for the conductivity of the polymer [43]. A detailed description of polaron and bipolaron are given in section 1.1.3.1.

In the dedoped state, the energy gap is about 3.16 eV which is too wide for electrons to move from the valence to the conduction band at room temperature. They behave as insulators. The generation of

polaron induces two new intermediate states (bonding and antibonding) in the band gap, where the energy of HOMO is increased and that of LUMO is decreased. On further oxidation, bipolarons are formed and hence the energy gap is further decreased. As the degree of oxidation increases, these bipolaron states overlap to form two wide bipolaron bands in the energy gap with a minimum energy gap minimum energy gap [85].

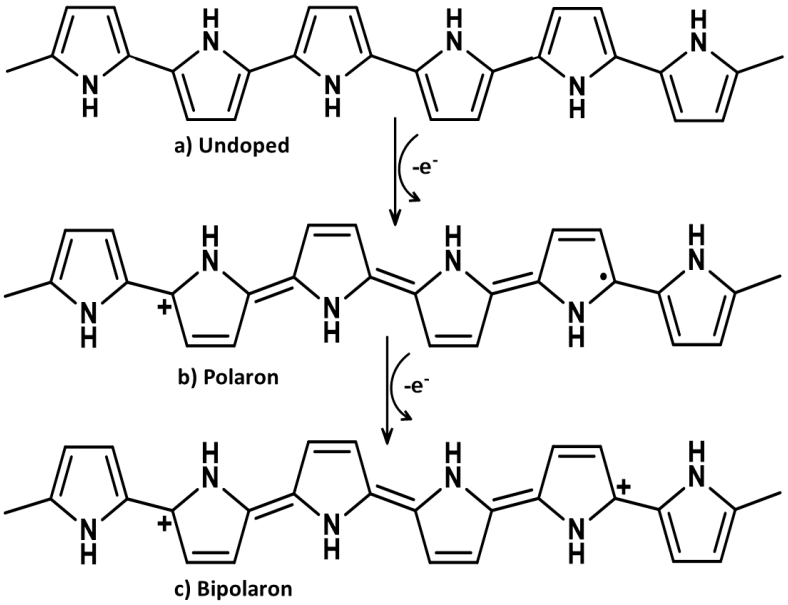

Figure 1.11 *Structures of (a) undoped, (b) polaron and (c) bipolaron of PPy*

1.2.4. Charge transport in Polypyrrole

The electrical conductivity of PPy is the product of two important factors, concentration of charge carriers and their mobility. In fully doped PPy, the concentration of carriers ranges from 10^{21} to $10^{23}/cm^3$, which is higher than that of inorganic semiconductors. PPy possess low mobility of charge carriers due to low degree of crystallinity and many

other defects. The mobility of charge carriers of PPy depends on both intrachain mobility and interchain mobility. The intrachain mobility is the charge transfer along the PPy chain. The interchain mobility requires energy more than that of intrachain mobility as it involves the hopping or tunneling of the charge from one chain to other. In the presence of an applied electric field, the polarons and bipolarons of PPy move along the chain by single and double bond rearrangements. When they reach at the end of a chain or approach any kind of defect, they hop or tunnel to neighboring chains and deliver the charges [35].

1.2.5. Synthesis of Polypyrrole

There are diverse techniques used for the synthesis of PPy. Among them, chemical oxidative polymerization and electrochemical polymerization are the two most commonly used techniques. Moreover, other conventional methods such as plasma polymerization, photochemical polymerization, radiolysis polymerization, vapor phase polymerization and concentrated emulsion polymerization are also employed to some extent. Whether PPy is synthesized chemically or electrochemically, the initial stage involves the formation of highly reactive free radical cations. This radical cation then reacts with a second radical cation or with neutral monomers to give radical dimers. On further reaction they are converted to trimer and build up the long polymer chains. The oxidation potential of oligomer of polymer is lower than that of the monomer and hence the radical coupling reaction is favored. When the length of the polymer chain exceeds the solubility limit of solvent, precipitation occurs. The polymerization steps are given in Figure 1.12.

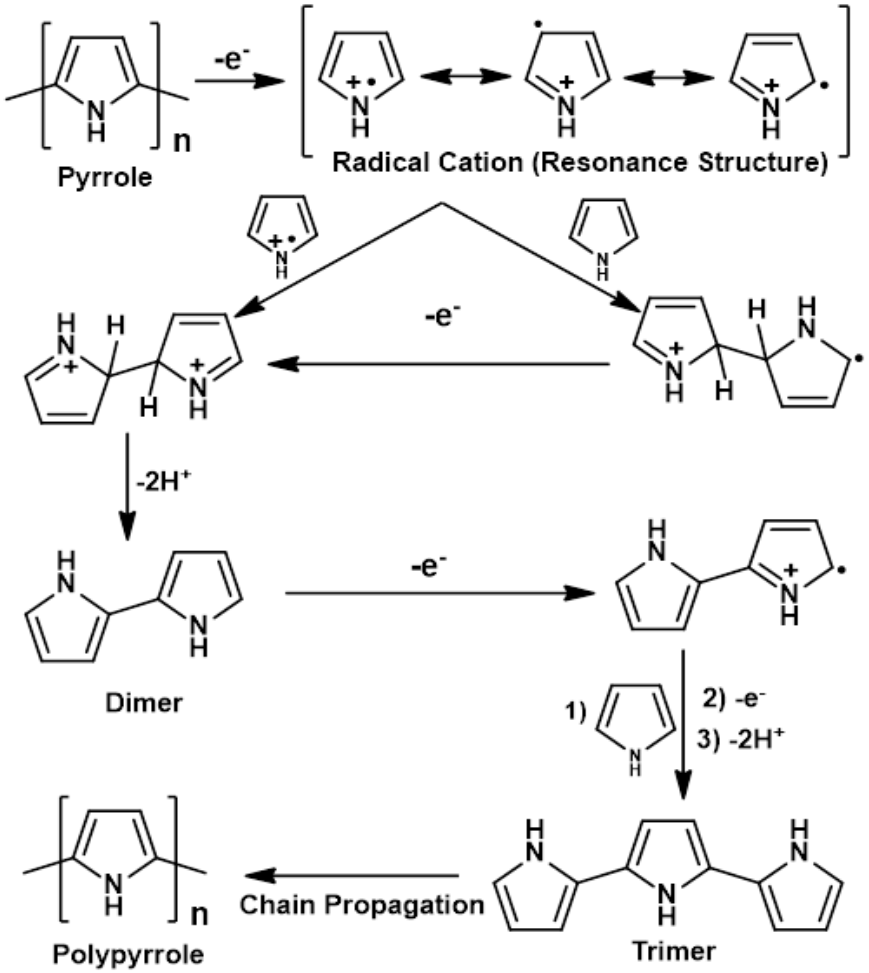

Figure 1.12 *Schematic representation of the mechanism of polymerization of pyrrole through the coupling of two radical cations*

1.2.5.1. Chemical synthesis

(a) Chemical oxidative polymerization: In the chemical oxidation method, an oxidant lead dioxide, quinones, ferric chloride, permanganate, dichromate or persulfates is added to the pyrrole monomer with dopant dissolved in a suitable solvent [86]. As a result doped PPy powder is precipitated. Usually the conductivity of PPy

synthesized by chemical method is lower than that of PPy synthesized electrochemically. The chemical synthesis is suitable for large scale production of processable PPy at a reasonable cost [87, 88]. Here, we can control the molecular weight and structural feature of the resulting polymer to a greater extent when compared to electrochemical method. An additional advantage is that, this method can be employed to produce all types of novel CPs which cannot be produced by electrochemical method. The yield of the PPy synthesized, conductivity, morphology and stability depends on many factors such as initial pyrrole/oxidant ratio, type of oxidant, purity of solvent used, concentration of reagent, reaction time and polymerization temperature. Lower temperature, low pH and shorter polymerization time enhances the conductivity of PPy formed. The major drawback of this technique is the inability to form thin films [89]. $FeCl_3$ is found to be the best oxidant and the yield of PPy approaches 100% [87]. The overall stoichiometric equation for the chemical polymerization of pyrrole using $FeCl_3$ as oxidant can be represented by Equation 1.7 [90].

$$nC_4H_5N + (2+y)n\,FeCl_3 \rightarrow \left[(C_4H_3N)_n^{y+}\, nyCl^-\right] + (2+y)FeCl_2 + 2n\,HCl \qquad (1.7)$$

where *y* represents degree of oxidation.

(b) Interfacial polymerization: Unlike chemical oxidative polymerization the reaction rate is slow and occurs at the interface/ boundary of two immiscible phases (liquid/air or liquid/liquid). Generally, one of the phases is an aqueous phase containing the oxidant and the other is an organic phase containing the PPy monomer. The reactants diffuse towards the interface and

polymerization occurs. This method possesses benefits over other techniques. The polymer is formed in a controlled manner due to slower reaction kinetics [91, 92].

(c) Template-mediated polymerization: This method involves two types of templates: soft and hard templates. In soft template method the surfactant micelles and porphyrin undergoes self-organization and traps the monomers resulting in polymerization. The commonly used surfactants for this method are cetyltrimethylammonium bromide, dodecylltrimethylammonium bromide and octyltrimethylammonium bromide [93]. The mechanism involves the formation of lamellar structure between cations of the surfactants and the anions of the oxidizing agents in the aqueous solution. Here the template is self-degradable and hence can be easily removed during washing. Hard templates act as physical templates in which polymerization occurs either chemically or electrochemically [94]. After polymerization, the polymer need to be removed from the template [95]. The commonly used hard templates are polycarbonate, anodic aluminium oxide, filtration membranes, mesoporous silica and nanotubular titania [96].

1.2.5.2. Electrochemical synthesis

Electrochemical polymerization is an elegant method for the deposition of conducting PPy films on the anodic electrode with a well-controlled thickness and morphology [97, 98]. The electropolymerization does not require the use of oxidants, and is achieved by electron transfer between the substrate and the electrode by

applying potential that permits coupling reaction between the radical cations or anions leading to the growth of the polymer chain [99]. One of the key advantages of the electrochemical method is that the technique allows the deposition of highly conducting insoluble PPy films in a simple, fast, clean and cost effective manner. Under appropriate conditions it is possible to control the growth rate and film thickness. The properties of the deposited films depend on several parameters of electropolymerization including the deposition charge, deposition time, the doping agent, the solvent, the temperature, the pH and the electrode system [100-104]. The electrochemical polymerization occurs only if the monomer undergoes oxidation in the presence of an applied potential. [97]. Electropolymerization can be performed either in a two electrode (working electrode (WE) and counter electrode (CE)) or a three electrode system (i.e. working, counter and reference electrodes (RE)). Electrochemical synthesis of PPy can be performed in both aqueous and non-aqueous media (acetonitrile, dichloromethane, propylene carbonate, etc.) [105, 106]. The film formation does not occurs in nucleophilic aprotic solvents like hexamethyl phosphoramide, dimethyl formamide, dimethyl sulfoxide etc. without the addition of some protic solvent to reduce the nucleophilicity [107].

Generally, Electropolymerization process of PPy can be carried out in three ways: the galvanostatic, the potentiostatic and potentiodynamic techniques [108].

(a) Potentiostatic method: The potential between the WE and RE is controlled, while the current varies [109]. The transport of current or

monomers occurs through convection, migration or diffusion. This method is used to obtain thin films. The potential should be lower than 1V, otherwise overoxidation or chain degradation occurs resulting in poor quality film formation.

(b) Galvanostatic method: In this method, the potential varies and the current is controlled. That is the rate at which the PPy is deposited is steady and can be accurately controlled [109, 110]. This method provides a better control over thickness and commonly used to obtain thick polymer films. The thicker growth of polymer is also achieved due to the passivation of the electrode surface by considerable polymer deposition.

(c) Potentiodynamic method (cyclic voltammetry): This method involves sweeping the polymerization potential of the WE between a low and high potential limit in cycles with respect to the RE at a certain scan rate [111]. This method allows the polymer to be deposited in layers and each layer is electrically active [112]. The polymer alternates between different redox states during potential cycling and gives information about the redox potentials of polymer and monomer. This method is useful to produce PPy films with different surface morphology.

1.2.5.3. Other methods

(a) Plasma polymerization: Plasma polymerization is a novel process used to obtain thin films of PPy without any chemical oxidants from a group of organic and organometallic preliminary materials [113]. The reaction takes place in gas phase and plasma-polymerized PPy are

highly linked, chemically inert, thermally stable, insoluble and mechanically strong. The fragment formation, trapped radicals, and a higher degree of branching and crosslinking is responsible for these properties [114].

(b) Photochemical polymerization: Polymerization of pyrrole done by this method, involves the irradiation with visible light as a photosensitizer electron acceptor. This method is fast, inexpensive and not destructive to the surroundings [115].

(c) Radiolysis polymerization: This method involves the radiolysis of an aqueous solution of monomer by gamma rays [116]. This method is simple, easy to conduct in different environments and requires less complicated set up for polymerization. By adjusting the dose of radiation it is possible to synthesize polymers with different properties.

(d) Vapor phase polymerization: In this technique, the monomer in the vapor form is introduced into the oxidant coated substrate and polymerization takes place at the interface [117]. It is a solvent free technique and no liquids act as transport medium for the agglomeration of particles [117]. This method can be used to deposit CP coating on a particular substrate. However, PPy produced using this method exhibits lower conductivity.

(e) Concentrated emulsion polymerization: This is a heterophase procedure, which requires an emulsifier or a surfactant for the polymerization to take place [118]. It consists of an aqueous phase (containing water soluble initiator), an organic phase (containing a water insoluble monomer) and certain emulsifiers or micelle-forming

surfactants [119]. The radical polymerization is the prime mechanism involved. Here the surfactant acts either as a template or as a co-dopant.

1.2.6. Applications of Polypyrrole

The amazing properties of PPy make it an efficient candidate for potential applications in multidisciplinary fields. Some of them are outlines in Figure 1.13.

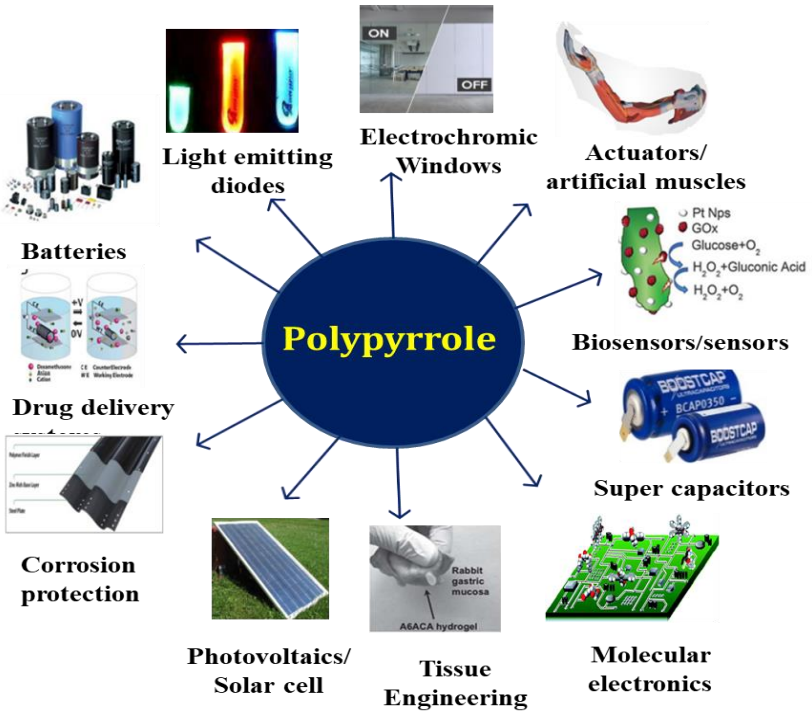

Figure 1.13 *Potential applications of PPy*

(a) Sensors: PPy has been widely used as chemical, electrochemical, physical or biological sensors due to their stimuli responsive behavior. Based on PPy, highly selective electrochemical sensors have been developed for the determination of p-nitrophenol [120],

benzimidazole [121], nitrite [122], hydroxylamine [123], xanthine [124], cholesterol [125], and so on. Here, the measured signals can be current flow, change in potential or change in resistance. As biosensors they are used for DNA sensing [126], dopamine [127] and ascorbic acid sensing [128], glucose sensing [129], hydrogen peroxide sensing [130] and so on. In addition, electrochemical immunosensors were also developed based on PPy [131]. The dependence of electrical conductivity of PPy on the kind or concentration of gases makes it efficient for gas sensing applications [132]. Nanocomposites of PPy with iron oxide were reported for humidity and gas sensing applications [133].

(b) Actuators: PPy has been considered as an excellent material for actuator applications, because it undergoes reversible dimensional changes during the oxidation/reduction processes [134]. The electrochemically synthesized PPy films show fast and intensive bending in air without using electric field, ions or heat [135]. PPy has gained a reputable status from their use as actuators due to their biocompatibility, moderately high actuation strain, low operational voltage, and ability to generate forces similar to natural muscle. Toribio et.al demonstrated the linear and bending (bilayer and trilayer) actuators of PPy [136-138].

(c) Supercapacitors: The use of PPy is particularly promising in the field of supercapacitors because of its high energy storage capacity, excellent doping-dedoping properties, good electrical conductivity, ease of synthesis, and stability in air [139]. Though, PPy exhibit high theoretical capacitance, it suffers from poor cycling stability in

long-term charge-discharge processes. This poor cycling stability can be enhanced by making composites with suitable materials [140].

(d) Batteries: PPy has been used in rechargeable batteries due to its lightweight and capacity to store recoverable charge [141]. The various synthetic conditions influences the specific charge density of PPy and Li/PPy batteries with excellent performance was reported [63].

(e) Electromagnetic Interference Absorbing Material: PPy is capable of reflecting as well as absorbing the electromagnetic waves and therefore exhibit a significant advantage as EMI shielding materials [60].

(f) Electrochromic devices: CPs like PPy have advantages over many other electrochromic materials owing to their high contrast and coloration efficiency, ease of processing, fast switching time and tunable band gap [142]. A movable electrochromic pixel based on PPy was fabricated by Smela et al. [143].

(g) Protective coating: PPy can be used as a protective coating for semiconducting anodes in photo electrochemical cells. The PPy coatings prevents passivation of its surface and allows the formation of electron holes [144].

(h) Light emitting diodes: PPy is used as a transparent anode in polymer light-emitting diodes with a quantum efficiency of 0.5 % [18]. Here, the carrier injection from the PPy anode occurs by a combination of tunneling through the barrier and thermionic emission over the barrier. Organic light emitting diodes using photolithographically

patterned PPy films for patterned growth of hole transport is reported very recently [17].

(i) Solar cells: PPy has been widely applied as counter electrodes in dye-sensitized solar cells owing to their unique properties such as good specific capacitances, low cost, remarkable stabilities, high conductivity and catalytic activity for I_2 reduction [65].

(j) Biomedical applications: In the biomedical field, PPy find applications in drug delivery, tissue engineering, clinical therapies, biosensors as well as stimuli-responsive biomimetic polymeric materials [145, 146]. The electrical conductivity, electroactivity, microstructures and biocompatibility plays an important role for all those applications. PPy also has the ability to modulate cellular activities like proliferation, cell adhesion and differentiation via electrical stimuli [147].

1.2.7. Limitations of Polypyrrole

Despite of various interesting properties, extensive application of PPy is limited in innovative areas of technology to certain extent due to some of its inherent limitations.

- Due to the presence of conjugated double bonds in the backbone, PPy is inherently rigid, brittle and possess high stiffness. Thus they exhibit poor mechanical properties.
- PPy is infusible in nature and insoluble in most of the common organic and aqueous solvents, which give rise to processing difficulties.

- The poor cycling stability and low rate capability as a result of the structural instability due to swelling and shrinking of the polymer constitute the major limiting factor for the practical application of PPy for energy storage devices [148].
- They are generally hydrophobic in nature due to the presence of aromatic rings in the backbone causing π–π stacking of the chains.

These limitations restrict the potential applications of PPy. Hence systematic efforts are undertaken by the various research groups to improve the properties and performance of PPy and make it suitable for applications in more advanced and technological fields which is also one of the objectives of the present study.

1.2.8. Strategies adopted to overcome the limitations of Polypyrrole

In order to overcome the limitations of PPy which limits their applicability in various technological fields, various strategies have been adopted by the scientific community. Some of the strategies are given below.

- The mechanical properties and processability of PPy can be improved by making composites/hybrids/blends with other processable polymers like hydrogels.
- Solubility and processability can also be improved by the use of surfactants or emulsifiers.
- Attempts to overcome the limitations associated with the low cyclic stability and rate capability of PPy have centered on combining it with suitable materials such as carbon nanotubes,

graphene, activated carbon or metal oxides. These materials enhance the pseudocapacitance of PPy as they can provide high surface area. The incorporation of these materials also improves the conductivity of PPy. Besides, these materials with suitable functional groups enhance the stability of PPy.

Among various strategies adopted to improve the performance of PPy by overcoming its inherent limitations, the strategy of synthesizing or fabricating hybrid systems of PPy with hydrogels is an effective method to improve the mechanical properties of PPy, which can lead to their direct applicability in devices. This is one of the major objectives of the present study. The hydrogels are promising candidates due to their swelling-deswelling properties, biocompatibility, mechanical stability, stimuli-responsive behavior, porous structure, low cost , etc.

1.3. Hydrogels

Hydrogels, as the name implies, are three dimensional hydrophilic polymeric networks that can swell in water and hold a large volume of aqueous solvents within their porous structures and rendered insoluble by virtual, electrostatic or covalent crosslinking [149-151]. The first synthetic hydrogel is poly-2-hydroxyethyl methacrylate reported by Wichterle and Lím in 1960 [152]. Hydrogels can imbibe large quantity of water, resulting in an elastic network by filling the interstitial spaces. It is due to the presence of hydrophilic functional groups (-NH_2, -COOH, -OH, - CONH -, -$CONH_2$ and -SO_3H.) in the polymer chains. In addition, they can also hold other reactive, monomeric and potentially polymerizable species within their network

structures. In general, water content of hydrogel may vary from 10 % to thousands of times of the total weight and if water is present more than 95 %, then it is called superabsorbent. The environmental factors like temperature, pH, presence of magnetic field, electric field, type of solvent, ionic strength of the medium and chemical architecture of the gel determine the water absorbing capacity of the hydrogels. One of the important intrinsic characteristics of hydrogels is their wide range of stimuli-responsive behavior or the gel-sol phase transition in response to certain physical and chemical stimuli [150]. Physical stimuli include temperature, electric field, magnetic field, pressure, light intensity, and solvent composition. Chemical stimuli comprise pH, ionic strength, ions or specific molecular recognition events and specific chemical compositions. The hydrogel response is reversible and can preserve its overall shape during the swelling and shrinking process. The extent of swelling or response of hydrogels to external stimuli depends on the nature (mainly hydrophilicity) of the monomer, degree of cross-linking, charge density, pendant chains and applied external stimulus.

In order to retain the three-dimensional structures, the polymer networks of hydrogels are usually cross-linked through chemical or physical interactions [149]. Chemically cross-linked hydrogels are often connected by covalent bonds, while physically cross-linked hydrogels are resulted from non-covalent interactions such as van der Waals interactions, ionic interactions, hydrogen bonding, or hydrophobic interactions [153]. They closely resemble biological tissue than any other synthetic biomaterials due to their higher swelling capacity, porosity, permeability and soft nature. Hydrogels have gained

considerable attention in last 50 years due their exceptional properties like swelling-deswelling properties, biocompatibility, flexibility, mechanical stability, stimuli-responsive behavior and so on and can be utilized for various potential applications such as sensors [154], biosensors [155], artificial muscles [156], tissue engineering [157], wound dressings [158], drug delivery [159], cosmetics [160], superabsorbents [161] and controlled-release fertilizer [162]. Some of the functional features of an ideal hydrogel material are listed below:

- High water absorption capacity without loss of structural integrity. The equilibrium swelling rate of the hydrogel depends on degree of cross-linking, interaction with the counter ion and hydrophobic/hydrophilic interactions.
- High mechanical strength, durability and stability in the swelling state and during the storage. The polymer structure, cross-linking density and degree of swelling determines the mechanical properties of the hydrogel.
- They possess high degree of flexibility and softness similar to natural tissues.
- Stimuli-responsive behavior.
- High biodegradability without the formation of toxic products during degradation.
- Biocompatibility.
- Rate of absorption depending on the desired application.
- Most of them are non-toxic, colorless and odorless.
- They possess re-wetting capability depending on the application requirements.

Hydrogels can be classified on the basis of their origin/source into natural, synthetic and hybrid or semi-synthetic [163, 164]. Natural hydrogels are derived from natural sources such as plants and animals. Examples are chitosan, collagen, gelatin, alginate, fibrin etc. Synthetic hydrogels are derived from synthetic sources by conventional polymerization. Examples are polyvinyl alcohol, polyethylene glycol, polyacrylic acid, poly ethylene oxide, etc. Over the last two decades synthetic polymers have attracted significant attention over natural hydrogels because of their water absorption capacity, strength, well-defined structures, stability and higher durability. The present study comprises of two hydrogels: chitosan (Cs) - a natural hydrogel and polyvinyl alcohol (PVA) – a synthetic hydrogel.

1.4. Conducting polymer/hydrogel systems

The search for CPs satisfying technological and industrial requirements by the scientific community led to the development of conducting polymer/hydrogel systems (CPHs) as an efficient free standing electrode material for many potential applications. CPHs are gels combining the CP moieties in the insulated porous polymer network of hydrogels. Such systems can show the combined properties of both hydrogel and conductive polymers. In 1994, Gilmore et al. have reported the first CPH system which is a hybrid composite based on PPy and polyacrylamide [165]. Improvements are expected from these hybrid systems in which the CPs provide the essential building bloke of conducting phase, while the hydrogel enhances the mechanical properties. They can effectively combine the respective properties of both CPs and hydrogels including conductivity, electroactivity,

swelling property, flexibility, in vitro and in vivo biocompatibility, porosity, mechanical strength, high specific surface area, high diffusivity, electrochemical switching between redox forms, and macroscopic homogeneity [166, 167]. The fabrication of CPHs helped in overcoming the inherent limitations associated with CPs such as poor mechanical strength, poor processability and brittleness [151, 168]. The CPH can change their shape, size, volume, etc., in response to external stimuli such as electric field, pH, temperature, solvent, light, ionic strength etc. Since both the components are stimuli responsive materials, CPHs have enhanced properties compared to CPs and since they are flexible in nature, they are recently receiving considerable attention in the field of sensors, supercapacitors, actuators, biomedical applications and optics. They offer excellent processability and can be simply cast into films, fibers, wires, microspheres or any other desired shapes at the gelation stage. They can improve the various electrode interfaces such as electronic and ionic transport phases, soft and hard materials as well as synthetic and biological systems [169].

1.4.1. Fabrication of conducting polymer/hydrogel systems

Several methods have been reported in the literature for the fabrication of CPHs [169, 170]. The final properties of CPHs depend on the concentration and structure of the CP within the hydrogel and synthetic conditions. Some of the important methods are discussed below.

(a) Polymerization of conducting polymer within a prefabricated hydrogel matrix: It is the widely used method for the fabrication of

CPHs. During chemical oxidation method, a prefabricated dried hydrogel is immersed in the monomer solution of CP for sufficient time to attain equilibrium. The monomers also get penetrated inside the hydrogel matrix. Then the solution is exposed to the oxidant solution resulting in the polymerization of CP inside and outside the hydrogel [171]. The electrochemical polymerization technique can also be employed for the fabrication of CPHs instead of chemical oxidation method. Here, a hydrogel coated electrode is used as the anode and the CP is electrodeposited on it by the application of potential [172]. Another method adopted for the synthesis of CPHs is interfacial polymerization [173], where the monomer and the oxidant are in two immiscible liquid phases. The hydrogel is permitted to swell in an aqueous oxidant solution for attaining equilibrium and then exposed to the organic layer containing the monomer and the polymerization reaction occurs at the interface of two liquids.

(*b) CPHs formed by blending of conducting polymer with hydrogel:* It is an alternative method employed to fabricate CPHs. It consists of blending CP with hydrogel in the solution state or melt state [174]. In order to disperse CP uniformly throughout the hydrogel matrix, the solution/dispersion of CP is mixed with hydrogel solution with constant stirring. Crosslinking agents like glutaraldehyde are used if needed. Since CPs exhibits poor solubility in common solvents, this method limits the versatility.

(c) Polymerization of conducting polymer in the presence of matrix polymer solution/dispersion: It is a one-pot synthesis of CPHs involving the chemical polymerization of CP within a solution of a

suitable supporting hydrogel instead of polymerizing in the presence of a prefabricated hydrogel. When the polymerization of pyrrole/aniline takes place in presence of water soluble polymers, usually a colloidal dispersion of CPH is formed. It can be then precipitated with the help of a suitable solvent like ethanol, methanol, ethanol/ether mixture or acetone or can be cast into a film, fibers or to any other desired shape [175, 176].

(d) CPHs Formed from mixed precursors: This is a less common method used for the fabrication of CPHs. This method is employed for the hydrogels that can be easily prepared from their monomer. Here the CP and hydrogel precursors are placed in the same vessel and allowed to polymerize either simultaneously or in a two-step process [177].

(e) Synthesis of CPHs by cross-linking with dopant molecule: The CPHs formed from conventional methods are usually in the form of gels, which is having conductivity lower than that of the conducting polymer component due to the incorporation of nonconductive hydrogels. It is found that molecules such as phytic acid, amino trimethylene phosphonic acid and copper phthalocyanine-3,4′,4″,4‴-tetrasulfonic acid tetrasodium salt (CuPcTs) with multiple acid functional groups can cross-link with the polymer chains of CP, results in the formation of CP gels with 3D networked structures free of insulating components [178]. They are having good electronic and electrochemical properties [179]. A two-component mixing strategy was used to produce CP gels. That is a solution containing the oxidative initiator was mixed with the second solution containing the CP

monomer and crosslinking dopant, resulting the formation of a gel within a few minutes [180].

1.4.2. Applications of conducting polymer/hydrogel systems

The CPHs have drawn greater attention in diverse field of applications not only because of their interesting electronic properties but also of the expected synergistic effects of both the components. Due to the availability of large number of CPs and hydrogels, there has been an increase in the number of articles in the literature dealing with the applications of CPHs.

(a) Sensors: The high flexibility, sensitivity, robustness, stability of CPHs in comparison to pristine CPs, making them promising candidates for and different types of sensors such as chemical, environmental, gas and biosensors [181, 182]. CPHs are promising for biosensor applications because of their porous nature that makes them permeable to water soluble chemicals and facilitate their diffusion [183].

(b) Energy storage devices: CPHs show better performance such as high specific capacitance, high conductivity, high cycling stability, large surface area, structural tunability, hierarchical porosity, mechanical stability, flexibility and ease of preparation. Therefore they can be used in the development of the next generation energy storage devices (supercapacitors, solar cells, biofuel cells etc.) [184, 185]. The synergized properties can meet the essential requirements for flexible, lightweight, and environmentally friendly energy storage devices [186].

They showed better cycling stabilities at high current densities due to the highly porous nature that can accommodate the swelling and shrinking of the polymer network during cycling processes [170].

(c) Actuators/artificial muscles: Since both the components of CPHs share a common feature of stimuli responsive behavior, they exhibit enhanced chemical and electrochemical actuation in responses to pH and electrical stimuli over pure CPs and hence they find potential applications in the field of actuators [187, 188].

(d) Electronic devices: Due to high electrical conductivity and mechanical flexibility, CPHs are widely used for the development of flexible electronic devices such as light emitting diodes [64], electrochromic windows [189], transistors and diodes [190], and photovoltaic devices [67, 191]. CPHs have applied in the form of active layers in electrochromic devices owing to their ability to change the colour [192].

(e) Biomedical applications: CPHs have been primarily utilized as bioelectrodes due to the mechanical similarity to biointerfaces such as human skin and replace the metallic electrodes and enhances the mechanical properties and long-term stability of the electrodes within living systems. They are used in the field of tissue engineering because of their good electrical property, electroactivity, biocompatibility, large surface area, high porosity, and biodegradability [193]. CPH can acts as an enhanced neural interface material and exhibit low impedance, high charge density, soft nature and showed controlled release of nano biomaterials, which are the necessary requirement for getting high quality signals [194].

1.5. Supercapacitors : An overview

Supercapacitors, otherwise called ultracapacitors or electrochemical capacitors are energy storage devices that bridge the gap flanked by traditional electrolytic capacitors and conventional batteries with long life and the eco-friendly operation. They are having energy density higher than traditional electrolytic capacitors and power density greater than conventional batteries as evident from the Ragone plot shown in Figure 1.14a. Over the past few years, the field of electrochemical supercapacitors has witnessed phenomenal growth due to their outstanding electrochemical performances such as high power density, high cyclic stability, shelf life, fast charge-discharge cycles and higher energy storage as compared with the Li-ion batteries. The supercapacitors are broadly classified on the basis of charge storage principle into electrochemical double-layer capacitors (EDLC), pseudocapacitors, and hybrid capacitors as shown in Figure 1.14b.

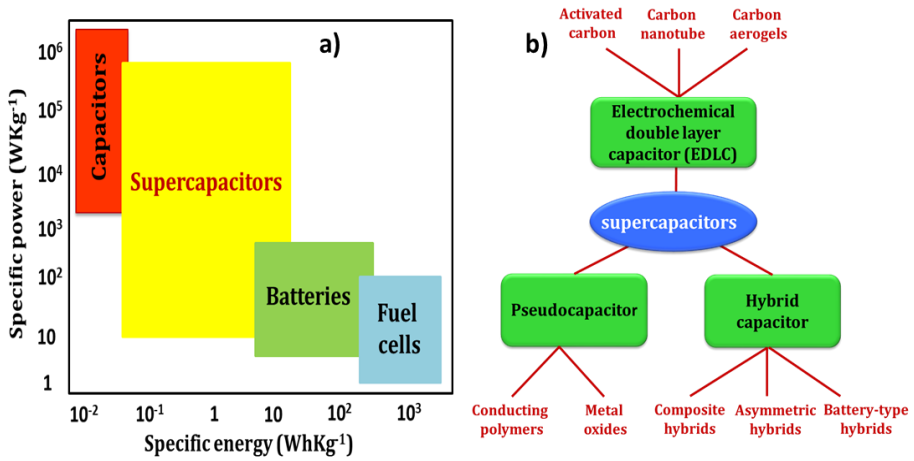

Figure 1.14 (a) *Ragone plot for typical energy storage devices, and (b) Classification of supercapacitors based on the charge storage mechanism*

1.5.1. Electrical double layer capacitors

EDLCs can store charge electrostatically or through a non-faradaic process and there is no charge transfer takes place between the electrolytes and electrodes. When a voltage is applied across the electrodes, a potential difference is generated across the electrolytic medium. As a result the positive and negative electrolytic ions migrate to the oppositely charged electrodes as shown in Figure 1.15a. Therefore accumulation of charges occurs at the surface of the electrodes. To prevent recombination of ions at electrodes, a Helmholtz double layer is developed. The double-layers combined with enhanced specific surface area decreases the distance between electrodes and enables EDLCs to produce higher energy densities. Carbon based materials such as activated carbon, carbon nanotubes, graphene, carbon aerogels etc. are most extensively used as supercapacitor electrode materials.

1.5.2. Pseudocapacitors

Pseudocapacitors are based on faradaic redox reactions which involves the transfer of charge between electrode and electrolyte. They offer high energy density and much higher specific capacitance than EDLCs, but their cycle life is inferior. Pseudocapacitors generally involve the use of CPs and transition metal oxides since they can be promptly charged and discharged by converting between their different redox states. When a potential is applied to a pseudocapacitor, some specifically adsorbed ions of the electrolyte diffuse into the double layer and transfer their charge with the electrodes. The schematic

representation of a pseudocapacitor is shown in Figure 1.15b. The oxidation/reduction reactions take place at the electrode material allows the passage of charge across the double layer and the flow of faradaic current through the supercapacitor cell. The pseudocapacitors utilize the bulk of the electrode for the redox reaction rather than the surface as in the case of EDLC.

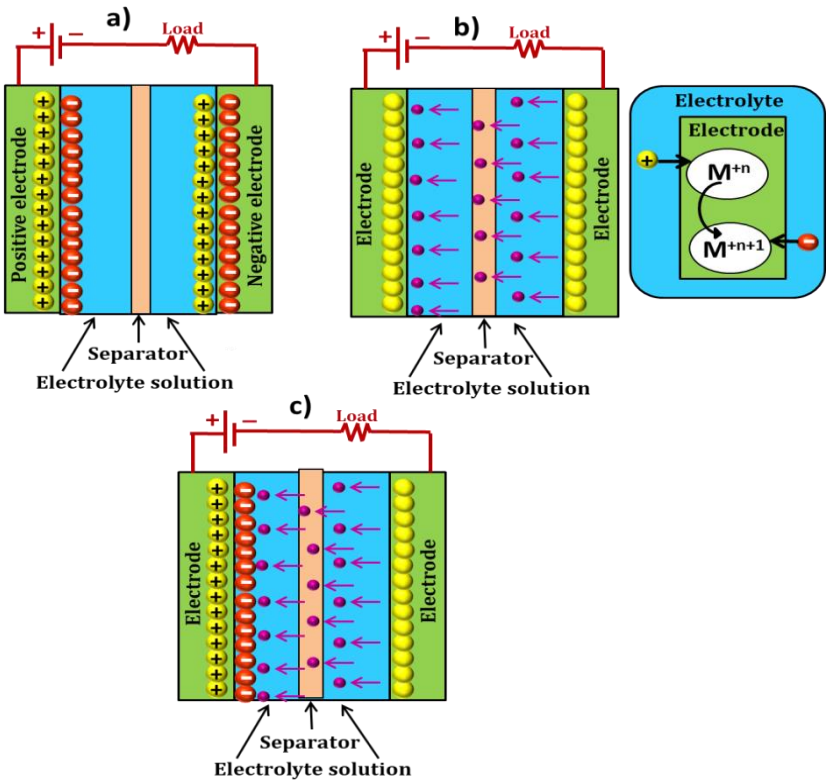

Figure 1.15 *schematic representations of different types of supercapacitor: (a) EDLC (b) pseudocapacitor and (c) hybrid capacitor*

1.5.3. Hybrid capacitors

Hybrid capacitors utilize both faradaic and non-faradaic mechanism for storage of charges. Here two types of electrodes

i.e., a battery-like electrode and a capacitor-like electrode are combined within the same cell and gives excellent cyclic stability. The schematic representation of a hybrid capacitor is shown in Figure 1.15c. The three main types of hybrid capacitor configurations are composite, asymmetric and battery-type. It is also possible to fabricate hybrid capacitors by combining composites of pseudocapacitive materials with double-layer capacitive materials. Hybrid capacitors synergize the advantageous features of both EDLCs and pseudocapacitors to achieve high electrochemical performance such as high energy density and power density.

Among many candidates, CPs are widely explored for energy storage materials and modifying the present energy storage devices towards the future advanced cutting-edge electronic applications owing to their low cost, light weight, ease of synthesis, high theoretical capacitance, environmental stability, excellent doping-dedoping properties, high intrinsic flexibility and tunable electrical conductivity in contrast to the expensive metal oxides. However, CP based supercapacitors still struggle against poor processability and brittleness especially under large deformations. They show poor cycling stability as a consequence of the structural instability due to swelling (oxidation) and shrinking (reduction) of the polymer chains. Therefore, the development of supercapacitors based on CP/hydrogel hybrid systems with stable mechanical properties and electrochemical performance has become one of the research hotspots in this field. The combination of hydrogels with CPs facilitates efficient electron/ion transport and suppresses the structural collapse of the electrodes.

1.6. Present investigation

During the last two decades, CPs have been exploited thoroughly for their potential applications, most of them by considering the material composition constant. They still remain as a less explored material based on their composition dependent properties, i.e., their ability to change the material composition by several orders of magnitude during electrochemical reactions has not been exploited for potential applications. At the same time, the scientific community has been searching for multi-sensing intelligent motors capable of sensing surrounding variables at any instant, without physical separation using the same two connecting wires. Inspired by these, the present research is aimed at exploring the composition dependent properties of PPy and to fabricate self sensing macromolecular motors based on PPy redox reactions.

This work is a part of our approach on CPs to establish the fact that the simultaneous sensing properties are a general property of all CPs. That is, unlike other researches where the property changes when the material changes, here the faradaic redox reactions in all CP is a general property which can be exploited to design biomimetic self sensing devices. The investigation starts with exploring the electrochemical properties of chemically synthesized PPy powder. A detailed investigation was done on the structural faradaic processes occurring in PPy by coulovoltammetry.

The traditional electrochemical or potentiometric sensors work under equilibrium conditions and follow the Nernst equation, whereas

the CPs, because of the continuous variation of composition, are visualized as working outside the chemical equilibrium condition. Therefore, the typical Le-Chatelier principle and Nernst equation are not directly applicable for CPs. Otero's principle proposed by reformulating the Le-Chatelier principle is only applicable to such condensed systems. This principle is the very foundation of reaction driven sensing characteristics of CPs. In this thesis, one of our objectives is to verify the reaction driven sensing characteristics of chemically synthesized PPy through chronopotentiometry and to verify the electrical energy can act as the sensing parameter, and through cyclic voltammetry to verify electrical charge can act as the sensing parameter. We argue that, any device based on the electrochemical reactions of PPy can sense the working energetic conditions at any instant, using the same two connecting wires.

Poor mechanical strength and low processability of PPy limits its extensive application in diverse fields ranging from electronics to energy devices. Therefore, another objective of our research is directed to fabricate mechanically stable free standing electrode materials based on PPy reaction. Centered on this, we have fabricated two CP/hydrogel hybrid films through a facile and low cost method: (1) PPy/Chitosan hybrid films and (2) PPy/PVA hybrid films. Both the hybrid films were fabricated through in situ chemical polymerization of pyrrole on pre-fabricated hydrogel matrix. We have extended the sensing principle to PPy/Chitosan hybrid films and the objective is to verify the whether the PPy/Chitosan films can act as a multi-sensing electrode materials capable of sensing its surrounding electrical, chemical and thermal

conditions. Besides, we wanted to explore their performance as a free-standing supercapacitor electrode material.

Final objective of this study is to fabricate a mechanically stable self-sensing macromolecular device based on the faradaic reactions of PPy capable of working both in dry and wet conditions. Though PPy/Chitosan films showed a reasonably good mechanical strength in the dry state, they are mechanically less stable in the wet state and found not suitable for such device fabrications. Accordingly our research was directed to search for a highly electroactive hybrid films which are mechanically highly stable both in the dry and wet states. PPy/PVA hybrid films were fabricated and studies were directed to prove their reaction driven sensing characteristics, the influence of the size of anions on the reaction driven sensing characteristics and to explore the various reaction conditions such as chemical, thermal and electrical energetic conditions influence the cooperative actuation of multistep molecular motors of PPy. The charge storage characteristics of the hybrid films were studied by cyclic voltammetry and galvanostatic charge discharge method. Finally, we have moved to device fabrication. Here, we have demonstrated the charge storage and sensing characteristics of a self sensing motor, i.e. a self sensing supercapacitor device.

1.7. References

1. H. Shirakawa, A. McDiarmid, A. Heeger, Chemical Communications, 2003 (2003) 1-4.
2. A.G. MacDiarmid, Reviews of Modern Physics, 73 (2001) 701.
3. A. Bakhshi, G. Bhalla, (2004).

4. D. Ateh, H. Navsaria, P. Vadgama, Journal of the royal society interface, 3 (2006) 741-752.
5. T.A. Skotheim, Handbook of conducting polymers, CRC press, 1997.
6. J.H. Burroughes, D.D. Bradley, A. Brown, R. Marks, K. Mackay, R.H. Friend, P.L. Burns, A.B. Holmes, nature, 347 (1990) 539-541.
7. M. Belhadi, S. Kheffache, International Scholarly Research Notices, 2012 (2012).
8. T.F. Otero, J.G. Martinez, L. Valero, K. Asaka, Y.A. Ismail, Advances in Science and Technology, Trans Tech Publ, 2013, pp. 16-25.
9. F.G. Córdova, Y.A. Ismail, J.G. Martinez, A.S. Al Harrasi, T.F. Otero, Electroactive Polymer Actuators and Devices (EAPAD) 2013, SPIE, 2013, pp. 29-43.
10. Y.A. Ismail, J.G. Martínez, T.F. Otero, Electrochimica Acta, 123 (2014) 501-510.
11. Y.A. Ismail, J.G. Martinez, T.F. Otero, Journal of Electroanalytical Chemistry, 719 (2014) 47-53.
12. R. Prakash, K. Santhanam, Journal of Solid State Electrochemistry, 2 (1998) 123-125.
13. Y.A. Ismail, J. Chang, S.R. Shin, R.S. Mane, S.-H. Han, S.J. Kim, Journal of the Electrochemical Society, 156 (2009) A313.
14. P. Novák, K. Müller, K. Santhanam, O. Haas, Chemical Reviews, 97 (1997) 207-282.
15. J. Killian, B. Coffey, F. Gao, T. Poehler, P. Searson, Journal of the Electrochemical Society, 143 (1996) 936.
16. R. Gupta, R. Singh, Journal of Polymer Research, 11 (2005) 269-273.
17. J. Li, Y. Hu, X. Liang, J. Chen, L. Zhong, L. Liao, L. Jiang, H. Fuchs, W. Wang, Y. Wang, Advanced Optical Materials, 8 (2020) 1902105.
18. J. Gao, A. Heeger, J. Lee, C. Kim, Synthetic Metals, 82 (1996) 221-223.
19. Y.A. Ismail, Desalination, 250 (2010) 523-529.
20. A. Yahya, A. Ahmad, F. Mohammad, (2004).
21. A. Bhattacharya, B. Misra, Progress in polymer science, 29 (2004) 767-814.
22. S. Xing, G. Zhao, Journal of applied polymer science, 104 (2007) 1987-1996.
23. K. Maksymiuk, Electroanalysis: An International Journal Devoted to Fundamental and Practical Aspects of Electroanalysis, 18 (2006) 1537-1551.
24. A. Chithrambattu, Y.A. Ismail, Journal of Adhesion Science and Technology, 34 (2020) 2685-2702.
25. Y.A. Ismail, J.G. Martínez, A.S. Al Harrasi, S.J. Kim, T.F.F. Otero, Electroactive Polymer Actuators and Devices (EAPAD) 2011, SPIE, 2011, pp. 450-461.

26. L. Dai, Intelligent macromolecules for smart devices: from materials synthesis to device applications, Springer Science & Business Media, 2004.
27. C. Chiang, M. Druy, S. Gau, A. Heeger, E. Louis, A.G. MacDiarmid, Y. Park, H. Shirakawa, Journal of the American Chemical Society, 100 (1978) 1013-1015.
28. A.G. MacDiarmid, A.J. Epstein, Faraday Discussions of the Chemical Society, 88 (1989) 317-332.
29. O. Dimitriev, Macromolecules, 37 (2004) 3388-3395.
30. A. Nenashev, S. Baranovskii, M. Wiemer, F. Jansson, R. Österbacka, A. Dvurechenskii, F. Gebhard, Physical Review B, 84 (2011) 035210.
31. H. Chan, S. Ng, W. Sim, K. Tan, B. Tan, Macromolecules, 25 (1992) 6029-6034.
32. A.G.B. da Cruz, J.L. Wardell, A.M. Rocco, Journal of materials science, 43 (2008) 5823-5836.
33. T. Bashir, A. Shakoor, E. Ahmed, N. Niaz, S. Iqbal, M.S. Akhtar, M.A. Malik, Polymer Science, Series A, 59 (2017) 902-908.
34. J.F. Rubinson, Y.P. Kayinamura, Chemical Society Reviews, 38 (2009) 3339-3347.
35. S.D. Kang, G.J. Snyder, Nature materials, 16 (2017) 252-257.
36. S. Iqbal, S. Ahmad, Journal of industrial and engineering chemistry, 60 (2018) 53-84.
37. M. Kim, S. Park, J. Park, Polymers, 9 (2017) 452.
38. D.L. Gochnauer, T. Gilani, Am. J. Undergrad. Res, 14 (2018) 49-56.
39. R. Menon, current science, 79 (2000) 1632-1635.
40. A.K. Singh, R. Prakash, 2008 2nd National Workshop on Advanced Optoelectronic Materials and Devices, IEEE, 2008, pp. 65-74.
41. J.L. Bredas, G.B. Street, Accounts of chemical research, 18 (1985) 309-315.
42. T.H. Gilani, T. Masui, G.Y. Logvenov, T. Ishiguro, Synthetic metals, 78 (1996) 327-331.
43. G. Verbist, F. Peeters, J. Devreese, Physical Review B, 43 (1991) 2712.
44. G. Čík, F. Šeršeň, L. Dlháň, Synthetic metals, 151 (2005) 124-130.
45. T.S.K.M.T. FJ, Chem. Phys. Lett, 394 (2004) 339.
46. A.A. Syed, M.K. Dinesan, Talanta, 38 (1991) 815-837.
47. L. Bay, T. Jacobsen, S. Skaarup, K. West, The Journal of Physical Chemistry B, 105 (2001) 8492-8497.
48. W. Takashima, S.S. Pandey, M. Fuchiwaki, K. Kaneto, Japanese journal of applied physics, 41 (2002) 7532.
49. Y. Zhu, J. Li, M. Wan, L. Jiang, Macromolecular rapid communications, 29 (2008) 239-243.
50. S. Balasubramaniam, A. Mohanty, S.K. Balasingam, S.J. Kim, A. Ramadoss, Nano-Micro Letters, 12 (2020) 1-46.

51. R. Jain, N. Jadon, A. Pawaiya, TrAC Trends in Analytical Chemistry, 97 (2017) 363-373.
52. J. Bautista-Quijano, F. Avilés, J. Aguilar, A. Tapia, Sensors and Actuators A: Physical, 159 (2010) 135-140.
53. M.C. Lonergan, E.J. Severin, B.J. Doleman, S.A. Beaber, R.H. Grubbs, N.S. Lewis, Chemistry of Materials, 8 (1996) 2298-2312.
54. X. Chen, H. Liu, Y. Zheng, Y. Zhai, X. Liu, C. Liu, L. Mi, Z. Guo, C. Shen, ACS applied materials & interfaces, 11 (2019) 42594-42606.
55. V. Giurgiutiu, A. Zagrai, J. Jing Bao, Structural Health Monitoring, 1 (2002) 41-61.
56. G. Pioggia, F.D. Francesco, M. Ferro, F. Sorrentino, P. Salvo, A. Ahluwalia, Microchimica Acta, 163 (2008) 57-62.
57. F. Jasmi, N.H. Azeman, A.A.A. Bakar, M.S.D. Zan, K.H. Badri, M.S. Su'ait, Ieee Access, 6 (2018) 47355-47363.
58. B. Muthulakshmi, D. Kalpana, S. Pitchumani, N. Renganathan, Journal of Power Sources, 158 (2006) 1533-1537.
59. H. Ghenaatian, M. Mousavi, M. Rahmanifar, Electrochimica acta, 78 (2012) 212-222.
60. R. Gregory, W. Kimbrell, H. Kuhn, Synthetic Metals, 28 (1989) 823-835.
61. L. Olmedo, P. Hourquebie, F. Jousse, Advanced Materials, 5 (1993) 373-377.
62. M. Kim, H. Kim, S. Byun, S. Jeong, Y. Hong, J. Joo, K. Song, J. Kim, C. Lee, J. Lee, Synthetic metals, 126 (2002) 233-239.
63. T. Osaka, T. Momma, H. Ito, B. Scrosati, Journal of power sources, 68 (1997) 392-396.
64. X. Liu, Z. Zhong, Y. Tang, B. Liang, Journal of Nanomaterials, 2013 (2013).
65. W. Wang, L. Chi, Accounts of Chemical Research, 45 (2012) 1646-1656.
66. M. Josowicz, J. Janata, Analytical chemistry, 58 (1986) 514-517.
67. M. Maggini, G. Possamai, E. Menna, G. Scorrano, N. Camaioni, G. Ridolfi, G. Casalbore-Miceli, L. Franco, M. Ruzzi, C. Corvaja, Chemical communications, (2002) 2028-2029.
68. V. Nguyen, K. Potje-Kamloth, Thin Solid Films, 338 (1999) 142-148.
69. Z.-B. Huang, G.-F. Yin, X.-M. Liao, J.-W. Gu, Frontiers of Materials Science, 8 (2014) 39-45.
70. C.R. Broda, J.Y. Lee, S. Sirivisoot, C.E. Schmidt, B.S. Harrison, Journal of biomedical materials research Part A, 98 (2011) 509-516.
71. G. Kang, R.B. Borgens, Y. Cho, Langmuir, 27 (2011) 6179-6184.
72. R.D. Rauh, Electrochimica Acta, 44 (1999) 3165-3176.
73. B.P. Jelle, G. Hagen, Solar Energy Materials and Solar Cells, 58 (1999) 277-286.
74. A. Olad, A. Rashidzadeh, Iran J Chem Eng, 5 (2008) 45-54.

75. J. Alam, U. Riaz, S. Ashraf, S. Ahmad, Journal of Coatings Technology and Research, 5 (2008) 123-128.
76. X. Liu, L. Cai, Applied Surface Science, 445 (2018) 242-254.
77. M. Dennstedt, J. Zimmermann, Berichte der deutschen chemischen Gesellschaft, 21 (1888) 1478-1481.
78. A. Angeli, L. Alessandri, Gazzetta Chimica Italiana, 46 (1916) 283-300.
79. J.M. Fonner, L. Forciniti, H. Nguyen, J.D. Byrne, Y.-F. Kou, J. Syeda-Nawaz, C.E. Schmidt, Biomedical materials, 3 (2008) 034124.
80. A. Dallolio, G. Dascola, V. Varacca, V. Bocchi, Comptes Rendus Hebdomadaires Des Seances De L Academie Des Sciences Serie C, 267 (1968) 433-&.
81. C. He, C. Yang, Y. Li, Synthetic metals, 139 (2003) 539-545.
82. A. Mahun, S. Abbrent, P. Bober, J. Brus, L. Kobera, Synthetic Metals, 259 (2020) 116250.
83. A.L. Pang, A. Arsad, M. Ahmadipour, Polymers for Advanced Technologies, 32 (2021) 1428-1454.
84. S. Roth, Physica B+ C, 127 (1984) 151-157.
85. J. Kaufman, N. Colaneri, J. Scott, G. Street, Physical review letters, 53 (1984) 1005.
86. F.-W. Zeng, X.-X. Liu, D. Diamond, K.T. Lau, Sensors and Actuators B: Chemical, 143 (2010) 530-534.
87. S.P. Armes, Synthetic Metals, 20 (1987) 365-371.
88. P. Calvo, J. Rodrıguez, H. Grande, D. Mecerreyes, J. Pomposo, Synthetic Metals, 126 (2002) 111-116.
89. N. Guimard, N. Gomez, C. Schmidt, Prog Polym Sci, 32 (2007) 876-892.
90. S. Machida, S. Miyata, A. Techagumpuch, Synthetic metals, 31 (1989) 311-318.
91. C. Bora, S. Dolui, Polymer, 53 (2012) 923-932.
92. G. Qi, Z. Wu, H. Wang, Journal of Materials Chemistry C, 1 (2013) 7102-7110.
93. L. Mao, H.S.O. Chan, J. Wu, RSC advances, 2 (2012) 10610-10617.
94. S. De Vito, C.R. Martin, Chemistry of materials, 10 (1998) 1738-1741.
95. K. Jackowska, A.T. Bieguński, M. Tagowska, Journal of Solid State Electrochemistry, 12 (2008) 437-443.
96. D. Zhang, L. Luo, Q. Liao, H. Wang, H. Fu, J. Yao, The Journal of Physical Chemistry C, 115 (2011) 2360-2365.
97. N.K. Guimard, N. Gomez, C.E. Schmidt, Progress in polymer science, 32 (2007) 876-921.
98. P. Herrasti, L. Dıaz, P. Ocón, A. Ibáñez, E. Fatas, Electrochimica acta, 49 (2004) 3693-3699.

99. A. Ramanavicius, K. Habermüller, J. Razumiene, R. Meškys, L. Marcinkeviciene, I. Bachmatova, E. Csöregi, V. Laurinavicius, W. Schuhmann, Surface and Colloid Science, Springer, 2001, pp. 143-148
100. D.-H. Han, H.J. Lee, S.-M. Park, Electrochimica acta, 50 (2005) 3085-3092.
101. K.J. Gilmore, M. Kita, Y. Han, A. Gelmi, M.J. Higgins, S.E. Moulton, G.M. Clark, R. Kapsa, G.G. Wallace, Biomaterials, 30 (2009) 5292-5304.
102. S. Meng, M. Rouabhia, G. Shi, Z. Zhang, Journal of Biomedical Materials Research Part A: An Official Journal of The Society for Biomaterials, The Japanese Society for Biomaterials, and The Australian Society for Biomaterials and the Korean Society for Biomaterials, 87 (2008) 332-344.
103. D.A. Kaplin, S. Qutubuddin, Polymer, 36 (1995) 1275-1286.
104. A. Kaynak, Materials Research Bulletin, 32 (1997) 271-285.
105. S. Asavapiriyanont, G. Chandler, G. Gunawardena, D. Pletcher, Journal of electroanalytical chemistry and interfacial electrochemistry, 177 (1984) 229-244.
106. B. Scharifker, E. Garcia-Pastoriza, W. Marino, Journal of electroanalytical chemistry and interfacial electrochemistry, 300 (1991) 85-98.
107. A. Diaz, J.C. Lacroix, New journal of chemistry (1987), 12 (1988) 171-180.
108. D.H. Kim, S.M. Richardson-Burns, J.L. Hendricks, C. Sequera, D.C. Martin, Advanced Functional Materials, 17 (2007) 79-86.
109. G. Wallace, M. Smyth, H. Zhao, TrAC Trends in Analytical Chemistry, 18 (1999) 245-251.
110. D.D. Zhou, X.T. Cui, A. Hines, R.J. Greenberg, Implantable Neural Prostheses 2: Techniques and Engineering Approaches, (2010) 217-252.
111. S.K. Mondal, K.R. Prasad, N. Munichandraiah, Synthetic metals, 148 (2005) 275-286.
112. T. Girija, M. Sangaranarayanan, Synthetic Metals, 156 (2006) 244-250.
113. F. Arefi, V. Andre, P. Montazer-Rahmati, J. Amouroux, Pure and applied chemistry, 64 (1992) 715-723.
114. R.K. John, D.S. Kumar, Journal of applied polymer science, 83 (2002) 1856-1859.
115. A. Deronzier, J.-C. Moutet, Coordination Chemistry Reviews, 147 (1996) 339-371.
116. M. Karim, C. Lee, M. Lee, Polymers for Advanced Technologies, 18 (2007) 916-920.
117. A.T. Lawal, G.G. Wallace, Talanta, 119 (2014) 133-143.
118. Z. Gu, C. Li, G. Wang, L. Zhang, X. Li, W. Wang, S. Jin, Journal of Polymer Science Part B: Polymer Physics, 48 (2010) 1329-1335.

119. F. Khadem, M. Pishvaei, M. Salami-Kalajahi, F. Najafi, Journal of Applied Polymer Science, 134 (2017).
120. A.D. Arulraj, M. Vijayan, V.S. Vasantha, Analytica chimica acta, 899 (2015) 66-74.
121. A. Nezhadali, L. Mehri, R. Shadmehri, Sensors and Actuators B: Chemical, 171 (2012) 1125-1131.
122. D. Ye, L. Luo, Y. Ding, Q. Chen, X. Liu, Analyst, 136 (2011) 4563-4569.
123. J. Li, H. Xie, Y. Li, Journal of Solid State Electrochemistry, 16 (2012) 795-802.
124. R. Devi, M. Thakur, C. Pundir, Biosensors and Bioelectronics, 26 (2011) 3420-3426.
125. K. Singh, P.R. Solanki, T. Basu, B. Malhotra, Polymers for Advanced Technologies, 23 (2012) 1084-1091.
126. H. Lê, S. Chebil, B. Makrouf, H. Sauriat-Dorizon, B. Mandrand, H. Korri-Youssoufi, Talanta, 81 (2010) 1250-1257.
127. T. Qian, C. Yu, X. Zhou, P. Ma, S. Wu, L. Xu, J. Shen, Biosensors and Bioelectronics, 58 (2014) 237-241.
128. D. Tonelli, B. Ballarin, L. Guadagnini, A. Mignani, E. Scavetta, Electrochimica Acta, 56 (2011) 7149-7154.
129. [M. Singh, P.K. Kathuroju, N. Jampana, Sensors and Actuators B: Chemical, 143 (2009) 430-443.
130. Y. Tao, E. Ju, J. Ren, X. Qu, Chemical Communications, 50 (2014) 3030-3032.
131. S. Zang, Y. Liu, M. Lin, J. Kang, Y. Sun, H. Lei, Electrochimica Acta, 90 (2013) 246-253.
132. F. Selampinar, L. Toppare, U. Akbulut, T. Yalçin, Ş. Süzer, Synthetic metals, 68 (1995) 109-116.
133. K. Suri, S. Annapoorni, A. Sarkar, R. Tandon, Sensors and Actuators B: Chemical, 81 (2002) 277-282.
134. J.D. Madden, P.G. Madden, I.W. Hunter, Smart Structures and Materials 2001: Electroactive Polymer Actuators and Devices, SPIE, 2001, pp. 72-83.
135. H. Okuzaki, T. Kunugi, Journal of Polymer Science Part B: Polymer Physics, 34 (1996) 1747-1749.
136. A.-P. Joaquín, F.O. Toribio, G.M. José, A.I. Yahya, (2012).
137. T. Otero, M. Cortes, Electrochemical characterization and control of triple-layer muscles, SPIE, 2000.
138. C. Plesse, F. Vidal, D. Teyssié, C. Chevrot, Chem. Commun., 46 (2010) 2910-2912.
139. Y. Huang, H. Li, Z. Wang, M. Zhu, Z. Pei, Q. Xue, Y. Huang, C. Zhi, Nano Energy, 22 (2016) 422-438.
140. D. Zhang, X. Zhang, Y. Chen, P. Yu, C. Wang, Y. Ma, Journal of Power Sources, 196 (2011) 5990-5996.

141. S. Kuwabata, S. Masui, H. Tomiyori, H. Yoneyama, Electrochimica acta, 46 (2000) 91-97.
142. C. Dulgerbaki, A.U. Oksuz, Polymers for Advanced Technologies, 27 (2016) 73-81.
143. E. Smela, Advanced Materials, 11 (1999) 1343-1345.
144. A.J. Frank, K. Honda, Journal of Photochemistry, 29 (1985) 195-204.
145. S. Meng, Z. Zhang, M. Rouabhia, Journal of bone and mineral metabolism, 29 (2011) 535-544.
146. G. Tai, M. Tai, M. Zhao, Burns & trauma, 6 (2018).
147. E. Stewart, X. Liu, G. Clark, R. Kapsa, G.G. Wallace, Acta biomaterialia, 8 (2012) 194-200.
148. K. Wang, H. Wu, Y. Meng, Z. Wei, Small, 10 (2014) 14-31.
149. H. Park, K. Park, Hydrogels in bioapplications, ACS Publications, 1996.
150. M. Bahram, N. Mohseni, M. Moghtader, An introduction to hydrogels and some recent applications, Emerging concepts in analysis and applications of hydrogels, IntechOpen, 2016.
151. A. Guiseppi-Elie, Biomaterials, 31 (2010) 2701-2716.
152. W. Otto, L. Drahoslav, Nature, 185 (1960) 117-118.
153. S. Ma, B. Yu, X. Pei, F. Zhou, Polymer, 98 (2016) 516-535.
154. D. Buenger, F. Topuz, J. Groll, Progress in Polymer Science, 37 (2012) 1678-1719.
155. A. Herrmann, R. Haag, U. Schedler, Advanced Healthcare Materials, 10 (2021) 2100062.
156. B. Xu, H. Jiang, H. Li, G. Zhang, Q. Zhang, RSC Advances, 5 (2015) 13167-13170.
157. I. Frisman, Y. Shachaf, D. Seliktar, H. Bianco-Peled, Langmuir, 27 (2011) 6977-6986.
158. W. Xu, Q. Song, J.-F. Xu, M.J. Serpe, X. Zhang, ACS applied materials & interfaces, 9 (2017) 11368-11372.
159. X. Fu, L. Hosta-Rigau, R. Chandrawati, J. Cui, Chem, 4 (2018) 2084-2107.
160. M. Parente, A. Ochoa Andrade, G. Ares, F. Russo, Á. Jiménez-Kairuz, International journal of cosmetic science, 37 (2015) 511-518.
161. M. Zohuriaan-Mehr, H. Omidian, S. Doroudiani, K. Kabiri, Journal of materials science, 45 (2010) 5711-5735.
162. A.H. Basta, V.F. Lotfy, C. Eldewany, Polymer-Plastics Technology and Materials, 60 (2021) 1884-1897.
163. S. Aswathy, U. Narendrakumar, I. Manjubala, Heliyon, 6 (2020) e03719.
164. F. Ali, I. Khan, J. Chen, K. Akhtar, E.M. Bakhsh, S.B. Khan, Gels, 8 (2022) 205.
165. K. Gilmore, A. Hodgson, B. Luan, C. Small, G. Wallace, Polymer Gels and Networks, 2 (1994) 135-143.

166. D. Mawad, A. Lauto, G.G. Wallace, Polymeric hydrogels as smart biomaterials, (2016) 19-44.
167. D. Wei, X. Lin, L. Li, S. Shang, M.C.-w. Yuen, G. Yan, X. Yu, Soft Matter, 9 (2013) 2832-2836.
168. T.Y. Dai, X.T. Qing, C. Shen, J. Wang, Y. Lu, Advanced Materials Research, Trans Tech Publ, 2010, pp. 117-120.
169. Y. Zhao, B. Liu, L. Pan, G. Yu, Energy & Environmental Science, 6 (2013) 2856-2870.
170. Y. Shi, L. Peng, G. Yu, Nanoscale, 7 (2015) 12796-12806.
171. A. Shabeeba, L. Rajan, M.P. Sidheekha, M.S. Thayyil, Y.A. Ismail, Journal of Energy Storage, 55 (2022) 105724.
172. X. Zhang, J. Zhao, T. Xia, Q. Li, C. Ao, Q. Wang, W. Zhang, C. Lu, Y. Deng, Energy Storage Materials, 31 (2020) 135-145.
173. Y. Shi, L. Pan, B. Liu, Y. Wang, Y. Cui, Z. Bao, G. Yu, Journal of Materials Chemistry A, 2 (2014) 6086-6091.
174. T. Tungkavet, N. Seetapan, D. Pattavarakorn, A. Sirivat, Polymer international, 61 (2012) 825-833.
175. I.Y. Dmitriev, P.V. Vlasov, M.F. Lebedeva, I.V. Gofman, V.Y. Elokhovsky, E.N. Popova, M.S. Lozhkin, E.N. Vlasova, I.S. Kuryndin, M.A. Smirnov, G.K. Elyashevich, Materials Chemistry and Physics, 187 (2017) 88-95.
176. L. Li, J. Ge, B. Guo, P.X. Ma, Polymer Chemistry, 5 (2014) 2880-2890.
177. Q. Tang, J. Wu, H. Sun, J. Lin, S. Fan, D. Hu, Carbohydrate Polymers, 74 (2008) 215-219.
178. L.-H. Xu, J.-j. Li, H.-B. Zeng, X.-J. Zhang, S. Cosnier, R.S. Marks, D. Shan, Biosensors and Bioelectronics, 143 (2019) 111601.
179. W. Jiang, Y. Liu, J. Wang, M. Zhang, W. Luo, Y. Zhu, Advanced Materials Interfaces, 3 (2016) 1500502.
180. L. Pan, G. Yu, D. Zhai, H.R. Lee, W. Zhao, N. Liu, H. Wang, B.C.-K. Tee, Y. Shi, Y. Cui, Proceedings of the National Academy of Sciences, 109 (2012) 9287-9292.
181. D.-H. Kim, J.A. Wiler, D.J. Anderson, D.R. Kipke, D.C. Martin, Acta biomaterialia, 6 (2010) 57-62.
182. S.I. Brahim, D. Maharajh, D. Narinesingh, A. Guiseppi-Elie, Analytical letters, 35 (2002) 797-812.
183. R.E. Rivero, M.A. Molina, C.R. Rivarola, C.A. Barbero, Sensors and Actuators B: Chemical, 190 (2014) 270-278.
184. X. Han, G. Xiao, Y. Wang, X. Chen, G. Duan, Y. Wu, X. Gong, H. Wang, Journal of Materials Chemistry A, 8 (2020) 23059-23095.
185. Z. Tang, J. Wu, Q. Li, Z. Lan, L. Fan, J. Lin, M. Huang, Electrochimica acta, 55 (2010) 4883-4888.
186. Z. Chen, J.W. To, C. Wang, Z. Lu, N. Liu, A. Chortos, L. Pan, F. Wei, Y. Cui, Z. Bao, Advanced energy materials, 4 (2014) 1400207.

187. Y.A. Ismail, A. Shabeeba, M.P. Sidheekha, L. Rajan, Actuators: Fundamentals, Principles, Materials and Applications, (2020) 211-252.
188. P. Marcasuzaa, S. Reynaud, F. Ehrenfeld, A. Khoukh, J. Desbrieres, Biomacromolecules, 11 (2010) 1684-1691.
189. Y. Bashtyk, A. Fechan, O. Grytsenko, Z. Hotra, I. Kremer, O. Suberlyak, O. Aksimentyeva, Y. Horbenko, M. Kotsarenko, Molecular crystals and liquid crystals, 672 (2018) 150-158.
190. S. Park, S.-W. Chung, C.A. Mirkin, Journal of the American Chemical Society, 126 (2004) 11772-11773.
191. D. Yu, Y. Yang, M. Durstock, J.-B. Baek, L. Dai, ACS nano, 4 (2010) 5633-5640.
192. Y. Kim, J. Baek, M.-H. Kim, H.-J. Choi, E. Kim, Ultramicroscopy, 108 (2008) 1224-1227.
193. A. Phadke, C. Zhang, B. Arman, C.-C. Hsu, R.A. Mashelkar, A.K. Lele, M.J. Tauber, G. Arya, S. Varghese, Proceedings of the National Academy of Sciences, 109 (2012) 4383-4388.
194. V. Guarino, M.A. Alvarez-Perez, A. Borriello, T. Napolitano, L. Ambrosio, Advanced healthcare materials, 2 (2013) 218-227.

Chapter 2

MATERIALS AND METHODS

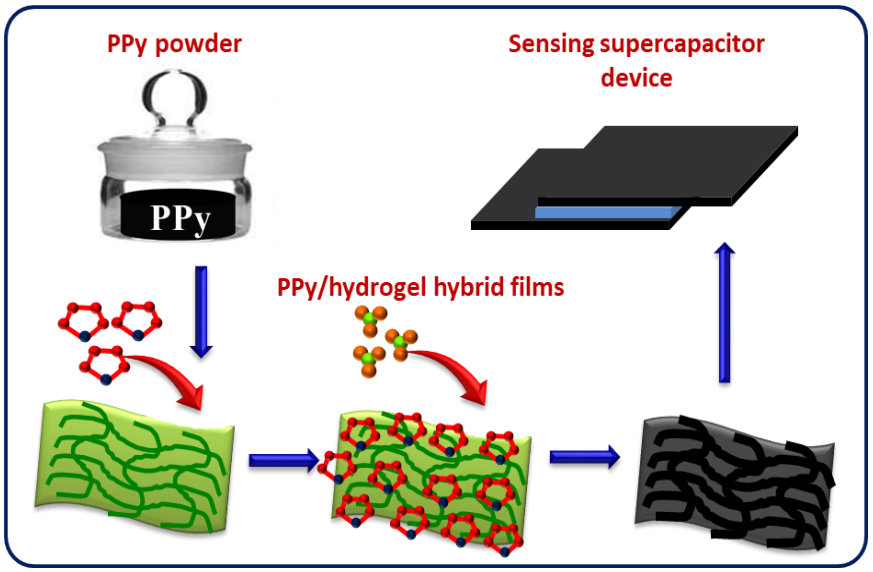

The studies described in the thesis involve chemical synthesis of PPy and fabrication of PPy/hydrogel hybrid films for electrochemical sensing and supercapacitor applications. This chapter encompasses the various materials and methods used for the synthesis and fabrication of the polymers and hybrid films. The various analytical techniques adopted to characterize the materials generated and electrochemical methods employed to explore their potential applications are also outlined.

2.1. Materials

All the chemicals and reagents used for the investigation were of A.R. grade unless specified otherwise. Pyrrole monomer was purified by double distillation under vacuum prior to use. Chitosan with an average molecular weight of 190,000–310,000 was used as received. Double distilled water was employed throughout the experiments. Lists of chemicals used are displayed in Table 2.1.

Table 2.1 *List of chemicals used for the present study and their make*

Sl. No.	Chemicals	Manufacturer/Supplier
1	Pyrrole (C_4H_5N)	Spectrochem, India
2	Chitosan	Sigma Aldrich, USA
3	Polyvinyl alcohol	Himedia, India
4	Ferric chloride ($FeCl_3$)	Merck, India
5	Sodium chloride (NaCl)	Merck, India
6	Sodium hydroxide (NaOH)	Merck, India
7	Glacial acetic acid (CH_3COOH)	Spectrochem
8	Ethanol (C_2H_5OH)	Merck, India
9	Methanol (CH_3OH)	Merck, India
10	Conductive carbon paste	MG chemicals, USA
11	Isopropanol (C_3H_8O)	Merck, India
12	Acetonitrile (CH_3CN)	Spectrochem, India
13	Lithium bis(triflouromethane sulfonyl) imide	TCI, India
14	Lithium perchlorate ($LiClO_4$)	Himedia, India
15	Lithium chloride (LiCl)	Himedia, India

2.2. Experimental procedures

2.2.1. Chemical synthesis of Polypyrrole

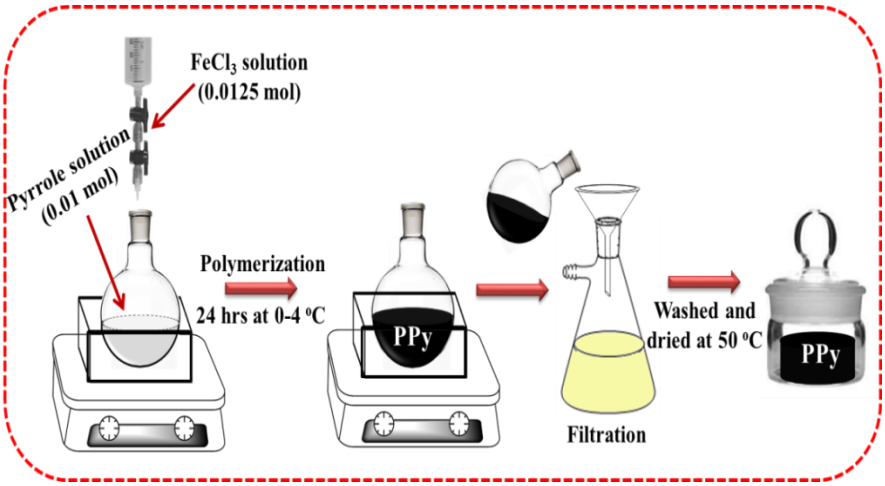

Figure 2.1 *Schematic representation of the synthesis of PPy through in situ chemical polymerization*

PPy powder was synthesized through in situ chemical oxidative polymerization of pyrrole using anhydrous $FeCl_3$ as an oxidizing agent. For the chemical polymerization, 0.01 mol of pyrrole was added to 100mL of water and kept at a temperature range of 0 ˚C – 4 ˚C in an ice bath. Then 0.0125 mol of $FeCl_3$ solution in 100 mL of water was added into the above solution at a rate of 1 mL/minute with constant stirring. Here the ratio of monomer to oxidant was fixed at 1:1.25. The reaction was carried out at low temperature for 24 hours with constant stirring. The fine black precipitate of PPy was immediately filtered through a Whatman no.1 filter paper and repeatedly washed with double distilled water to remove excess oxidants followed by acetone to remove low molecular weight oligomers. Then the product was dried

in hot air oven at 55 ˚C for about 24 hours to remove the moisture, ground and stored in a desiccator for further use. A schematic representation of the synthesis of PPy is displayed in Figure 2.1.

2.2.2. Fabrication of Chitosan films

A homogenous, bubble-free 1 wt% solution of Cs in 2 % acetic acid was prepared. It was filtered, poured into a glass plate and placed in a hot air oven for 2 to 3 days and allowed the solvent to evaporate without any disturbance. The film was then peeled off and suspended in NaOH (1 M) solution for another 24 hours. It was further washed with distilled water and allowed to dry at ambient conditions in a vertical position until a constant weight was attained.

2.2.3. Fabrication of Polypyrrole/Chitosan hybrid films

Polypyrrole/chitosan (PPy/Cs) hybrid films were fabricated through an in situ chemical polymerization of pyrrole using $FeCl_3$ as a catalyst. Cs films were soaked in a monomer solution containing 0.01 mol of pyrrole in 100 mL of 1:1 mixture of water and ethanol for 2 hours. A solution of 0.0125 moles of $FeCl_3$ in 100mL of 1:1 mixture of ethanol and water was slowly added to the solution containing the film at a rate of 1 mL/minute with gentle stirring for 24 hours. The polymerization reaction was carried out at a temperature of 5±1 ˚C. The single coated hybrid films (PCF1) were removed from the solution, washed with methanol several times for removing the oligomers, oxidant and the unreacted monomer, and dried at room temperature. The schematic illustration of the fabrication of PPy/Cs hybrid film is

shown in Figure 2.2. The same experimental procedure was repeated by using the single coated hybrid film PCF1 under the same experimental conditions to obtain a second coated hybrid film PCF2. The coating procedure was repeated on PCF2 to get a third coated hybrid film PCF3. Fourth coated hybrid film PCF4 was fabricated using PCF3 through repeating the same experimental procedures.

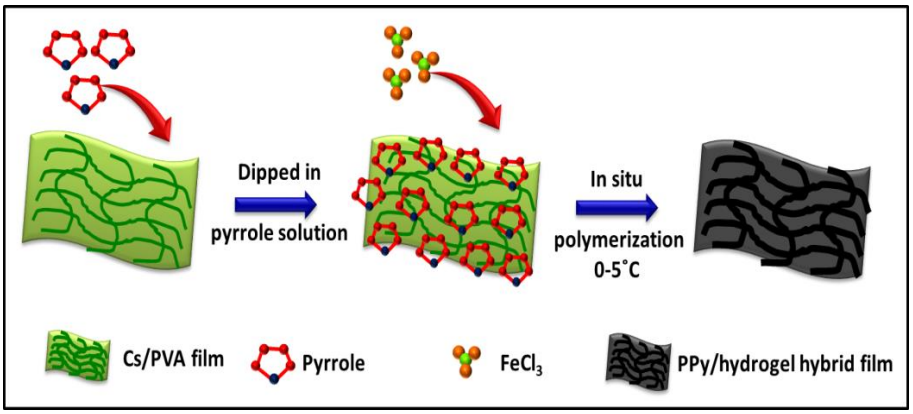

Figure 2.2 *Schematic diagram of the fabrication of the PPy/hydrogel hybrid films through in situ chemical polymerization*

2.2.4. Fabrication of Polyvinyl alcohol films

PVA films were prepared by solution casting technique. A 2 wt% homogenous solution of PVA was prepared by dissolving 5 g in 250 mL of distilled water at 80 ˚C by continuous stirring for 30 min. The solution was filtered, poured into a glass plate by taking care to avoid bubbles and allowed to evaporate in a hot air oven at 50 ˚C for 2 or 3 days. The film was then peeled off carefully, washed with distilled water and allowed to dry at ambient condition until a constant weight was achieved.

2.2.5. Fabrication of Polypyrrole/PVA hybrid films

Electroactive PPy/PVA hybrid films were fabricated through the chemical coating of PPy using PVA films as template and employing an in situ chemical polymerization of pyrrole in an aqueous medium using ferric chloride as a catalyst. The fabrication procedure was similar to that employed for the fabrication of PPy/Cs hybrid films. After the polymerization, the single coated hybrid films (PPF1) were taken out, washed thoroughly with water and methanol and dried in air at room temperature. The schematic representation of the fabrication of PPy/PVA hybrid film is shown in Figure 2.2. The same experimental procedure was repeated by using PPF1 under the same experimental conditions to obtain a second coated hybrid film PPF2. The coating procedure was repeated on PPF2 to get a third coated hybrid film PPF3. Fourth coated hybrid film PPF4 was fabricated using PPF3 through repeating the same experimental procedures.

2.2.6. Fabrication of working electrode for sensing and three electrode supercapacitor studies

(a) PPy powder: 0.2 mg of the synthesized PPy powder and 0.2 mg of conductive carbon paste binder was dispersed in 20 µL of isopropanol. The dispersion was ultrasonicated for 1 hour to make it homogeneous. Then 5 µL of this homogeneous slurry was pipetted out and coated on the tip of the glassy carbon electrode (GCE) having 3 mm diameter. It was then dried in hot air oven at 55 ˚C. The total weight of active material on the electrode was maintained as 0.05 mg. Prior to the coating of active material, the tip of the GCE is sequentially polished

with a wetted micro cloth containing alumina powder and cleaned in double distilled water and by ultrasonication.

***(b) PPy/hydrogel hybrid films*:** The hybrid film was cut into a rectangular piece of 1 cm length and 0.2 cm breadth and fixed on a clean Pt wire using conductive carbon paste.

2.2.7. Fabrication of symmetric supercapacitor device

To fabricate an all-solid-state symmetric supercapacitor, PVA/NaCl gel electrolyte was sandwiched between two identical pieces of the PPy/PVA hybrid film electrodes (PPF4). Here, the PVA/NaCl gel electrolyte was prepared by mixing 1 g of NaCl, 1 g of PVA and 10 mL of deionized water through vigorous stirring at 85 ˚C until it became transparent. The PPy/PVA hybrid film was cut into rectangular pieces having a dimension of 1×2 cm^2 and were stacked and pressed together with PVA/NaCl gel electrolyte as the middle layer in such a way that it leaves 1×1.5 cm^2 film dimension for contacting each other. We have employed a simple method for the fabrication of a supercapacitor electrode which avoids the use of auxiliary materials. The schematic representation of the fabrication of the device is shown in Figure 2.3.

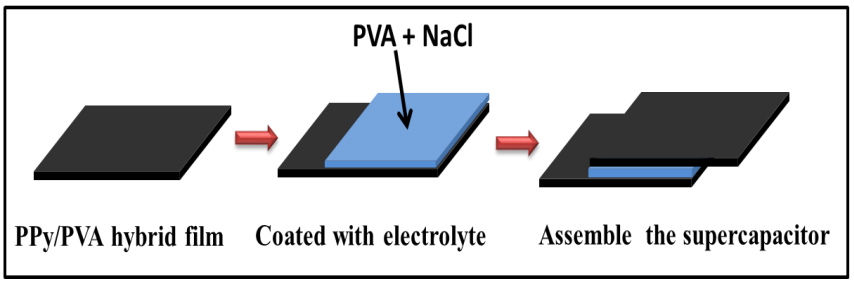

Figure 2.3 *Schematic representation of the fabrication of all-solid-state symmetric supercapacitor*

2.3. Characterization techniques

The synthesized PPy powder, PPy/Cs hybrid films and PPy/PVA hybrid films were well characterized using different analytical methods. The characterization tools such as Fourier transform infrared (FTIR), Field emission scanning electron microscope (FESEM), Energy dispersive X-ray spectroscopy (EDX) and Thermogravimetric analysis (TGA) were used to study the spectral characteristics, morphology, elemental composition and thermal behaviour of the synthesized materials. The electrical conductivity studies were performed using Broadband dielectric spectrometer (BDS). A Universal test frame machine (UTM) was employed to study the mechanical characteristics of the hybrid films. To evaluate the electrochemical characteristics of the synthesized materials cyclic voltammetry (CV), chronopotentiometry, galvanostatic charge discharge (GCD) and electrochemical impedance spectroscopy (EIS) were employed. For studying the supercapacitor behaviour, we have employed both three electrode and two electrode configurations and studied using GCD and CV.

The fundamental principles of the aforementioned techniques are briefly outlined below.

2.3.1. Fourier transform infrared spectroscopy (FTIR)

FTIR spectroscopy is one of the comprehensive analytical tools that provides information about the chemical structure and composition of the molecule [1, 2]. For the powder sample, the JASCO FTIR 4100 instrument in the absorption range of 600 cm^{-1} to 3600 cm^{-1} was

employed using the KBr pellets. FTIR spectral measurements of the film samples were carried out using JASCO FTIR 4700 spectrometer (using attenuated total reflectance - ATR technology) in the same wavelength range. Infrared spectroscopy is based on the interaction of the vibrating dipole moments of molecules with IR radiation. When exposed to IR radiation, the sample selectively absorb a particular wavelength, experience a change in dipole moment and consequently excitations occurs between the ground and excited vibrational states. In a typical IR spectra, each absorption peaks are ascribed to different vibrational modes of a particular molecule. An IR spectrum is generally used to find the functional groups present in a molecule. Every sample has a unique combination of atoms, gives unique infrared spectrum and is considered as a fingerprint of a molecule for its structural elucidation. The quantity of a specific moiety exist in a sample can be determined from the intensity of the corresponding peaks. The experimental set up of a FTIR instrument consists of a light source, sample holder, interferometer, a detector and a computer. It can also functioned in ATR mode which requires minimum sample preparation procedure compared to KBr disc method.

2.3.2. Field emission scanning electron microscope (FESEM)

FESEM is a widely used microscopic technique that analyses the surface morphology of a material by scanning with a focused beam of high energy electrons to generate a variety of signals and converted it into a high-resolution image [3, 4]. In the present study, the CARL ZEISS GeminiSEM-300 (Germany) instrument operated at an accelerating voltage of 5 kV was used to study the surface morphology

of the samples. The basic components of the instrument are electron gun, sample stage, electron lenses, scanning coils, detector, and output display units. When an electron beam is irradiated on the surface, it interacts with the atoms of the sample, resulting in the ejection of secondary electrons, backscattered electrons, and auger electrons. The secondary electrons generated by the inelastic interactions between the surface and high energy electrons are most preferably collected by the detector and produce various signals giving information about the morphology and compositions of the surface as images with higher magnification and resolution. The intensity of the signal produced is directly proportional to the number of secondary electrons generated. The materials to be examined should be electrically conducting, and otherwise they are coated with thin layer of a conducting material like gold or silver via sputtering method.

2.3.3. Energy dispersive X-ray spectroscopy (EDX)

Energy dispersive X-ray spectroscopy is a versatile tool employed to determine the elemental composition of materials [5]. EDX is usually combined with electron microscopes SEM or TEM. In the present study, elemental analysis of the films was carried out by employing Energy Dispersive X-ray spectral attachment with the SEM using Gemini 300/EDS. When a sample is bombarded with the electron beam, the inner electrons get excited as a result of inelastic collision between the incident beam and the inner shell electrons of an atom [6]. Then they return to a lower energy state by emitting X-rays of fixed wavelength. The energy and intensity of these X-rays is a characteristic of the element from which it was emitted and compared

to get the elemental composition of the sample. The EDX spectrum contains peaks corresponding to the elements present in the material.

2.3.4. Electrical conductivity studies

Electrical conductivity is the intrinsic ability of a material to transport an electric charge [7, 8]. The electrical conductivity measurements of the samples were performed using two point probe method at room temperature and ambient pressure within the frequency range of 10^{-2} Hz to 10^{7} Hz employing Broadband dielectric spectrometer (Novocontrol technologies, Germany). The samples (vacuum dried pellets and films) were sandwiched between a couple of gold-plated parallel copper electrodes. The film samples were cut into round pieces of 2 cm diameter. The PPy powder sample was pressed into a pellet using a stainless steel dye of 1.3 cm diameter and by employing hydraulic press. The thicknesses of the samples were measured using an electronic screw gauge. All the measurements were carried out in triplicate and the mean values are reported. The DC electrical conductivity can be derived by fitting the frequency-dependent conductivity data to the universal power law known as Jonscher's power law. This law is expressed as:

$$\sigma\,(\omega) = \sigma_0 + A\omega^n \qquad (2.1)$$

where, $\sigma(\omega)$ represents the AC conductivity at frequency ω, σ_0 is the DC conductivity, A is a constant related to the strength of the AC conductivity, ω is the angular frequency ($\omega=2\pi f$) and n is the frequency exponent, usually lies between 0 and 1, and gives information about the distribution of relaxation times in the material.

2.3.5. Mechanical studies

A Universal testing machine (UTM), is employed to examine the mechanical characteristics of the films [9]. In the present investigation, A UTM, Shimadzu AGX-PLUS-10 kN with a crosshead speed of 5 mm/min was used. All the film samples having a dimension of 6 cm × 2 cm were taken and clamped between two mechanical gripping units of the machine, which leaves 3 cm gauge length for mechanical loading and is stretched apart until it breaks. It provides information about Young's modulus, tensile strength and percentage elongation of the hybrid films. The Young's modulus was obtained by submitting the samples to a steady stretching force (F). Young's modulus is calculated using the equation 2.2.

$$\text{Young's modulus} = {}^{\text{stress}}/_{\text{strain}} \qquad (2.2)$$

where stress is the force (F) in newton (N) per unit area (A) in mm^2 and strain is the length variation (ΔL) per initial length (L_0). After the testing, the results were reported as stress-strain curves. All the tests were performed in triplicate and the mean values were taken for comparison.

2.3.6. Thermo gravimetric analysis (TGA)

TGA is a tool which measures the rate of change in weight of a substance as a function of temperature in a controlled atmosphere [10]. The thermal behaviors of the vacuum dried samples (PPy powder, bare hydrogel film and PPy/Hydrogel hybrid films) were investigated using a TG analyzer (TA Q50) instrument under nitrogen atmosphere from

30 ˚C to 650 ˚C with a heating rate of 10 ˚C per minute. TGA determines the thermal stability of a sample and gives information about various steps involved in the thermal decomposition of the materials [11]. The temperature range, the rate of decomposition and the extent of decomposition helps us to distinguish one substance from other. TGA provides information about thermal stability, composition of a mixture, oxidative stability, product lifetime, moisture, volatiles and filler content of materials and their decomposition kinetics. A thermogram is a plot of weight change with respect to the temperature and its first derivative curve gives the point at which weight loss is more apparent. The weight loss of the sample is recorded either isothermally at a temperature of interest or subjected to a programmed heating rate in a dynamic mode of operation.

2.3.7. Electrochemical characterizations

The instrument used for electrochemical studies execute a number of techniques like CV, GCD, Chronopotentiometry and EIS that can be applied to study electrochemical sensing, supercapacitors, batteries, electropolymerization, solar cells etc. In the present research work, all electrochemical studies were performed using a single compartment cell, together with a galvanostat-potentiostat electrochemical workstation (Zahner Zennium Pro, Canada) operating with computer-controlled Thales XT analysis software. It was carried out in a conventional three-electrode electrochemical cell with the hybrid film or modified GCE as the WE, Ag/AgCl (3 M KCl) as the RE and Pt mesh as the CE or auxiliary electrode using aqueous NaCl

solution as electrolyte at ambient conditions. For film samples, a film of length 1 cm and breadth 0.2 cm fixed on a Pt wire using conductive carbon paste was taken as the WE and for PPy powder sample, the WE was fabricated by mixing the PPy powder with conducting carbon paste and then coated on GCE. The samples were allowed to equilibrate in the electrolyte before the application of electrical signals. In voltammetric studies, the current flow between WE and CE and the potential is measured between WE and RE. The RE should have a well-defined and stable electrode potential and it should be non-polarizable. The potential of the WE is controlled with respect to RE by the potentiostat.

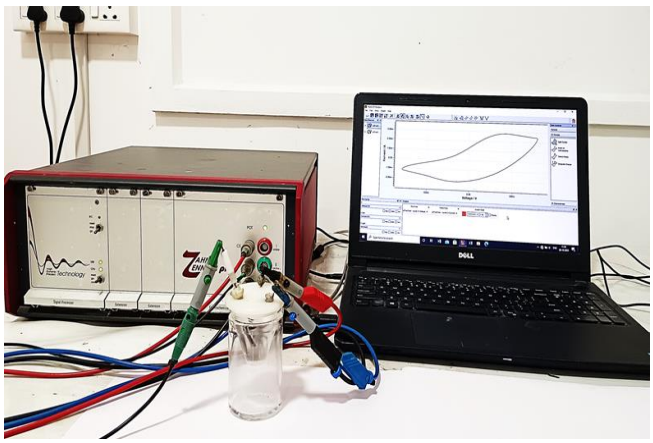

Figure 2.4 *Zahner Zennium Pro electrochemical workstation used for electrochemical studies*

2.3.7.1. Cyclic voltammetry

CV is a very useful potentiodynamic electroanalysis technique to get information about the simple and complex redox chemistry of electroactive species, interfacial processes at electrode surface, kinetics

and mechanism of electron transfer reactions and electrochemical nature of a moiety diffusing towards electrode surface [12, 13]. CV comprises of ceaselessly scanning the potential of the WE in a controlled manner between two selected potential limits and measures the resulting current as a function of applied potential. A typical cyclic voltammogram for a reversible redox species is a plot of current at the WE (vertical axis) versus applied potential (horizontal axis) [14]. In CV, the potential is ramped in cyclic phases. During the initial forward scan in the positive region, from the lower potential to higher potential, anodic reaction (oxidation) occurs and the reverse scan results in cathodic reaction (reduction) and returns to the original (initial) potential. The rate at which the potential is swept in an experiment is termed as scan rate or slew rate. As the scan rate increases, the potential sweeps in a faster way and requires lesser time to complete one cycle. The reversible electrochemical reactions are characterised by Nernst Equation,

$$E = E^0 - \frac{RT}{nF} ln \frac{[Ox]}{[Red]} \tag{2.3}$$

where E^0 is the standard reduction potential for the redox couple, R is the universal gas constant, T is the absolute temperature, n is the number of electrons transferred, F is the Faraday's constant, [Ox] and [Red] is the concentration of oxidized and reduced species at equilibrium. For diffusion controlled process, the peak current (i_p) linearly varies with square root of the scan rate through Randles-Sevcik equation,

$$i_p = (2.687 \times 10^5) n^{3/2} v^{1/2} D^{1/2} AC \tag{2.4}$$

where, *n* is the number of electrons involved in the redox process, *v* is the scan rate in V s^{-1}, *D* is the diffusion coefficient in cm^2 s^{-1}, A is the surface area of the electrode in cm^2 and C is the concentration of the electroactive species in mol cm^{-3}.

In our studies, CV is used to evaluate the reaction driven sensing capabilities (sensing electrical, chemical and thermal energetic conditions) and supercapacitor performance of the samples. The specific capacitance (C) was also estimated from the CV curves according to Equation 2.5,

$$C = \frac{1}{m\upsilon\Delta V}\int_{V1}^{V2} I\Delta V \qquad (2.5)$$

where, ∫IΔV represents the integrated area of the CV curve, m is the mass of active material, υ is the scan rate and ΔV is the operating potential window.

2.3.7.2. Chronopotentiometry

Chronopotentiometry is a galvanostatic electrochemical method in which a square wave of current is applied between two electrodes and the resulting potential is monitored as a function of time [15, 16]. In the present investigation, chronopotentiometry is employed to study the reaction driven sensing characteristics (current, concentration and temperature sensing) of the generated materials. Chronopotentiometry is widely used to study the mechanism and kinetics of electrochemical reactions. The plot of the potential evolved (vertical axis) versus time (horizontal axis) is called a chronopotentiograms. A potential step is observed initially due to various types of resistance (solution resistance,

film resistance, counterion resistance and interfacial resistance) associated with the sample and then the potential gradually changes [17]. When the current exceeds the limiting value, the diffusion process could not produce the flux required to sustain the current, the potential shoots up until it reaches the electrode potential of the following reaction. When the applied current is reversed an anodic to a cathodic one, the anodic product starts reduction process and the potential shifts to the cathodic direction. The electric energy consumed (U) by the reaction at any time of the current flow can be expressed in terms of evolved potential (E) and the driving current as,

$$U = I \int Edt \qquad (2.6)$$

Where ∫ Edt is the area under the chronopotentiograms.

2.3.7.3. Galvanostatic Charge Discharge (GCD)

GCD is a commonly used well-grounded technique to evaluate the performance of supercapacitors and batteries under controlled current conditions [18]. The charging and discharging processes are continuous and provides information about IR drop, electrochemical double layer characteristics and faradaic charge-discharge processes. When compared to other techniques, GCD provides precise specific capacitance values [19]. We have employed GCD is used to study the supercapacitor behavior of PPy/hydrogel hybrid films. It is regarded as the experimental antonym of CV since a constant current is applied to the WE and the resulting potential is measured as a function of the time. The shape of the GCD curves provides information about the

charge-discharge processes occur in the supercapacitor. For an ideal supercapacitor, the GCD curve is linear, with alternating positive and negative slopes. For pseudocapacitive behavior, deviations from linearity occur in which series resistance causes the rapid drop in cell voltage. In addition, irreversible redox reactions and electrolyte degradation may also results in inflection points and plateaus in the plot. From the GCD curves, the specific capacitance (C) was calculated according to equation 2.7,

$$C = \frac{I\Delta t}{m\Delta V} \tag{2.7}$$

where, I is the discharge current, Δt is the time elapsed for the discharge, m is the active mass and ΔV is the potential interval of the discharge [20]. For the supercapacitor device, the amount of energy that can be stored per unit weight is represented in terms of energy density (E) and the rate at which the energy can be transferred is given by the power density (P). For the solid-state symmetric supercapacitor device the energy density and power density are calculated by the equations 2.8 and 2.9 respectively.

$$E = \frac{0.5 \times C \times \Delta V^2}{3.6} \tag{2.8}$$

$$P = \frac{3600 \times E}{\Delta t} \tag{2.9}$$

2.3.7.4. Electrochemical Impedance Spectroscopy

EIS is the most strenuous and sophisticated technique that gives valuable information about the resistance, capacitance, and inductance

of the sample as a function of frequency by applying a low-amplitude alternative voltage superimposed on a steady-state potential [21]. It consists of applying a sinusoidal potential to the cell from high frequency to low frequency for monitoring the current response [22]. EIS can be graphically expressed as Nyquist plot and Bode plot. A Nyquist plot displays the imaginary and real components of impedance measurements and its semicircle and linear portions indicates the charge transfer and diffusion-controlled processes respectively [23]. In the present investigation, EIS measurements of the samples were performed at an open-circuit voltage of 10 mV in a frequency range from 0.1 Hz to 100 kHz. The results obtained were interpreted in terms of an equivalent circuit model proposed by Zman software. EIS is widely explored in the field of supercapacitors, batteries, sensors, biosensors and corrosion studies.

2.4. References

1. D.L. Pavia, G.M. Lampman, G.S. Kriz, J.A. Vyvyan, Introduction to spectroscopy, Cengage learning, 2014.
2. N. Colthup, Introduction to infrared and Raman spectroscopy, Elsevier, 2012.
3. R.J. Keyse, A.J. Garratt-Reed, P.J. Goodhew, G.W. Lorimer, Introduction to scanning transmission electron microscopy, Routledge, 2018.
4. N. Brodusch, H. Demers, R. Gauvin, Field emission scanning electron microscopy: New perspectives for materials characterization, Springer, 2018.
5. G. Piburn, A. Barron, Physical methods in chemistry and nano science, (2013) 90-98.
6. D. Shindo, T. Oikawa, Energy dispersive x-ray spectroscopy, Analytical electron microscopy for materials science, Springer, 2002, pp. 81-102.
7. W.H. Woodward, Broadband Dielectric Spectroscopy—A Practical Guide, Broadband Dielectric Spectroscopy: A Modern Analytical Technique, ACS Publications, 2021, pp. 3-59.

8. Y.P. Kalmykov, (2012).
9. E. Huerta, J. Corona, A. Oliva, F. Avilés, J. González-Hernández, Revista mexicana de física, 56 (2010) 317-322.
10. A. Coats, J. Redfern, Analyst, 88 (1963) 906-924.
11. B. Lothenbach, P. Durdzinski, K. De Weerdt, A practical guide to microstructural analysis of cementitious materials, 1 (2016) 177-211.
12. R.S. Nicholson, Analytical chemistry, 37 (1965) 1351-1355.
13. J.J. Van Benschoten, J.Y. Lewis, W.R. Heineman, D.A. Roston, P.T. Kissinger, Journal of Chemical Education, 60 (1983) 772.
14. N. Elgrishi, K.J. Rountree, B.D. McCarthy, E.S. Rountree, T.T. Eisenhart, J.L. Dempsey, Journal of chemical education, 95 (2018) 197-206.
15. A.J. Bard, L.R. Faulkner, H.S. White, Electrochemical methods: fundamentals and applications, John Wiley & Sons, 2022.
16. J. Wang, J. Schultze, Angewandte Chemie-English Edition, 35 (1996) 1998-1998.
17. A. Testa, W. Reinmuth, Analytical chemistry, 33 (1961) 1320-1324.
18. A. Burke, M. Miller, Electrochimica Acta, 55 (2010) 7538-7548.
19. B. Conway, Dordrecht, 1999.
20. D. Guo, M. Zhang, Z. Chen, X. Liu, Materials Research Bulletin, 96 (2017) 463-470.
21. M.F. Dupont, A.F. Hollenkamp, S.W. Donne, Journal of The Electrochemical Society, 161 (2014) A648.
22. P. Taberna, P. Simon, J.-F. Fauvarque, Journal of the Electrochemical Society, 150 (2003) A292.
23. J. Li, Y. Liu, D. Zhan, Y. Zou, F. Xu, L. Sun, C. Xiang, J. Zhang, Journal of Energy Storage, 39 (2021) 102665.

Chapter 3

CHARACTERIZATIONS OF POLYPYRROLE WITH A SPECIAL EMPHASIS ON ELECTROCHEMICAL CHARACTERIZATION

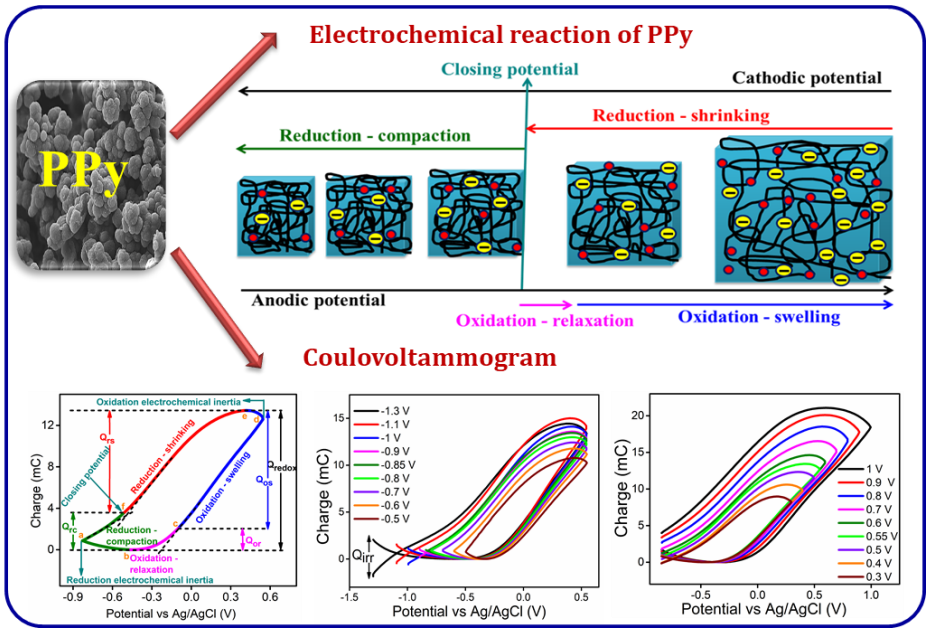

This chapter presents a detailed study of chemically synthesized PPy powder through oxidative polymerization of pyrrole. The synthesized PPy is characterized using FTIR spectroscopy, FESEM, electrical conductivity measurement and TGA. The electrochemical characteristics of the synthesized PPy have been explored using cyclic voltammetric and coulovoltammetric techniques. This chapter also encompassed a detailed study of the reaction driven structural faradaic processes in PPy and analysed the influence of cathodic and anodic potential limits on the voltammetric and coulovoltammetric responses of PPy.

3.1. Introduction

The modern world is constantly witnessing an upsurge in the demand for smart materials capable of stimulating the advancement of human civilization. The advancement of material science research intensely influences day-to-day lives and changes the mode of living. After the discovery of electrically conducting trans-polyacetylene, CPs have received much attention from both academic and industrial communities because of their impressive electrical and electronic properties. This made many researchers all around the world to exploit the marvelous properties of CPs. The present technology urges the researchers to search for lightweight, safer, flexible and high-performance electronic devices based on smart materials. Considering the materials regime, CPs are one of the most suitable materials for the said applications. Apart from this, scientific world is searching for materials and devices capable of sensing the surrounding while working without having additional connectivities. CPs are very special with respect to these applications. The interaction of human systems with the surrounding environment occurs through a series of polymer-based sensors that convert physical or chemical stimuli into electrical impulses and transmit them along the nerves to the brain. The CPs, water and ions are the simplest systems that can mimic the biological functions in their most elemental expression during the electrochemical reactions and produce the basis for the simultaneous sensing while working.

Most of the investigations related to CPs were based on keeping the material composition constant, whereas applications focused on

their composition-dependent properties are not well explored. CPs are multifunctional materials because they drive simultaneous variation of different material properties and functions such as conductivity, stored charge, stored conformational energy, stored counterions, porosity, volume, color and wettability by several orders of magnitude through the same electrochemical reaction, i.e. through electrochemical switching between oxidized and reduced states. These composition-dependent properties of CPs mimic parallel reactions that occur in biological organs such as volume change in muscles, change in the potential in biosensors, color change in skins, changes in the intrachain distances in ion channels and so on. These transformations can effectively be employed in the fabrication of electrochemical devices and products: supercapacitors [1, 2], actuators [3, 4], sensors [5, 6], light-emitting diodes [7, 8], microelectronics [9], polymeric batteries [10, 11], smart drug delivery devices [12, 13], electrochromic windows [14, 15], etc.

As a representative CP, PPy has been profusely studied due to its high electrical conductivity (1-1000 S cm^{-1}), high electrochemical activity over a wide range of pH, lightweight, low operational voltage, large potential window, ease of synthesis ,high stability and biocompatibility [16, 17]. It is noteworthy to mention that the high sensitivity of PPy towards the working conditions leading to its applications towards developing sensing motors has not been well addressed by the scientific community. In the present investigation, we have synthesized PPy powder through chemical oxidative polymerization of pyrrole using anhydrous $FeCl_3$ as an oxidizing agent.

This chapter focuses on detailed electrochemical characterization of chemically synthesized PPy using cyclic voltammetric and coulovoltammetric techniques. This chapter also encompasses a detailed study of the reaction driven structural faradaic processes in PPy and analysed the influence of cathodic and anodic potential limits on the voltammetric and coulovoltammetric responses of PPy.

3.2. Results and discussion

The synthesis of PPy powder has been carried out through chemical oxidative polymerization of pyrrole using anhydrous $FeCl_3$ as an oxidizing agent. After the chemical oxidative polymerization, a dark black powder of PPy was obtained. A schematic representation of the synthesis of PPy is presented in Figure 2.1.

3.2.1. General characterizations

3.2.1.1. FTIR Analysis

FTIR spectrum of the synthesized PPy powder recorded in a wavelength range of 600-3600cm^{-1} is displayed in Figure 3.1. The typical –N–H stretching vibration was observed at 3440 cm^{-1} [18]. The characteristic absorption peak at 1632 cm^{-1} corresponds to the C=C stretching vibration of the pyrrole ring. The absorption peaks at 1545 cm^{-1} and 1460 cm^{-1} are attributed to the characteristic asymmetric and symmetric ring stretching vibrations of PPy [19]. The peaks at 1305 cm^{-1} and 1175 cm^{-1} are ascribed to the C-N stretching vibrations of PPy. The C–H in-plane vibration and the N–H wagging of secondary amine present in the pyrrole unit were observed at 1039 cm^{-1} and 786 cm^{-1} respectively [20, 21]. The peak present at 922 cm^{-1} proves

the out-of-plane ring deformation due to the bipolaronic structure of PPy [22]. The peaks at 2922 cm^{-1} and 2855 cm^{-1} correspond to C-H asymmetric and symmetric stretching vibrations.

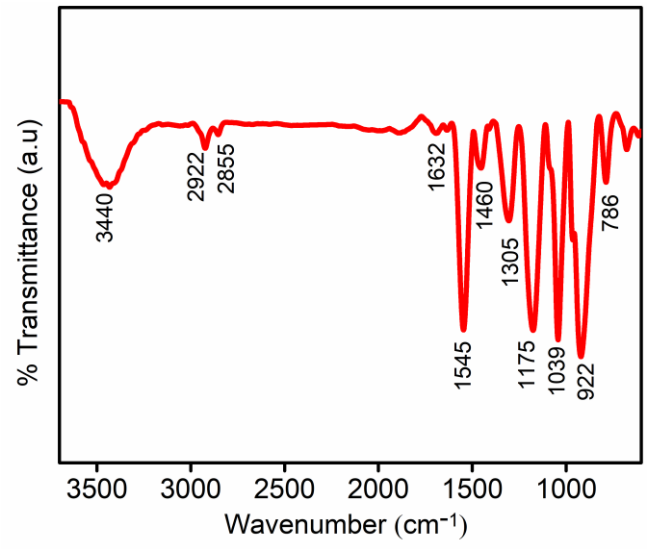

Figure 3.1 *FTIR spectrum of PPy powder*

3.2.1.2. Surface morphology

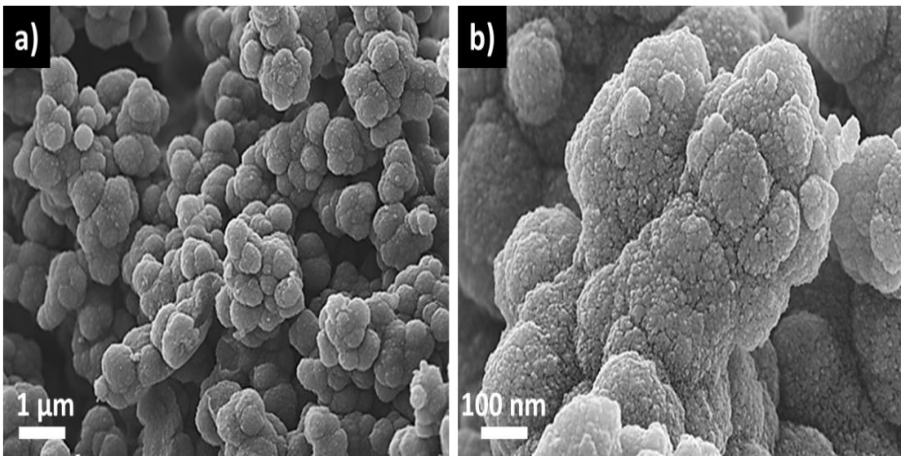

Figure 3.2 *SEM images of PPy powder (a) at low resolution, and (b) at high resolution*

The surface morphological features of PPy powder were examined by recording FESEM and the low and high resolution SEM images are presented in Figure 3.2. From the SEM images, it can be seen that, chemically generated PPy has an agglomerated granular morphology comprising aggregations of particles with nanometer dimensions. The material possesses sufficient porosity that enables the efficient diffusion of ions and solvents through the electrochemical reaction with the electrolyte during potential cycling and it accounts for the efficient electrochemical activity.

3.2.1.3. Electrical conductivity

The frequency-dependent electrical conductivity of the PPy powder investigated using broadband dielectric spectroscopy within the frequency range of 10^{-2} Hz to 10^{7} Hz is presented in Figure 3.3. The total conductivity of the PPy powder depends on the content of PPy, doping level, nature of dopants, method of synthesis, polymerization temperature, etc. Our PPy sample showed a high electrical conductivity of 2.4×10^{2} S cm^{-1} and this high value enables better electrical contact to allow electrochemical reactions and leading to the demonstration of reaction driven sensing characteristics. There is not much variation in the conductivity with frequencies up to 10^{6} Hz. At high frequency, the AC conductivity increases because the electrons are sufficiently excited and hop from one conducting region to another through the extremely small inter-particle gap [23]. The higher value of electrical conductivity of PPy suggests that it has a higher number of charge carriers present in the polymer chain.

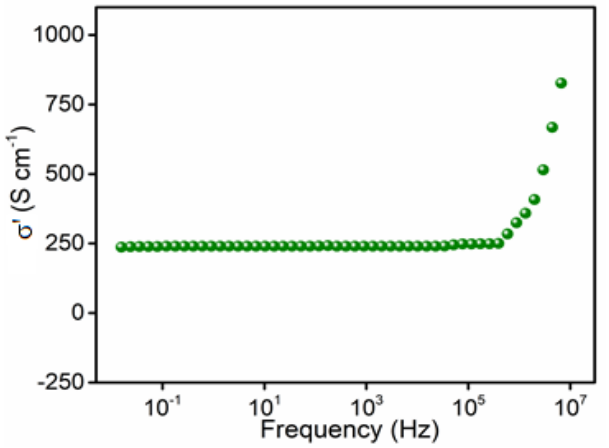

Figure 3.3 *Frequency dependence of electrical conductivity of PPy*

3.2.1.4. Thermogravimetric analysis

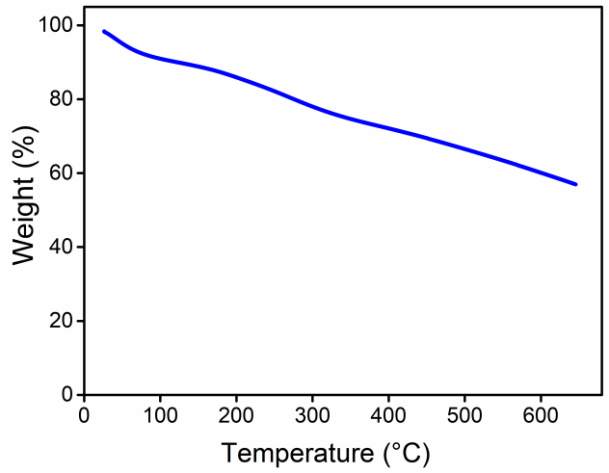

Figure 3.4 *Thermogram of PPy*

TGA was used to assess the thermal stability and the degradation behaviour of the synthesized PPy powder. The resultant thermogram is presented in Figure 3.4. As can be seen, the pure PPy showed three-stage degradation. The initial stage up to 120 ˚C is related to the loss of moisture from the polymer matrix about a weight loss

of 9 % [24]. The slow weight loss upto 210 ˚C is ascribed due to the removal of dopant ions. The polymer degradation begins approximately at 280 ˚C and progresses gradually until 650 ˚C [25]. A residual weight of 57 % is observed at 650 ˚C.

3.2.2. Electrochemical characterizations

3.2.2.1. Cyclic voltammetry

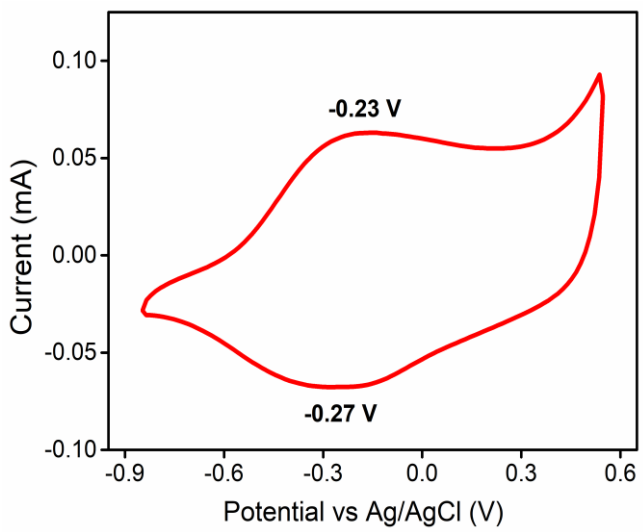

Figure 3.5 *Cyclic voltammogram of PPy electrode at a scan rate of 5 mV s^{-1} in 1 M NaCl aqueous solution when it is subjected to potential cycles between −0.85 V and 0.55 V vs. Ag/AgCl electrode*

The electrochemical activity of PPy was evaluated by cyclic voltammetry in a three-electrode cell assembly at room temperature. The stationary CV recorded for the PPy powder on a glassy carbon electrode at a scan rate of 5 mV s^{-1} in 1 M NaCl solution within the potential interval of -0.85 V and 0.55 V after 10 consecutive cycles (for stabilizing the material and erasing previous structural memory) is presented in Figure 3.5. The obtained CV curve shows a pair of redox

peaks due to faradaic redox behavior. The voltammograms consist of a broad anodic maximum corresponding to PPy oxidation at -0.23 V and a broad cathodic maximum at -0.27 V corresponding to reduction of PPy. When the scan rate is low, the oxidation and reduction potentials are applied for a large time interval and thus promote deeper conformational changes. Hence an increased amount of free volume is generated/destroyed to insert/eject an increased number of counterions and solvent molecules, with the consumption of a large amount of redox charge. Thus we get deeper oxidation/reduction states at low scan rates. The absence of additional peaks due to overoxidation on repeated potential cycling indicates the excellent stability of our PPy sample.

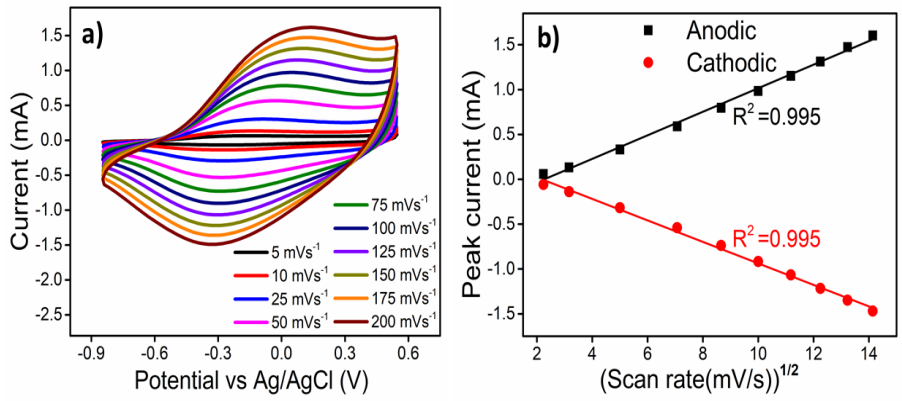

Figure 3.6 *(a) Stationary CV responses of PPy electrode at different scan rates and (b) The linear variation of the peak current obtained from the voltammograms with the square root of the scan rate*

The relationship between scan rate and oxidation-reduction processes was investigated. The CVs of the PPy powder recorded at various scan rates ranging from 5 mV s^{-1} to 200 mV s^{-1} are depicted in Figure 3.6a. Due to the rapid response of the oxidation/reduction to the

current changes, the current of the anodic and cathodic peaks increases dramatically with the increase of the scan rate. At higher scan rates, the intensity of redox peaks is weakened due to the fact that there is less time for the electrolyte to interact with the electrode in the fast electrochemical processes. The variation of the cathodic/anodic peak current versus the square root of the scan rate of the PPy powder is shown in Figure 3.6b. The Figure shows a smooth linear relationship for the current and square root of the scan rate with a higher correlation coefficient (R^2=0.995), suggesting a diffusion-controlled electrochemical process is occurring up to 200 mV s^{-1}.

The electrochemical reversible reaction driving the exchange of anions by a p-doping/p-dedoping process (oxidation/reduction) in PPy can be represented in its simplest form as,

$$(PPy^*)_S + n(X^-)_{sol} + m(H_2O) \rightleftharpoons [(PPy)^{n+}(X^-)_n(H_2O)_m]_{gel} + ne^- \quad (3.1)$$

where PPy* denotes the active centers in the polymer chain (indicated by the sub-index s means solid) that store the positive charges (polaron/bipolaron, in physical terminology) by oxidation, X^- is the monovalent anion exchanged with the electrolyte solution (indicated by the sub-index sol means solution) to balance the positive charge of the chain, *n* is the number of electrons removed per polymer chain or the concomitant number of anions exchanged for charge balance. Neutral PPy exhibits a compact and closed polymer structure by virtue of the attractive Van der Waals interaction between the neighbouring polymer chains. During electrochemical oxidation, electrons are ejected from the

polymer chain and there occurs a strong coulombic repulsion between the emerging polarons. As a result, interchain distances increase and generate free volume to lodge anions and solvent molecules. Thus, anions (X^-) and solvent molecules (H_2O) enter into the polymer matrix for charge and osmotic balance. That is, PPy swells during oxidation to form a dense reactive gel $[(PPy)^{n+}(X^-)_n(H_2O)_m]$. During reduction, electrons are injected; positive charges are terminated and reverse process occurs. Thus, the polymer shrinks to recover the original structure [26]. The schematic representation of the redox process in PPy is shown in Figure 3.7. The forward and backward reactions drive conformational and structural changes accompanied by the volume changes and thus, every chain act as a reversible molecular machine. As the energy needed for extracting the first, second . . ., n^{th} electron from the polymer chain is different, the *n* electrons are extracted one by one through *n* consecutive steps (energetic conformational states), and the PPy chain behaves as a multistep molecular machine [27].

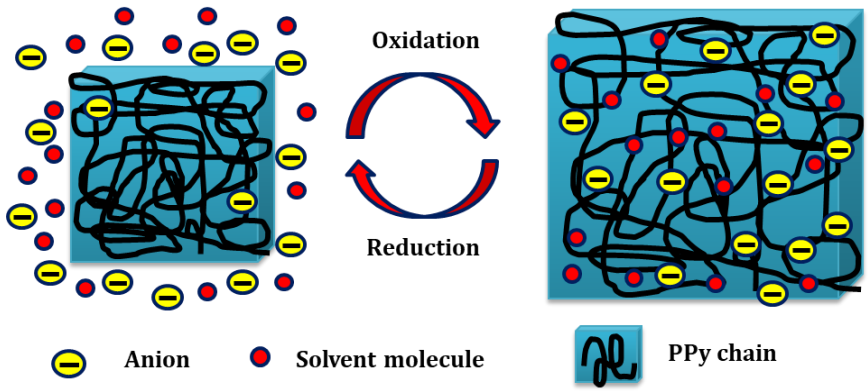

Figure 3.7 *Schematic representation of the electrochemical redox reaction of PPy*

Neutral PPy chains allow free rotation of the consecutive monomeric units as they contain only σ bonds between the monomer units. So the polymer chain can exhibit different conformations and finally gives a coil-like structure. During electrochemical oxidation (Reaction 3.1) the double bond structure is modified. The oxidized chains have a planar structure due to the formation of radical cations or bications having several monomeric units linked through conjugated double bonds which hinders the free rotation of polymer chains. That is, through oxidation, the neutral coil-like structure is transformed into a conjugated rod-like structure. During reduction, reversible conformational movements occur and the coil-like structure is recovered [28]. That means, the reversible redox reactions of CPs control the reverse conformational movements of the polymer chains.

3.2.2.2. Coulovoltammograms

The charge consumed during potential cycling (obtained through CV) can be represented in terms of coulovoltammograms (QV, consumed charge vs. applied potential). The QVs, obtained by integrating the CVs, can be used as a powerful tool for the characterization of reaction-driven conformational changes that occurs in CP electrodes. It helps to reveal, detect and quantify reversible and irreversible electrode reactions in CPs. Positive increments quantify the charge consumed during the oxidation process while negative increments indicate the charge consumed during the reduction process. The QV obtained by integrating the CV (Figure 3.5) of our PPy sample is displayed in Figure 3.8a. The QV of our PPy sample constitutes a closed loop in the studied potential interval revealing that only

reversible oxidation/reduction reactions take place in the PPy powder: the specific oxidation charge equals the specific reduction charge and the overall number of anions and water molecules entered during oxidation equals those expelled during reduction. If there is no such balance, the QV loops are either open or give a closed loop along with an open fraction [29, 30]. The open part present at relatively low cathodic potentials represents that some charge is spent for the parallel irreversible generation of hydrogen by water electrolysis. The minimum of QV is considered as the zero-charge reference and the difference between the closed QV loop maximum and minimum points defines the charge (13.44 mC) consumed during the reversible PPy oxidation-reduction reaction.

The closed loop of the QV is associated with abrupt slope (Q/E) changes. According to Faraday's second law, the charge (Q) involved in the reversible reaction defines the number of exchanged counterions (*n*) through Equation 3.2:

$$n = \frac{Q}{wzF} \tag{3.2}$$

where *z* represents the charge of the exchanged ion, *w* is the polymer mass and *F* is the Faraday constant. For any empirical potential sweep rate, $v = {dE}/{dt}$, the reaction rate (r) is the rate of change of the specific concentration of the ions in the reacting polymer [31]:

$$r = \frac{dn}{dt} = \frac{d(Q/wzF)}{d(E/v)} = \frac{v}{wzF}\frac{dQ}{dE} \tag{3.3}$$

Where dQ/dE is the slope at any point of the QV in Figure 3.8 and the slope changes represent the change in reaction rate associated with each of the structurally induced processes.

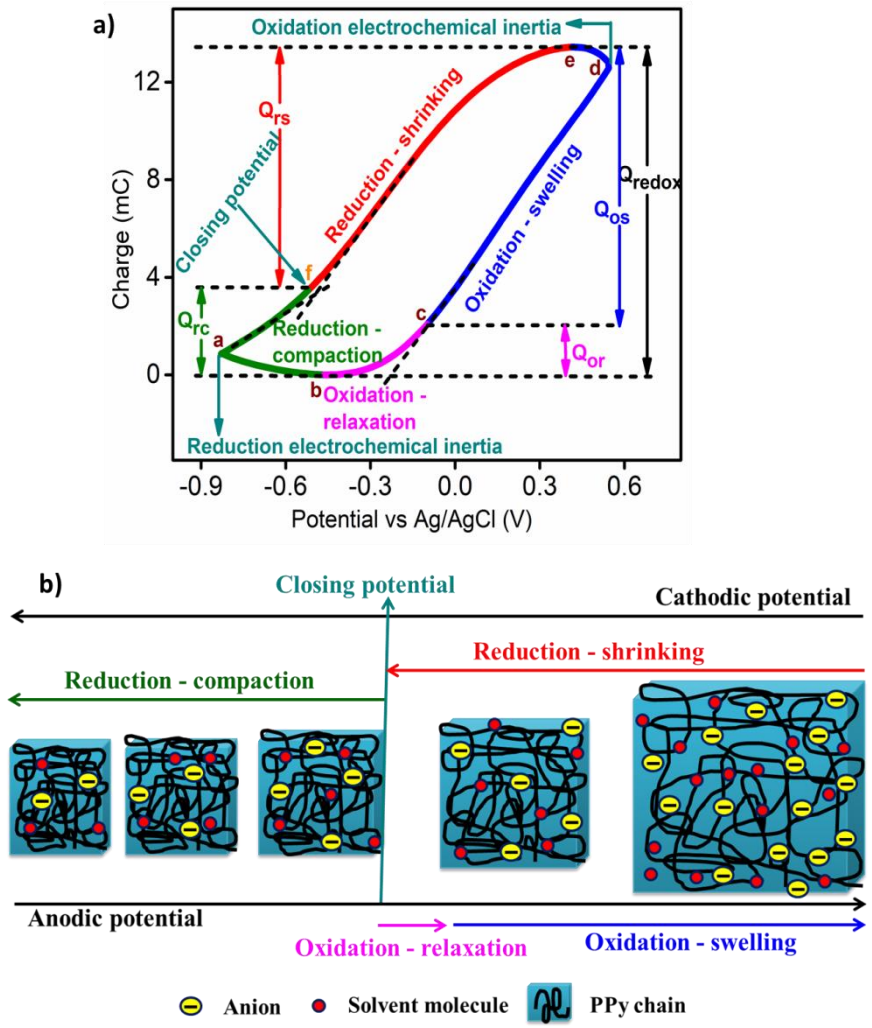

Figure 3.8 *(a) Stationary coulovoltammetric response of PPy at a scan rate of 5 mV s^{-1} in 1M NaCl aqueous solution, the different colors indicate the different structural process and (b) A schematic representation of the corresponding structural changes during the reversible oxidation/reduction reactions*

3.2.2.3. Reaction-driven structural changes in Polypyrrole: potential ranges and related consumed charges

QVs are used for the identification, separation and quantification of the different structural processes during electrochemical reactions. These structural changes are theoretically described and quantitatively determined by the electrochemically stimulated conformational relaxation model (ESCR) [32, 33]. Inside the closed QV loop of PPy, only one oxidation and one reduction reaction occurs (Figure 3.8a) and narrates four basic structural slope variations: viz. reduction-shrinking, reduction-compaction, oxidation-relaxation and oxidation swelling as a result of exchanging anions during electrochemical reactions [28]. Any variation of the charge/potential slope inside the closed-loop indicates a change of reaction rate during the different electrochemical processes (different structural processes) [29, 30, 34].

The QV maximum (point *e*) presents the most oxidized-swollen state by the consumption of 13.44 mC of charge (Figure 3.8a). As like any other faradaic system, the numbers of exchanged ions and solvent molecules and the concomitant volume variation to insert/expel those ions are controlled by the redox charge [35, 36]. When starting from the most oxidized swollen state (point *e*), a fast reduction (high slope) with the expulsion of counterions and water molecules takes place until point *f*. This process is under diffusion kinetic control of the counterions across the PPy chain. This fast reduction causes fast shrinking of the polymer chains (**reduction-shrinking**). As the fast reduction continues and reaches point *f*, the average distance between neighbouring polymeric chains equals the diameter of the hydrated

counterion unit and the dense polymer gel closes the gel structure. Thus point *f* represents the reduction maximum and the corresponding potential is the **closing potential (Ec)**. At this stage, a major portion of the counterions involved in the oxidation process of the polymer chains get trapped between the chains [37, 38].

The material is still a soft wet substance and therefore the reduction does not stop at point *f* and continues with a slower rate (lower slope) as the cathodic potential increases. The trapped counterions expelled from the material must push away the polymer chains apart (conformational movements) to open their way toward the solution. Thus the slow reduction beyond point *f* occurs under the kinetic control of these slow conformational movements of chains. The volume of the film gets more compacted due to the conformational movements of the polymer chain and this process is the **reduction-compaction**. The compaction does not stop at point *a* and continues at the beginning of the anodic potential sweep with a slower rate until point *b* is reached (QV minimum). This is because the reduction overpotential and the conformational mobility are still high at the beginning of the anodic sweep. The reduction occurring at the beginning of the anodic potential sweep is the **reduction electrochemical inertia**.

The material oxidation started after point *b*. But the packed conformational structure undergoes oxidation only after getting extra energy to relax the packed conformations (**oxidation-relaxation**). During the conformational relaxation, the σ bond between the carbon atoms of consecutive monomeric units changes to conjugated π-bonds

and gives a stick-like conformation. This produces sufficient free volume to accommodate anions and solvent molecules. The potential at the minimum of QV is termed **relaxation potential** (Er). That is oxidation starts with an oxidation-relaxation step and once the packed conformation is relaxed (point *c*), a fast oxidation process occurs (high anodic slope). The fast oxidation results in the fast swelling of the polymer chain. This process of **oxidation-swelling** is under the kinetic control of counterion diffusion from the solution. The oxidation does not stop at the maximum anodic potential (point *d*) and continues at the beginning of the cathodic potential sweep until point *e* is reached (QV maximum). This is termed as **oxidation electrochemical inertia.** The potential range corresponding to each structural process described here is given in Table 1.

Here the QV contains only a closed loop corresponding to the reversible redox reaction and within the closed loop, the oxidation charge (Q_{ox}) equals the reduction charge (Q_{red}) and also equals the reversible charge (Q_{redox})

$$Q_{redox} = Q_{ox} = Q_{red} \qquad (3.4)$$

The difference in charge between the QV maximum and the closing potential gives the charge consumed during the reduction-shrinking process (Q_{rs}). After the closing potential, the reduction-compaction starts and does not stop at the potential minimum and continues up to the QV minimum. The corresponding charge difference gives the reduction-compaction charge (Q_{rc}) which is the combination of charge consumed up to the potential minimum and the reduction

electrochemical inertia. The oxidation is initiated from the QV minimum with an oxidation-relaxation step by consuming an oxidation-relaxation charge (Q_{or}). Once the packed conformation is relaxed, fast oxidation-swelling occurs and does not stop at the end of the anodic potential sweep and continues to the QV maxima. Thus the oxidation-swelling charge (Q_{os}) is the sum of both the oxidation up to potential maximum and oxidation electrochemical inertia. The charge consumed during oxidation and reduction reaction is given as:

$$Q_{ox} = Q_{or} + Q_{os} \tag{3.5}$$

$$Q_{red} = Q_{rs} + Q_{rc} \tag{3.6}$$

The consumed charge corresponding to each structural process is given in Table 1.

Table 3.1 *The potential ranges and consumed charges related to the reaction driven structural changes*

Structural changes	**Potential range (V)**	**Charge (mC)**
Reduction-shrinking	0.416 to -0.521	Q_{rs} = -9.98
Reduction-compaction	-0.521 to -0.85 to -0.099	Q_{rc} = -3.46
Total reduction process	0.416 to -0.85 to -0.099	Q_{red} = -13.44
Oxidation-relaxation	-0.099 to -0.463	Q_{or} = 2.07
Oxidation-swelling	-0.463 to 0.55 to 0.416	Q_{os} = 11.37
Total oxidation process	-0.099 to 0.55 to 0.416	Q_{ox} = 13.44

3.2.2.4. Influence of cathodic potential limit on voltammetric and coulovoltammetric responses

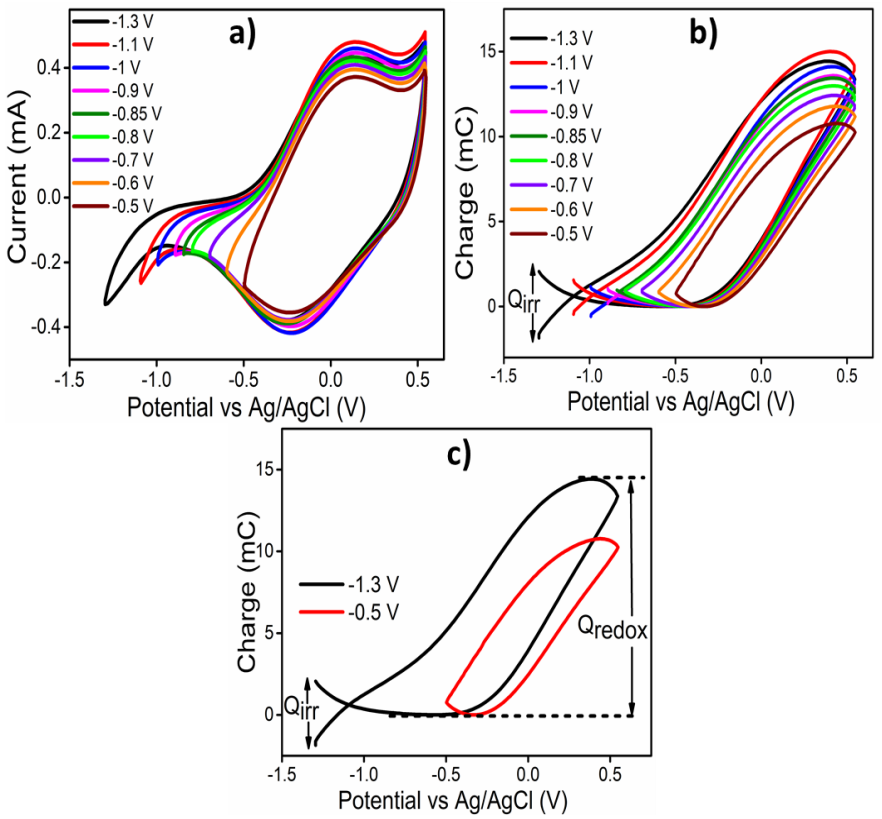

Figure 3.9 *(a) Stationary CVs obtained for PPy at different cathodic potential limits ranging from –0.5 V to −1.3 V for the same anodic potential limit of 0.55 V at 5 mV s^{-1} in 1 M NaCl aqueous solution, (b) Contaminant QV responses obtained by integration of the CVs and (c) QVs obtained by integration of the stationary voltammograms from two different cathodic potential limits: -0.5 V (a closed QV) and -1.3 V (a closed loop and an open part)*

Figure 3.9a depicts the stationary CVs of the PPy powder in 1 M NaCl aqueous solution at 5 mV s^{-1} between a fixed anodic potential limit of 0.55 V and rising cathodic potential limits (ranging from -0.5 V up to -1.3 V) by keeping rest of the experimental

conditions constant. The third stationary CV is taken each time so as to erase any possible material memory. For rising cathodic potential limits the peak current increases upto -1.1 V and then decreases for the cathodic limit of -1.3 V. As the cathodic potential limit increases beyond -0.85 V, small current flows at the cathodic side and this continues to the subsequent anodic potential sweep.

By the integration of the voltammetric responses in Figure 3.9a, the concomitant QV responses were obtained which are presented in Figure 3.9b. These QVs are used for the better characterization and visualization of the structural changes and the possible presence of irreversible reactions in the studied PPy powder in the studied potential ranges. There occurs a continuous variation of charge with varying cathodic potential limits, indicating the presence of a faradaic reaction in the full potential range. For cathodic potential limits lower than -0.85 V, closed QV loops were obtained, indicating that only reversible redox reactions occur (where oxidation charge equals reduction charge). For cathodic potential limits greater than -0.85 V, every QV contains a closed loop on the right side and a small open fraction on the left side [39]. The closed loop defines the presence of reversible oxidation and reduction processes. The open part present at relatively low cathodic potentials represents that some charge is spent for the parallel irreversible reactions like the generation of hydrogen by water electrolysis. The charge consumed by an irreversible reduction reaction (Q_{irr}) is obtained from the negative charge increment between the initial and final point of the open fraction (Figure 3.9c). This irreversible reduction charge is not recovered during the potential

cycling [40]. That is beyond -0.85 V, the reversible reactions overlap with the irreversible reactions and $Q_{reduction} = Q_{redox} + Q_{irr}$

Table 3.2 *Evolution of Q_{redox} (closed loop), Q_{irr} (open part) and $Q_{reduction}$ of the QV responses from different cathodic limits*

Cathodic limit (V)	**Q_{redox} (mV)**	**Q_{irr} (mV)**	**$Q_{reduction}$ (mV)**
-0.5	10.77	-	10.77
-0.6	11.79	-	11.79
-0.7	12.42	-	12.42
-0.8	12.99	-	12.99
-0.85	13.44	-	13.44
-0.9	13.58	1.23	14.81
-1	14.11	1.75	15.86
-1.1	15	2.01	17.01
-1.3	14.43	3.91	18.34

As the cathodic potential limit increases or the reduction goes on beyond the voltammetric reduction maximum the reversible charge (Q_{redox}) increases upto -1.1 V and then decreases for the cathodic limit of -1.3 V. This is because, at higher cathodic potential limits, higher charges should be consumed by the system to reduce it. But here, the oxidation maximum shifts to higher potentials and result in the incomplete oxidation of the reduced material within the applied anodic

limit of 0.55 V. Thus the whole reduced material is not get oxidized within the applied anodic limit. For increasing the cathodic potential limit beyond -0.85 V, the irreversible charge (Q_{irr}) consumed by the irreversible reactions increases as seen in Figure 3.9b. Table 2 represents the charge consumed by the redox reaction, by the parallel irreversible reduction reactions and the total reduction charge at different cathodic limits.

3.2.2.5. Influence of anodic potential limit on voltammetric and coulovoltammetric responses

From Figure 3.9b, it is clear that only reversible structural reactions giving closed charge loops are present for cathodic potential limits ranging from -0.5 V to -0.85 V. Now a potential of -0.85 V is taken as the cathodic potential limit and the anodic potential limits are varied from a potential of 0.3 V to 1 V to study the influence of the anodic potential limit on reversible and irreversible electrode processes in our chemically synthesized PPy. The third stationary CVs attained for the PPy electrode for different anodic intervals in 1 M NaCl aqueous solution at a scan rate of 5 mV s^{-1} are depicted in Figure 3.10a. By the integration of those CVs, the concomitant QV responses are given in Figure 3.10b. For anodic potential limits lower than 0.55 V, QV responses show two parts: a closed loop that quantifies the reversible charge consumed by the redox process and an open part that quantifies the charge consumed by irreversible reduction reactions (hydrogen evolution) (Figure 3.10e). At an anodic potential limit of 0.55 V, the QV response shows only a closed loop showing the presence of reversible reactions (Figure 3.10d). For anodic potential

limits beyond 0.55 V a new irreversible oxidation or overoxidation occurs and gives open QV loops (Figure 3.10b and 3.10c) where the oxidation charges overcome the reduction charges [41].

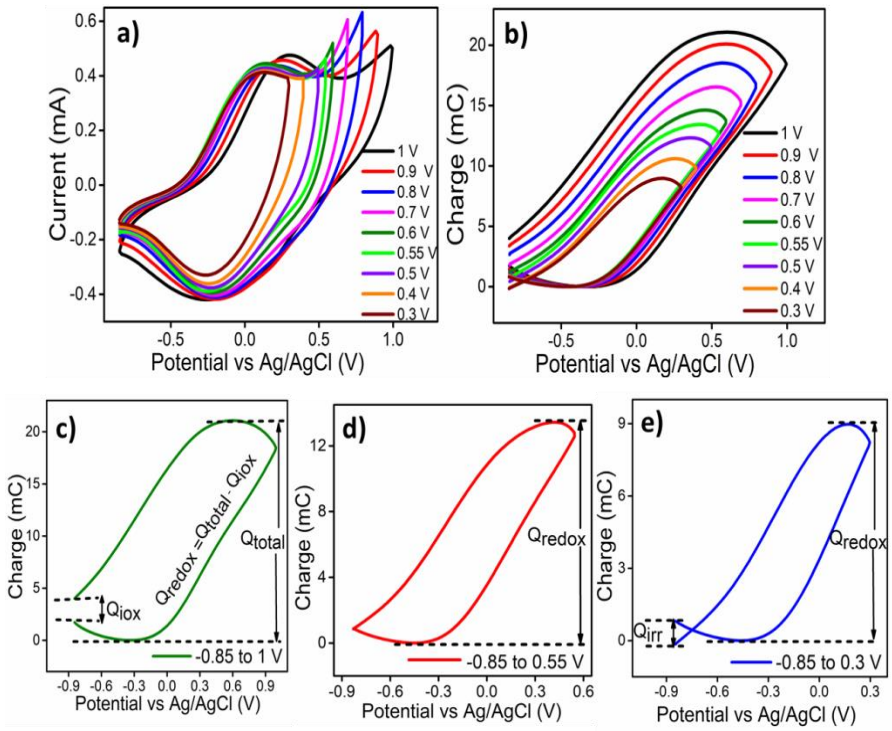

Figure 3.10 *(a) Stationary CVs obtained for PPy at different anodic potential limits ranging from 0.3 V to 1.0 V at the same cathodic potential limit of -0.85 V at 5 mV s^{-1} in 1 M NaCl aqueous solution, (b) Contaminant QV responses obtained by integration of the voltammograms and (c-e) Selected QVs from (b) up to different anodic potential limits to show reversible/irreversible charges*

The charge consumed by irreversible oxidation processes (Q_{iox}) is equal to the difference between the initial and final point of the open loop (Figure 3.10c). Then the reversible charge is obtained by subtracting Q_{iox} from the QV total charge (difference between QV

maximum and minimum): $Q_{redox} = Q_{total} - Q_{iox}$. Beyond the anodic potential limit of 0.55 V the charge consumed by the irreversible oxidation reaction increases for rising anodic potential limits. Overoxidation promotes polymer degradation followed by changes in the electrochemical properties of the polymer. Table 3 represents the charge consumed during the redox reaction, during the parallel irreversible oxidation/reduction reactions and the total charge at different anodic potential limits. Within the studied potential ranges, the QV narrates four basic structural processes: viz. reduction-diffusion, reduction-compaction, oxidation-relaxation and oxidation-diffusion.

Table 3.3 *Evolution of Q_{redox} (closed loop), Q_{irr} (open part) and $Q_{reduction}$ of the QV responses from different anodic limits*

Cathodic limit (V)	**Q_{redox} (mV)**	**Q_{iox} (mV)**	**Q_{irr} (mV)**	**Q_{total} (mV)**
0.3	8.97	-	0.965	9.935
0.4	10.6	-	0.925	11.525
0.5	12.33	-	0.558	12.888
0.55	13.44	-	-	13.44
0.6	14.48	0.15	-	14.63
0.7	15.91	0.63	-	16.54
0.8	17.13	1.39	-	18.52
0.9	18.18	1.92	-	20.1
1	18.81	2.27	-	21.08

3.3. Conclusion

Electroactive PPy powder constituted by multistep macromolecular machines (the PPy chains) was synthesized through chemical oxidative polymerization of pyrrole employing anhydrous $FeCl_3$ as an oxidizing agent. The as-synthesized PPy powder was characterized with FTIR spectroscopy, FESEM, electrical conductivity measurement and TGA. The SEM images revealed that the synthesized PPy has an agglomerated granular morphology comprising aggregations of particles with nanometer dimensions. The electrical conductivity of PPy was found to be 2.4×10^{2} S cm^{-1} and this high value is good enough to impart high electrochemical activity for the synthesized PPy. The excellent electrochemical activity of PPy was confirmed through recording CV in an aqueous solution of NaCl. The coulovoltammetric response of the PPy electrode is closed in NaCl aqueous solution, suggesting that only reversible PPy redox reactions take place in the studied potential interval (-0.85 V and 0.55 V). The coulovoltammetric responses detect and quantify the charge consumed by the reaction and narrate four basic reaction-driven structural slope variations: viz. reduction-shrinking, reduction-compaction, oxidation-relaxation and oxidation swelling. The influence of potential limit on voltammetric and coulovoltammetric responses was analyzed by varying the cathodic and anodic potential limits. The reversible process overlaps with irreversible reduction reactions beyond the cathodic potential limit of -0.85 V, and with irreversible oxidation reactions beyond the anodic limit of 0.55 V.

3.4. References

1. M.P. Sidheekha, K. Nufaira, A. Shabeeba, L. Rajan, Y.A. Ismail, Materials Today: Proceedings, 51 (2022) 2286-2292.
2. R.B. Choudhary, S. Ansari, B. Purty, Journal of Energy Storage, 29 (2020) 101302.
3. F. García-Córdova, L. Valero, Y.A. Ismail, T.F. Otero, Journal of Materials Chemistry, 21 (2011) 17265-17272.
4. E.W. Jager, E. Smela, O. Inganas, Science, 290 (2000) 1540-1545.
5. A. Ramanavičius, A. Ramanavičienė, A. Malinauskas, Electrochimica acta, 51 (2006) 6025-6037.
6. H. Wei, A. Li, D. Kong, Z. Li, D. Cui, T. Li, B. Dong, Z. Guo, Advanced Composites and Hybrid Materials, 4 (2021) 86-95.
7. J. Gao, A. Heeger, J. Lee, C. Kim, Synthetic Metals, 82 (1996) 221-223.
8. J. Li, Y. Hu, X. Liang, J. Chen, L. Zhong, L. Liao, L. Jiang, H. Fuchs, W. Wang, Y. Wang, Advanced Optical Materials, 8 (2020) 1902105.
9. R. Gupta, R. Singh, Journal of Polymer Research, 11 (2005) 269-273.
10. Z. Yin, Q. Zheng, Advanced Energy Materials, 2 (2012) 179-218.
11. P. Novák, K. Müller, K. Santhanam, O. Haas, Chemical Reviews, 97 (1997) 207-282.
12. M. Sharma, G.I. Waterhouse, S.W. Loader, S. Garg, D. Svirskis, International journal of pharmaceutics, 443 (2013) 163-168.
13. R.T. Richardson, A.K. Wise, B.C. Thompson, B.O. Flynn, P.J. Atkinson, N.J. Fretwell, J.B. Fallon, G.G. Wallace, R.K. Shepherd, G.M. Clark, Biomaterials, 30 (2009) 2614-2624.
14. P.M. Beaujuge, J.R. Reynolds, Chemical reviews, 110 (2010) 268-320.
15. B. Yang, D. Ma, E. Zheng, J. Wang, Solar Energy Materials and Solar Cells, 192 (2019) 1-7.
16. V.V. Tat'yana, O.N. Efimov, Russian chemical reviews, 66 (1997) 443.
17. E.W. Jager, E. Smela, O. Inganas, I. Lundstroem, Smart Structures and Materials 1999: Electroactive Polymer Actuators and Devices, SPIE, 1999, pp. 377-384.
18. N. Antony, S. Mohanty, S.K. Nayak, Journal of applied polymer science, 137 (2020) 49561.
19. C. MA, P. SG, G. PR, M. RN, S. Shashwati, P. VB, Soft nanoscience letters, 2011 (2011).
20. Y. Fu, Y.-S. Su, A. Manthiram, Journal of the Electrochemical Society, 159 (2012) A1420.
21. T. Dai, X. Yang, Y. Lu, Materials Letters, 61 (2007) 3142-3145.
22. Y.A. Ismail, J.G. Martínez, A.S. Al Harrasi, S.J. Kim, T.F.F. Otero, Electroactive Polymer Actuators and Devices (EAPAD) 2011, SPIE, 2011, pp. 450-461.
23. M. Ramesan, K. Greeshma, K. Parvathi, T. Anilkumar, Journal of Vinyl and Additive Technology, 26 (2020) 187-195.

24. M. Cabuk, Y. Alan, M. Yavuz, H.I. Unal, Applied Surface Science, 318 (2014) 168-175.
25. M. Ramesan, Journal of applied polymer science, 128 (2013) 1540-1546.
26. T.F. Otero, RSC advances, 11 (2021) 21489-21506.
27. T.F. Otero, S. Beaumont, Sensors and Actuators B: Chemical, 263 (2018) 493-501.
28. T.F. Otero, Journal of Materials Chemistry B, 1 (2013) 3754-3767.
29. T.F. Otero, Electrochimica Acta, 212 (2016) 440-457.
30. T.F. Otero, M. Alfaro, V. Martinez, M.A. Perez, J.G. Martinez, Advanced Functional Materials, 23 (2013) 3929-3940.
31. T.F. Otero, Physical Chemistry Chemical Physics, 19 (2017) 1718-1730.
32. T.F. Otero, H. Grande, I. Cantero, A. Sarasola, Smart Structures and Materials 1999: Electroactive Polymer Actuators and Devices, SPIE, 1999, pp. 122-132.
33. T. Otero, H. Grande, J. Rodriguez, The Journal of Physical Chemistry B, 101 (1997) 8525-8533.
34. T.F. Otero, The Chemical Record, 18 (2018) 788-806.
35. M. Fuchiwaki, J.G. Martinez, T.F. Otero, Electrochimica Acta, 195 (2016) 9-18.
36. T.F. Otero, J. Schumacher, V.H. Pascual, RSC advances, 6 (2016) 68538-68544.
37. B. Malinowska, K. Maksymiuk, Electroanalysis: An International Journal Devoted to Fundamental and Practical Aspects of Electroanalysis, 15 (2003) 263-269.
38. G.r. Frenning, A. Razaq, K. Gelin, L. Nyholm, A. Mihranyan, The Journal of Physical Chemistry B, 113 (2009) 4582-4589.
39. M. Fuchiwaki, T.F. Otero, Journal of Materials Chemistry B, 2 (2014) 1954-1965.
40. T.F. Otero, J. Schumacher, Journal of Electroanalytical Chemistry, 782 (2016) 182-191.
41. J.G. Martinez, S. Aznar-Cervantes, A.A. Lozano-Pérez, J.L. Cenis, T.F. Otero, Electrochimica Acta, 209 (2016) 521-528.

Chapter 4

POLYPYRROLE AS REACTIVE SENSORS OF WORKING AMBIENT: CHRONOPOTENTIOMETRIC AND VOLTAMMETRIC INVESTIGATIONS

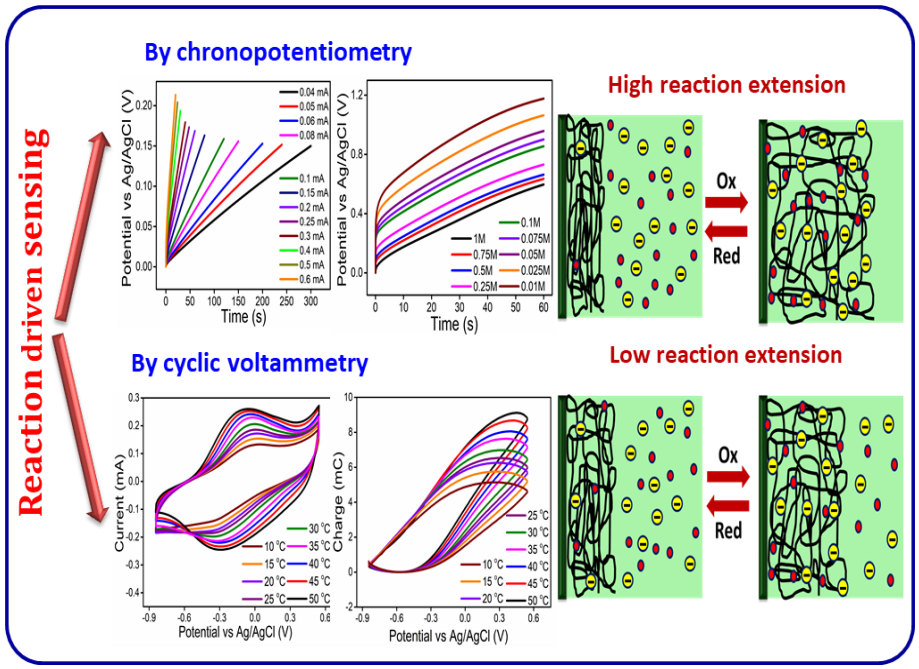

This chapter encompasses a detailed study of the reaction driven sensing characteristics: sensing working electrical, chemical and thermal condition of the chemically synthesized PPy by galvanostatic and potentiodynamic methods. The consumed electrical energy and electrical charge during the redox reactions of PPy are the sensing magnitudes. The results offer the emergence of electrochemical devices based on the reversible redox reactions of PPy which can act as an electrical, thermal and chemical sensor.

4.1. Introduction

CPs are unique reactive materials capable of undergoing electrochemically-driven oxidation/reduction reactions with associated exchange of ions and solvent molecules. When a neutral CP attached to a metal electrode is immersed in an aqueous electrolyte, the polymer-polymer Van der Waals interactions overcome the polymer-solvent interactions and give a coil-like structure. During electrochemical oxidation, electrons are extracted from the chain and form a conjugated planar structure due to the formation of radical cations or bications. Thus the polymeric chain expands by the insertion of counterions and solvent molecules for charge and osmotic pressure balance and gives a rod-like structure. All the processes are reversed during reduction: the expulsion of anions promotes polymer shrinking. These intra and intermolecular interactions can lead the CPs to act as reversible molecular motors in solution. Under electrochemical control, they can go through *n* consecutive chemical equilibrium steps or *n* consecutive fundamental conformational energetic states progressively and reversibly and therefore they can act as multi-step macromolecular motors [1, 2].

Though CPs have been exploited thoroughly for their potential applications in electronics due to their tunable electrical conductivity, they still remains as a less exploited material based on their composition dependent properties, i.e., their ability to change the material composition during the electrochemical reactions by several orders of magnitude. Since the electron extraction during oxidation occurs through *n* consecutive steps, any infinitesimally small changes

in the polymer composition is possible by applying infinitesimally small anodic or cathodic potential changes to the material. This give rise to the existence of a range of intermediate compositions for CPs during potential cycling. Accordingly, any properties (the temperature, the driving current, any mechanical force or pressure acting on the material, any chemical change inside the solution and so on) associated with the volume variations in CPs during the electrochemical reaction also experience associated changes [3]. These changes influence the energy of the electrons and the potential evolution in CPs. Thus it is expected that CPs or any devices of CPs designed based on the above principle work simultaneously as a sensor of the surrounding variables acting on them.

Chemists, physicists and engineers use various classes of electroactive materials as electrodes to develop traditional electrochemical sensors of an analyte in electrolyte solution or adsorbed on the electrode. While Otero and co-workers proposed a different approach to investigating the ability of the polymeric reactions to self-sense the working energetic (chemical, electrical, thermal and mechanical) conditions using different electrochemical methodologies. During the forward reaction 3.1, i.e., oxidation, the *n* electrons cannot be extracted simultaneously from the polymer chains, but are extracted through *n* consecutive steps (energetic conformational states) each involving one electron extraction at *n* ionization potentials of increasing energies. Thus reaction 3.1 (forward and backward) is working outside the chemical equilibrium and the typical Le-Chatelier principle is not applicable. Otero's principle proposed by reformulating the

Le-Chatelier principle applies to such systems. It states that any physical or chemical perturbation (current, active site concentration, electrolyte concentration, mechanical stress and temperature) acting on the electrochemical reaction rate should modify the reaction overpotential (electrical energy) to self-adapt to the newly imposed energetic requirements [4]. That is, the potential evolution between two different oxidation states or the consumed electrical energy during the reaction senses the electrical, thermal, mechanical, or chemical conditions while working. During any electrochemical reaction, the energy consumed is the product of the electrical potential (E) and the consumed charge (Q). Thus the sensing parameter must be any of those above-described parameters or any other quantity related to them. That means, any reactive device such as sensor, supercapacitor, actuator, smart membrane, electrochromic devices etc. based on the ion and solvent molecule exchanges between the CP chains and the electrolyte driven by the electrochemical reactions can respond to, adapt to and sense the working energetic conditions while working.

The reactive polymer chains, ions, and water are the simplest system that replicates the electro-biological reactions in haptic muscles and can be considered as a material model for designing biomimetic devices [5]. The electrochemical reactions of CPs can self-sense any perturbation (internal or external) of their surrounding working conditions at any reaction moment, using the same two connecting wires without physical separation just like biological muscles do [6, 7]. Thus, the CPs offer full integration of multi-sensing properties in a single device through their unique electrochemical reactions. Hence a

new unexplored scientific arena of multi-sensing systems is emerging, opening a new world for the development of sensing motors responding to their surroundings while working. The scientific community working in this field has been trying to establish the fact that, all the CPs behaves in a similar way and the reaction driven (intrinsic) sensing capability is a general property of all CPs such as PPy, PANI, PT, PIN, etc.

This chapter explores the ability of the electrochemical reactions of PPy synthesized through an in situ chemical polymerization of pyrrole in an aqueous medium to sense the electrical, chemical and thermal variations of the ambient environment through chronopotentiometry (galvanostatic method) and CV (potentiodynamic method). We proved that the consumed electrical energy and the consumed electrical charge (extension of reaction) during the reactions are the sensing magnitude for chemically synthesized PPy.

4.2. Results and discussion

4.2.1. Reaction driven sensing characteristics of Polypyrrole: Chronopotentiometric investigation

4.2.1.1. Theoretical description

In the complex electrochemical reactions of CP (Equation 3.1), the forward process represents the anodic oxidation and the reverse process represents the cathodic reduction. Such types of reactions involving two or more reactants and having reaction orders other than one have been studied by Prof K. J. Veter [8]. Then the rate of oxidation reaction (r) can be expressed as;

$$r = k_a[PPy^*]^x[X^-]^y \quad (4.1)$$

where k_a is the anodic rate constant, [PPy*] is the concentration of active centers of the polymer chains, [X^-] is the concentration of counterions, the superscripts x and y are the reaction orders concerning the concentration of active centers of the polymer chains and counterions in the solution respectively.

As mentioned earlier, the reaction takes place outside the equilibrium conditions. According to electrochemical kinetics, under the flow of constant anodic currents (i_a), the oxidation empirical reaction rate for the complex reaction can be expressed as [9];

$$r = k_a[PPy^*]^x[X^-]^y = \frac{i_a}{FV} \quad (4.2)$$

where, i_a is the applied anodic current, F is the Faraday constant (F = 96485 C mol^{-1}), and V is the volume of the electrode material. For the cathodic reduction reactions, the rate of reaction is

$$r = k_c[(PPy)^{n+}(X^-)_n]^z = \frac{i_c}{FV} \quad (4.3)$$

where k_c is the reduction rate constant, $[(PPy)^{n+}(X^-)_n]$ is the concentration of the oxidized species, z is the reaction orders concerning the concentration of oxidized species and i_c is the applied cathodic current.

According to the Butler-Volmer equation, the rate constant depends on the potential evolution during anodic and cathodic reactions. For the

anodic process under galvanostatic experiment, the current passing through the electrode material becomes [10];

$$i_a = FVk_a[PPy^*]^x[X^-]^y$$

$$= FVk_{a0}[PPy^*]^x[X^-]^y \exp\left(\frac{(1-\alpha)nF(E-E_0)}{RT}\right) \quad (4.4)$$

where α is the symmetry factor, E is the electrode potential, E_0 is the standard electrode potential, k_{a0} is the anodic rate constant or rate coefficient, for $E = E_0$, n is the number of electrons removed per polymer chain, R is the universal gas constant ($R = 8.314\ J\ K^{-1}\ mol^{-1}$) and T is the reaction temperature.

For the cathodic process under galvanostatic experiment, the current passing through the electrode material becomes;

$$i_c = FVk_c[(PPy)^{n+}(X^-)_n]^z$$

$$= FVk_{c0}[(PPy)^{n+}(X^-)_n]^z \exp\left(\frac{\alpha nF(E-E_0)}{RT}\right) \quad (4.5)$$

where k_{c0} is the cathodic rate constant or rate coefficient for $E = E_0$. under the flow of anodic or cathodic currents, the expression for the evolution of the material potential (E_a or E_c) can be obtained by taking the logarithm on both sides of equations and then rearranging the equation;

$$E_a = E_0 + \frac{RT}{(1-\alpha)nF}\left(ln\left(\frac{i_a}{FV}\right) - yln[X^-] - xln[PPy^*] - lnk_{a0}\right) \quad (4.6)$$

$$E_c = E_0 + \frac{RT}{\alpha nF}\left(ln\left(\frac{i_c}{FV}\right) - zln[(PPy)^{n+}(X^-)_n] - lnk_{c0}\right) \quad (4.7)$$

Equations 4.6 and 4.7 describe the material potential evolution during the reaction as a function of the physical and chemical variables such as the reaction temperature (T); the imposed current (i_a or i_c); the concentration of electrolyte [X^-]; the concentration of active centers [PPy*]; and the mechanical or structural conditions (conformations of a polymer chain) through V and k_{a0}. Moreover, Equations 4.6 and 4.7 describe the ability of the material potential evolution to sense and to respond to the reaction conditions (working temperature, electrolyte concentration, imposed current and mechanical conditions) while working.

The concentration of active centers of the polymeric chain ([PPy*]) is related to the points on the PPy chains that can store positive charges at the end of the anodic oxidation process. Under the current flow, the concentration of active centers with time (t) decreases as a function of consumed charge per unit volume (Q/V). The consumed charge (Q = it) is related to the number of moles of electrons extracted from the polymer chain (n = Q/F) and to the number of counterions entered into the polymer chain from the electrolyte solution for balancing the charge [11]. Thus,

$$[PPy^*] = [PPy^*]_{initial} - [PPy^*]_{consumed}$$
$$= [PPy^*]_{initial} - \frac{Q}{FV} \quad (4.8)$$

$$[PPy^*] = [PPy^*]_{initial} - \frac{it}{FV} \quad (4.9)$$

From equations 4.6 and 4.7, the material potential evolution during the anodic process can be given as a function of the time of current flow and different experimental variables as,

$$E_a(t) = E_0 + \frac{RT}{(1-\alpha)nF}\left[ln\left(\frac{i_a}{FV}\right) - yln[X^-] - xln\left([PPy^*]_{initial} - \frac{i_a t}{FV}\right) - lnk_{a0}\right] \quad (4.10)$$

The concentration of the oxidized species $[(PPy)^{n+}(X^-)_n]$ is related to the concentration of the reactants through the expression for the equilibrium constant of reaction 3.1;

$$K = \frac{k_c}{k_a} = \frac{[(PPy)^{n+}(X^-)_n]^z}{[PPy^*]^x[X^-]^y} \quad (4.11)$$

Then the concentration of the oxidized species becomes,

$$[(PPy)^{n+}(X^-)_n]^z = \frac{k_c}{k_a}[PPy^*]^x[X^-]^y \quad (4.12)$$

From equation 4.6, 4.9 and 4.12, the material potential evolution during the anodic process can be expressed as a function of the time of current flow and different experimental variables as,

$$E_c(t) = E_0 + \frac{RT}{\alpha nF}\left[ln\left(\frac{i_c}{FV}\right) - \frac{k_c}{k_a}yln[X^-] - \frac{k_c}{k_a}xln\left(\frac{i_c t}{FV}\right) - lnk_{c0}\right] \quad (4.13)$$

During oxidation, the *n* electrons cannot be extracted simultaneously from the polymer chains but through *n* consecutive steps (energetic conformational states) each involving one electron extraction at

n ionization potentials of increasing energies. That is the reaction goes on through *n* consecutive chemical equilibrium states at increasing standard potentials. That is, $E_{01} < E_{02} < E_{03} < \cdots \ldots \ldots < E_{0(n-1)} < E_{0n}$. Then the material potential evolution at any intermediate state is given by,

$$E_{an}(t) = E_{0n} + \frac{RT}{(1-\alpha)F}\left[ln\left(\frac{i_a}{FV}\right) - yln[X^-] - xln\left([PPy^*]_{initial} - \frac{i_a t}{FV}\right) - lnk_{a0}\right] \quad (4.14)$$

$$E_{cn}(t) = E_{0n} + \frac{RT}{\alpha F}\left[ln\left(\frac{i_c}{FV}\right) - \frac{k_c}{k_a}yln[X^-] - \frac{k_c}{k_a}xln\left(\frac{i_c t}{FV}\right) - lnk_{c0}\right] \quad (4.15)$$

For any intermediate step, the initial potential is equal to the final potential reached during the previous step (E_{n-1}) with an increment (ΔE). By considering the increment as a constant we have,

$$E_{0n} = E_{n-1} + \Delta E$$

$$= E_{n-2} + \Delta E + \Delta E$$

$$= E_0 + (n-1)\Delta E \quad (4.16)$$

By substituting Equation 4.13 in 4.11 and 4.12,

$$E_{an}(t) = E_0 + (n-1)\Delta E + \frac{RT}{(1-\alpha)F}\left[ln\left(\frac{i_a}{FV}\right) - yln[X^-] - xln\left([PPy^*]_{initial} - \frac{i_a t}{FV}\right) - lnk_{a0}\right] \quad (4.17)$$

$$E_{cn}(t) = E_0 + (\mathrm{n}-1)\Delta\mathrm{E} + \frac{RT}{\alpha F}\left[ln\left(\frac{i_c}{FV}\right) - \frac{k_c}{k_a}yln[\,X^-\,] - \frac{k_c}{k_a}xln\left(\frac{i_c t}{FV}\right) - lnk_{c0}\right] \quad (4.18)$$

During galvanostatic experiments potential evolution takes place at higher potentials for higher anodic currents, indicating the effect of electrical resistances (opposing the current flow) in the system on the potential evolution. In electrochemistry, electrical resistances include the electric flow through the electrolyte and the interfacial ionic and electronic transfer processes on both electrodes. Thus by considering the system impedance (Z) resulting from the electrical resistances, a new term of the potential described by Ohm's law ($E_Z = i_aZ$) is added to equations 4.17 and 4.18. Then the most general equation for the material potential evolution as a function of the time of current flow and different experimental variables for a system working outside the equilibrium is attained as;

$$E_{an}(t) = E_0 + i_a\mathrm{Z} + (\mathrm{n}-1)\Delta\mathrm{E} + \frac{RT}{(1-\alpha)F}\left[ln\left(\frac{i_a}{FV}\right) - yln[\,X^-] - xln\left([PPy^*\,]_{initial} - \frac{i_a t}{FV}\right) - lnk_{a0}\right] \quad (4.19)$$

$$E_{cn}(t) = E_0 + i_c\mathrm{Z} + (\mathrm{n}-1)\Delta\mathrm{E} + \frac{RT}{\alpha F}\left[ln\left(\frac{i_c}{FV}\right) - \frac{k_c}{k_a}yln[\,X^-\,] - \frac{k_c}{k_a}xln\left(\frac{i_c t}{FV}\right) - lnk_{c0}\right] \quad (4.20)$$

This equation describes the effect of applied current, electrolyte concentration and temperature on the potential evolution. In other words, the evolution of material potential during the electrochemical

reactions of the CPs can sense or respond to the physical and chemical working ambient.

The electrical energy (U(t)) consumed by the reaction at any time of the current flow can be expressed in terms of potential evolution (E) and the flowing current(i_a) as;

$$U_a(t) = i_a \int E dt \tag{4.21}$$

Thus by substituting the equation 4.19 for E, consumed energy in terms of experimental variables can be obtained.

$$U_a(t) = i_a t[E_0 + Z i_a + (n-1)\Delta E] + \frac{RTi_a t}{(1-\alpha)F}\left[ln\left(\frac{i_a}{FV}\right) - yln[X^-] - lnk_{a0}\right] + \frac{RTVx}{(1-\alpha)}\left[ln\left([PPy^*]_{initial} - \frac{i_a t}{FV}\right) - 1\right]\left[\left([PPy^*]_{initial} - \frac{i_a t}{FV}\right)\right] \tag{4.22}$$

Similarly for the cathodic process;

$$U_c(t) = i_c \int E dt \tag{4.23}$$

$$U_c(t) = i_c t[E_0 + Z i_c + (n-1)\Delta E]$$

$$+ \frac{RTi_c t}{\alpha F}\left[ln\left(\frac{i_c}{FV}\right) - \frac{k_c}{k_a} yln[X^-] - lnk_{c0} + \frac{k_c}{k_a} xln\left(\frac{i_c t}{FV}\right) - \frac{k_c}{k_a} e\right] \tag{4.24}$$

Equations 4.22 and 4.24 describes the consumed electrical energy as a function of the experimental variables such as driving current (i_a), time of current flow (t), temperature (T), electrolyte concentration ($[X^-]$) and film volume (V). These equations are the sensing equations, and the sensing parameter is the consumed electrical energy U(t).

Thus we can state that **'any electrochemical device based on the electrochemical reactions of PPy can sense the physical and chemical reaction conditions through the potential evolution between two defined oxidation states and/or consumed electrical energy'**.

Sensing characteristics of the PPy towards driving current, experimental temperature and electrolyte concentration was monitored by recording chronopotentiograms under galvanostatic conditions after stabilizing the hybrid film by recording 10 consecutive cycles of CV between the specified potential limits (to erase any previous structural memory). The potential cycling was stopped at the cathodic potential limit and each experiment was initiated from a reduced state of the material. Then consecutive square current waves were applied.

4.2.1.2. Sensing working electrical conditions: Current sensor

For studying the current sensing characteristics, the PPy was stimulated by four consecutive square waves of currents of different magnitudes ranging from ±0.04 mA to ±0.6 mA (positive current for anodic and negative current for cathodic processes) in 1 M NaCl aqueous solution as the electrolyte. The time period for square waves is varied in accordance with the applied current to consume a constant charge of ±12 mC (Q = it, kept constant) for attaining the same reaction extension (or for attaining the same initial and final oxidation states). Figures 4.1a and 4.1b respectively show the stabilized fourth normalized chronopotentiometric responses for the anodic and cathodic processes. In Figures 4.1a and 4.1b, a potential step is observed initially

due to various types of resistances (solution resistance, film resistance, counterion resistance and interfacial resistance) associated with the material. Then the anodic and cathodic potential increases gradually. As the anodic current increases, the potential evolution takes place at higher potentials and the potential gradually decreases towards higher negative potentials for increasing values of the cathodic currents.

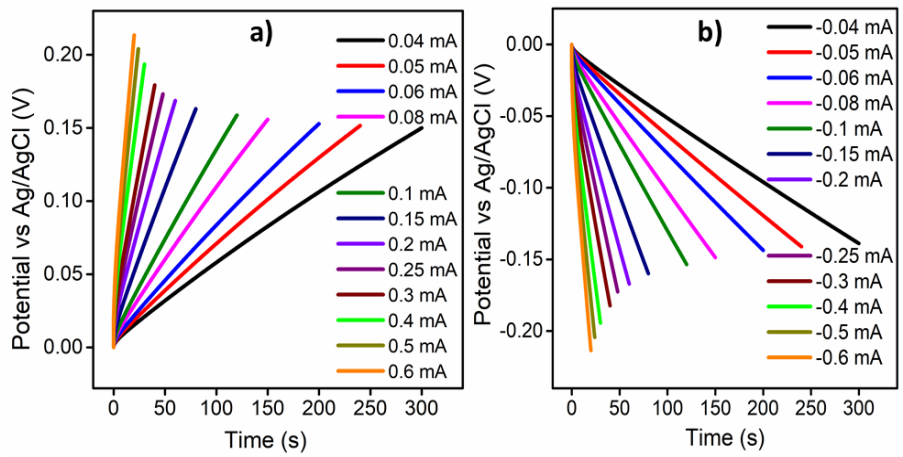

Figure 4.1 *Chronopotentiograms obtained when different constant (a) anodic and (b) cathodic currents were applied to PPy by passing a constant electrical charge of ±12 mC in 1 M NaCl aqueous solution*

The electrical energy (U) consumed by the PPy during each oxidation and reduction step is the area under the experimental chronopotentiograms multiplied by the current. This was calculated as $U = I \int Edt$ where I is the constant current density, t is the time and E is the potential. Figure 4.2 shows the variation of the consumed electrical energy by consumption of the same charge as a function of applied current. The result shows that the consumed electrical energy during the redox reactions of PPy is a linear function of applied current. It suggests that PPy can sense or responds to the locally imposed

electrical conditions during the electrochemical reaction. In this regard, Figure 4.2 represents the sensor calibration line. The slope of the curves (1.041 mJ mA^{-1} for oxidation and -1.253 mJ mA^{-1} for reduction) represents the sensitivity of the sensor to the applied current. The experimental results support the argument that any device based on the electrochemical reactions PPy can sense the working electrical condition (driving current).

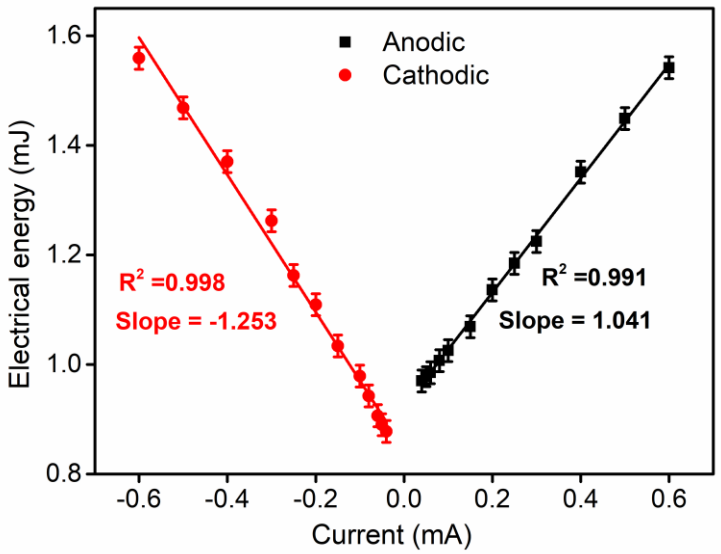

Figure 4.2 *Linear variation of electrical energy consumed during the redox reactions of PPy with applied current*

4.2.1.3. Sensing working chemical conditions: Concentration sensor

To investigate the concentration sensing ability of the redox reactions of PPy, the normalized chronopotentiometric responses were recorded at different concentrations of NaCl (from 0.01 M to 1 M) at a constant applied current of ± 0.2 mA for 60s (the consumed charge was

kept constant at 12 mC) at room temperature. Figures 4.3a and 4.3b show the normalized chronopotentiometric responses for the anodic and cathodic processes respectively. It can be seen that under the same physical and chemical conditions with the same time of current flow, for increasing the concentration of electrolyte, the potential evolution occurs at lower values. That is, as the available chemical energy increases, the consumption of electrical energy occurs at lower potentials for attaining the same reaction extension.

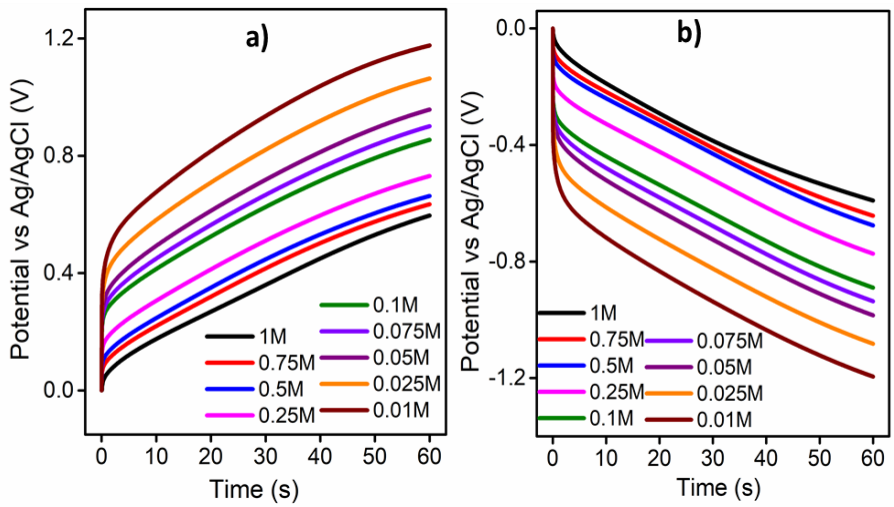

Figure 4.3 *Normalized chronopotentiograms obtained at different concentrations of NaCl when (a) +0.2 mA (anodic) and (b) -0.2 mA (cathodic) current were applied to PPy for 60s in aqueous solutions of NaCl at room temperature*

According to equations 4.19 and 4.20, a logarithmic dependence of electrical energy is expected for various concentrations of electrolyte under constant temperature and current (Figure 4.4). Upon integrating the chronopotentiometric responses of various concentrations, the electrical energy consumed during the reaction is obtained.

Figure 4.4 shows a logarithmic decrease of consumed electrical energy with a gradual increase of working electrolyte concentrations by consumption of the same charge. This means that the energy consumed to achieve a constant volume senses (adapts) the chemical energy (electrolyte concentration) of the ambient. Thus PPy is proven to be working as a concentration sensor. The slope of the curves (-1.455 mJ M^{-1} for oxidation and -1.456 mJ M^{-1} for reduction) provides the concentration sensitivity of the sensor.

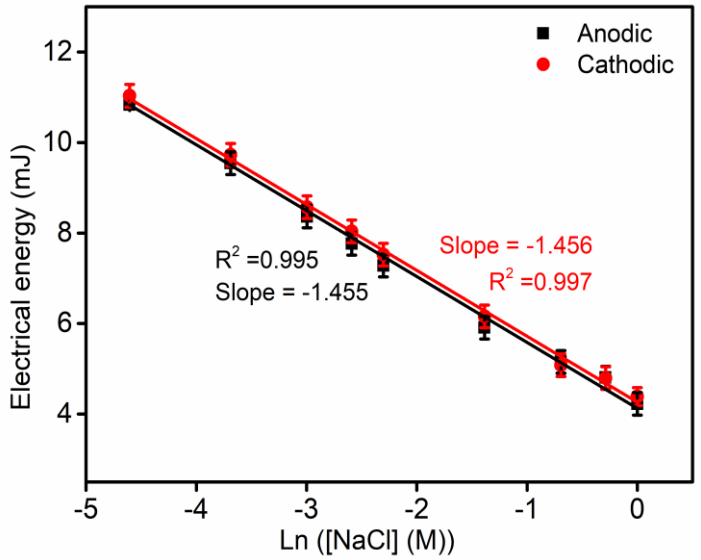

Figure 4.4 *Logarithmic variation of electrical energy consumed by the redox reactions of PPy with the electrolyte concentration by the flow of ± 0.2 mA for 60s at room temperature*

4.2.1.4. Sensing working thermal conditions: Temperature sensor

For studying the temperature sensing characteristics, the PPy was subjected to consecutive square current waves of ±0.2 mA for 60s (at a constant charge of 12 mC for attaining the same reaction extension) at different temperatures ranging from 10 ˚C to 50 ˚C in 1 M NaCl

solution using a thermostat while keeping all other experimental variables constant. The resulted stationary and normalized chronopotentiometric responses for the anodic and cathodic processes are presented in Figure 4.5a and 4.5b respectively.

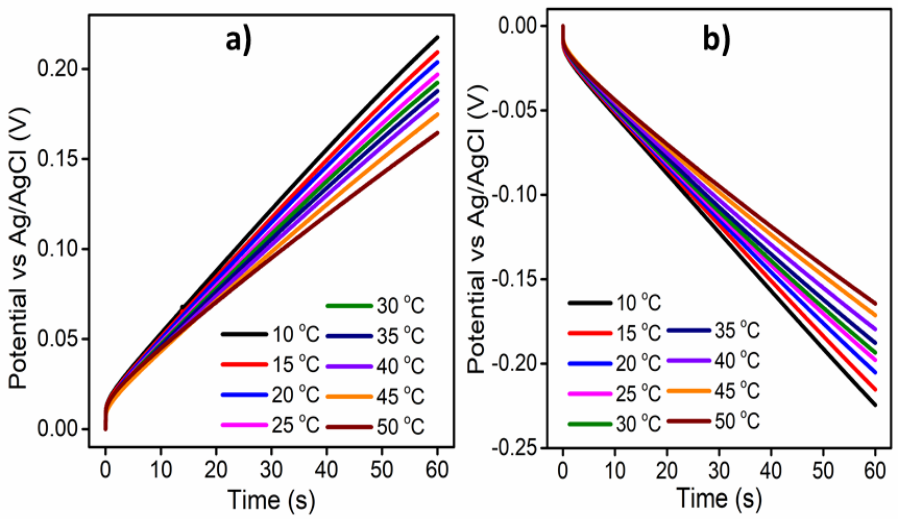

Figure 4.5 *Chronopotentiometric responses attained at various temperatures when (a) +0.2 mA (anodic) and (b) -0.2 mA (cathodic) currents were applied to PPy for 60s in 1 M NaCl solution*

According to the Arrhenius concept, the rate of a chemical or electrochemical reaction (anodic or cathodic) is expected to increase with increasing experimental temperature. As the available thermal energy increases, there occurs faster and longer conformational movements of the polymer chains and the electrode reaction require lower electrical energies. This is equivalent to saying that if a reaction is carried out at a constant rate by passing a constant current for the same duration, the reaction requires lower consumption of electrical energies to achieve the same reaction extension. Thus for rising

temperatures at a constant current applied for the same time (constant charge), the reaction occurs at lower potentials (lower resistance).

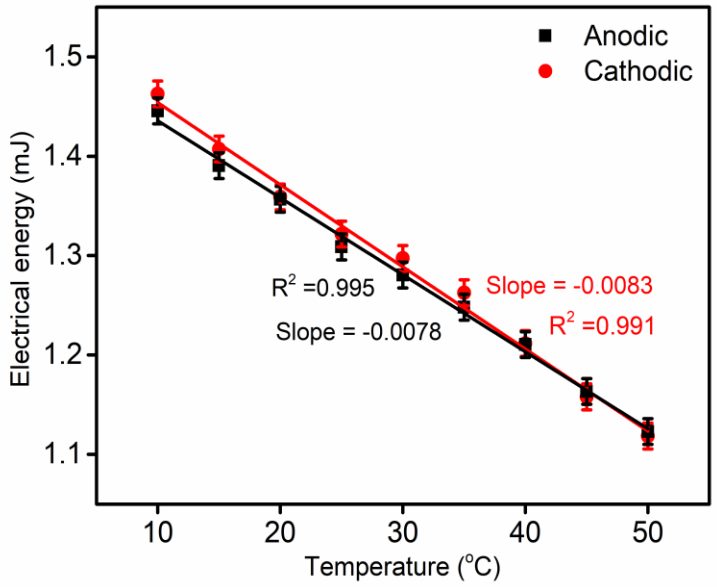

Figure 4.6 *Variation of electrical energy consumed by PPy at different temperatures for anodic and cathodic processes*

From Figure 4.6 it is evident that the electrical energies consumed during the oxidation and reduction processes show a linear increase with decreasing working temperature. Thus the reaction energy senses or responds to the working thermal condition and the concomitant line is the calibration curve. The slope of the curves represents the temperature sensitivity of the chemically synthesized PPy: -7.8 μJ K^{-1} for the oxidation and -8.3 μJ K^{-1} for the reduction processes. The experimental results are in good agreement with the sensing equations 4.19 and 4.20. This proves that the chemically generated PPy can act as a temperature sensor.

4.2.2. Reaction driven sensing characteristics of Polypyrrole: Voltammetric investigation

4.2.2.1. The reaction extension senses the scan rate

Here we have studied the influence of the scan rate on the extension of the reaction (consumed charge) by keeping other experimental conditions (thermal, mechanical and chemical) constant.

a) Theoretical description

From the theoretical point of view, the rate of the forward reaction 3.1 can be written as:

$$R = k[PPy^*]^x[Cl^-]^y \quad (4.25)$$

where R is the rate of the reaction, k is the rate constant and the superscripts x and y are the orders of the reaction concerning the counterion concentration in solution and the concentration of active polymeric centers, respectively. The volume of the material changes during the electrochemical reaction. By taking it into consideration the rate of the reaction in terms of the specific concentration of active centers (r) can be expressed as:

$$r = \frac{R}{m} = \frac{k}{m}[PPy^*]^x[Cl^-]^y \quad (4.26)$$

where m is the unit mass of the dry material reacting inside the electrolyte during reaction 3.1.

Here we tried to study the influence of the experimental electrical variable (the scan rate of the reaction) on the reaction extension (consumed charge). According to Faraday's law, the variation of the

concentration of active centers, [PPy*], during the reaction can be expressed in terms of the involved reaction charge (Q) as:

$$[PPy^*] = \frac{Q}{mzF} = \frac{q}{zF} \tag{4.27}$$

where Q is the charge involved, q is the specific charge ($q = Q/m$), z is the valence of the active center (taken as 1 in this case), and F is the Faraday constant (F = 96485 C mol^{-1}). The reaction rate can also be defined in terms of the variation of the specific concentration of active centers [PPy*] in the material per unit of time. The time can be expressed in terms of the potential and the scan rate v ($v = \partial E/\partial t,\ \partial t = \partial E/v$).

$$r = \frac{\partial[PPy^*]}{\partial t} = \frac{\partial}{\partial t}\frac{q}{F} = \frac{1}{F}\frac{\partial q}{\partial t} = \frac{v}{F}\frac{\partial q}{\partial E} \tag{4.28}$$

The average rate of the reaction ($\bar{r}$) in terms of the consumed coulovoltammetric charge (Q) and the time required for a potential sweep ($\Delta E/v$) can be given as:

$$\bar{r} = \frac{\Delta[PPy^*]}{\Delta t} = \frac{q}{F\Delta t} = \frac{qv}{F\Delta E} \tag{4.29}$$

From equations 4.26, 4.27 and 4.29

$$\frac{qv}{F\Delta E} = \frac{k}{m}[PPy^*]^x[Cl^-]^y = \frac{k}{m}\left(\frac{q}{F}\right)^x[Cl^-]^y \tag{4.30}$$

The relationship between the consumed charge during the reaction of PPy and the scan rate is obtained by rearranging equation 4.30 as:

$$q^{1-x} = \frac{kF^{1-x}\Delta E}{m}[Cl^-]^y\frac{1}{v} \tag{4.31}$$

The constant terms in equation 4.31 are considered as a new constant, $k_1'\left[k_1' = \frac{kF^{1-x}\Delta E}{m}[Cl^-]^y\right]$, then

$$q^{1-x} = k_1'\frac{1}{v} \tag{4.32}$$

This equation correlates the reaction extension (specific reversible charge, q) and the potential scan rate (v): the reaction extension decreases with increasing scan rates when the rest of the experimental variables (concentration of electrolyte, experimental pressure, experimental temperature, potential interval, etc.) kept constant. Taking logarithms on both sides, we get a double logarithmic relation between the reversible specific charge consumed during the reaction and the scan rate as:

$$(1-x)\ln q = \ln k_1' - \ln v \tag{4.33}$$

$$\ln q = c_1 - d_1 \ln v \tag{4.34}$$

Equation 4.34 represents a straight line equation with slope c_1 and intercept d_1 given by equations 4.35 and 4.36 respectively:

$$c_1 = \frac{\ln k_1'}{1-x} \tag{4.35}$$

$$d_1 = \frac{1}{1-x} \tag{4.36}$$

Equation 4.34 is the sensing equation which shows how the reaction extension (the charge consumed during the reaction) senses or responds to the scan rate of the experiment. The consumed charge is a double

logarithmic function of the reaction energetic conditions (the scan rate here) [4, 12].

b) Influence of the frequency on the extension of the reaction

Here we have studied the influence of experimental frequency (*f*, number of potential cycles per second, s^{-1}) on the extension of reaction (consumed charge) by keeping all other experimental variables constant. In equation 4.29 the time interval of the experiment can be redefined in terms of frequency ($\Delta t = 1/\Delta f$). Then,

$$\bar{r} = \frac{\Delta[PPy^*]}{\Delta t} = \frac{q}{F\Delta t} = \frac{qf}{F} \tag{4.37}$$

From equations 3.32, 3.33 and 3.43

$$\frac{qf}{F} = \frac{k}{m}\left(\frac{q}{F}\right)^x [Cl^-]^y \tag{4.38}$$

The relationship between the consumed charge during the reaction of PPy and the experimental frequency is obtained by rearranging Equation 4.38 as:

$$q^{1-x} = \frac{kF^{1-x}}{m}[Cl^-]^y \frac{1}{f} \tag{4.39}$$

The constant terms in equation 4.39 are considered as a new constant, $k_2'\left[k_2' = \frac{kF^{1-x}}{m}[Cl^-]^y\right]$, then

$$q^{1-x} = k_2'\frac{1}{f} \tag{4.40}$$

This equation correlates the reaction extension (specific reversible charge, *q*) and the frequency (*f*): the reaction extension decreases with

increasing frequency when the rest of the experimental variables (concentration of electrolyte, experimental pressure, experimental pressure, potential interval, etc.) are kept constant. Taking logarithms on both sides, we get a double logarithmic relation between the reversible specific charge consumed during the reaction and the frequency:

$$(1-x)\ln q = \ln k_2{}' - \ln f \tag{4.41}$$

$$\ln q = c_2 - d_2 \ln f \tag{4.42}$$

Equation 4.42 represents a straight line equation with slope c_2 and intercept d_2 given by equations 4.43 and 4.44 respectively:

$$c_2 = \frac{\ln k_2{}'}{1-x} \tag{4.43}$$

$$d_2 = \frac{1}{1-x} \tag{4.44}$$

Equation 4.42 is the sensing equation which shows how the reaction extension (the charge consumed during the reaction) varies with the frequency of the experiment. The consumed charge is a double logarithmic function of the experimental frequency [13, 14].

c) Experimental results

In order to investigate the influence of scan rate or frequency on the extension of reaction defined by the consumed charge, the CV responses were recorded at different scan rates by keeping other experimental conditions constant. The stationary CV responses obtained after three consecutive potential cycles, for the PPy at

different scan rates in 1 M NaCl aqueous solution within the potential interval of −0.85 V and 0.55 V is shown in Figure 4.7a. Due to the rapid response of the oxidation/reduction reactions to the current changes, the current of the anodic and cathodic peaks increases dramatically with the increase of the scan rate.

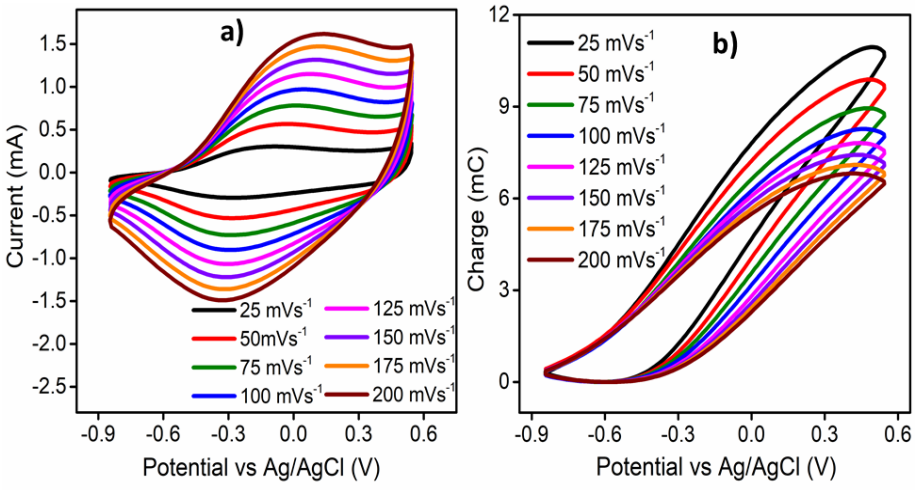

Figure 4.7 *(a) Stationary CV responses of PPy at different scan rates in 1 M NaCl aqueous solution and (b) Concomitant QV responses obtained at different scan rates*

Upon integrating the CVs, the coulovoltammetric responses are obtained. The stationary QV responses corresponding to the CVs from Figure 4.7a were presented in Figure 4.7b. It is observed that all the QVs constitute a closed loop in the studied potential interval related to the PPy reversible oxidation/reduction reaction. As the scan rate rises, the redox charge consumed during the reversible reactions driving the conformational movements of the reactive polymeric chain decreases under the same chemical, physical and mechanical energetic conditions.

When the scan rate is low, the oxidation and reduction potentials are applied for large time intervals. It promotes deeper conformational changes of the polymer chains. Hence an increased amount of free volume is generated/destructed to insert/eject an increased amount of counterions and solvent molecules with the consumption of large redox charges. Thus we get deeper oxidation/reduction states at low scan rates. That is extension of the reaction is greater when the scan rate is low. As the scan rate increases, the time available for reaction 3.1 to extract the electrons from the polymer chain and to drive the conformational movements of the polymeric chains is low and thus free volume generated is low. Thus the amount of anions and solvent that can be inserted by reaction 3.1 is relatively low with concomitant consumption of low oxidation charge and the polymer chains become partially oxidized. The above described events are summarized in Figure 4.8.

Figure 4.9a displays the double logarithmic variation of the consumed charge or extension of the reaction with the scan rate. The experimental results are in good agreement with the sensing equation 4.34. The slope of the curve (-0.236) represents the sensitivity of the sensor, that is how fast the reaction extension decreases per unit variation of the scan rate. The linear fit of the curve corroborates that the consumed electrical charge during the redox reactions of PPy can act as a robust sensor of the imposed electrical condition (scan rate). Thus we can say that any electrochemical device (sensors, supercapacitors, actuators, batteries, etc.) driven by redox reactions of PPy will sense (respond) while working, any perturbation of the working electrical conditions, as the natural organs do.

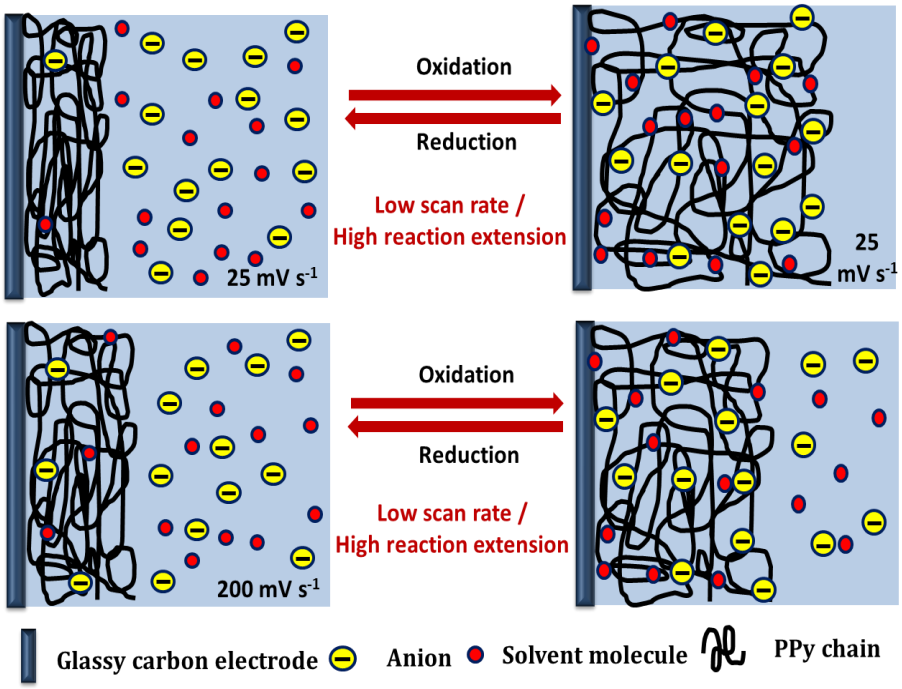

Figure 4.8 *Schematic representation of the extension of the structural changes (swelling/shrinking) by the reversible redox reaction of PPy at low and high scan rates*

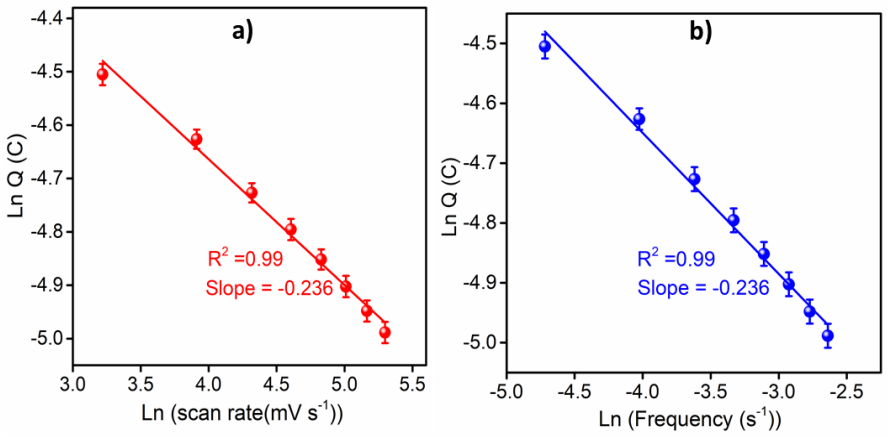

Figure 4.9 *Linear variations showing the double-logarithmic relationship between the charge consumed by the reversible reactions of PPy with the (a) scan rate and (b) frequency*

The variation of the consumed charge through the redox reaction of PPy with frequency is shown in Figure 4.9b. The reaction extension has a double logarithmic dependence with frequency, which fits the theoretical sensing equation 4.42. Figure 4.9b represents the sensing calibration curve. The slope of the curves (-0.236) represents the sensitivity of the sensor indicating how fast the consumed charge decreases with the experimental frequency. The attained linear relationship (R^2 = 0.99) indicates that the charge consumed during the reactions of PPy senses or responds to the experimental frequency.

4.2.2.2. The reaction extension senses the electrolyte concentration

Here we have studied the influence of concentration of the electrolyte on the extension of the reaction i.e., consumed charge while keeping other experimental conditions constant.

a) Theoretical description

By rearranging equation 4.30, the relationship between the consumed charge during the reaction of PPy and the electrolyte concentration can be given as;

$$q^{1-x} = \frac{kF^{1-x}\Delta E}{mv}[Cl^-]^y \qquad (4.45)$$

The constant terms in equation 4.45 are considered as a new constant, $k_3'\left[k_3' = \frac{kF^{1-x}\Delta E}{mv}\right]$, then

$$q^{1-x} = k_3'\,[Cl^-]^y \qquad (4.46)$$

This equation correlates the extension of the reaction (specific reversible charge, q) and the concentration of the electrolyte: the reaction extension increases with increasing electrolyte concentration when the rest of the experimental variables (scan rate, experimental pressure, experimental temperature, potential interval, etc.) are kept constant. Taking logarithms on both sides, we get a double logarithmic relation between the reversible specific charge consumed during the reaction and the electrolyte concentration:

$$(1-x)\ln q = \ln k_3{}' + y\ln[Cl^-] \tag{4.47}$$

$$\ln q = c_3 + d_3\ln[Cl^-] \tag{4.48}$$

Equation 4.48 represents a straight line equation with slope c_3 and intercept d_3 given by equations 4.49 and 4.50 respectively:

$$c_3 = \frac{\ln k_3{}'}{1-x} \tag{4.49}$$

$$d_3 = \frac{y}{1-x} \tag{4.50}$$

Equation 4.48 is the sensing equation which shows how the reaction extension (the charge consumed during the reaction) senses or responds to the concentration of the electrolyte. The consumed charge is a double logarithmic function of the chemical ambient (here, the electrolyte concentration) [10].

b) Experimental results

The stationary CV responses obtained after three consecutive potential cycles for the PPy at different concentrations of the electrolyte

within the potential interval of −0.85 V and 0.55 V at 10 mV s^{-1} are shown in Figure 4.10a. It can be seen from Figure 4.10a that, the peak current increases gradually with an increase in electrolyte concentration under the same thermal, mechanical and electrical conditions. The stationary QV responses corresponding to the CVs from Figure 4.10a were presented in Figure 4.10b. By adjusting the QV minimum to zero, the redox charge consumed during the reversible reactions rises for increasing the concentration of the electrolyte.

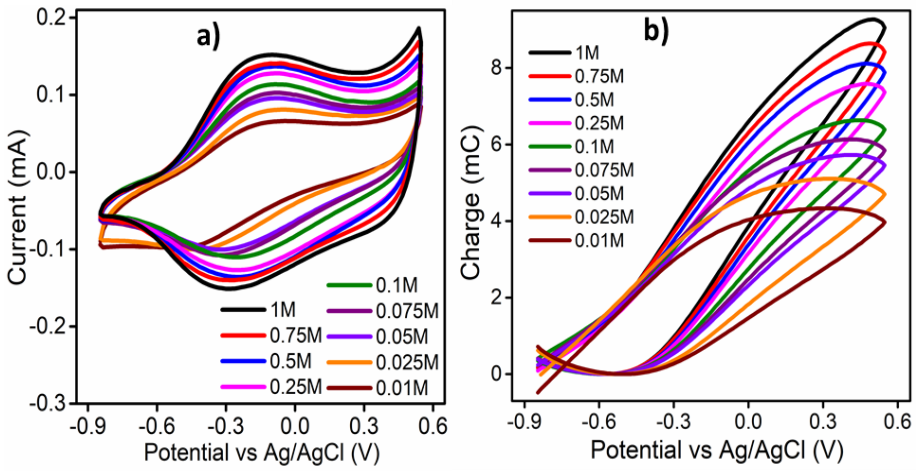

Figure 4.10 *(a) Stationary CV responses of PPy at different concentrations of NaCl solutions and (b) Concomitant QV responses obtained at different electrolyte concentrations*

The ion and solvent exchange occurs between the PPy and electrolyte solution for charge and osmotic balance change with the electrolyte concentration. At a low concentration of electrolyte, the chemical energy available for reaction 3.1 to extract the electrons from the polymer chain and to drive the conformational movements from the reactant polymeric chains is low and hence producing a small amount

of free volume. Thus the amount of anions and solvent molecules that can be inserted by reaction 3.1 is relatively low with concomitant consumption of low oxidation charge and the polymer chains become partially oxidized. When the concentration of the electrolyte increases, the available chemical energy increases, the free volume generated increases, thus inserting more anions and solvent molecules with concomitant consumption of large oxidation charges. Thus we get a deeper oxidation state at high concentrations under the same thermal, mechanical and electrical conditions. The above described conformational movements are schematically represented in Figure 4.11. When the electrolyte concentration increases the redox charge consumed by the reversible reaction driving conformational movements of the polymer chains also increases.

The variation of charge consumed by the reaction of the PPy with the electrolyte concentration is shown in Figure 4.12. The reaction extension has a double logarithmic linear dependence on the concentration of the electrolyte. Figure 4.12 represents the sensing calibration curve. The slope of the curve (0.16) represents the sensitivity of the sensor. The linear fit of the curve corroborates that the consumed energy during the reaction of the PPy can act as a robust sensor of the electrolyte concentration under constant thermal, mechanical and electrical conditions. Thus we can say that any electrochemical device (sensors, supercapacitors, actuators, batteries, etc.) driven by redox reactions PPy will sense (respond) while working, any perturbation of the chemical working energetic conditions, as the natural organs do [15].

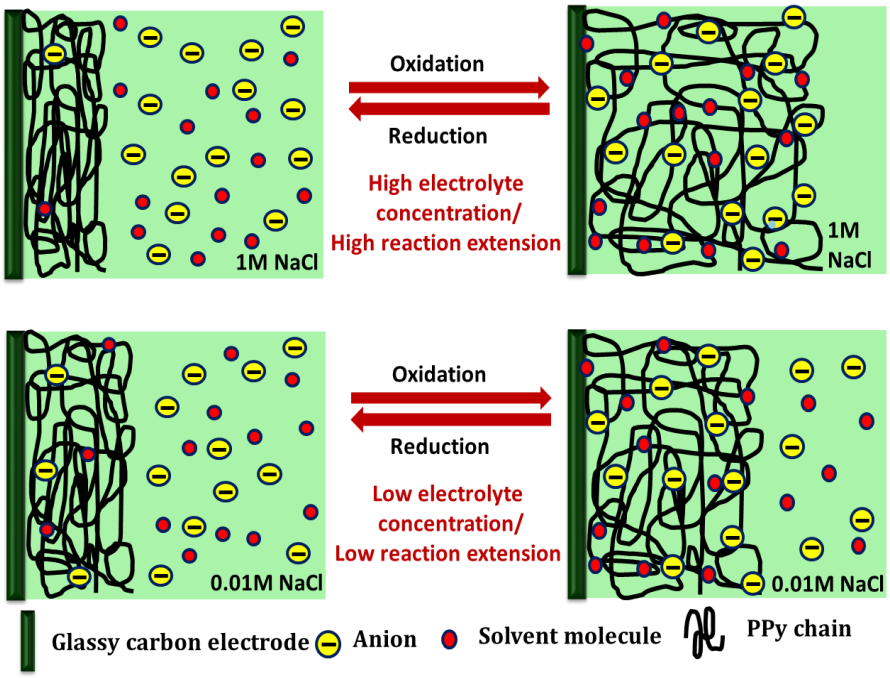

Figure 4.11 *Schematic representation of the extension of the structural changes (swelling/shrinking) by the reversible redox reaction of PPy at high and low electrolyte concentrations*

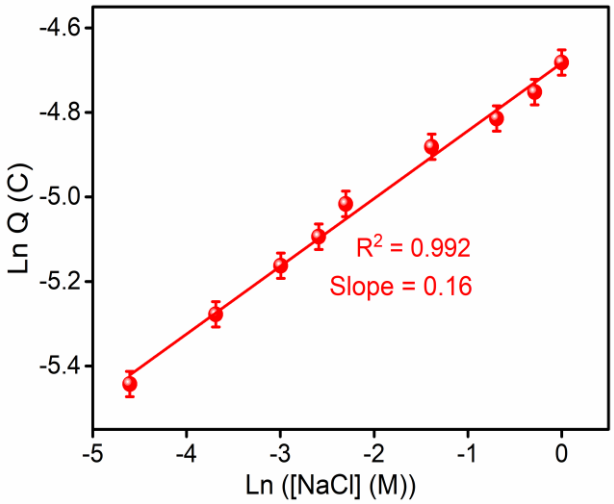

Figure 4.12 *Double logarithmic variation of the electrical charge consumed by the reversible reactions of PPy with the NaCl concentration*

4.2.2.3. The reaction extension senses the working temperature

Here we have studied the influence of the experimental temperature on the extension of the reaction i.e., consumed charge while keeping other experimental conditions constant.

a) Theoretical description

According to the Arrhenius temperature dependence on reaction rate:

$$k = Ae^{-\left(E_a/RT\right)} \tag{4.51}$$

where A is the pre-exponential factor, E_a is the activation energy of the electrochemical reaction, R is the universal gas constant and T is the working absolute temperature. Substituting equation 4.51 in equation 4.30, we get:

$$\frac{qv}{F\Delta E} = \frac{Ae^{-\left(E_a/RT\right)}}{m}[PPy^*]^x[X^-]^y = \frac{Ae^{-\left(E_a/RT\right)}}{m}\left(\frac{q}{F}\right)^x[X^-]^y \tag{4.52}$$

The relationship between the consumed charge during the electrochemical reaction and the experimental temperature is obtained by rearranging equation 4.52 as:

$$q^{1-x} = \frac{F^{1-x}\Delta E[X^-]^y A}{mv}e^{-\left(E_a/RT\right)} \tag{4.53}$$

The constant terms in equation 4.53 are considered as a new constant k_4' $\left[k_4' = \frac{F^{1-x}\Delta E[X^-]^y A}{mv}\right]$, then

$$q^{1-x} = k_4' e^{-\left(E_a/RT\right)} \tag{4.54}$$

Taking logarithms on both sides, we get a semilogarithmic relation between the redox charge consumed during the reaction and the experimental temperature at constant chemical, physical and mechanical conditions:

$$(1-x)\ln q = \ln k_4{}' - \frac{E_a}{RT} \tag{4.55}$$

$$\ln q = c_4 - d_4 \frac{1}{T} \tag{4.56}$$

Equation 4.56 represents a straight-line equation with a slope c_4 and intercept d_4 given by equations 4.57 and 4.58 respectively:

$$c_4 = \frac{\ln k_4{}'}{1-x} \tag{4.57}$$

$$d_4 = \frac{E_a}{(1-x)R} \tag{4.58}$$

Equation 4.56 describes how the redox charge or reaction extension during the potentiodynamic conditions responds to the experimental thermal conditions. The redox charge defined by the coulovoltammetric charge varies as a semilogarithmic function of the inverse of temperature. In other words, the electrochemical reaction of PPy senses the experimental temperature (available thermal energy) [9].

b) Experimental results

Figure 4.13a displays the stationary voltammetric response of the PPy at different temperatures ranging from 10 ˚C to 50 ˚C under constant chemical, physical and mechanical conditions. Voltammetric responses illustrate the increase of both the anodic and cathodic peak

currents with the increase in temperature. The stationary QV responses obtained by integrating the CVs from Figure 4.13a are presented in Figure 4.13b. It is observed that all the QVs constitute a closed loop in the studied potential interval related to the PPy reversible oxidation/reduction reaction and guarantee the absence of any simultaneous irreversible reaction like solvent electrolysis taking place in the studied potential interval. As the experimental temperature increases, the redox charge consumed during the reversible reactions driving the conformational movements of the reactive polymeric chain increases under the same chemical, physical and mechanical energetic conditions. Thus we get deeper oxidation/reduction states at higher temperatures.

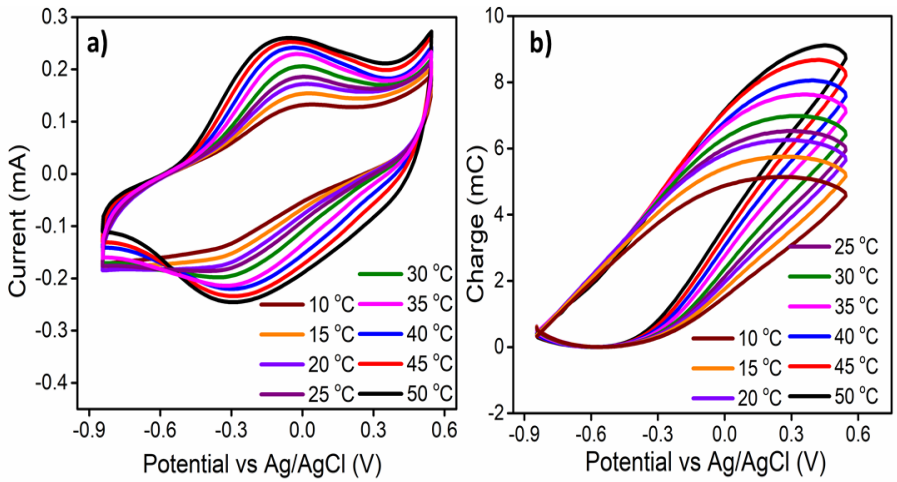

Figure 4.13 *(a) Stationary CV responses of PPy obtained at different temperatures when cycled between −0.85 V and 0.55 V at 10 mV* s^{-1} *in 1 M NaCl aqueous solution and (b) Stationary QVs obtained at different experimental temperatures*

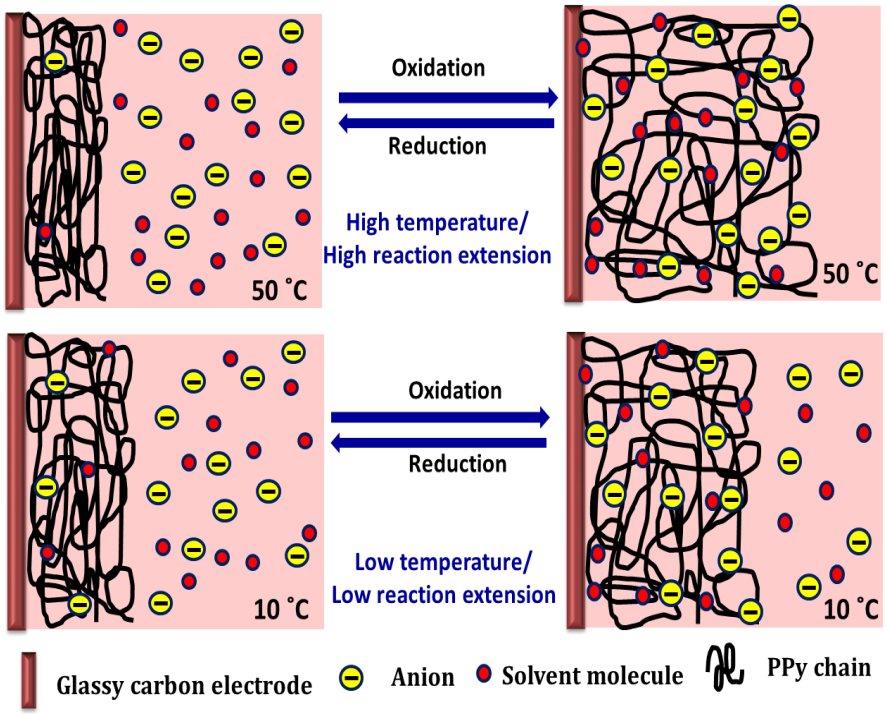

Figure 4.14 *Schematic representation of the extension of the structural changes (swelling/shrinking) by the reversible redox reaction of PPy at high and low experimental temperatures*

Working at a low temperature means that the reaction occurs under the demand of low available thermal energies and allows partial conformational movements of the reactant polymeric chains. The partial conformational relaxation of the polymeric chains generates a low amount of free volume to insert the counterions and the solvent molecules with concomitant consumption of low oxidation charge [16]. Due to the partial exchange of counterions and the solvent molecules, the polymer chains undergo partial oxidation/reduction at low temperatures [17, 18]. As the experimental temperature increases, the increased available thermal energy allows faster and longer conformational movements of the polymeric chains,

producing/destroying increasing amounts of free volume to enter/eject increasing amounts of counterions and solvent molecules with the consumption of increasing redox charges [19]. Thus, under the same chemical, mechanical and electrical conditions, we get deeper oxidation/reduction states at higher temperatures. The above described conformational movements are schematically represented in Figure 4.14.

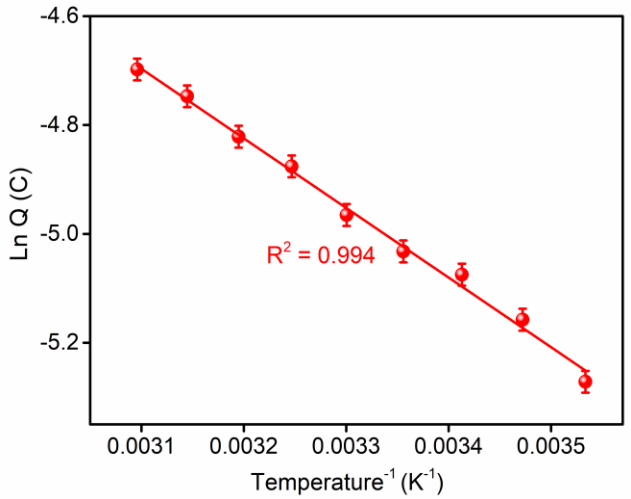

Figure 4.15 *Logarithmic variation of the electrical charge consumed by the reversible redox reactions of PPy with the inverse of the temperature*

Figure 4.15 displays the logarithmic variation of the redox charge or reaction extension with the inverse of the temperature while keeping other experimental variables constant. The experimental results are in good agreement with the sensing equation 4.56. The slope of the linear dependency (-1278.5) gives the thermal sensitivity of the sensor. Thus for any chemical or biochemical reaction based on the electrochemical reactions of chemically generated PPy the extension of the reaction varies, at any instant, as a function of the temperature. That is, the

redox charge acts as a self-sensor of the reaction thermal ambient similar to that of natural muscles. While translating this concept to design biomimetic molecular motor which can act as a temperature sensor, it is noteworthy to mention here that that higher redox charges are consumed by the muscular reactions occurring at higher temperatures.

4.3. Conclusion

The reactive sensing capabilities of PPy constituted by macromolecular electrochemical machines synthesized through chemical oxidative polymerization of pyrrole have been studied by chronopotentiometry and cyclic voltammetry. The PPy can go through *n* consecutive fundamental conformational energetic states progressively and reversibly under electrochemical control and acts as a multi-step macromolecular motor. Here, the driving (current and charge) and sensing (material potential, reaction energy) signals are present and, are detected/controlled by the computer at any working instant, through the same two connecting wires. It is proved that the consumed electrical energy and electric charge during the reaction are the sensing magnitudes. Under galvanostatic conditions (square current waves) at a constant charge (to achieve the same reaction extension), the PPy electrode senses or responds to the electrical, thermal and chemical energetic perturbation of the reaction ambient by modifying the consumed electric energy to self-adapt the newly imposed energetic states. The consumed electrical energy has a linear relation with the applied current (working electrical condition) and experimental temperature (working thermal condition) and a logarithmic relation

with the concentration of electrolyte (working chemical condition) as described by the sensing equations.

Under potentiodynamic conditions (constant electrochemical stimulus), the reaction extension or the consumed charge obtained from the closed coulovoltammetric loops respond to, adapt to, or can act as sensors of the electrical, thermal and chemical working condition as described by the sensing equations. The consumed charge varies as a double logarithmic function of the scan rate or scan frequency (working electrical ambient) as well as electrolyte concentration (working chemical ambient) and acts as a self-sensor of reaction electrical and chemical conditions (reaction self-awareness). At any reaction time, the coulovoltammetric charge varies as a logarithmic function of the inverse of temperature and acts as a self-sensor of reaction thermal conditions (reaction self-awareness). The results offer the emergence of biomimetic sensing devices based on PPy redox reactions imitating biological functions in which the driving and sensing signals can be read at any instant of the reaction, through the same two connecting wires.

4.4. References

1. T.F. Otero, M.J. Ariza, The Journal of Physical Chemistry B, 107 (2003) 13954-13961.
2. T.F. Otero, Journal of Materials Chemistry, 19 (2009) 681-689.
3. T. Otero, M. Cortes, G.V. Arenas, Smart Sensors, Actuators, and MEMS II, SPIE, 2005, pp. 477-483.
4. T.F. Otero, J.G. Martinez, Progress in Polymer Science, 44 (2015) 62-78.
5. T.F. Otero, Polymer Reviews, 53 (2013) 311-351.
6. T.F. Otero, J.G. Martinez, Advanced Functional Materials, 23 (2013) 404-416.

7. F. García-Córdova, L. Valero, Y.A. Ismail, T.F. Otero, Journal of Materials Chemistry, 21 (2011) 17265-17272.
8. K. Vetter, New York., (1967).
9. T.F. Otero, J.J. Sanchez, J.G. Martinez, The Journal of Physical Chemistry B, 116 (2012) 5279-5290.
10. J.G. Martinez, T.F. Otero, The Journal of Physical Chemistry B, 116 (2012) 9223-9230.
11. T.F. Otero, J.G. Martinez, L. Valero, K. Asaka, Y.A. Ismail, Advances in Science and Technology, Trans Tech Publ, 2013, pp. 16-25.
12. J.G. Martinez, T.F. Otero, Sensors and Actuators B: Chemical, 195 (2014) 365-372.
13. R. Kiefer, J.G. Martinez, A. Kesküla, G. Anbarjafari, A. Aabloo, T.F. Otero, Sensors and Actuators B: Chemical, 233 (2016) 328-336.
14. N. Aydemir, P.A. Kilmartin, J. Travas-Sejdic, A. Kesküla, A.-L. Peikolainen, J. Parcell, M. Harjo, A. Aabloo, R. Kiefer, Sensors and Actuators B: Chemical, 216 (2015) 24-32.
15. T. Otero, M. Cortes, Sensors and Actuators B: Chemical, 96 (2003) 152-156.
16. L. Valero, J.G. Martinez, T.F. Otero, Journal of Solid State Electrochemistry, 19 (2015) 2683-2689.
17. T. Otero, H. Grande, Journal of Electroanalytical Chemistry, 414 (1996) 171-176.
18. H. Grande, J. Rodríguez, Synthetic metals, 85 (1997) 1077-1078.
19. A.A. Entezami, B. Massoumi, (2006).

Chapter 5

POLYPYRROLE/CHITOSAN HYBRID FILMS FOR REACTIVE SENSING AND SUPERCAPACITOR APPLICATIONS

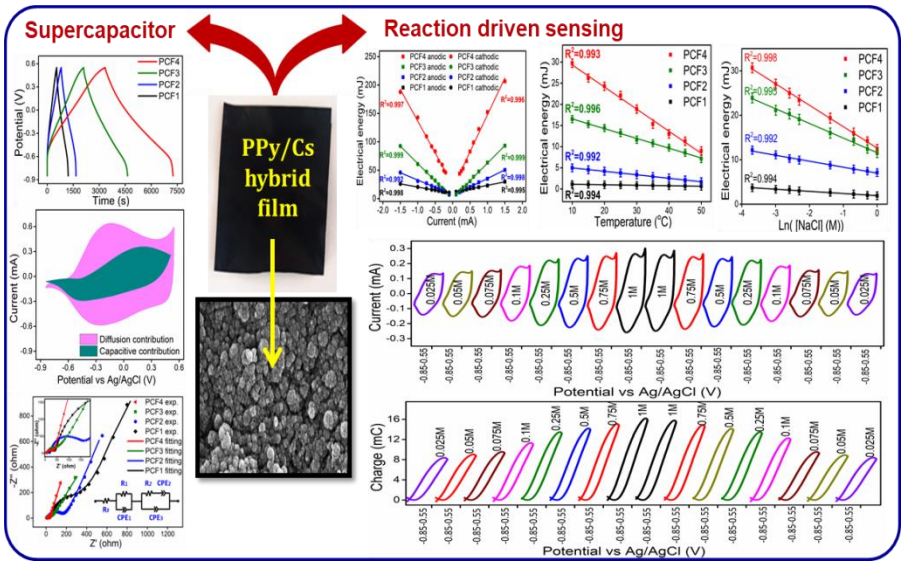

Here, Polypyrrole/chitosan (PPy/Cs) hybrid film supercapacitors constituted by multistep macromolecular machines (PPy chains) capable of sensing working energetic conditions were fabricated. Under galvanostatic conditions, the hybrid film supercapacitors sense or respond to the electrical, thermal and chemical energetic perturbation of the reaction ambient. Under potentiodynamic conditions, the extension of the reaction (coulovoltammetric charges) involving conformational movements of the reacting polymeric chains is a function of and senses the working chemical, electrical and thermal ambient. This chapter also encompasses the effect of number of times of coating on the capacitive behavior and sensing capabilities of the hybrid films.

5.1. Introduction

The scientific community has been dreaming for decades for the development of multi-sensing intelligent motors integrated into a single reactive chemical device capable of sensing surrounding variables (any physical or chemical) at any instant, without physical separation using the same two connecting wires. To date, most of such devices are functioning with additional connectivity or by integrating individual specific functionalities in series and require complex software to take autonomous decisions. Therefore, the realization of a single device with multiple functionalities is highly desired. The burgeoning demand for efficient and sustainable electrochemical energy storage systems in electronic equipment, medical electronics, military devices, portable batteries, etc. created enthusiasm for the development of lightweight, safer, flexible and high-performance supercapacitor gadgets. In this scenario, the fabrication of multi sensing supercapacitor electrodes and evaluating their electrochemical performance is of great importance. Still it remains a great challenge to design lightweight high performance supercapacitor electrodes capable of sensing themselves. Among many candidates, CPs are widely explored for energy storage materials owing to their low cost, lightweight, ease of synthesis, excellent doping-dedoping properties, high theoretical capacitance, environmental stability and tunable electrical conductivity in contrast to the expensive metal oxides. Moreover, CPs are prove to show reactive sensing capabilities also.

The chapter 4 covers the reaction driven sensing capabilities of PPy in detail. Free standing PPy films can be prepared by

electrochemical methods [1-3]. But the extensive application of PPy is limited in diverse fields ranging from electronics to energy devices due to some inherent limitations. Like any other conducting polymer, PPy lacks processability, flexibility and mechanical integrity. Also CP film are found to be more brittle [4, 5]. Along with it, comparatively low cycling stability of the polymer limits their practical applications for designing energy storage devices.

Numerous approaches have been proposed for the property enhancement of PPy to overcome such drawbacks. Among these co-polymerization with substituted monomers [6], use of surfactants [7, 8], the formation of blends [9], composites or hybrids with mechanically strong polymers [10-12] are explored recently. Hydrogels have received considerable attention as a prominent material for constructing different kinds of intelligent materials due to their structural and functional characteristics, for example, their wide range of stimuli-responsive behavior, non-toxicity, biocompatibility, hydrophilicity, mechanical stability, high-quality adhesion etc. [13-15]. The incorporation of a CP into a hydrogel synergizes the advantageous features of two relatively low-cost materials to obtain good electrical conductivity, electroactivity (from the CP), good processability and mechanical strength (from the hydrogels) [16-18].

5.1.1. Chitosan

Chitosan (Cs), (1-4)-linked 2-amino-2-deoxy-β-D-glucopyranose, is a naturally abundant and non-toxic cationic polyelectrolyte polymer hydrogel obtained by the alkaline deacetylation of chitin. Chitin is chemically poly (β-(1→4)-N-acetyl-D-glucosamine) present in the

exoskeletons of crustaceans, fungal cell walls, plankton and endoskeletons of cephalopods [19, 20]. Chitin is the second most abundant natural polymer in the earth's crust and when its degree of deacetylation reaches 50 %, it is termed as Cs. The structures of chitin and Cs are given in Figure 5.1.

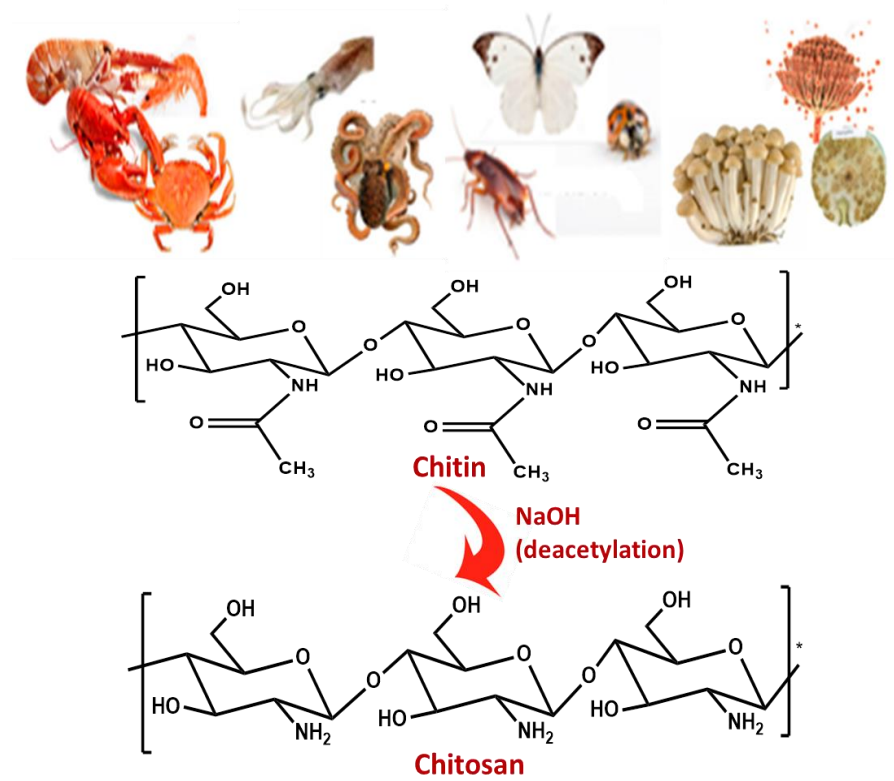

Figure 5.1 *Sources and structure of chitin and chitosan*

Cs has a flexible backbone, and has received considerable attention as a prominent material for constructing different kinds of intelligent materials due to its structural and functional characteristics (for example, stimuli responsive behavior, hydrophilicity, mechanical stability, adsorption properties, non-toxicity, biodegradability,

biocompatibility, and high-quality film-forming properties) [21-23]. The presence of reactive functional groups, amino and hydroxyl groups in its repeating structural unit is responsible for the hydrophilic interaction between the chain segments and the ability to form hydrogen bonds. The amino groups get protonated in dilute acidic solutions which make Cs positively charged. Thus the polymer becomes soluble and form rubbery hydrogel in water [24]. The production of Cs from chitin is environment friendly and economical and has been better researched for several decades for artificial muscles, sensors [18, 25], biosensors, wound healing, tissue engineering, paint and ink industries, drug carriers, pharmaceuticals etc. [20].

In this chapter attempts were made to explore the reaction driven sensing capabilities and energy storage characteristics of PPy/Cs hybrid film supercapacitors fabricated through in situ chemical polymerization of pyrrole on Cs film employing different electrochemical methodologies. This chapter also describes the effect of coating on the reaction driven sensing characteristics (sensing working electrical, chemical and thermal conditions) of the PPy/Cs hybrid films through galvanostatic and potentiodynamic methods. Here we also explored the efficacy of PPy/Cs hybrid films as a supercapacitor electrode with high specific capacitance and long-term cycling stability and examined how the number of times of coating affects the capacitive behavior of PPy/Cs hybrid films. Thus a new paradigm of sensing supercapacitors (sensing motors) capable of sensing electrical, thermal and chemical ambient is proposed.

5.2. Results and discussion

PPy/Cs hybrid films were fabricated through an in situ chemical polymerization of pyrrole in an aqueous medium using $FeCl_3$ as oxidant as explained in chapter 2. A schematic representation of the fabrication of PPy/Cs hybrid film is displayed in Figure 2.2. This method allows the large-scale fabrication of CP/hydrogel hybrid films with superior electrochemical activity. After the in situ chemical polymerization, the Cs film (thickness = 0.108 ± 0.005 mm) turned black in color, suggesting the coating of PPy on Cs film. Here, four different types of films where fabricated, which are designated as PCF1, PCF2, PCF3 and PCF4 (as explained in section 2.2.3). The thickness of PCF1, PCF2, PCF3 and PCF4 were found to be 0.113 ± 0.005 mm, 0.121 ± 0.005 mm, 0.128 ± 0.005 mm and 0.136 ± 0.005 mm respectively. The photographs of the pure Cs film and PCF4 are shown in Figure 5.2a and b, respectively.

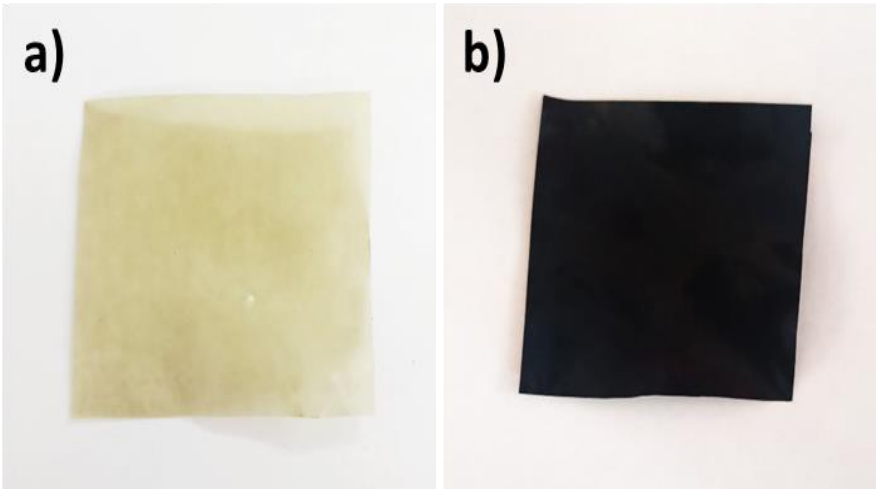

Figure 5.2 *Photographs of (a) the Cs film, (b) the fabricated PCF4 film*

When the Cs film is immersed in the monomer solution, there is a possibility of aligning the pyrrole monomer along the Cs chain assisted through intermolecular hydrogen bonding [26]. The intermolecular hydrogen bonding interaction of the C=O group of Cs with the –NH group of pyrrole is observed in the IR spectra. During the in situ chemical polymerization process, the pyrrole monomers are penetrated through the Cs hydrogel matrix and got polymerized inside the hydrogel. It resulted in a homogeneous distribution of PPy on the surface as well as inside the Cs matrix.

5.2.1. Characterizations of PPy/Cs hybrid films

5.2.1.1. FTIR Analysis

Figure 5.3 shows the FTIR spectra of PPy, Cs film and all four PPy/Cs hybrid films. The FTIR spectrum of Cs exhibits a broad peak around 3280 cm^{-1} due to the axial stretching of O-H and N-H bonds [27, 28]. The peaks at 1642 $cm^{-1}$and 1559 cm^{-1} are assigned to the C=O stretching of the acetyl group and NH bending (amide II) respectively. The peaks at 2915 $cm^{-1}$and 2870 cm^{-1} correspond to C-H asymmetric and symmetric stretching vibrations. The peak at 1320 cm^{-1} is associated with the C-O stretching of the alcohol group. The peaks at 1142 cm^{-1}, 1056 cm^{-1}, and 1020 cm^{-1} are due to the C-O-C stretching vibration in the glucosamine rings. The characteristic peaks in the FTIR spectrum of PPy have been discussed in section 3.2.1.1.

The FTIR spectra of all four PPy/Cs hybrid films show the characteristic absorption peaks corresponding to both PPy and Cs with slight modifications, which confirm that definite interaction exist

between them. The FTIR spectra of the films were recorded by ATR technology and hence, the major absorptions that emerged from the surface of the film correspond to PPy. In the FTIR spectra of PCF4, as a result of the intermolecular hydrogen bonding interaction of the C=O group of Cs with the N-H group of PPy, the C=O stretching vibration is shifted to 1679 cm^{-1}. It shows a broad peak around 3330 cm^{-1} which is consistent with the overlapping of N-H stretching of pyrrole and O-H stretching of Cs. The peaks at 1516 $cm^{-1}$and 1434 cm^{-1} are attributed to the characteristic asymmetric and symmetric ring stretching vibrations of PPy respectively [29]. Similar peaks were exhibited by all other hybrid films and are summarized in Table 5.1. The presence of characteristic peaks of PPy on the hybrid films confirms the successful coating of PPy on the surface of Cs films.

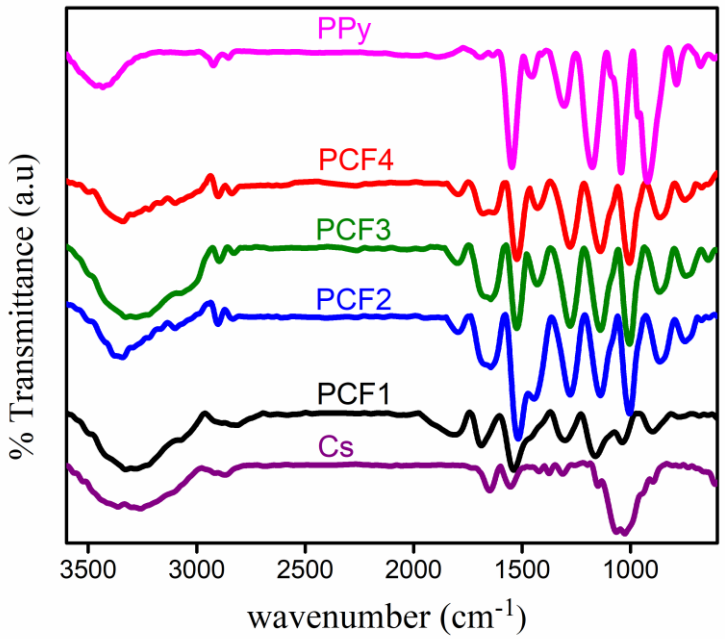

Figure 5.3 *FTIR spectra of PPy, PCF1, PCF2, PCF3, PCF4 and Cs film*

Table 5.1 *Major FTIR spectral absorptions of Cs, PPy, PCF1, PCF2, PCF3 and PCF4 films*

Absorption peaks	Cs	PPy	PCF1	PCF2	PCF3	PCF4
N-H and O-H stretching (cm^{-1})	3280	3440	3317	3348	3313	3330
C=O stretching (cm^{-1})	1642	-	1681	1679	1672	1679
C-H asymmetric and symmetric stretching (cm^{-1})	2915, 2870	2922, 2825	2913, 2825	2902, 2834	2896, 2827	2900, 2838
Asymmetric and symmetric ring stretching (cm^{-1})	-	1545, 1460	1537, 1455	1518, 1442	1526, 1432	1516, 1434
C-N stretching (cm^{-1})	-	1305, 1175	1301, 1144	1285, 1141	1283, 1140	1281, 1139

5.2.1.2. Surface morphology and EDX analysis

The morphological behavior of the PPy/Cs hybrid films was investigated using FESEM and the resulting images are presented in Figure 5.4. Cs film has a smooth and homogenous surface morphology without any voids or cracks. After the in situ chemical polymerization with pyrrole, a complete coating of PPy is present on the surface of the Cs film. All the hybrid films exhibit an agglomerated granular morphology composed of an aggregation of particles with nanometer

dimensions of PPy grown on the surface of Cs film. The whole structure provides sufficient porosity which facilitates the diffusion of ions and solvents and therefore, improve the electrochemical characteristics. No distinct differences were noted in the morphologies of all the hybrid films.

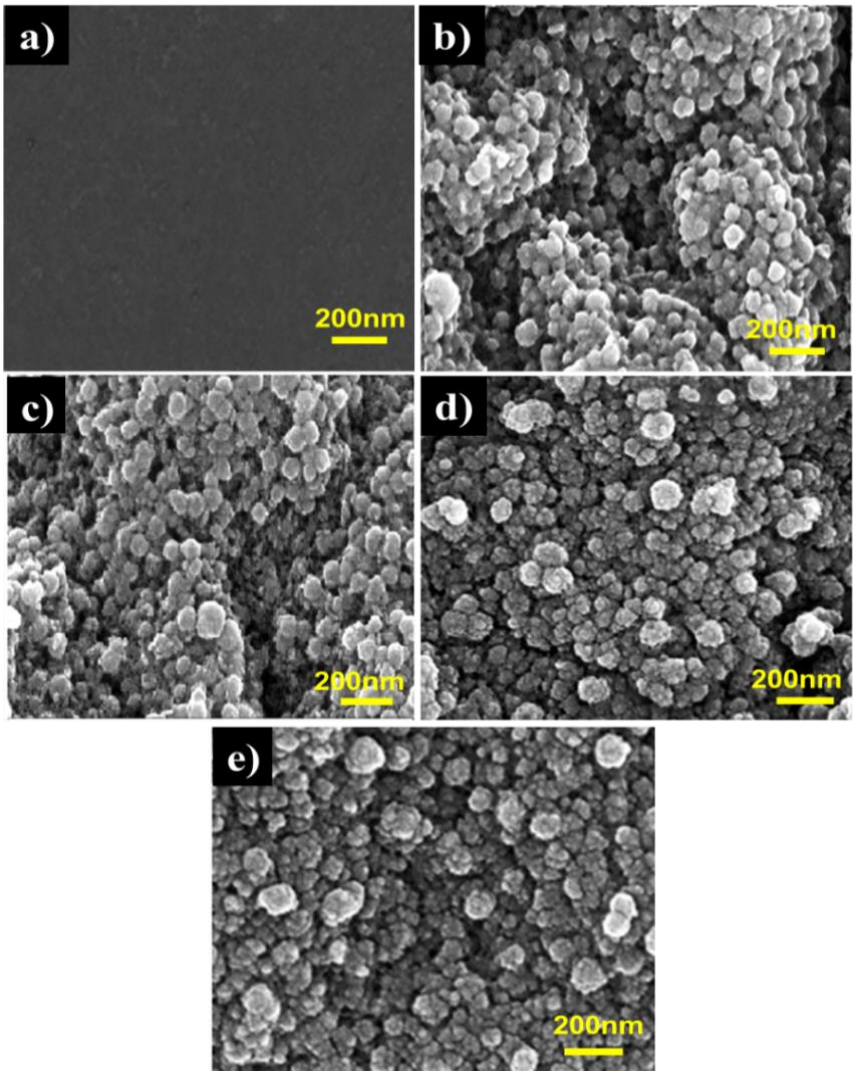

Figure 5.4 *SEM images of (a) Cs film, (b) PCF1, (c) PCF2, (d) PCF3 and (e) PCF4*

The EDX spectra confirmed that all the hybrid films consist of only the elements C, N, O, and Cl on the surface (Figure 5.5) and the percentage of Cl is associated with the Cl^- ions (counter ions) introduced during the doping of PPy. There is no extra peak corresponding to Fe in the EDX spectrum, which indicates that no residual $FeCl_3$ is present on the film. The EDX table data gives the weight percentages of individual elements in the sample.

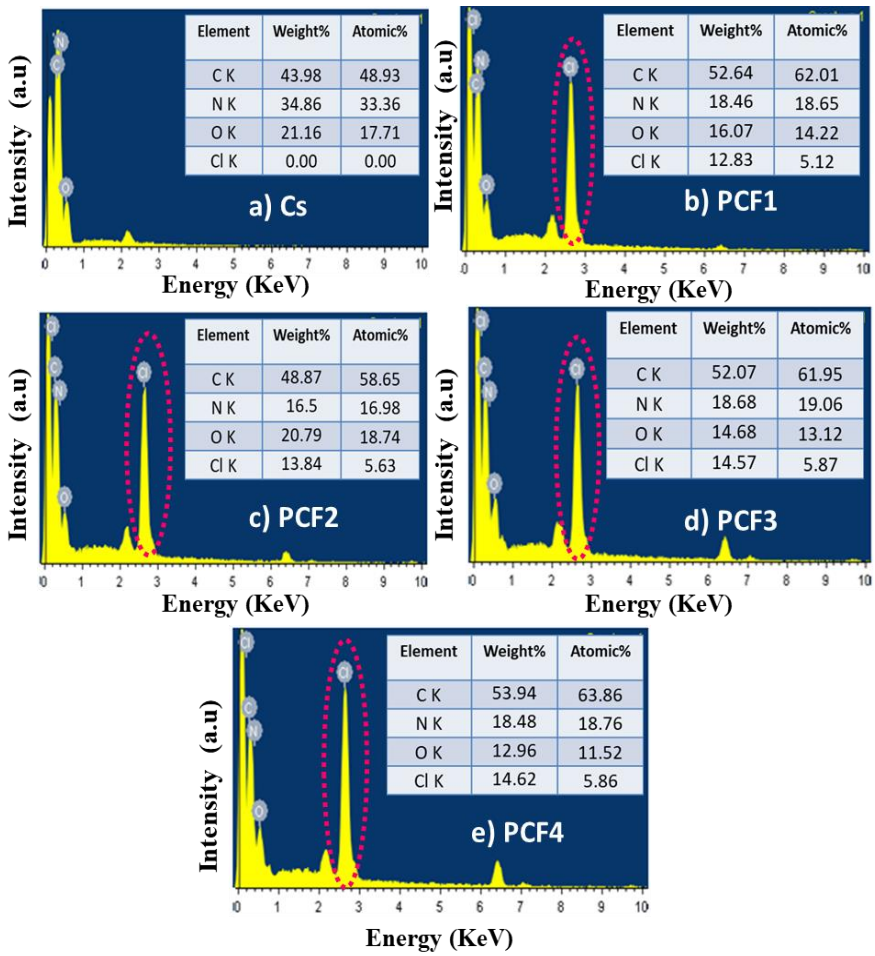

Figure 5.5 *EDX spectrum of (a) Cs (b) PCF1, (c) PCF2, (d) PCF3 and (e) PCF4*

5.2.1.3. Electrical conductivity

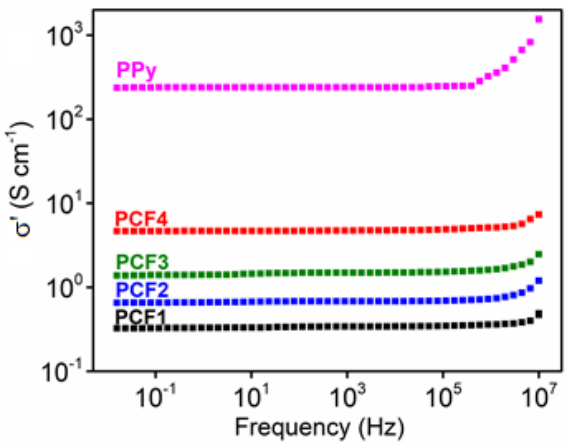

Figure 5.6 *Frequency dependence of electrical conductivity of PPy and PPy/Cs hybrid films*

Table 5.2 *Electrical conductivities of all the hybrid films*

Material	PCF1	PCF2	PCF3	PCF4
Conductivity (S cm^{-1})	3.4×10^{-1}	6.7×10^{-1}	1.4	4.55

The electrical conductivity of the PPy/Cs hybrid films was investigated using broadband dielectric spectroscopy. The frequency-dependent conductivities of the hybrid films with in the frequency range of 10^{-2} Hz to 10^{7} Hz are presented in Figure 5.6. It is evident from Figure 5.6 that the conductivity of hybrid films is improved by the increase in the content of PPy (number of times of coating) from PCF1 to PCF4. This increase in conductivity is due to the increase in the number of charge carriers with increase in the number of times of coating. For all the hybrid films there is not much variation in the conductivity with frequencies up to 10^{6} Hz. The electrical conductivities of all the hybrid films are presented in

Table 5.2 and PPF4 have the highest electrical conductivity of 3.15 S cm^{-1}. The conductivity values of all hybrid films are found to be lower than that of pure PPy (2.4×10^{2} S cm^{-1}); The lower conductivity of the hybrid film is due to the fact that the main constituent of the hybrid films is Cs, which is insulating in nature and served as a skeleton for the polymerization of pyrrole. However, it is large enough for demonstrating its capacitance and sensing applications. Thus the relatively good conductivity of our hybrid films suggests that PPy has been penetrated through the Cs matrix.

5.2.1.4. Thermogravimetric analysis

TGA was used to assess the thermal stability and the degradation behavior of the Cs film, PPy/Cs hybrid films and pure PPy. The results obtained are presented in Figure 5.7. The thermogram of Cs showed two stages of weight reduction behavior: In the first stage a 14 % weight loss observed up to 137 °C is attributed to the loss of water molecules, and the second stage of 52 % weight loss observed between 230 °C and 340 °C is attributed to the decomposition of Cs. The residual weight is found to be 34 %. The degradation temperature of Cs is observed to be 286 °C. Pure PPy showed three-stage degradation which is explained in section 3.2.1.4.

The thermal behavior of all PPy/Cs hybrid films is similar to that of Cs with two stages of weight loss. The first stage is related to the loss of water molecules absorbed. The second stage corresponds to the loss of dopants and polymer degradation, which begins at approximately 170 °C. The degradation temperature of PCF1, PCF2,

PCF3 and PCF4 are 190 °C, 191 °C, 194 °C and 196 °C respectively. The hybrid films exhibited a lower degradation temperature when compared to that of Cs because of the presence of dopant ions incorporated with PPy. After the end of the process at 650 °C, the residual weights of PCF1, PCF2, PCF3 and PCF4 are found to be 32 %, 36 %, 41 % and 40 % respectively. It is observed that the residual weight of hybrid films is slightly higher than that of Cs except that of PCF1 due to the presence of relatively high content of thermally stable PPy. The thermal stability of the hybrid films increases from PCF1 to PCF4.

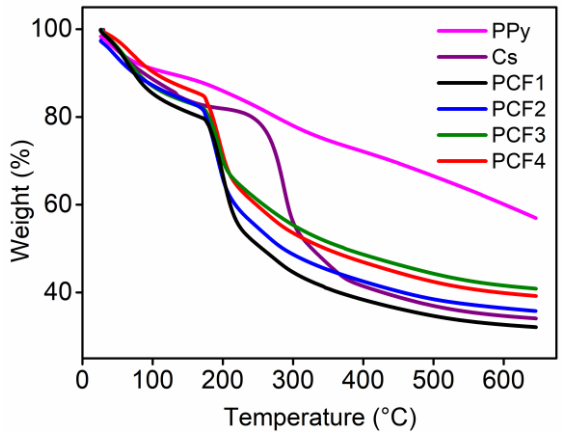

Figure 5.7 *Thermographs of PPy, Cs and PPy/Cs hybrid films*

5.2.1.5. Mechanical studies

The mechanical properties of the PPy/Cs hybrid films were evaluated from the stress-strain curves (Figure 5.8a) and the results are displayed in Figures 5.8b-d. The tensile strength of the hybrid film increases as the content of PPy increases from PCF1 to PCF4. The incorporation of more PPy into the Cs matrix increases the

interaction between PPy and Cs, and restricts the free movement of polymer segments leading to higher tensile strength. The percentage elongation of the hybrid films was also affected by the incorporation of PPy in the Cs matrix. It is observed that the hybrid films show lesser percentage elongation. This decrease in the percentage elongation for the hybrid films from PCF1 to PCF4 is due to the incremental increase in the stiffness of hybrid films that restricts the free mobility of polymer chains and increases the resistance to stretching upon the application of strain. The Young's modulus increases as the number of the coating increase from PCF1 to PCF4. The mechanical characteristics of the hybrid films were good enough to be used as a free standing working electrode for electrochemical studies and the associated applications (sensors, actuators, etc.).

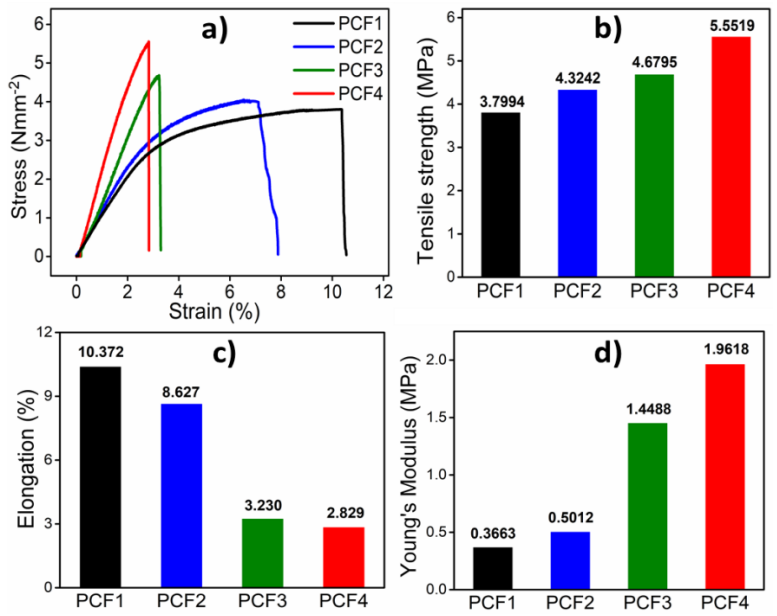

Figure 5.8*(a) Stress-strain curve of PPy/Cs hybrid films, (b) Tensile strength (c) Percentage elongation and (d) Young's modulus of PPy/Cs hybrid films evaluated from the stress-strain curves*

5.2.1.6. Electrochemical characterizations

(a) Cyclic voltammetry

The stationary CVs of all the hybrid films were taken in a conventional three-electrode electrochemical cell with the PPy/Cs hybrid film as the WE, Ag/AgCl (3 M KCl) as the RE and Pt mesh as the CE using aqueous NaCl solution as electrolyte at ambient conditions. A film of length 1 cm and breadth 0.2 cm fixed on a Pt wire by conductive carbon paste was used as the WE. All the hybrid films were allowed to equilibrate in the electrolyte before the application of electrical signals. CVs of the hybrid films were recorded within a potential window of -0.85 V and 0.55 V at a scan rate of 5 mV s^{-1} and the fourth stationary voltammetric responses were taken for the study to remove any structural memory.

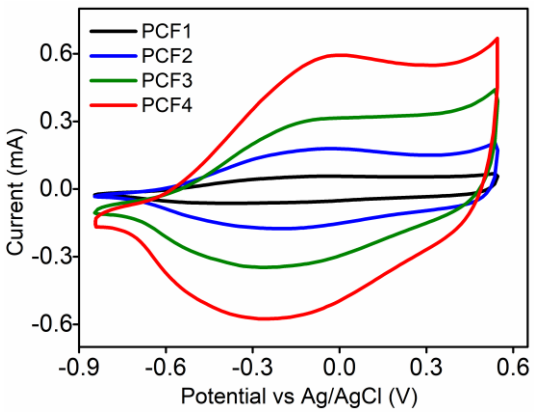

Figure 5.9 *CVs of all PPy/Cs hybrid films at a scan rate of 5mV s^{-1} in 1 M NaCl aqueous solution within a potential window of -0.85 V and 0.55 V*

The stationary CVs of all the hybrid films obtained are presented in Figure 5.9. The CVs revealed that all the hybrid films are electroactive and the electrochemical activity was imparted by PPy.

All the voltammograms consist of a broad anodic peak corresponding to PPy oxidation and a broad cathodic peak corresponding to PPy reduction. The peak potential values are presented in Table 5.3. The scan rate is slow enough to show the redox peaks clearly in the studied potential range. The presence of redox peaks in the CV curves of the hybrid films corresponds to their faradaic redox behavior and also reveals the pseudocapacitance behavior of PPy. Over repeated cycling between the studied potential ranges, no additional peaks (as a result of overoxidation) were generated, indicating excellent stability of the hybrid films. This cyclic voltammogram also illustrates the dominant mechanism of the anion exchange. These anions enter the film during the oxidation process and leave during the reduction process (along with the water molecules). From the CVs, it is observed that as the number of times of coating increases from PCF1 to PCF4, the peak current also increases.

Table 5.3 *Anodic and cathodic potentials of PPy/Cs hybrid films obtained from CV*

Hybrid film	Anodic potential (V)	Cathodic potential (V)
PCF1	-0.06	-0.33
PCF2	-0.04	-0.20
PCF3	-0.07	-0.25
PCF4	-0.02	-0.26

The relationship between scan rate and oxidation-reduction processes was investigated. The cyclic voltammetric responses of all

the hybrid films recorded at different scan rates are presented in Figure 5.10. At higher scan rates, there exists a noticeable deviation in the voltammetric responses than those recorded at lower scan rates. As the scan rate increases from 5 mV s^{-1} to 200 mV s^{-1}, the reduction peaks shift to more negative potentials and the oxidation peaks to more positive potentials. This is convincing because, at higher scan rates, the redox reaction becomes more resistive due to the slow entry/ejection of counter ions through the matrix. The potential shifting and current increase suggest kinetic limitations of the concomitant electrochemical reactions [30]. At lower scan rates, the applied oxidation and reduction potentials promote deeper conformational changes due to the generation/destruction of the increased quantity of free volume to enter/eject an increased number of counterions and solvent molecules.

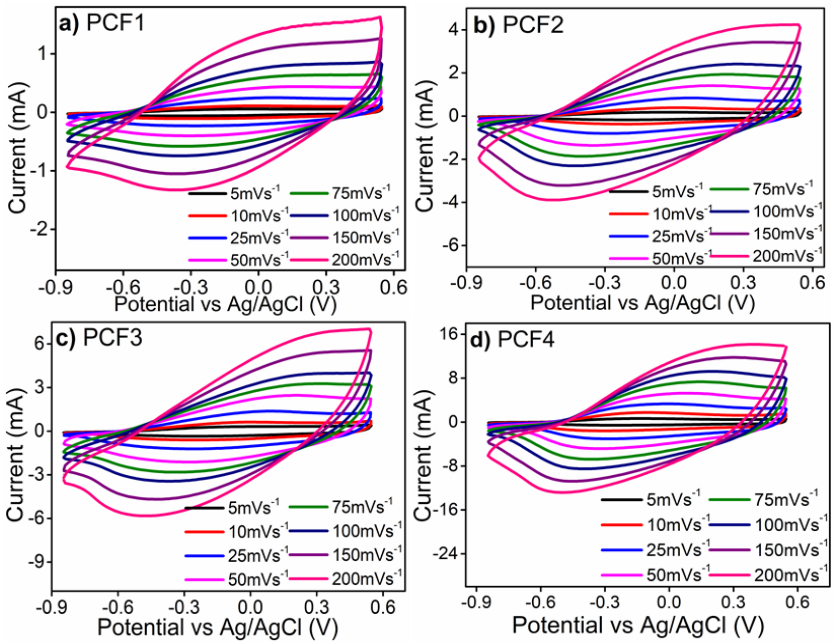

Figure 5.10 *CVs of (a) PCF1, (b) PCF2, (c) PCF3 and (d) PCF4 at different scan rates ranging from 5 mV s^{-1} to 200 mV s^{-1} in 1 M NaCl aqueous solution*

Figure 5.11 exhibits a smooth linear relation of oxidation/reduction peak currents with the square root of scan rates for all the hybrid films. The observed higher correlation coefficient (R^2=0.99) up to 200 mV s^{-1} reveals that the oxidation/reduction processes in PPy/Cs hybrid films are controlled by the ion diffusion process.

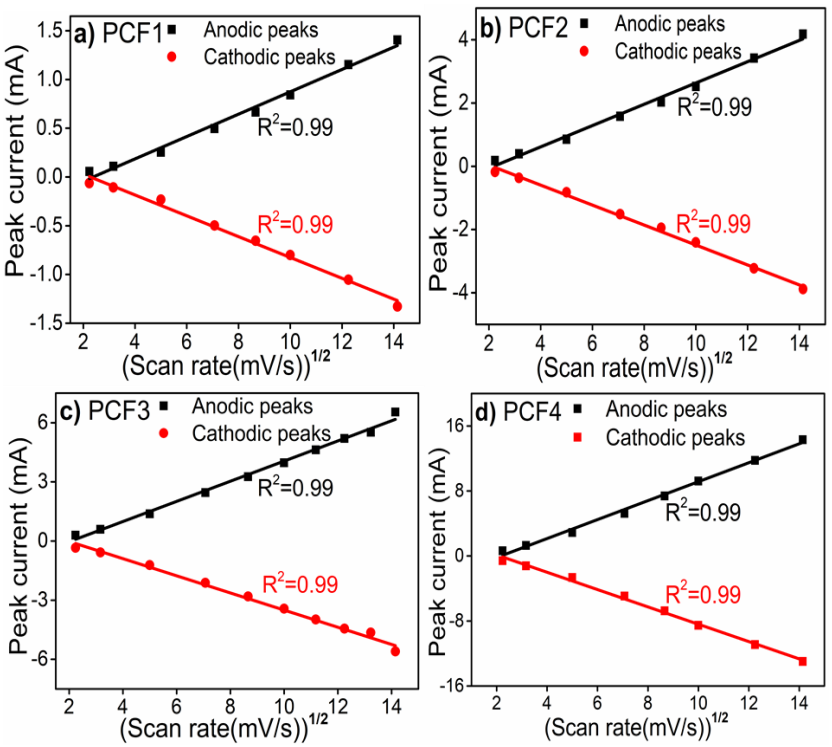

Figure 5.11 *Variation of the intensity of the cathodic/anodic peak current of (a) PCF1, (b) PCF2, (c) PCF3 and (d) PCF4 as a function of the square root of scan rates*

(b) Coulovoltammogram

Figure 5.12a represents the QVs attained by integrating the CVs present in Figure 5.9. It comprises of a closed part on the right and

a small open fraction on the left. The closed loop defines the presence of reversible reactions and the open part represents the parallel irreversible processes. The charge consumed by the reversible redox processes of all the hybrid films is given in Figure 5.12b. As the number of times of coating increases from PCF1 to PCF4, the redox charge (film oxidation/reduction charges) increases due to increase in the electroactive center. Higher PPy content increases the number of ions exchanged during the redox reaction and thus results in the consumption of higher charges.

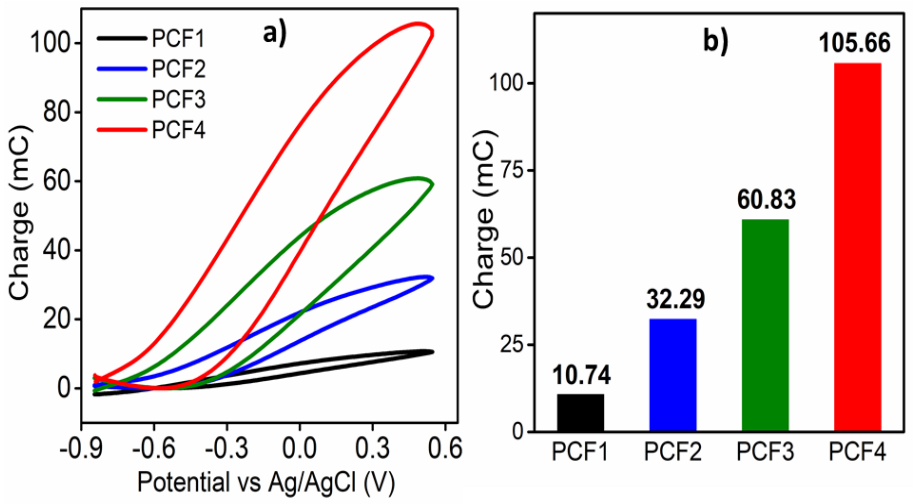

Figure 5.12 *(a) QVs of the hybrid films and (b) Redox charges of PPy/Cs hybrid films obtained from QVs*

5.2.2. Reaction driven sensing characteristics of PPy/Cs hybrid films: Chronopotentiometric investigation

Here, the reaction driven sensing characteristics of PPy/Cs hybrid films towards electrical, chemical and thermal working conditions are studied through chronopotentiometry to prove consumed electrical

energy can as the sensing magnitude. The sensing equations remain the same as that of PPy because the PPy is the electroactive material in the hybrid film.

5.2.2.1. Sensing working electrical condition: Current sensor

The normalized chronopotentiometric responses obtained by applying square current waves of different currents (±0.1 mA to ±1.5 mA) while keeping constant thermal, mechanical and chemical conditions for both the anodic and cathodic processes of all the hybrid films are depicted in Figure 5.13a-d and 5.13e-h respectively. The chronopotentiometric studies of the hybrid films were performed at a constant charge approximately equal to their redox charge obtained from the QVs. For both anodic (Figure 5.13a-d) and cathodic processes (Figure 5.13e-h), an initial potential step is observed before triggering the actual electrode process. As the anodic or cathodic current of the hybrid films increase, the potential evolution takes place at higher anodic or higher cathodic potentials respectively. Figure 5.14a shows a linear evolution (R^2 = 0.99) of consumed electrical energy during the electrochemical redox reaction of all the hybrid films (to attain the same reaction extension) in relation to the applied current. Therefore, consumed electrical energy is an excellent sensor of the working electrical condition (the driving current), and the concomitant line is the calibration line. The sensitivity (slope of the curve) of the hybrid films are improved by the increase in the content of PPy (number of times of coating) from PCF1 to PCF4 (Figure 5.14b). PCF4 shows the highest sensitivity of 129.89 mJ mA^{-1} and -111.80 mJ mA^{-1} for anodic and cathodic processes respectively.

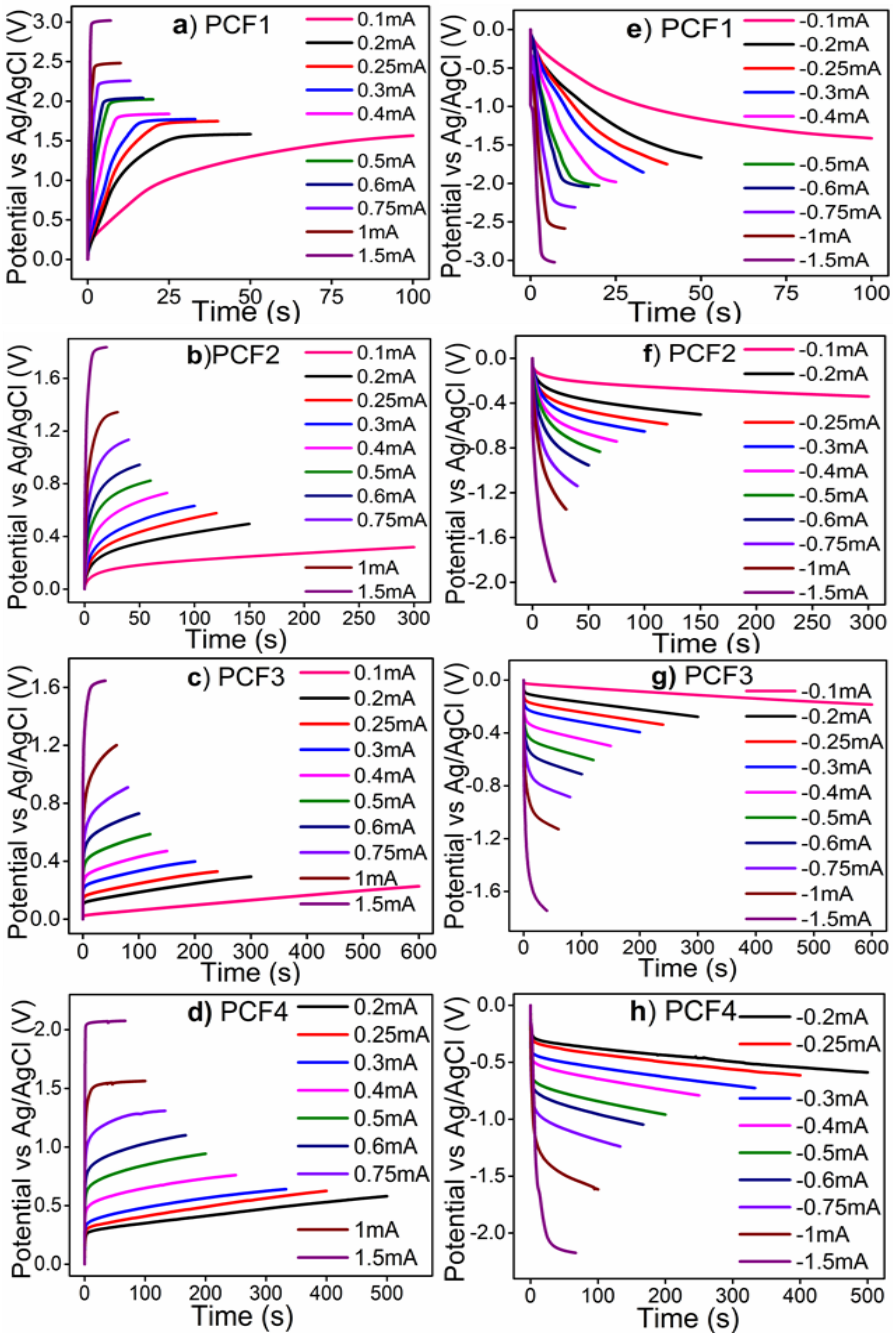

Figure 5.13 *Chronopotentiograms obtained when different constant (a-d) anodic and (e-h) cathodic currents were applied to PPy/Cs hybrid films by passing a constant electrical charge in 1 M NaCl aqueous solution*

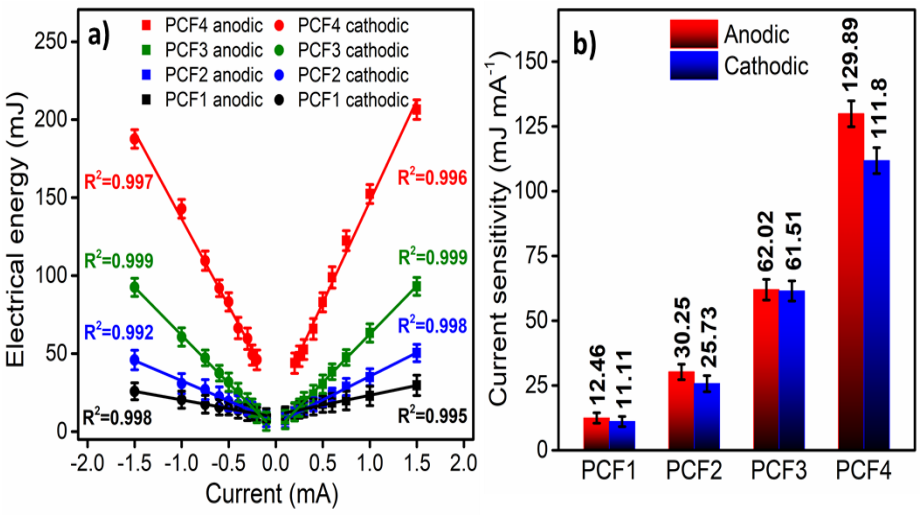

Figure 5.14 *(a) Variation of electrical energy consumed by the PPy/Cs hybrid films with the driving current and (b) Effect of number of times of coating of PPy on current sensitivity*

5.2.2.2. Sensing working chemical condition: Concentration sensor

The normalized chronopotentiometric responses of all the hybrid films were recorded at constant thermal and mechanical conditions by applying a constant current (±0.5 mA) for different concentrations of NaCl ranging from 0.025 M to 1 M at a constant charge approximately equal to their redox charge. Figure 5.15a-d and 5.15e-h show the normalized chronopotentiometric responses for the anodic and cathodic processes of all the hybrid films respectively. During the reversible redox reactions of the hybrid films under the same physical and chemical conditions, for increasing the concentration of electrolytes, the material potential evolution occurs at lower values as expected from the sensing equations 4.19 and 4.20.

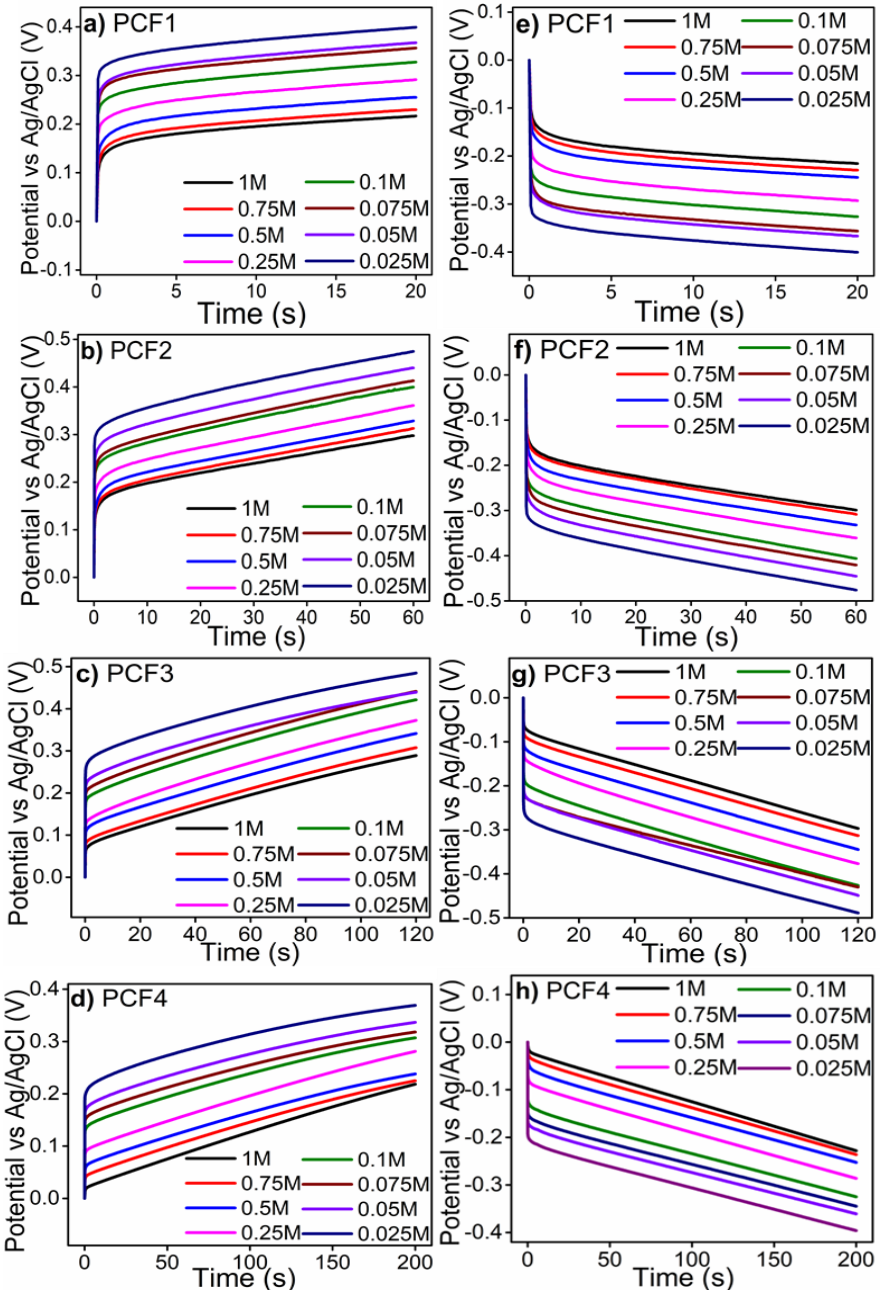

Figure 5.15 *Chronopotentiograms obtained when PPy/Cs hybrid films were subjected to different concentrations of NaCl by applying an anodic current of +0.5 mA (a-d) and a cathodic current of -0.5 mA (e-h) at a constant electrical charge*

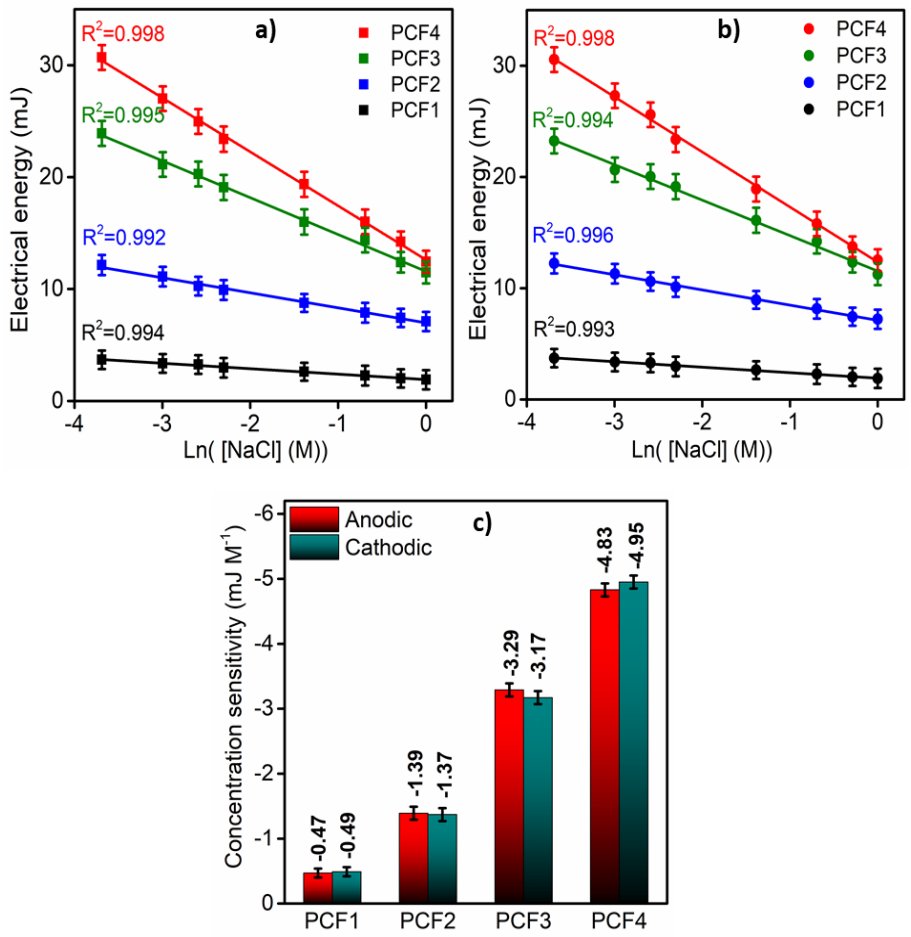

Figure 5.16 *Logarithmic variation of the consumed electrical energy of the hybrid films with the concentration of electrolyte by applying (a) an anodic current of +0.5 mA and (b) a cathodic current of -0.5 mA at a constant charge and (c) Effect of number of times of coating of PPy on anodic and cathodic concentration sensitivity*

Figure 5.16a and 5.16b corroborate the logarithmic dependence of the consumed electrical energy of the hybrid films with electrolyte concentration for the anodic and cathodic processes respectively. As the available chemical energy increases, the consumption of electrical energy occurs at lower values for attaining the same reaction

extension [31]. The attained linear relationships (R^2 = 0.99) indicate that the energy consumed by the hybrid films senses or responds to the working chemical condition (electrolyte concentration). The slope of the curves defines the chemical sensitivity of the hybrid film which is improved by the increase in the content of PPy (number of times of coating) from PCF1 to PCF4, and PCF4 (Figure 5.16c) shows the highest sensitivity of -4.83 mJ M^{-1} and -4.95 mJ M^{-1} for anodic and cathodic processes respectively. Thus PPy/Cs hybrid films are proven to be working as concentration sensor.

5.2.2.3. Sensing working thermal condition: temperature sensor

The temperature sensing capability of the PPy/Cs hybrid films was examined by recording chronopotentiometric responses at different temperatures ranging from 10 ˚C to 50 ˚C under consecutive square current waves of ±0.5 mA in 1 M NaCl aqueous solution by keeping all other variables constant (at a constant charge approximately equal to their redox charge). Figure 5.17a-d and 5.17e-h show the normalized chronopotentiometric responses of the hybrid films for the anodic and cathodic processes respectively. It can be seen that for the anodic processes, the potential decreases with a gradual increase of temperature and for the cathodic processes, a similar, but inverse, behavior is observed. As the available thermal energy increases, there occurs faster and longer conformational movements of the polymer chains and therefore, the reaction requires the consumption of lower electrical energies to achieve the same reaction extension. Thus for rising temperatures at a constant current applied for the same time, the reaction occurs at lower potentials (lower resistance).

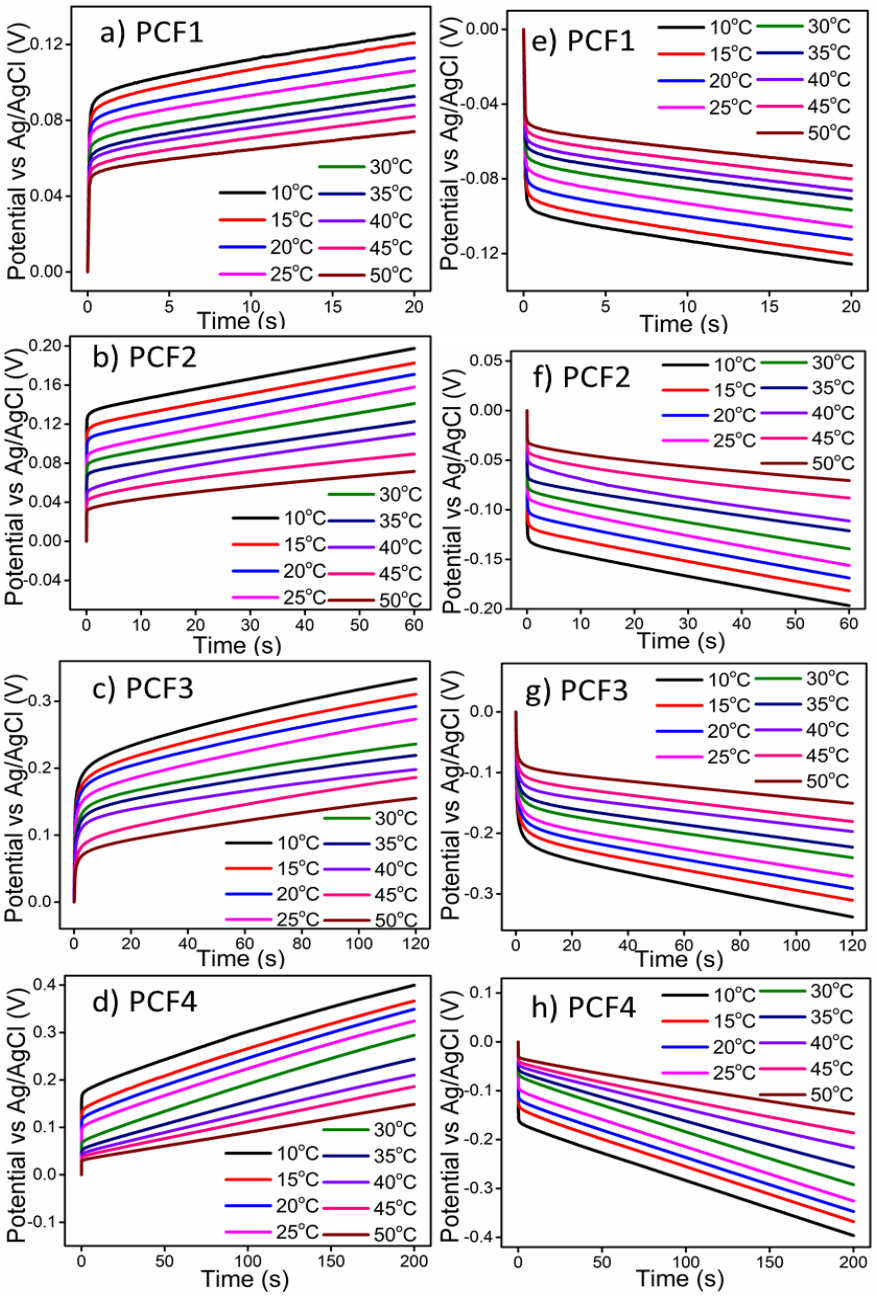

Figure 5.17 *Chronopotentiograms attained at different temperatures by applying an anodic current of +0.5 mA (a-d) and cathodic current of -0.5 mA (e-h) at a constant electrical charge*

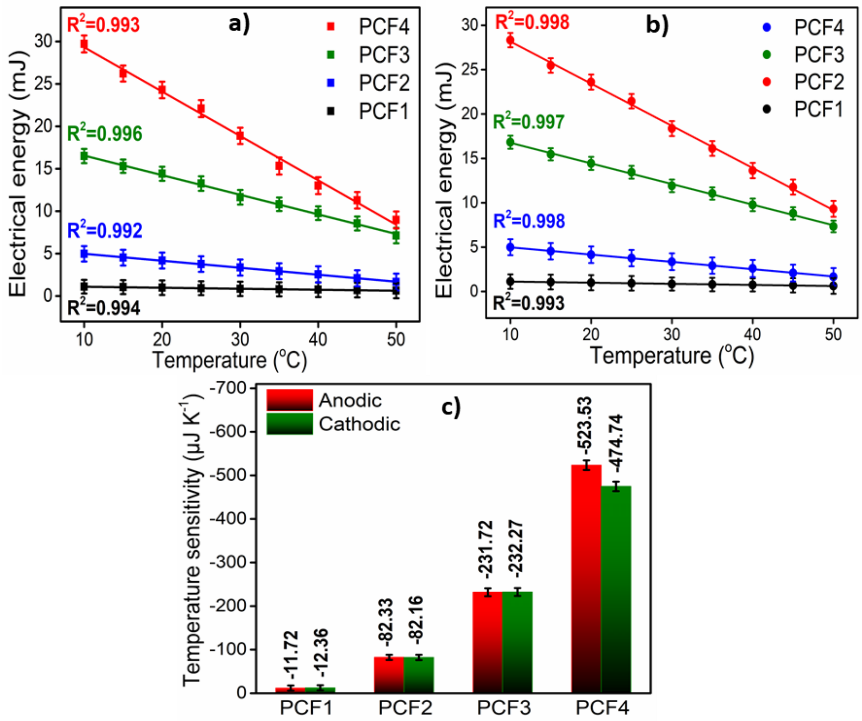

Figure 5.18 *Variation of electrical energy consumed by the PPy/Cs hybrid films with the experimental temperature by applying (a) an anodic current of +0.5 mA and (b) a cathodic current of -0.5 mA at a constant charge and (c) Effect of number of times of coating of PPy on temperature sensitivity*

Figure 5.18a and 5.18b shows a linear relationship of electrical energies consumed during the reactions with temperature of all the hybrid films. The energy consumed by the hybrid films (the macromolecular motors) to get the same reaction extension decreases when the temperature increases. Thus, at any time, the consumed energy of the hybrid films senses or responds to the temperature and the concomitant lines are the calibration lines. The sensitivities of the hybrid films to the experimental temperature being the slopes of the plots increases as the number of times of coating (the content of PPy) increases (Figure 5.18c). As a thermal sensor,

PCF4 having a high content of PPy presents the highest sensitivity of -523.53 μJ K^{-1} and -474.74 μJ K^{-1} for the oxidation and the reduction processes respectively.

5.2.3. Reaction driven sensing characteristics of PPy/Cs hybrid films: Voltammetric investigation

Here, the reaction driven sensing characteristics of PPy/Cs hybrid films towards electrical, chemical and thermal working conditions are studied through cyclic voltammetry to prove consumed electrical charge as the sensing parameter.

5.2.3.1. Sensing working electrical condition

The CV responses of all the hybrid films recorded at different electrical energetic conditions, i.e., scan rates, by keeping all other experimental conditions constant are displayed in Figure 5.10a-d. As the scan rate increases, the peak current corresponding to anodic and cathodic processes increases for all the hybrid films. The stationary QV responses corresponding to the CVs in Figure 5.10a-d are presented in Figure 5.19a-d. As the scan rate increases, the redox charge consumed during the reversible reactions driving the conformational movements of the reactive polymeric chain decreases for all the hybrid films. When the scan rate is low, the oxidation and reduction potentials are applied for large time intervals and promote deeper conformational changes with the consumption of large redox charges. Thus we get deeper oxidation/reduction states at low scan rates. As the scan rate increases, the time available for the reaction 3.1 to extract the electrons

from the polymer chain and to drive the conformational movements of the reactant polymeric chains is low and the polymer chains become partially oxidized.

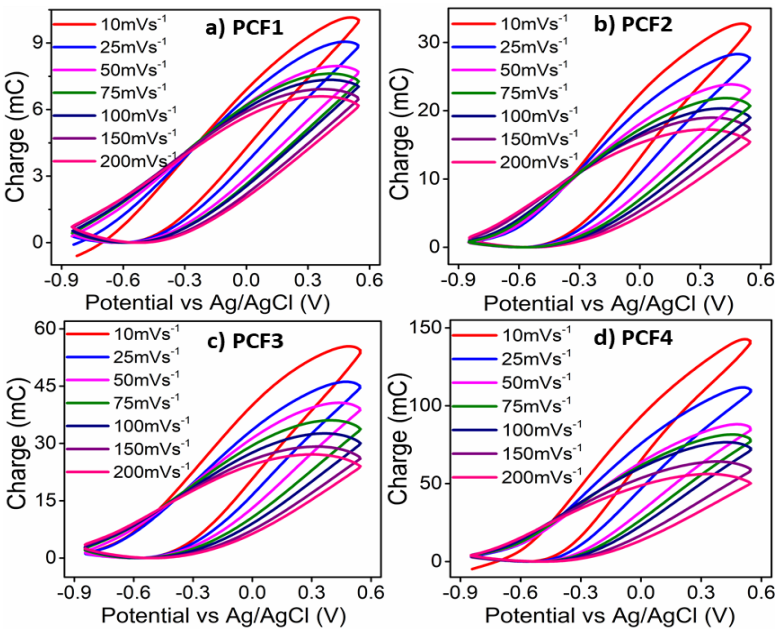

Figure 5.19 *QV responses of PPy/Cs hybrid films at different scan rates*

Figure 5.20a displays the double logarithmic variation of the consumed charge or extension of the reaction with the scan rate. The experimental results are in good agreement with the sensing equation 4.34. The slope of the calibration curves represents the sensitivity of the sensor. The sensitivity is improved as the number of times of coating increases, i.e., from PCF1 to PCF4 (Figure 5.20b). The linear fit of the curves corroborate that the consumed charge during the redox reactions of PPy can act as a robust sensor of the imposed electrical energetic condition while keeping all other surrounding variables (thermal, mechanical and chemical) constant.

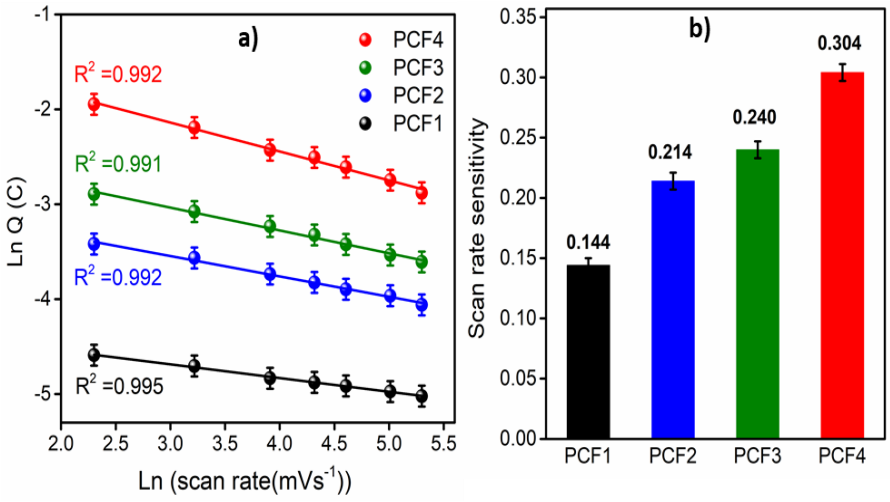

Figure 5.20 *(a) Linear variations showing the double-logarithmic relationship between the charges consumed by the reversible reactions of PPy/Cs hybrid films with the scan rate and (b) Effect of number of times of coating of PPy on scan rate sensitivity*

5.2.3.2. Sensing working chemical condition

Figure 5.21a-d represents the stationary voltammetric responses obtained for the hybrid films at different concentrations of the electrolyte when it is cycled between −0.85 V and 0.55 V versus Ag/AgCl at 10 mV s^{-1} at room temperature. The peak current increases gradually with an increase in electrolyte concentration for all the hybrid films as like pure PPy. The CVs in Figure 5.21a-d were integrated and the corresponding QV responses were presented in Figure 5.21e-h. The QV responses show a closed loop and a small open fraction in the investigated potential range for PCF1, PCF2 and PCF3. The sample PCF4 shows only a closed loop in the studied potential range. The redox charge consumed by the reaction of the hybrid films increases for increasing the concentration of the electrolyte.

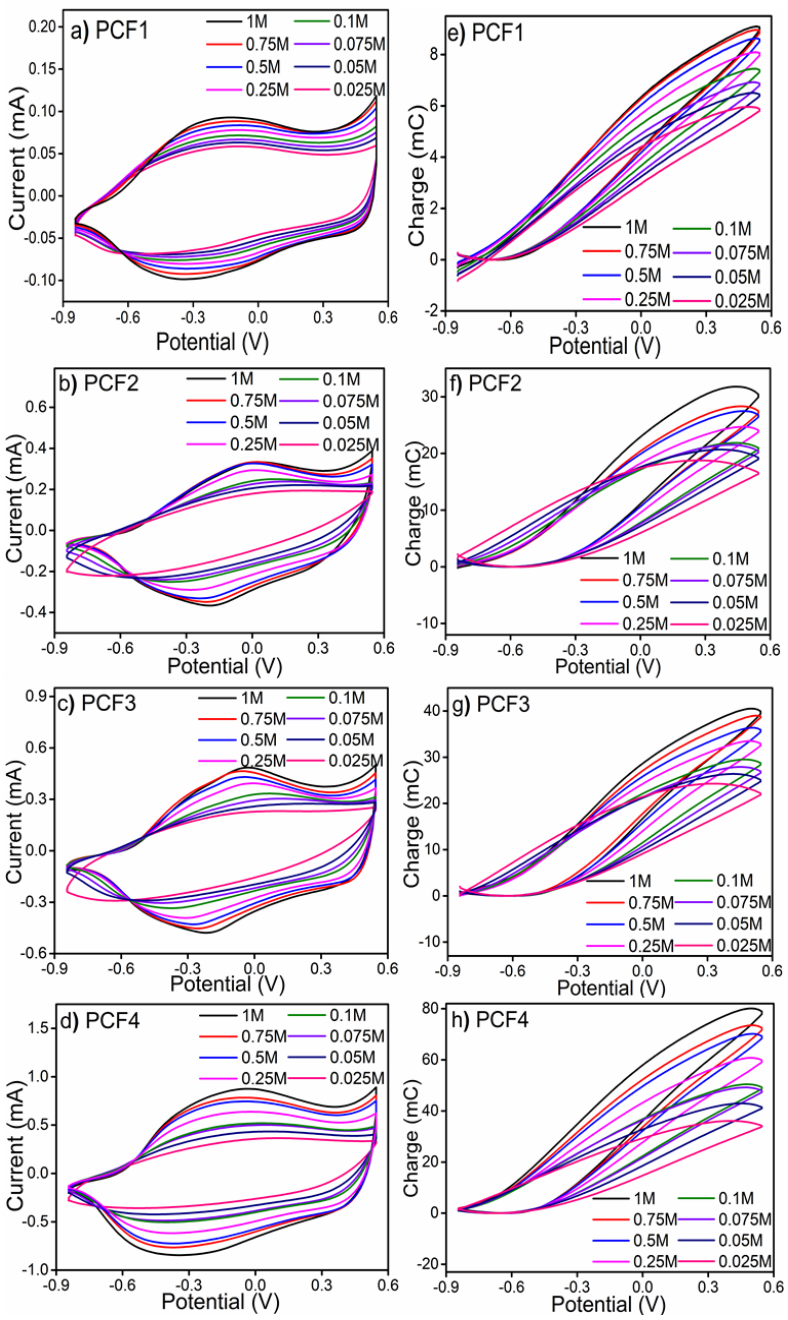

Figure 5.21 *(a-d) Stationary CV responses of PPy/Cs hybrid films at different concentrations of NaCl aqueous solutions and (e-h) QVs obtained at different electrolyte concentrations*

As mentioned earlier, at a low concentration of electrolyte, the chemical energy available for the reaction 3.1 to extract the electrons from the polymer chain and to drive the conformational movements from the reactant polymeric chains is low and the polymer chains become partially oxidized. When the concentration of the electrolyte increases, the available chemical energy increases and we get deeper oxidation states with the consumption of large charges.

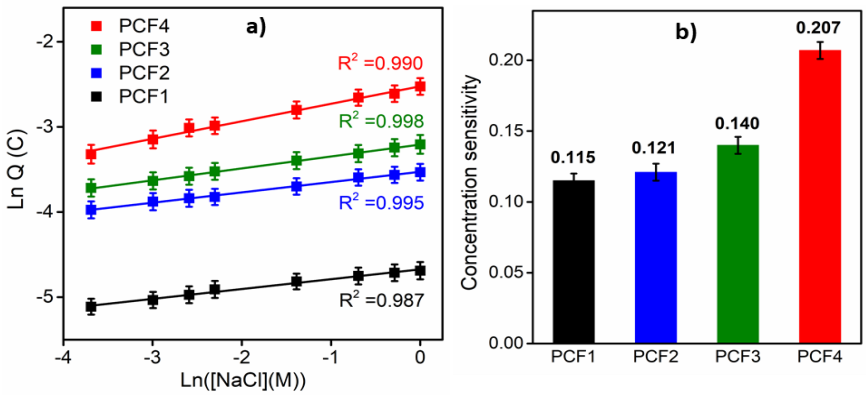

Figure 5.22 *(a) Double logarithmic variation of the consumed electrical charge of PPy/Cs hybrid films with concentration of electrolyte and (b) Effect of number of times of coating of PPy on concentration sensitivity*

Figure 5.22 shows the double logarithmic variation of the redox charge with the electrolyte concentration. The attained linear relationship indicates that the consumed redox charge of any electrochemical device based on the reversible reactions of PPy/Cs hybrid films can act as a self-sensor of surrounding chemical conditions. The chemical sensitivity of the fabricated hybrid films is quantified from the slope of the curves. It is found that the sensitivity increases as the PPy content in the hybrid film increases, and the highest sensitivity of 0.207 is obtained for PCF4.

5.2.3.3. Sensing working thermal condition

Figure 5.23a-d displays the stationary voltammetric response of the PPy/Cs hybrid films recoded at different temperatures ranging from 10 ˚C to 50 ˚C when it is cycled between −0.85 V and 0.55 V versus Ag/AgCl at 10 mV s^{-1} in 1 M NaCl aqueous solution. Both the anodic and cathodic peak currents increase with the increase of temperature. The stationary QV responses obtained by integrating the CVs shown in Figure 5.23a-d are presented in Figure 5.23e-h. We get deeper oxidation/reduction states at higher temperatures. It is observed that for PCF1, the QVs constitute a closed loop and a small open fraction in the studied potential interval. The QV of PCF2, PCF3 and PCF4 shows only closed loops in the studied potential range which is related to the PPy reversible oxidation/reduction reactions. For all the hybrid films, the redox charge consumed by the reversible electrochemical reaction that drives reversible conformational movements increases with increasing temperature.

The low temperature (low available thermal energy) allows partial conformational movements of the reactant polymeric chains and generates a low amount of free volume to insert the counterions and the solvent molecules with concomitant consumption of low oxidation charge [32]. Thus the polymer chains undergo partial oxidation/reduction at low temperatures [33]. As the experimental temperature increases, the increased available thermal energy allows faster and longer conformational movements of the polymeric chains with the consumption of increasing redox charges and we get deeper oxidation/reduction states at higher temperatures.

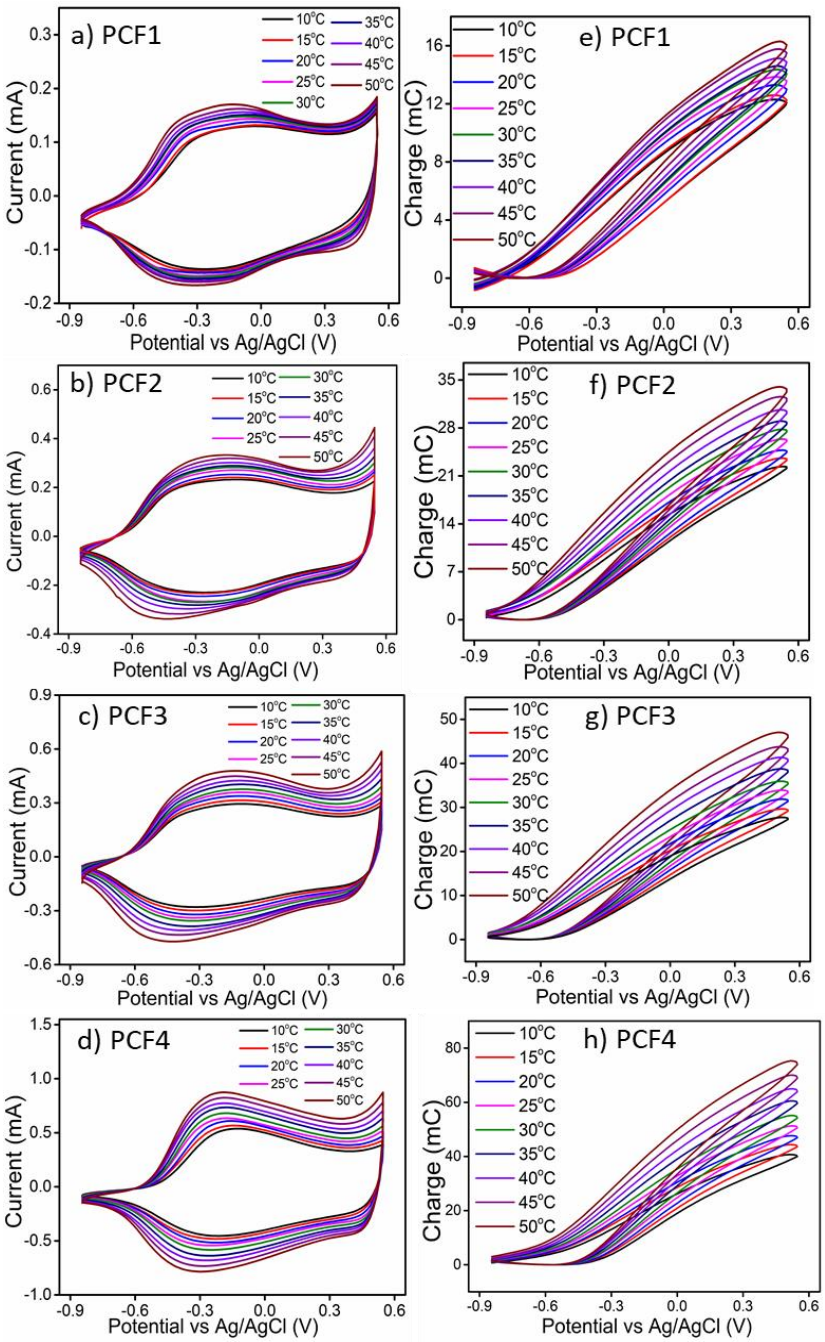

Figure 5.23 (*a-d) Stationary CV responses of PPy/Cs hybrid films at different temperatures and (e-h) QVs obtained at different temperatures*

Figure 5.24a shows the logarithmic variation of the redox charge with the experimental temperature. The attained linear relationships (R^2 = 0.99) indicates that the consumed redox charge of any electrochemical device based on the reversible reactions of PPy/Cs hybrid films senses or responds to the working thermal condition. The slope of the curves defines the temperature sensitivity of the hybrid films. The sensitivity is improved as the content of PPy increases i.e. as the number of times of coating increases from PCF1 to PCF4, and PCF4 presents the highest sensitivity of -1405.7 (Figure 5.24b).

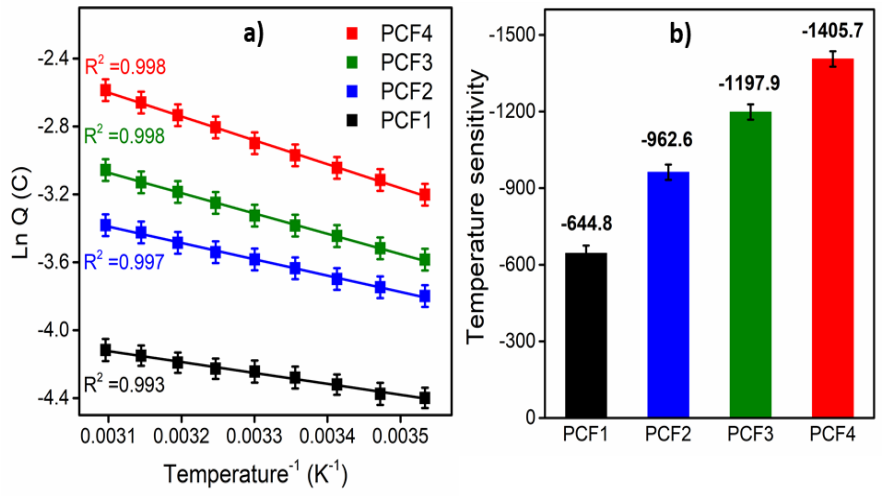

Figure 5.24 *(a) Logarithmic variation of the electrical charge consumed by the reversible redox reactions of the hybrid films with the inverse of the temperature and (b) Effect of number of times of coating of PPy on temperature sensitivity*

5.2.4. Supercapacitive studies

The feasibility of the use of all four PPy/Cs hybrid films as a free standing supercapacitor electrode material was evaluated using

GCD, CV and EIS measurements in a three electrode configuration. The GCD curves of the hybrid films operated at a current density of 0.2 A g^{-1} within the potential window of -0.85 V to 0.55 V in 1 M aqueous NaCl solution are given in Figure 5.25a. The GCD profiles are non-linear revealing the pseudocapacitive performance of the hybrid films. From the GCD plots, PCF4 exhibited the longest discharge period, indicating that it has the highest capacitance among all the films. The specific capacitance of the hybrid films was calculated using the equation 2.7. Through calculation, the specific capacitances achieved at a current density of 0.2 A g^{-1} for PCF1, PCF2, PCF3 and PCF4 are 95 F g^{-1}, 122 F g^{-1}, 362 F g^{-1} and 559 F g^{-1} respectively. That is, the supercapacitance increases as the number of times of coating (or electrical conductivity) increases (Figure 5.25b). The charge storage ability of the PPy/Cs hybrid films depends on the movement of electrons as well as the transfer of counterions.

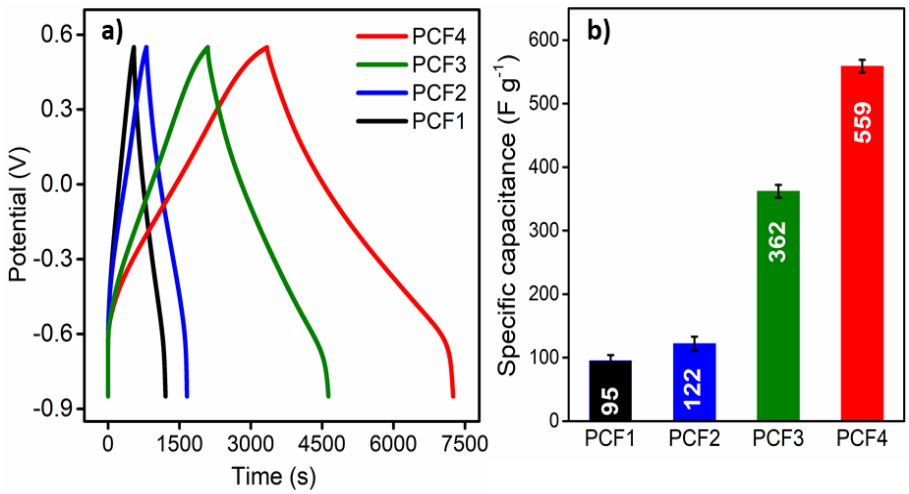

Figure 5.25 *(a) GCD curves of PPy/Cs hybrid films at a current density of 0.2 A g^{-1} and (b) The specific capacitance of all the hybrid films obtained from GCD profiles*

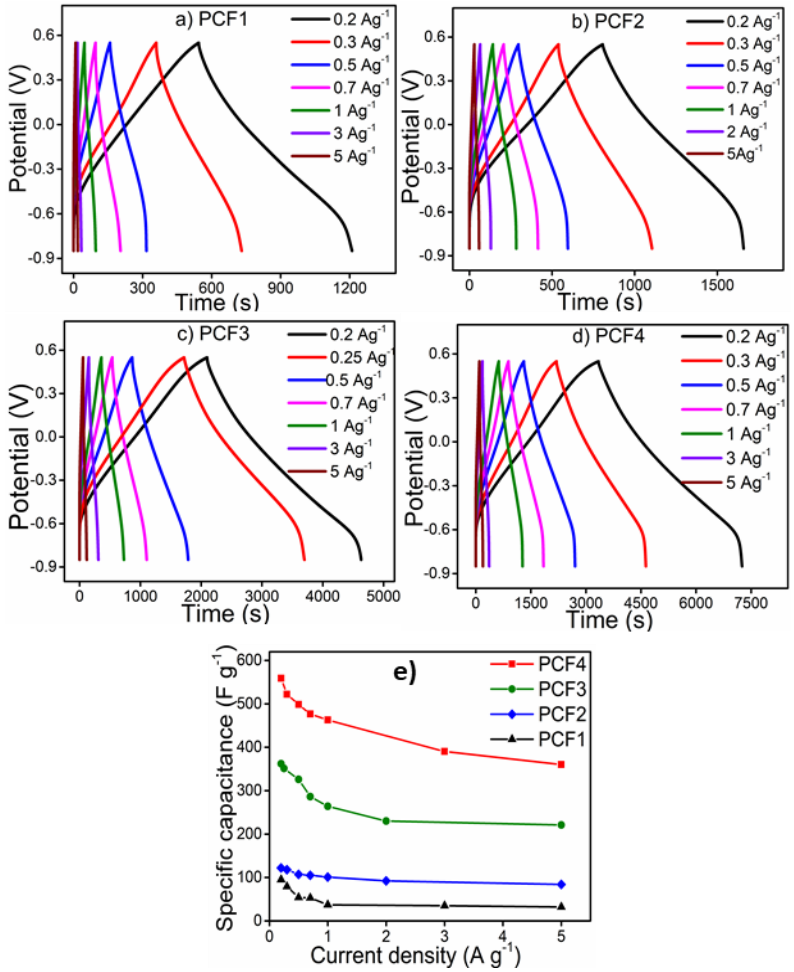

Figure 5.26 *GCD curves of (a) PCF1, (b) PCF2, (c) PCF3 and (d) PCF4 at different current densities, (e) The specific capacitance of all PPy/Cs hybrid films as a function of current density*

The charge-discharge properties of all the hybrid films were investigated under various current densities and the corresponding plots are shown in Figure 5.26a-d. Figure 5.26e represents the variation of specific capacitance as a function of specific current. There is less time for the electrolyte to interact with the hybrid film electrode at higher current densities and thus, the specific capacitance decreases with

increasing current density. The cycling stabilities of all the hybrid films were accessed over 1500 GCD profiles at 2 A g^{-1} and are shown in Figure 5.27a. The capacitance retention of the hybrid films continues to decline during the cycling process and is mainly attributed to the repeated swelling and shrinking that occurs in the polymer chains. It is worth mentioning that the cycle life is improved as the content of PPy or the number of times of coating increases (Figure 5.27b). Among the hybrid films, PCF4 retains 86 % of its initial capacitance after 1500 cycles indicating a good long-term cycle life.

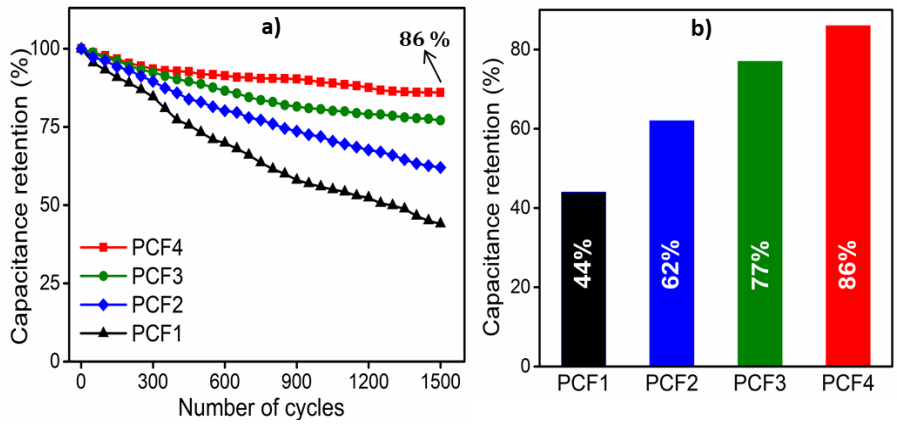

Figure 5.27 *(a) Cycling stability of all hybrid films for 1500 cycles and (b) Effect of number of times of coating of PPy on cycling stability of the hybrid films*

The capacitance of the hybrid film electrodes was further examined from CVs (Figure 5.9) using equation 2.5. The non-rectangular profile of the curves and the presence of a pair of redox peaks in the CV curves revealed the faradaic pseudocapacitive dominance prevailing in the hybrid films [34]. Moreover, the shift of oxidation peaks to more anodic potential and reduction peaks to more cathodic potentials is a common feature of pseudo-capacitive behavior.

The area encompassed by the CV profile is proportional to the capacitance of the hybrid films. PCF4 showed the largest area with much boosted current, revealing that it has the highest specific capacitance and lowest internal resistance than the other hybrid films. The specific capacitance values calculated at a scan rate of 5 mV s^{-1} for PCF1, PCF2, PCF3 and PCF4 are 79 F g^{-1}, 222 F g^{-1}, 414 F g^{-1} and 717 F g^{-1} respectively (Figure 5.28a). As the scan rate increases, the specific capacitance decreases (Figure 5.28b). This is because, at a low scan rate, the longer time allows the insertion of more anions into the electrode material. At high scan rates, the electrolyte does not have sufficient time to reach the internal sites of the electrode material effectively and has little contribution to the capacitive behavior resulting in a decrease in the specific capacitance values. The specific capacitance of PCF4 is compared with those of various PPy based supercapacitors reported in the literature, which are listed in Table 5.4.

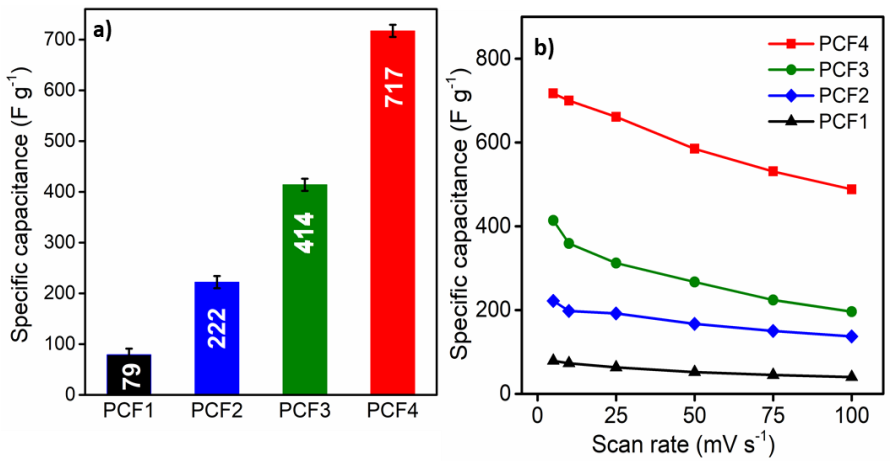

Figure 5.28 *(a) The specific capacitance of the hybrid films obtained from CV and (b) Variation of specific capacitance of all PPy/Cs hybrid films as a function of scan rate*

Table 5.4 *Capacitive performance of PPy based supercapacitors*

Electrode materials	Specific capacitance ($F\ g^{-1}$)	Capacitance retention	Ref.
PCF4	**559 at 0.2 A g^{-1} 717 at 5 mV s^{-1}**	**86 % (1500 cycles)**	**This work**
Graphene/PPy aerogel	253 at 0.5 A g^{-1}	93 % (2000 cycles)	[35]
RuO_2/PPy	302 at 0.5 A g^{-1}	90 % (300 cycles)	[36]
CNT/PPy/MnO_2 Sponges	325 at 2 mV s^{-1}	90 % (1000 cycles)	[37]
RGO-PPy-Mn hydrogel	356 at 1 A g^{-1}	-	[38]
PPy/rGO-CTAB composite	325 at 0.5 A g^{-1}	64 % (500 cycles)	[39]
PPy/GH	316 at 5 A g^{-1} 375 at 10 mVs^{-1}	87 % (4000 cycles)	[40]
CQDs/PPy-NW	306 at 0.5 A g^{-1}	-	[41]
PPy/RGO	280 at 5 mV s^{-1}	92 % (10000 cycles)	[42]
PPy/GNS	482 at 0.5 A g^{-1}	96 % (1000 cycles)	[43]
rGO/PPy aerogel	304 at 0.5 A g^{-1}	58.26 % (50 cycles)	[44]
PPy hydrogel	328 at 1 A g^{-1}	90 % (3000 cycles)	[45]
PPy hydrogel	380 at 0.2 A g^{-1}	93 % (3000 cycles)	[46]
PPy	329 at 5 mV s^{-1}	78 % (3000 cycles)	[47]

PPy/graphite	400 A g^{-1}	-	[48]
PPy nanoplates	533 at 5 mV s^{-1}	78 % (5000 cycles)	[49]
PPy nanoparticles	398 at 0.1 A g^{-1}	-	[50]
PPy/Nafion	380 at 10 mV s^{-1}	80 % (5000 cycles)	[51]
PPy/PTS	420 at 10 mV s^{-1}	-	[51]

CNT- carbon nanotube; RGO- reduced graphene oxide; CTAB- cetyltrimethylammonium bromide; GH- graphene hydrogel; CQDs- carbon quantum dots; NW- nanowire; GNS- graphene nanosheets; PTS- paratoluenesulfonate.

5.2.4.1. Charge Storage Kinetic Studies

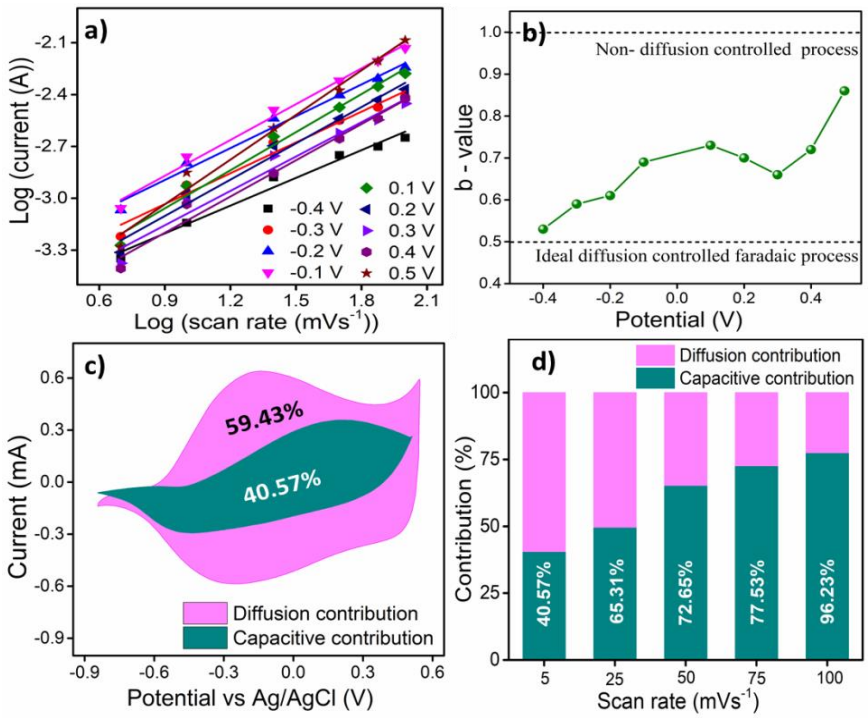

Figure 5.29 *(a) Linear relationship of log (current) versus log (scan rate) at different potentials, (b) The b-values at different potentials, (c) Separation of the pseudocapacitive and diffusion currents at a scan rate of 5 mV s^{-1} and (d) Contribution of capacitances from the surface-controlled pseudocapacitive reaction and diffusion-controlled processes at various scan rates*

The total capacitance of an electrode is contributed from both surface capacitive effects and diffusion-controlled faradaic processes. From the CV data at various scan rates, the current response of an electrode at a specific voltage is controlled by the following power-law equations 5.1 and 5.2 [52, 53].

$$i = av^b \tag{5.1}$$

$$\log i = \log\ a + b \log\ v \tag{5.2}$$

where i is the current, ν is the scan rate, a and b are constants. When the b value is 0.5, the electrochemical reaction at the electrode is limited by the diffusion controlled process (a pseudocapacitive feature), and when the b value is 1, the electrode shows capacitive-type behavior with a predominant surface controlled process (an EDLC feature). Figure 5.29a demonstrates a linear relationship of log (current) with log (scan rate) at different potentials and the b-value can be extracted from the slope of the linear fitting. The calculated b values of PCF4 hybrid film at different potentials are illustrated in Figure 5.29b and it lies between 0.5 and 1 for different potentials. Thus the electrode is expected to have both pseudocapacitive and EDLC like behavior. The respective contribution of both the processes can be quantified by the Dunn method by separating the current (i) into capacitive effects (k_1v) and diffusive effects ($k_2v^{1/2}$) as given below [54, 55].

$$i = k_1 v + k_2 v^{1/2} \tag{5.3}$$

where k_1 and k_2 represents the capacitive and diffusion contributions respectively and can be determined by plotting $i/v^{1/2}$ versus $v^{1/2}$.

Figure 5.29c shows that at a low scan rate of 5 mV s^{-1}, the capacitive (or pseudocapacitive) contribution is 40.57 % with a diffusive contribution of 59.43 %. The percentage of capacitive and diffusion contributions are measured at various scan rates. Figure 5.29d indicates that when the scan rate increases, the capacitive contribution increase and the diffusive contribution decrease. This is because at higher scan rates, the electrolyte does not have sufficient time to reach the internal sites of the electrode material effectively and therefore the surface controlled capacitive effects predominates.

5.2.4.2. Electrochemical impedance spectra

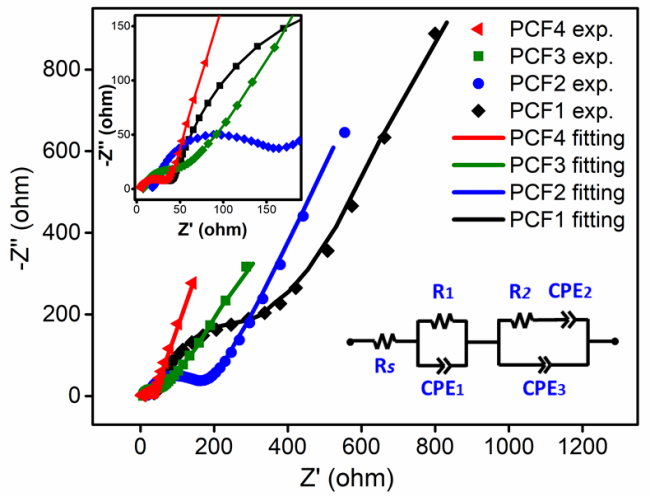

Figure 5.30 *Nyquist plot of PPy/Cs hybrid films (inset: equivalent circuit used to fit the impedance spectrum)*

EIS was performed to assess the fundamental behavior of PCF1, PCF2, PCF3 and PCF4 at an open-circuit voltage of 10 mV in a frequency range from 0.1 Hz to 100 kHz using a three electrode cell configuration .The Nyquist plots are shown in Figure 5.30.

The inset shows the magnified high-frequency region. The Nyquist plots of all the electrodes show a capacitive behavior, comprised of a semicircle in the high-frequency part and a nearly straight line in the low-frequency part. The equivalent series resistance (ESR) which is a combination of the solution resistance, intrinsic resistance and interfacial resistance between the electrode and current collector can be obtained from the intercept of the impedance curve at the real axis in the high-frequency region [40]. From the Nyquist plots, the ESR of PCF1, PCF2, PCF3 and PCF4 are 25.9 Ω, 16.69 Ω, 7.33 Ω and 2.45 Ω respectively. PCF4 shows the smallest ESR value compared with other electrodes, suggesting that more number of counterions and solvents can penetrate in and out of the hybrid film. The diameter of the semicircle at the high-frequency region displays the charge transfer resistance (Rct) resulting from faradaic reactions and double-layer capacitance at the interface of the electrode and electrolytic solution [56]. Here, as the content of PPy in the hybrid film increases, the diameter of the semicircle shows a decreasing tendency. It indicates that the charge transfer resistance of the hybrid films decreases as the number of times of coating or electrical conductivity increases, i.e., from PCF1 to PCF4. The faradaic reactions of PPy also cause an increase in the electrode/electrolyte interface. In the low-frequency region, the straight line is related to the diffusion-limited ion transport process and its slope gives the diffusion resistance. Among the hybrid films, PCF4 exhibited the highest slope and hence has a lower diffusion resistance. The highest slope also indicated that PCF4 have better supercapacitor behavior than other hybrid films. The EIS results are in agreement with the CV and GCD results.

An equivalent circuit model (inset of Figure 5.30) is proposed to fit the impedance curves by Zman software. In the circuit diagram, R_S, R_1 and R_2 signify the solution resistance, charge transfer resistance and diffusion resistance respectively. CPE_1, CPE_2 and CPE_3 are used to express the constant phase elements. The best fitting values are summarized in Table 5.5 with resistance values in ohm and CPE values in S s^{α}. The Y is the CPE parameter and α is the dispersion coefficient.

Table 5.5 *Equivalent circuit parameters of EIS of PPy/Cs hybrid films*

Electrode	**PCF1**	**PCF2**	**PCF3**	**PCF4**
R_S (Ω)	25.9	16.69	7.33	2.45
R_1 (Ω)	228.44	185.15	69.68	31.5
R_2 (Ω)	434.51	305.02	243.38	3.91
CPE_1-Y (S s^{α})	0.0000129	0.0002012	0.000189	.000208
CPE_1-α	0.814	0.623	0.898	0.662
CPE_2-Y (S s^{α})	0.00139	0.00372	0.00469	0.00528
CPE_2-α	0.637	0.688	0.722	0.764
CPE_3-Y (S s^{α})	0.00011	0.00072	0.0036	0.00404
CPE_3-α	0.566	0.636	0.732	0.831

5.3. Conclusion

Electroactive PPy/Cs hybrid films constituted by macromolecular electrochemical motors were fabricated using chemical coating of PPy on Cs film through an in situ chemical polymerization of pyrrole in an

aqueous medium employing ferric chloride as a catalyst. This strategy provides the basis for the large-scale fabrication of CP/hydrogel hybrid free standing films that can act as active electrode material for many electrochemical devices. The as-synthesized PPy/Cs hybrid films were well-characterized using FTIR spectroscopy, FESEM, electrical conductivity measurement, TGA, UTM analysis and cyclic voltammetry. The hybrid films comprised of agglomerated granular morphology of PPy grown on the surface of the Cs film with sufficient porosity enabling the efficient diffusion of ions and solvents for the electrochemical redox reaction with the electrolyte. The conductivity, tensile strength, Young's modulus and redox charge of hybrid films increases as the number of times of coating increases, i.e. from PCF1 to PCF4. The PPy component is accountable for the excellent electroactivity and good electronic conductivity of the hybrid films and chitosan provides mechanical stability.

During the reactions of electrochemical motors under galvanostatic conditions, the consumed electrical energy follows a linear relationship with driving current and experimental temperature and a logarithmic relationship with electrolyte concentration. The results prove that the films can act as sensors of imposed reaction ambient conditions while working. Under potentiodynamic conditions, the extension of the reaction or the consumed charge from the coulovoltammetric responses senses the working electrical, chemical and thermal ambient. Deeper oxidation/reduction states (with an increase of oxidation/reduction charge) were obtained for increasing energetic working conditions. At any reaction time, the consumed

charge varies as a double logarithmic function of scan rate and electrolyte concentration and a logarithmic function of the inverse of temperature (reaction self-awareness). The sensitivities of the hybrid films with regard to applied current, temperature and electrolyte concentration are improved by an increase in the number of times of coating or increase in the content of PPy and the fourth coated hybrid film (PCF4) shows best sensitivities. The hybrid film is considered here as a model material that replicates the reactions taking place in the biological muscles. The similarity of the polymeric chains with biological muscles in simultaneously sensing the working condition suggests the possibility of constructing biomimetic sensing motors using PPy/Cs films in which the driving and sensing signals can be read at any instant of the reaction, through the same two connecting wires. Thus, one reaction drives, many functions in a single material.

The non-rectangular profile of the CV curves and the presence of a pair of redox peaks revealed the faradaic pseudocapacitive dominance prevailing in the hybrid films. Related to the energy storage, the specific capacitance increases as the number of times of coating increase and PCF4 shows the highest capacitance (559 F g^{-1} at 0.2 A g^{-1}) and better cycle life (86 % retained capacitance after 1500 cycles at 2 A g^{-1}) than other films, suggesting it as a high-performance electrode material for the next-generation supercapacitors. The charge storage kinetic studies were analysed by Dunn's method and PCF4 shows 40.57 % the capacitive (or pseudocapacitive) contribution and 59.43 % diffusive contribution at a scan rate of 5 mV s^{-1}. EIS studies revealed that, due to better electrical conductivity

and electroactivity of PCF4, it shows low charge transfer resistance, solution resistance and diffusion resistance than other films indicating its high electrochemical performance. The highest slope exhibited by PCF4 in the low frequency region of EIS spectra also indicated its better supercapacitor behavior than other hybrid films.

5.4. References

1. M. Satoh, K. Kaneto, K. Yoshino, Synthetic metals, 14 (1986) 289-296.
2. C. Li, C. Sun, W. Chen, L. Pan, Surface and Coatings Technology, 198 (2005) 474-477.
3. T. Otero, E. De Larreta, Synthetic metals, 26 (1988) 79-88.
4. Y.A. Ismail, J.G. Martinez, T.F. Otero, Journal of Electroanalytical Chemistry, 719 (2014) 47-53.
5. A. Ben Slimane, M.M. Chehimi, M.-J. Vaulay, Colloid and Polymer Science, 282 (2004) 314-323.
6. D. Melling, S. Wilson, E. Jager, Rsc Advances, 5 (2015) 84153-84163.
7. M. Lu, R. Xie, Z. Liu, Z. Zhao, H. Xu, Z. Mao, Journal of Applied Polymer Science, 133 (2016).
8. K.-J. Ahn, Y. Lee, H. Choi, M.-S. Kim, K. Im, S. Noh, H. Yoon, Scientific reports, 5 (2015) 14097.
9. M. Pandey, K. Deshmukh, Journal of Applied Polymer Science, 139 (2022) e52450.
10. H. Yan, K. Kou, Journal of Materials Science, 49 (2014) 1222-1228.
11. A. Chithrambattu, Y.A. Ismail, Journal of Adhesion Science and Technology, 34 (2020) 2685-2702.
12. R. Rajamany, S. Prakash, Y.A. Ismail, Plastics, Rubber and Composites, 51 (2022) 240-249.
13. A. Karrat, A. Amine, Arab. J. Chem. Environ. Res, 7 (2020) 66-93.
14. A.N. Raja, International Journal of Biological Macromolecules, 164 (2020) 4231-4244.
15. F. Croisier, C. Jérôme, European polymer journal, 49 (2013) 780-792.
16. L. Rajan, M.P. Sidheekha, A. Shabeeba, Y.A. Ismail, Materials Chemistry Frontiers, 6 (2022) 1706-1718.
17. M.P. Sidheekha, L. Rajan, Y.A. Ismail, Materials Chemistry and Physics, 279 (2022) 125769.
18. Y.A. Ismail, J.G. Martínez, A.S. Al Harrasi, S.J. Kim, T.F. Otero, Sensors and Actuators B: Chemical, 160 (2011) 1180-1190.
19. R. Muzzarelli, C. Muzzarelli, Polysaccharides I: structure, characterization and use, (2005) 151-209.

20. M.N.R. Kumar, Reactive and functional polymers, 46 (2000) 1-27.
21. S. Yalçınkaya, C. Demetgül, M. Timur, N. Çolak, Carbohydrate polymers, 79 (2010) 908-913.
22. B. Rikhari, S.P. Mani, N. Rajendran, Carbohydrate polymers, 189 (2018) 126-137.
23. J. Berger, M. Reist, J.M. Mayer, O. Felt, N. Peppas, R. Gurny, European journal of pharmaceutics and biopharmaceutics, 57 (2004) 19-34.
24. T.M. M. Ways, W.M. Lau, V.V. Khutoryanskiy, Polymers, 10 (2018) 267.
25. A. Sugunan, C. Thanachayanont, J. Dutta, J. Hilborn, Science and Technology of Advanced Materials, 6 (2005) 335.
26. R.-J. Lee, R. Temmer, T. Tamm, A. Aabloo, R. Kiefer, Reactive and Functional Polymers, 73 (2013) 1072-1077.
27. G. Ruhi, O. Modi, S. Dhawan, Synthetic Metals, 200 (2015) 24-39.
28. S.-G. Anicuta, L. Dobre, M. Stroescu, I. Jipa, Analele Universită Ńii din Oradea Fascicula: Ecotoxicologie, Zootehnie şi Tehnologii de Industrie Alimentară, 2010 (2010) 1234-1240.
29. Y.A. Ismail, J.G. Martínez, A.S. Al Harrasi, S.J. Kim, T.F.F. Otero, Electroactive Polymer Actuators and Devices (EAPAD) 2011, SPIE, 2011, pp. 450-461.
30. T.F. Otero, M.J. Ariza, The Journal of Physical Chemistry B, 107 (2003) 13954-13961.
31. T.F. Otero, S. Beaumont, Sensors and Actuators B: Chemical, 263 (2018) 493-501.
32. T. Otero, H. Grande, J. Electroanal. Chem., 414 (1996) 171-176.
33. T. Otero, H. Grande, J. Rodriguez, J. Electroanal. Chem., 394 (1995) 211-216.
34. X. Zhang, R. Zhang, C. Xiang, Y. Liu, Y. Zou, H. Chu, S. Qiu, F. Xu, L. Sun, Ceramics International, 45 (2019) 13894-13902.
35. S. Ye, J. Feng, ACS applied materials & interfaces, 6 (2014) 9671-9679.
36. J. Zang, S.-J. Bao, C.M. Li, H. Bian, X. Cui, Q. Bao, C.Q. Sun, J. Guo, K. Lian, The Journal of Physical Chemistry C, 112 (2008) 14843-14847.
37. P. Li, Y. Yang, E. Shi, Q. Shen, Y. Shang, S. Wu, J. Wei, K. Wang, H. Zhu, Q. Yuan, ACS Applied Materials & Interfaces, 6 (2014) 5228-5234.
38. X. Gu, Y. Yang, Y. Hu, M. Hu, J. Huang, C. Wang, Journal of Materials Chemistry A, 3 (2015) 5866-5874.
39. X. Fan, Z. Yang, N. He, RSC advances, 5 (2015) 15096-15102.
40. F. Zhang, F. Xiao, Z.H. Dong, W. Shi, Electrochimica Acta, 114 (2013) 125-132.
41. X. Jian, J.-g. Li, H.-m. Yang, E.-h. Zhang, Z.-h. Liang, Carbon, 114 (2017) 533-543.
42. J. Zhu, Y. Xu, J. Wang, J. Lin, X. Sun, S. Mao, Physical Chemistry Chemical Physics, 17 (2015) 28666-28673.

43. D. Zhang, X. Zhang, Y. Chen, P. Yu, C. Wang, Y. Ma, Journal of Power Sources, 196 (2011) 5990-5996.
44. R. Sun, H. Chen, Q. Li, Q. Song, X. Zhang, Nanoscale, 6 (2014) 12912-12920.
45. J. Li, T. Que, J. Huang, Materials Research Bulletin, 48 (2013) 747-751.
46. Y. Shi, L. Pan, B. Liu, Y. Wang, Y. Cui, Z. Bao, G. Yu, Journal of Materials Chemistry A, 2 (2014) 6086-6091.
47. S.S. Shinde, G.S. Gund, V.S. Kumbhar, B.H. Patil, C.D. Lokhande, European polymer journal, 49 (2013) 3734-3739.
48. J.H. Park, J.M. Ko, O.O. Park, D.-W. Kim, Journal of Power Sources, 105 (2002) 20-25.
49. D. Dubal, S. Patil, A. Jagadale, C. Lokhande, Journal of Alloys and Compounds, 509 (2011) 8183-8188.
50. R. Devi, K. Patel, V. Sahu, K. Kashyap, K. Tapadia, T. Maharana, IOP Conference Series: Materials Science and Engineering, IOP Publishing, 2020, pp. 012034.
51. B. Kim, C. Too, J. Kwon, J. Ko, G. Wallace, Synthetic Metals, 161 (2011) 1130-1132.
52. L. Liu, Y. Chen, Y. Xie, P. Tao, Q. Li, C. Yan, Advanced Functional Materials, 28 (2018) 1801989.
53. Y. Gong, X.-G. Zeng, T. Luo, Z.-Y. Dai, Y.-Z. Jin, J. Chen, Y. Yi, T. Duan, Y.-J. Tang, Int J Electrochem Sci, 15 (2020) 7508-7519.
54. J. Wang, J. Polleux, J. Lim, B. Dunn, The Journal of Physical Chemistry C, 111 (2007) 14925-14931.
55. V. Augustyn, P. Simon, B. Dunn, Energy & Environmental Science, 7 (2014) 1597-1614.
56. J. Li, Y. Liu, D. Zhan, Y. Zou, F. Xu, L. Sun, C. Xiang, J. Zhang, Journal of Energy Storage, 39 (2021) 102665.

Chapter 6

POLYPYRROLE/PVA HYBRID FILMS AS SELF SENSING MACROMOLECULAR MOTORS: APPLICATION AS SENSING SUPERCAPACITOR

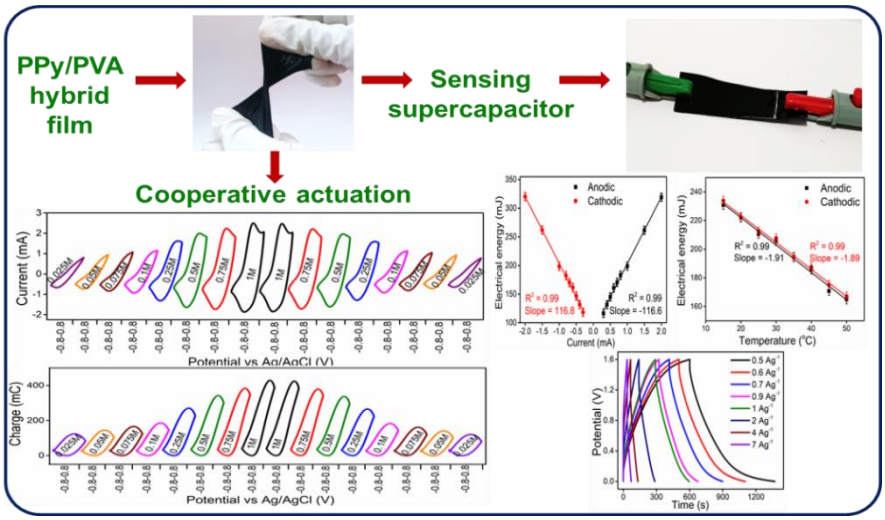

Highly mechanically stable and electroactive polypyrrole/PVA hybrid films were fabricated and were used to develop an all-solid-state symmetric supercapacitor device capable of sensing their surrounding conditions at any reaction moment, without physical separation through the same two connecting wires. The sensing characteristics of PPy/PVA hybrid films were studied through galvanostatic and potentiodynamic methods with special emphasis to the cooperative actuation of PPy chains. The charge storage capabilities of the hybrid films were studied by CV, GCD and EIS. This work open a facile and low-cost strategy to fabricate sensing motors (here, sensing supercapacitors) based on PPy/PVA hybrid systems and promote their practical applications in next generation energy storage devices.

6.1. Introduction

In the previous chapter, we have discussed the importance of multi sensing motors (sensing supercapacitors) capable of sensing their surrounding conditions at any reaction moment, without physical separation through the same two connecting wires. The PPy/Cs hybrid films have good reaction-driven sensing capabilities as well as charge storage properties. Although they have a reasonable mechanical strength in the dry state, it is observed that, they exhibit poor mechanical strength in the wet state due to high degree of swelling. Our aim is to fabricate a stable self sensing motor for which we get the insight from the biomimetic properties of CPs. Most of the applications of CPs mimicking the biological functions are working in wet conditions. Due to the poor mechanical strength of PPy/Cs hybrid films in the wet conditions, our search went into a direction to find mechanically more stable hydrogel in the wet state also. Accordingly we have succeeded in fabricating a highly electroactive PPy/PVA hybrid films which are mechanically highly stable in the wet state. These films are used as free standing electrode material for fabrication of self sensing supercapacitors.

6.1.1. Polyvinyl alcohol

PVA is the most commercially important biodegradable, colorless, odorless, translucent water-soluble hydrophilic synthetic polymer with an idealized formula of $[CH_2CH(OH)]_n$ (Figure 6.1). PVA was first prepared by Hermann and Haehnel in 1924 by hydrolyzing polyvinyl acetate in ethanol with potassium hydroxide.

It is insoluble in most organic solvents. The specific functional uses and the chemical, physical and mechanical properties of PVA depend on the degree of hydrolysis and the degree of polymerization [1]. PVA is unique among other polymers as it is not produced from the polymerization reactions of the corresponding monomer, but formed by polymerization of vinyl acetate to poly (vinyl acetate), and its subsequent hydrolysis [2, 3]. PVA has received considerable attention as an efficient candidate for various applications including sensors, pharmaceutical applications, tissue engineering, textiles, adhesives, etc. owing to its excellent film-forming capacity, biocompatibility, biodegradability, long-term temperature and pH stability, water absorption and water retention properties, elastic nature in the swollen state, adhesiveness, ductile nature, mechanical strength, less toxicity and non-carcinogenicity [4].

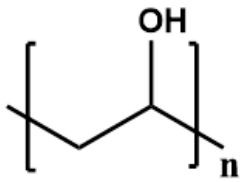

Figure 6.1 *Chemical structure of PVA*

This chapter presents a detailed study on highly mechanically stable and electroactive PPy/PVA hybrid films fabricated through in situ chemical polymerization of pyrrole on pre-fabricated PVA matrix. This chapter explores the ability of the electrochemical reactions of the hybrid film to sense the electrical, thermal and chemical energetic perturbation through chronopotentiometry by modifying the consumed electric energy to self-adapt the newly

imposed energetic conditions. Attempts were made to study the effect of size on anions in the electrolyte solution on the sensing characteristics of the hybrid film. The influence of various working energetic conditions on the conformational movements due to the cooperative actuation of the PPy chains have been studied by voltammetry with special emphasis to the reproducibility of the electroactivity. The charge storage capabilities of the hybrid films were studied by CV, GCD and EIS. As a proof-of-concept, we have fabricated an all-solid-state symmetric supercapacitor device capable of sensing their surrounding conditions at any reaction moment, without physical separation through the same two connecting wires.

6.2. Results and discussion

PPy/PVA hybrid films were fabricated through an in situ chemical polymerization of pyrrole in an aqueous medium using $FeCl_3$ as oxidant as explained in chapter 2. A schematic representation of the fabrication of PPy/PVA hybrid film is displayed in Figure 2.2. This method allows the large-scale fabrication of CP/hydrogel hybrid films with superior mechanical properties and electrochemical activity. After the in situ chemical polymerization, the PVA film (thickness = 0.091 ± 0.005 mm) turned black in color, suggesting the coating of PPy on PVA film. Here, four different types of films where fabricated, which are designated as PPF1, PPF2, PPF3 and PPF4 as explained in Chapter 2 (section 2.2.5). The thickness of PPF1, PPF2, PPF3 and PPF4 were found to be 0.102 ± 0.005 mm, 0.113 ± 0.005 mm, 0.119 ± 0.005 mm and 0.128 ± 0.005 mm respectively.

6.2.1. Characterizations of PPy/PVA hybrid films

6.2.1.1. FTIR Analysis

The FTIR spectra of PPy, PVA film and all four PPy/PVA hybrid films are presented in Figure 6.2. The FTIR spectrum of PVA shows a broad absorption peak at 3278 cm^{-1} due to O–H stretching vibration of the hydroxyl group [5]. C-H asymmetric and symmetric stretching vibrations are assigned at 2939 $cm^{-1}$and 2905 cm^{-1} respectively [6, 7]. The appearance of peaks at 1709 $cm^{-1}$and 1654 cm^{-1} is associated with the C=O stretching of acetyl group present on the PVA back bone and O–H bending vibrations. The peaks at 1429 cm^{-1} and 1323 cm^{-1} are attributed to the CH_2 bending and wagging vibrations respectively. The peak observed at 1234 cm^{-1} and 1087 cm^{-1} corresponds to C–O stretching of acetyl group of PVA. The characteristic peaks in the FTIR spectrum of PPy have been discussed in section 3.2.1.1.

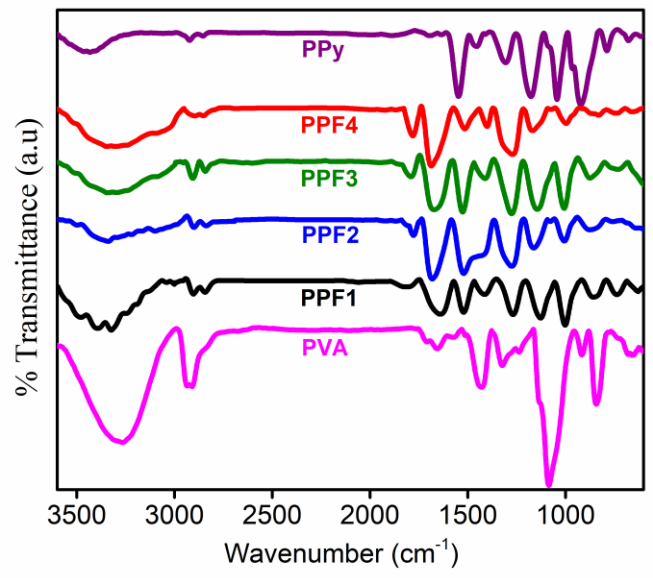

Figure 6.2 *FTIR spectra of PPy, PPF1, PPF2, PPF3, PPF4 and PVA film*

Table 6.1 *Major FTIR spectral absorptions of PVA, PPy, PPF1, PPF2, PPF3 and PPF4 films*

Absorption peaks	**PVA**	**PPy**	**PPF1**	**PPF2**	**PPF3**	**PPF4**
N-H and O-H stretching (cm^{-1})	3278	3440	3393	3338	3337	3347
O-H bending (cm^{-1})	1654	-	1642	1670	1680	1684
C-H asymmetric and symmetric stretching (cm^{-1})	2939, 2906	2922, 2825	2900, 2844	2907, 2846	2902, 2833	2896, 2850
Asymmetric and symmetric ring stretching (cm^{-1})	-	1545, 1460	1520, 1414	1524, 1410	1516, 1423	1513, 1402
C-N stretching (cm^{-1})	-	1305, 1175	1267, 1126	1274, 1143	1274, 1162	1266, 1168

The FTIR spectra of all the hybrid films exhibit the characteristic absorption peaks of both PPy and PVA with slight modifications confirming the interaction of PPy with the PVA matrix. The ATR technology is employed to record the FTIR spectra of the hybrid films and therefore the major absorption peaks emerged from the surface correspond to coated PPy. In the FTIR spectra of PPF4, the intense broad band at 3347 cm^{-1} is consistent with the overlapping of O-H stretching of PVA and N-H stretching of PPy. The peaks observed at 1513 cm^{-1} and 1404 cm^{-1} are attributed to the characteristic asymmetric and symmetric ring stretching vibrations of PPy respectively. Similar peaks were exhibited by all other hybrid films and

are summarized in Table 6.1. The presence of characteristic peaks of PPy on the hybrid films confirms the successful coating of PPy on surface of PVA film.

6.2.1.2. Surface morphology and EDX analysis

The FESEM images of PVA and PPy/PVA hybrid films showing their surface morphology are given in Figure 6.3. The surface of PVA film appears to be completely dark, smooth and homogenous without any beads or imperfections revealing that the casted films were free from air bubbles. After the in situ chemical polymerization with pyrrole, the impregnated PPy shows a complete coating on the surface of the PVA film. All the hybrid films composed of grain-like PPy nanostructures grown on the surface of PVA film with sufficient porosity. These PPy structures enable the easy diffusion of ions and solvents to the film through the electrochemical reaction and impart electroactivity to the films. As the number of times of coating increases, the PPy is grown on the surface of previously formed nanostructures and hence the surface morphology becomes more agglomerated.

The EDX spectra of PVA and PPy/PVA hybrid films are shown in Figure 6.4. The EDX spectra confirmed that after the in situ chemical polymerization with pyrrole, only the elements C, N, O, and Cl are present on the surface of hybrid films. The EDX spectra of the hybrid films show the presence of N and Cl in the surface of the film which confirms the existence of PPy and Cl^- ions associated with the polymer chain. We have not noticed any peak of Fe in the EDX

spectrum which indicates that no residual $FeCl_3$ is present on the hybrid film. Hence, the results of EDX analysis confirm the polymerization of pyrrole on the surface of the PVA film.

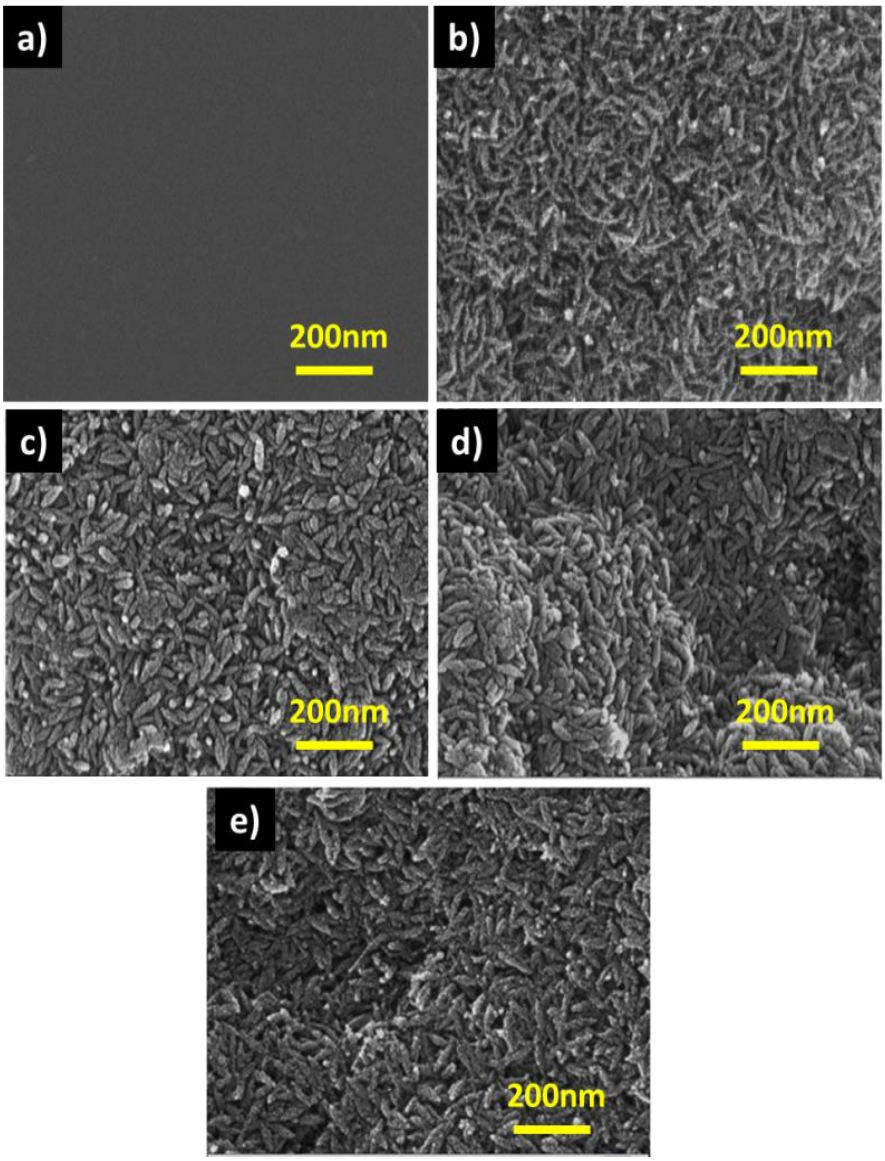

Figure 6.3 *SEM images of (a) PVA film, (b) PPF1, (c) PPF2, (d) PPF3 and (e) PPF4*

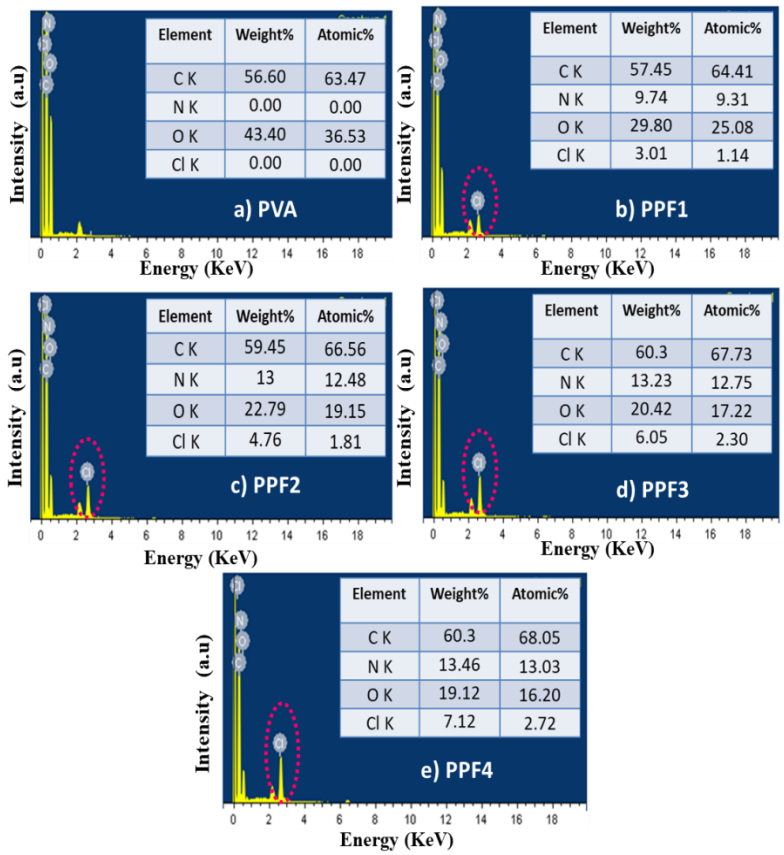

Figure 6.4 *EDX spectrum of a) PVA film, (b) PPF1, (c) PPF2, (d) PPF3 and (e) PPF4*

6.2.1.3. Electrical conductivity

The frequency-dependent electrical conductivities of the hybrid films investigated using broadband dielectric spectroscopy within the frequency range of 10^{-2} Hz to 10^{7} Hz is presented in Figure 6.5. It is evident from Figure 6.5 that the conductivity of hybrid films is improved significantly by increase in the number of times of coating from PPF1 to PPF4. This increase in conductivity is due to the increase in the number of charge carriers with increase in the number of times of coating. The electrical conductivities of all the hybrid films are

presented in Table 6.2 and PPF4 have the highest electrical conductivity of 3.15 S cm^{-1}. At lower frequencies, there is not much variation in the conductivity with frequency. At high frequency, the AC conductivity increases in all hybrid films because the electrons are sufficiently excited and hop from one conducting region to another through the extremely small inter-particle gap. The conductivity values of all hybrid films are found to be lower than that of pure PPy (2.4×10^{2} S cm^{-1}); however, it is large enough for the hybrid films to enable better electrical contact to allow electrochemical reactions and leading to the demonstration of supercapacitor and reaction driven sensing characteristics. The good conductivity of the hybrid films where the main constituent is insulating PVA, suggests that during the polymerisation process, pyrrole monomers are penetrated through the PVA hydrogel matrix and resulted in a homogeneous distribution of PPy in the surface as well as inside of the PVA film.

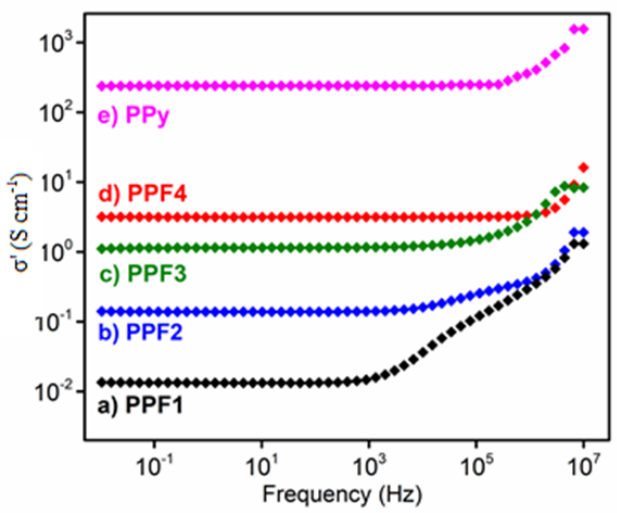

Figure 6.5 *Frequency dependence of electrical conductivity of PPy and PPy/PVA hybrid films*

Table 6.2 *Electrical conductivities of all the hybrid films*

Material	PPF1	PPF2	PPF3	PPF3
Conductivity (S cm^{-1})	1.33×10^{-2}	1.38×10^{-1}	1.14	3.15

6.2.1.4. Thermogravimetric analysis

The thermal stability of PPy/PVA hybrid films were evaluated by TGA and the results were compared with that of PVA and PPy (Figure 6.6). The thermogram of PVA showed a three-step degradation pattern. The first minor weight loss of 10 % observed at the temperature range 70 °C to 128 °C corresponds to the loss of bound water molecules during the chemical polymerization [8]. The second stage weight loss of 70 % at 239 °C to 311 °C, characterized by the sharp loss of weight in the graph, is probably due to the loss of side groups of the polymer chain [9, 10]. The degradation temperature of PVA is 263 °C. The third stage weight loss of 14.6 % occurred at 400 °C to 450 °C, which is due to the polymer main chain degradation. At 650 °C, the residual weight is found to be 5.4 %. PPy showed a three-stage degradation which is explained in section 3.2.1.4.

All PPy/PVA hybrid films exhibited three stages of thermal degradation. The first minor weight loss occurs around 70°C to 135 °C is due to the removal of bound water molecules while the second weight loss occurs at temperature range of 190 °C to 280 °C corresponds to the loss of dopants and oligomers. The third stage of weight loss begins at approximately 410 °C which is attributed to the characteristic degradation of a main polymer chain. The degradation

temperature of the main polymer chain of PPF1, PPF2, PPF3 and PPF4 are 434 °C, 439 °C, 433 °C and 439 °C respectively. It is observed that the incorporation of PPy into PVA matrix resulted in an enhancement in thermal stability of the hybrid films which is ascribed to (i) high contents of thermally stable PPy and (ii) restriction of the mobility of polymer chains (in PVA) by incorporation of PPy. After the end of the process at 650 °C, the residual weights of PPF1, PPF2, PPF3 and PPF4 are found to be 21 %, 29 %, 35 % and 42 % respectively. The residual weight of hybrid films is higher than that of PVA due to the high contents of thermally stable PPy.

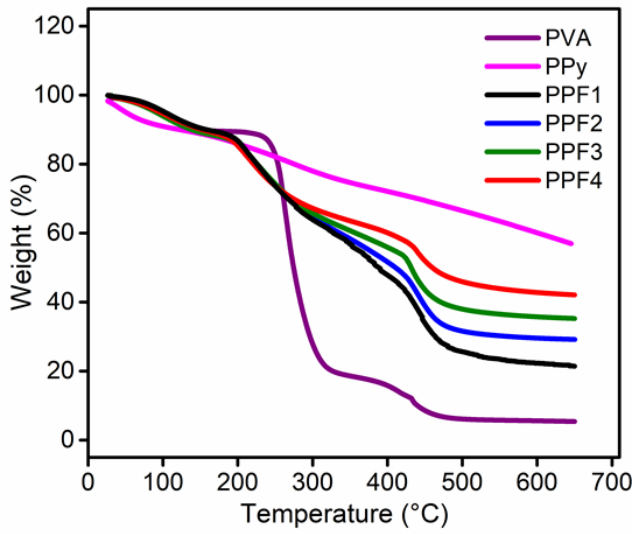

Figure 6.6 *Thermographs of PPy, PVA and PPy/PVA hybrid films*

6.2.1.5. Mechanical studies.

The photographs of PPF4 hybrid film in dry and wet states are shown in Figure 6.7 revealing that the film is mechanically stable, strong and flexible both in dry and wet states.

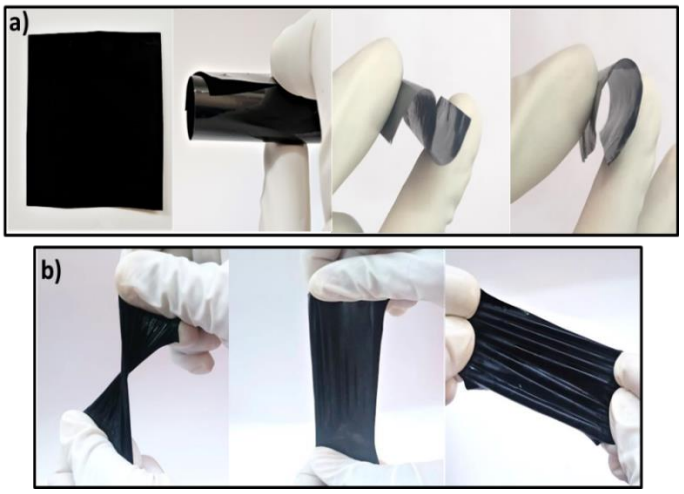

Figure 6.7 *Photographs of the PPF4 revealing its mechanical stability and flexibility in (a) dry state and (b) wet state*

The mechanical properties of the PPy/PVA hybrid films were analyzed both in dry and wet states and are evaluated from the experimental stress-strain curves (Figure 6.8a and 6.9a). The obtained results were presented in Figure 6.8b-d and 6.9b-d. The tensile strength and the Young's modulus of the hybrid films are much higher than that of the pure PVA film both in the dry and wet states. The incorporation of PPy into the PVA matrix results in strong hydrogen bonding interaction between PVA and PPy. This restricts the free movement of polymer segments leading to higher tensile strength [11]. In both dry and wet states, the tensile strength and Young's modulus increases gradually as the number of times of coating (content of PPy) increases in the hybrid films, i.e. increases from PPF1 to PPF4.

In both dry and wet states, the incorporation of PPy into PVA matrix resulted in reduction in percentage elongation of the hybrid films. As the number of times of coating increases,

i.e., from PPF1 to PPF4, the percentage of elongation is found to be reduced. It indicates that there occurs an incremental increase in the stiffness of hybrid films by the incorporation of more amount of PPy into PVA matrix and it restricts the free mobility of polymer chains. Even then all the hybrid films are found to be flexible. The percentage elongation of the hybrid films in the wet state is much higher than that in the dry state and maintains the mechanical stability. The percentage elongations of PPF4 in both dry and wet state are 19.17 % and 66.77 % respectively. As the hybrid films are mechanically more stable and flexible in the wet state, they may be used as stable free standing electrodes for various device applications.

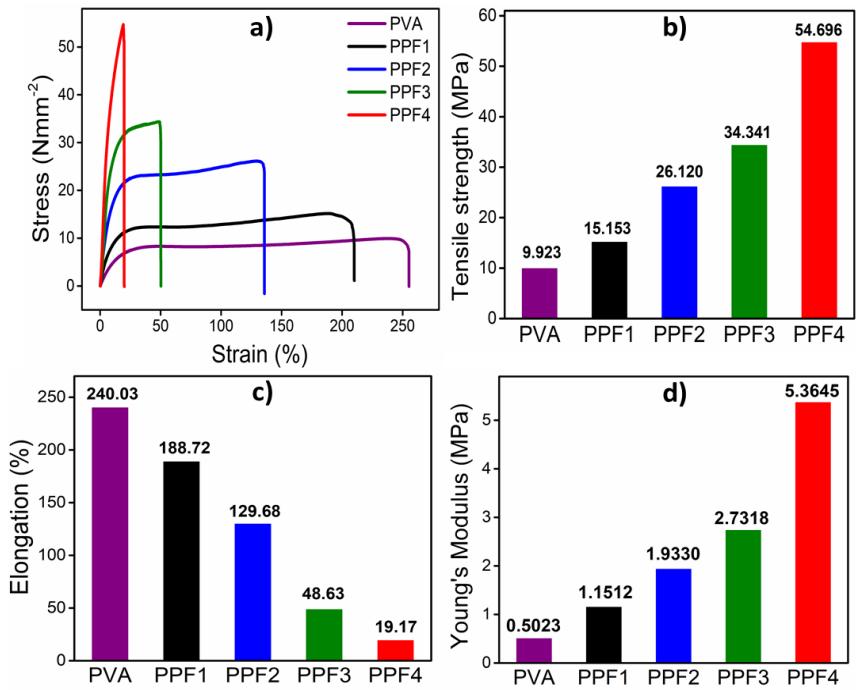

Figure 6.8 *(a) Stress-strain curve of PPy/PVA hybrid films in the dry state, (b) Tensile strength, (c) Percentage elongation and (d) Young's modulus of PPy/PVA hybrid films evaluated from the stress-strain curves in the dry state*

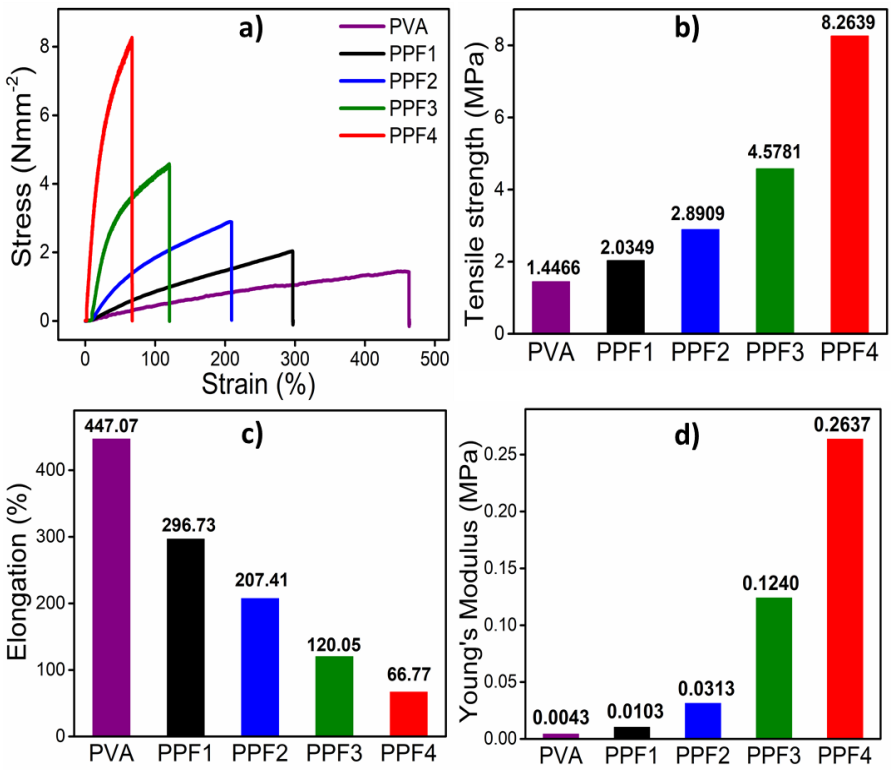

Figure 6.9 *(a) Stress-strain curve of PPy/PVA hybrid films in the wet state, (b) Tensile strength, (c) Percentage elongation and (d) Young's modulus of PPy/PVA hybrid films evaluated from the stress-strain curves in the wet state*

6.2.1.6. Electrochemical characterizations

(a) Cyclic voltammetry

The CVs of all the hybrid films were recorded in a conventional three-electrode electrochemical cell with the PPy/PVA hybrid films as the WE, Ag/AgCl (3 M KCl) as the RE and Pt mesh as the CE. Figure 6.10 shows the stationary CVs of all the hybrid films with in a potential window of -0.8 V and 0.8 V at a scan rate of 2 mV s^{-1} from 1 M NaCl solution at room temperature. The PPy/PVA hybrid films has a wider potential window compared to PPy/Cs hybrid films, which is

confirmed through the closed QV obtained for PPy/PVA hybrid films (Figure 6.13a). All the voltammograms consist of a broad anodic peak corresponding to PPy oxidation and a broad cathodic peak corresponding to PPy reduction, confirming the electroactivity of the hybrid films is imparted by PPy. The peak potential values are displayed in Table 6.3 [12]. The presence of redox peaks in the CV curves of the hybrid films correspond to their faradaic behavior and also reveals the pseudocapacitance behavior of PPy. The absence of any additional peaks which can arise due to overoxidation during the repeated potential cycling indicates the excellent stability of the hybrid films. From the CVs, it is observed that as the number of times of coating increases from PPF1 to PPF4, the peak current also increases. PPF4 having a high content of PPy and high conductivity shows the highest peak current.

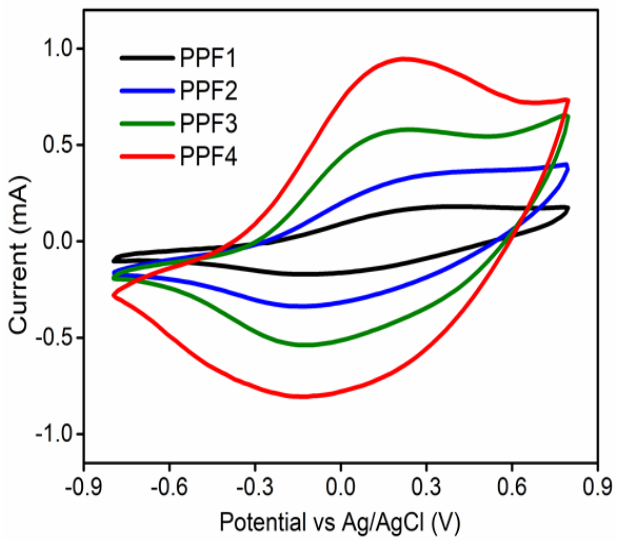

Figure 6.10 *CVs of all PPy/PVA hybrid films at a scan rate of 2 mV* s^{-1} *in 1M NaCl aqueous solution within a potential window of -0.8 V and 0.8 V*

Table 6.3 *Anodic and cathodic potentials of PPy/PVA hybrid films obtained from CVs*

Hybrid film	Anodic potential (V)	Cathodic potential (V)
PPF1	0.23	-0.12
PPF2	0.21	-0.13
PPF3	0.14	-0.12
PPF4	0.19	-0.13

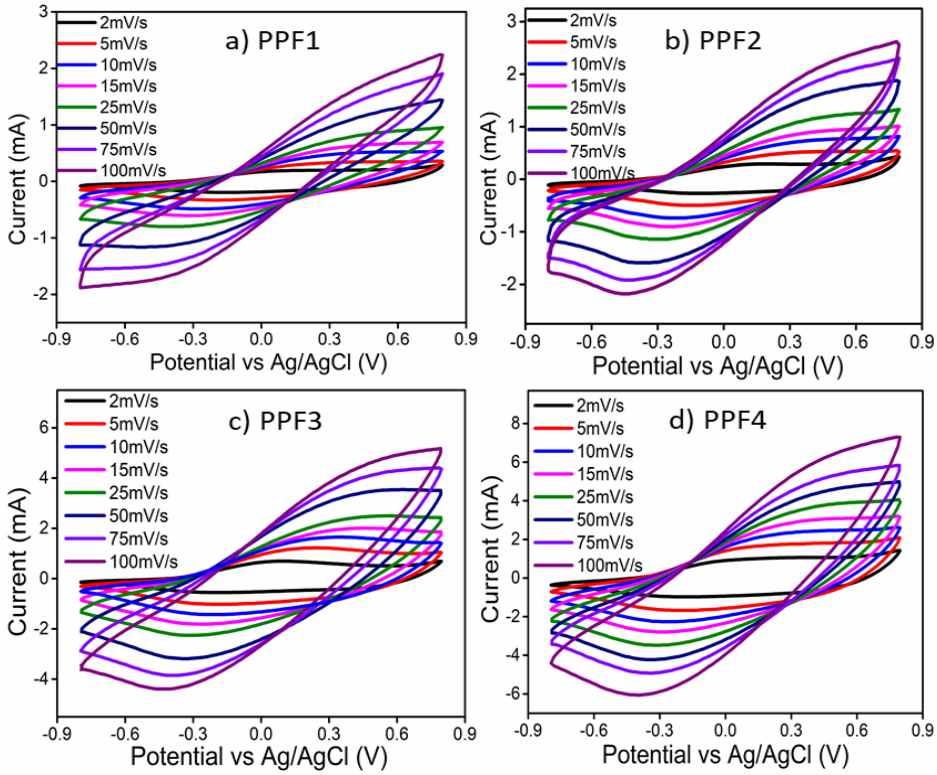

Figure 6.11 *CVs of (a) PPF1, (b) PPF2, (c) PPF3 and (d) PPF4 at various scan rates ranging from 5 to 100 mV* s^{-1} *in 1 M NaCl solution*

The CVs of all the hybrid films recorded at various scan rates from 2 mV s^{-1} to 100 mV s^{-1} to study the nature of the electrode process are depicted in Figure 6.11. As can be seen from the figure, the current of anodic and cathodic peaks increases with increasing the scan rate. Figure 6.12 shows the linear relationship between the anodic and cathodic peak currents with the square root of scan rates for all the hybrid films. The observed linear relationship indicates that the redox process in PPy/PVA hybrid films are controlled by ion diffusion up to 100 mV s^{-1} [13]. As the entry/ejection of counter ions through the polymer matrix is slow, the electrochemical process becomes more resistive at higher scan rates [14].

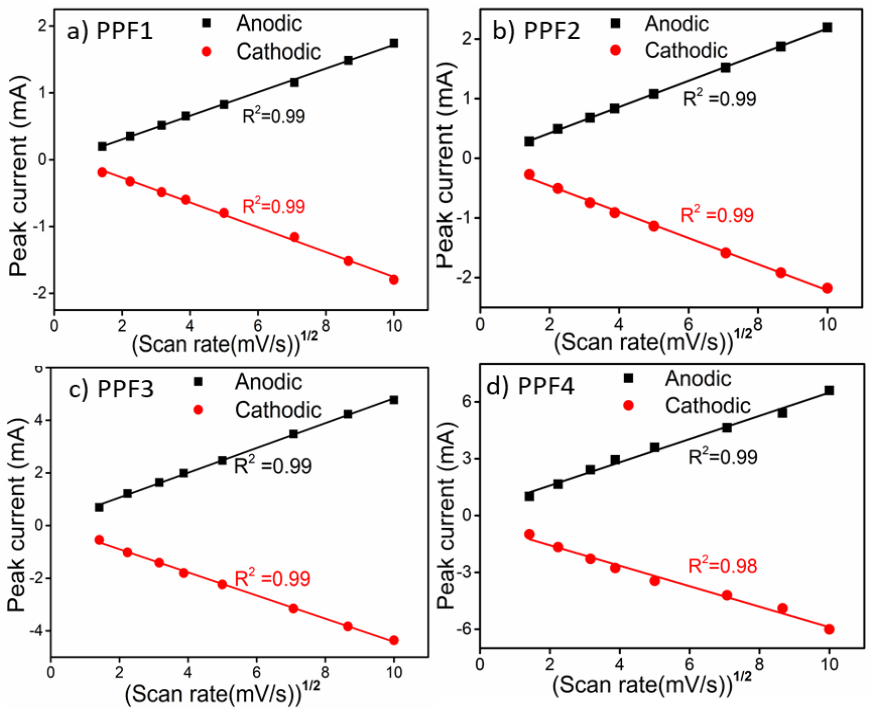

Figure 6.12 *Variation of the intensity of the cathodic/anodic peak current of (a) PPF1, (b) PPF2, (c) PPF3 and (d) PPF4 as a function of the square root of scan rates*

(b) Coulovoltammogram

Figure 6.13a presents the QVs obtained by integrating the CVs shown in Figure 6.10. All the hybrid films comprises a closed part in the QV revealing that only reversible oxidation/reduction reactions take place in the hybrid films in the studied potential interval [15]. The charge consumed by the reversible redox processes of all the hybrid films is presented in Figure 6.13b. It is observed that, as the number of times of coating increases from PPF1 to PPF4, the redox charge (film oxidation/reduction charges) increases due to increase in the electroactive center. Higher PPy content increases the number of ions exchanged during the redox reaction and thus results in the consumption of higher charges.

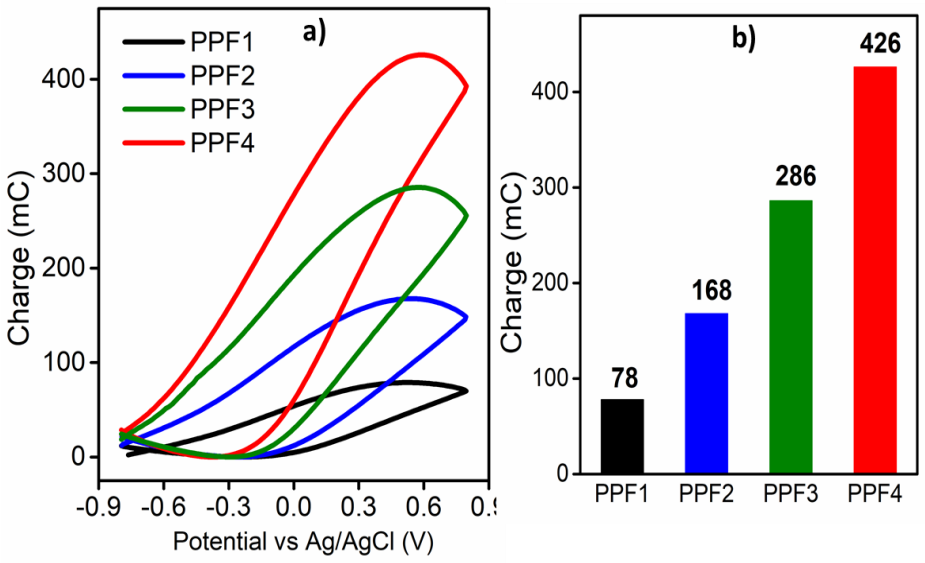

Figure 6.13 *(a) QVs of PPy/PVA hybrid films in 1 M NaCl aqueous solution and (b) Redox charges of PPy/PVA hybrid films obtained from QVs*

6.2.2. Reaction driven sensing characteristics of PPy/PVA hybrid films: Chronopotentiometric investigation

Here, the reaction driven sensing characteristics of PPy/PVA hybrid films towards electrical, chemical and thermal working conditions are studied through chronopotentiometry to prove that the consumed electrical energy can act as the sensing parameter. The sensing equations remain the same as that of PPy because the PPy is the electroactive material in the hybrid film.

6.2.2.1. Sensing working electrical condition: Current sensor

The normalized chronopotentiometric responses by applying square current waves of different magnitudes (±0.2 mA to ±2 mA) in 1 M NaCl aqueous solution while keeping the all other experimental variables constant for both the anodic and cathodic processes of all the hybrid films are depicted in Figure 6.14a-d and 6.14e-h respectively. The chronopotentiometric studies of the hybrid films were performed at a constant charge approximately equal to half of their redox charge obtained from the QVs. After the initial potential step, when the anodic or cathodic current of the hybrid films increases, the potential evolution takes place at higher anodic or higher cathodic potentials respectively [16]. Figure 6.15a shows that the consumed electrical energy during the electrochemical redox reaction of all the hybrid films varies linearly as a function of applied current. Thus, the consumed electrical energy is an excellent sensor of the locally imposed electrical energetic conditions i.e. the driving current, and the concomitant line is the sensor calibration line. The sensitivity of the hybrid films gradually

increases from PPF1 to PPF4 as the number of times of coating (content of PPy) increases (Figure 6.15b). PPF4 shows the highest sensitivity of 126.5 mJ mA^{-1} and -127.2 mJ mA^{-1} for the anodic and cathodic processes respectively.

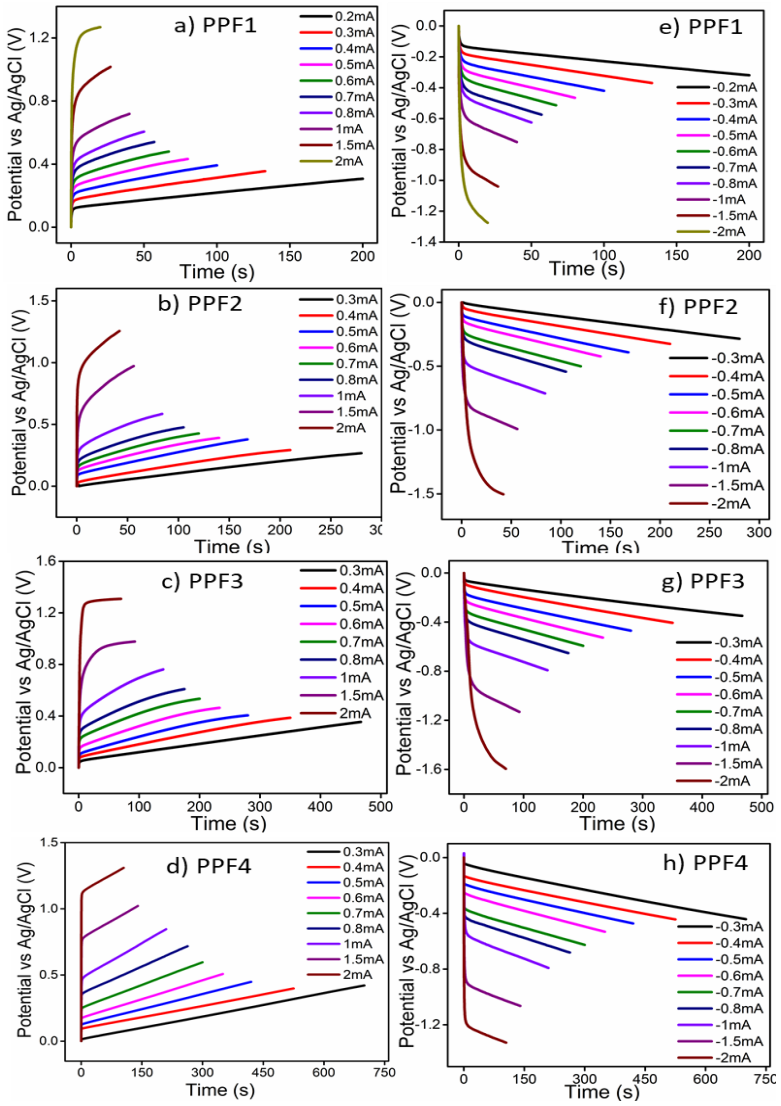

Figure 6.14 *(a-d) Anodic and (e-h) cathodic chronopotentiogranms obtained when different constant currents were applied to PPy/PVA hybrid films by passing a constant electrical charge in 1 M NaCl aqueous solution*

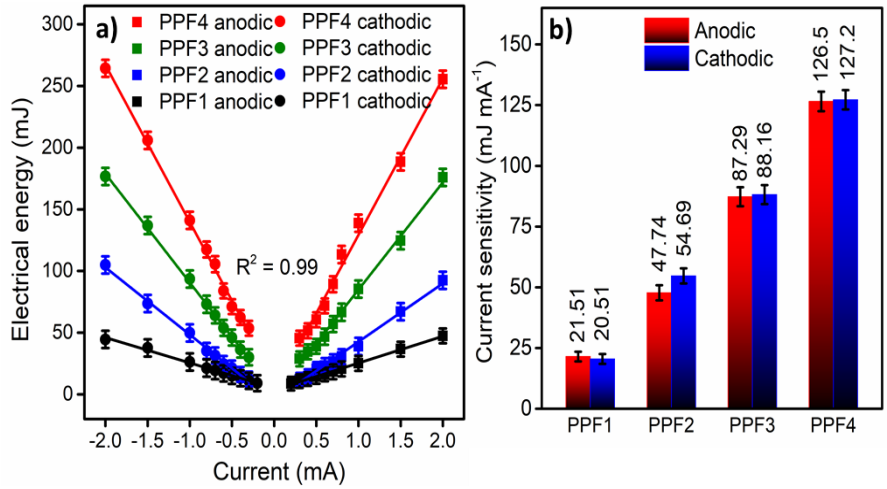

Figure 6.15 *(a) The linear variation of electrical energy consumed by the PPy/PVA hybrid films with the working current and (b) Effect of number of times of coating of PPy on current sensitivity*

6.2.2.2. Sensing working chemical condition: Concentration sensor

To investigate the concentration sensing ability of the PPy/PVA hybrid films the normalized chronopotentiometric responses were recorded at different concentrations of NaCl ranging from 0.01 M to 1 M at a constant current of ±1 mA by keeping constant charge approximately equal to half of their redox charge at room temperature. Figures 6.16a-d and 6.16e-h show the normalized chronopotentiometric responses for the anodic and cathodic processes of PPy/PVA hybrid films respectively. During the reversible redox reactions of the hybrid films under the same physical and chemical conditions, the anodic and cathodic potentials evolve at lower values for increasing electrolyte concentrations [15].

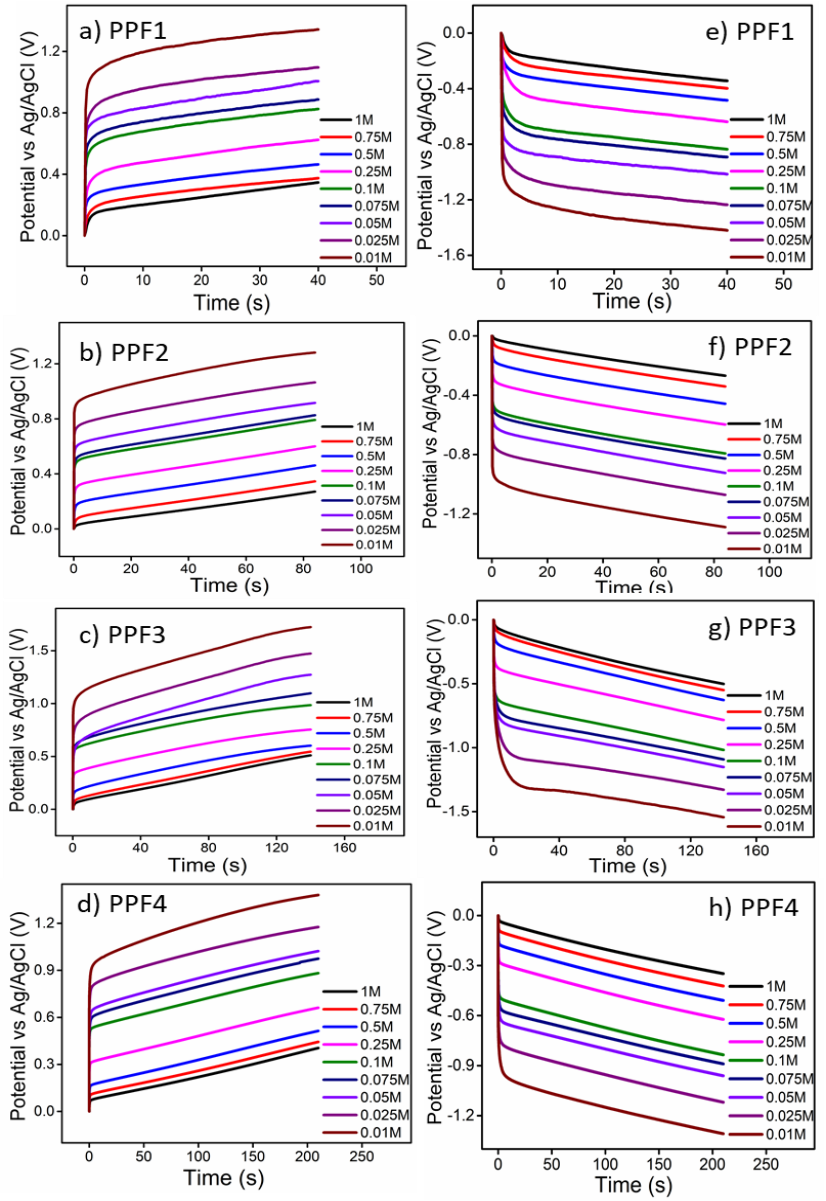

Figure 6.16 *(a-d) Anodic and (e-h) cathodic chronopotentiograms obtained when PPy/PVA hybrid films were subjected to different concentrations of NaCl by applying a constant current of ±1 mA at a constant electrical charge*

Figure 6.17a and 6.17b indicate the logarithmic dependence of the consumed electrical energy with the electrolyte concentration for

the anodic and cathodic processes respectively. It is observed that the lower available chemical energy requires the consumption of higher electrical energy for attaining the same reaction extension [17]. Hence, the electrical energy consumed by the hybrid films senses or responds to the working chemical condition (electrolyte concentration). The sensitivity (slope of calibration line) of the hybrid films gradually increases from PPF1 to PPF4 as the number of times of coating increases (Figure 6.17c) and PPF4 having a high content of PPy presents the highest sensitivity of -45.44 mJ M^{-1} and -42.78 mJ M^{-1} for the anodic and cathodic processes respectively.

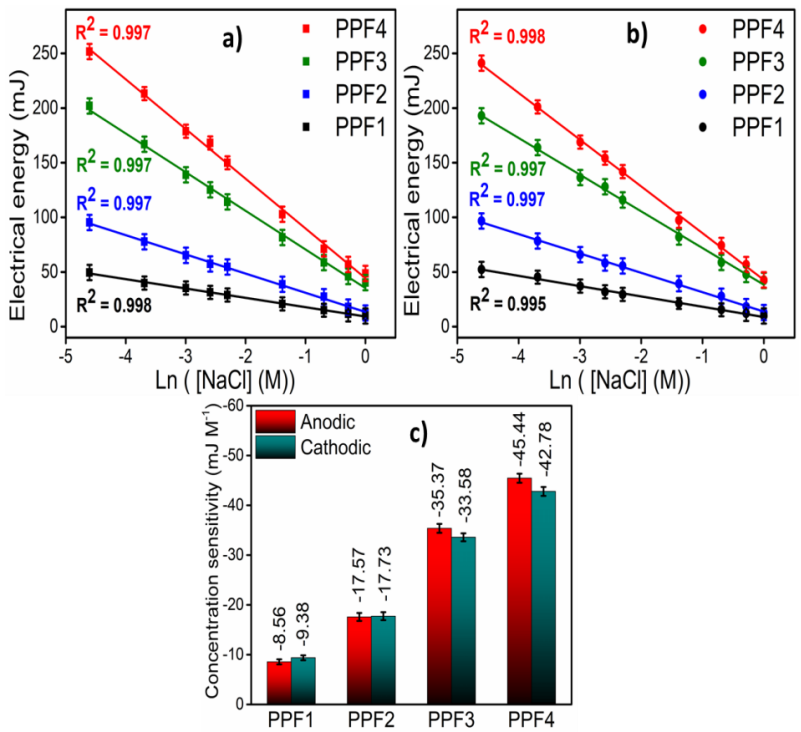

Figure 6.17 *Logarithmic variation of the consumed electrical energy of the hybrid films with the concentration of electrolyte for (a) anodic and (b) cathodic processes, (c) Effect of number of times of coating of PPy on concentration sensitivity*

6.2.2.3. Sensing working thermal condition: temperature sensor

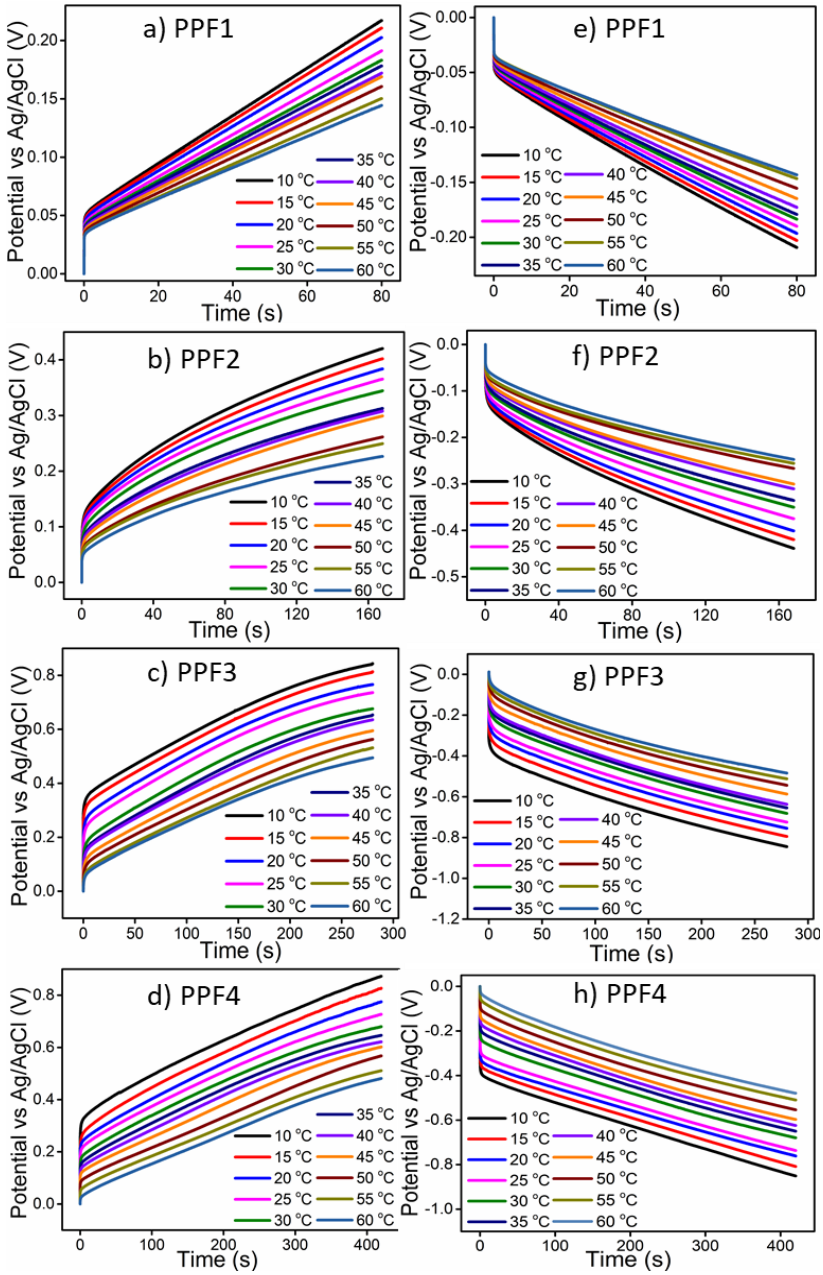

Figure 6.18 *(a-d) Anodic and (e-h) cathodic chronopotentiograms attained at different temperatures by applying a constant current of ±1 mA at a constant electrical charge in 1 M NaCl solution*

For studying the temperature sensing capability of the PPy/PVA hybrid films, chronopotentiometric responses were recorded at different temperatures ranging from 10 ^{o}C to 60 ^{o}C under consecutive square current waves of ±0.5 mA in 1 M NaCl solution by keeping all other experimental variables constant (at a constant charge approximately equal to half of their redox charge). The obtained stationary and normalized chronopotentiometric responses for the anodic and cathodic processes are presented in Figure 6.18a-d and 6.18e-h respectively. As the temperature increases, the anodic and cathodic potentials evolve at lower values for attaining the same reaction extension [18].

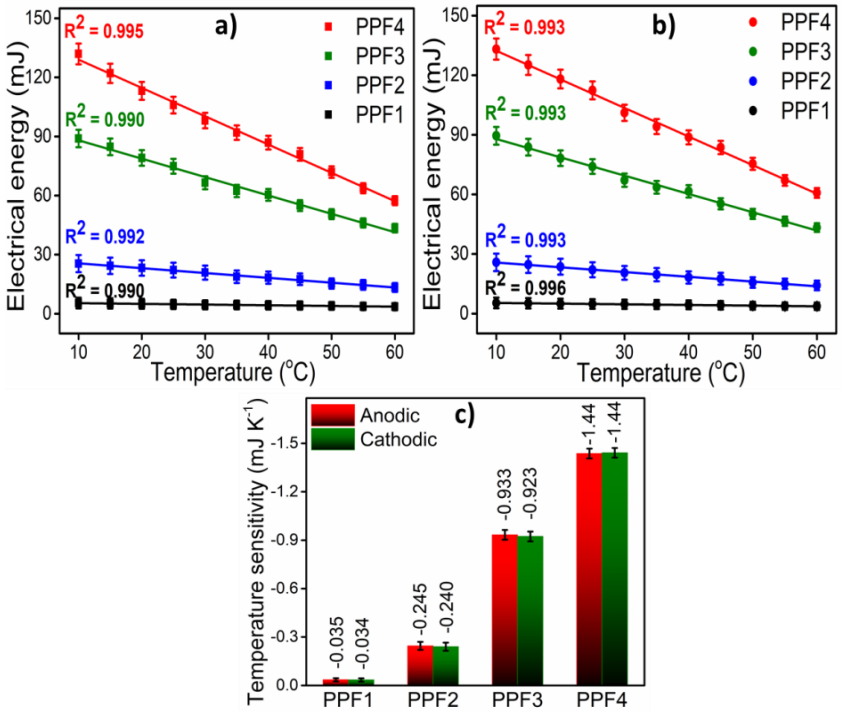

Figure 6.19 *Linear variation of electrical energy consumed by the PPy/PVA hybrid films with the working temperature for (a) anodic and (b) cathodic processes, (c) Effect of number of times of coating of PPy on temperature sensitivity*

The electrical energies consumed during the oxidation and reduction reactions of all the hybrid films have a linear relation with the experimental temperature as shown in Figure 6.19a and 6.19b. Thus all the hybrid films can act as sensors of the working temperature and the concomitant lines are the calibration lines. The sensitivities of the hybrid films to the experimental temperature increases as the number of times of coating increases from PPF1 to PPF4 (Figure 6.19c), and the highest sensitivity of -1.44 mJ K^{-1} for the anodic and -1.44 mJ K^{-1} for the cathodic processes are shown by PPF4.

6.2.3. Effect of size of anions on the reaction driven sensing characteristics of PPF4 film

The nature of anions in the electrolyte plays a key role in the electrochemical properties of CPs. Here, we have explored the influence of the size of anions in the electrolyte solution on the reaction driven sensing characteristics of PPF4 film. We have selected PPF4 film for this particular study primarily due to the fact that PPF4 film has the highest electroactivity among all the hybrid films studied. The electrolyte solutions used for this study are lithium bis(trifluoromethanesulfonyl)imide (LiTFMSI), lithium perchlorate ($LiClO_4$) and lithium chloride (LiCl), where the dominant mechanism of oxidation/reduction reactions is the exchange of anions. We have kept the same cation and varied the anions in our studies. The anionic size of the electrolyte increases in the order LiCl< $LiClO_4$<LiTFMSI. Figure 6.20a shows the CV responses of the PPF4 film in 1 M solution of these different electrolytes within a potential window of

-0.8 V and 0.8 V at a scan rate of 2 mV s^{-1}. The shapes of the CVs are affected by the nature of the anions present in the electrolyte solution. As can be seen from the figure, there is significant variations in the peak potential and peak current for both anodic and cathodic processes with change in electrolyte solution. As the size of anions decreases, the peak current increases. The obtained CVs were integrated and the corresponding QV responses are presented in Figure 6.20b. The redox charge consumed by the hybrid film increases when the size of anions in the electrolyte decreases (Figure 6.20c).

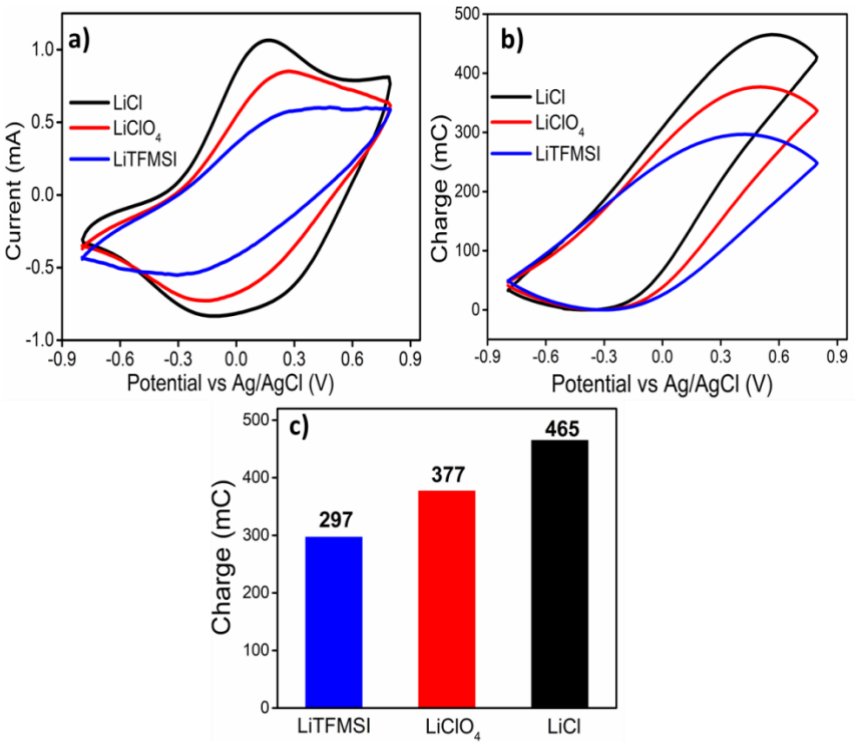

Figure 6.20 (a) *The CV responses and (b) QV responses of PPF4 film between -0.8 V and 0.8 V in 1 M of LiCl, $LiClO_4$, and LiTFMSI aqueous solutions as electrolyte, (c) Redox charges obtained from QVs for various electrolytes*

As the size of anion is small, there is easy penetration of anions into the polymer matrix, which in turn increases the ion diffusion rate. It promotes deeper conformational movements of the polymeric chains with the consumption of large redox charges. Thus we get deeper oxidation/reduction states when the size of anion is small. As the size of anion in the electrolyte solution increases, the amount of counterions penetrated into the polymer chain to drive the conformational movements of the reactant polymeric chains at a definite interval of time decreases. This result in the consumption of low oxidation charge and the polymer chains become partially oxidized. The water molecule also exchanged with the polymer matrix along the anions during the redox reactions, thus the CVs are also affected by the number of water molecules exchanged.

6.2.3.1. Effect of size of anions on the current sensing characteristics of PPF4

For studying the effect of size of anions in the electrolyte solution on the current sensing capability of PPF4 film, the normalized chronopotentiometric responses were recorded by applying square current waves of different magnitudes (±0.3 mA to ±1 mA) in different electrolytes while keeping all other experimental variables constant. In each electrolyte, the chronopotentiograms were recorded at a constant charge approximately equal to half of their redox charge obtained from the QVs at a scan rate of 2 mV s^{-1}. The obtained stationary and normalized chronopotentiometric responses for the anodic and cathodic processes of PPF4 in different electrolytes are shown in Figure 6.21a-c and 6.21d-f respectively.

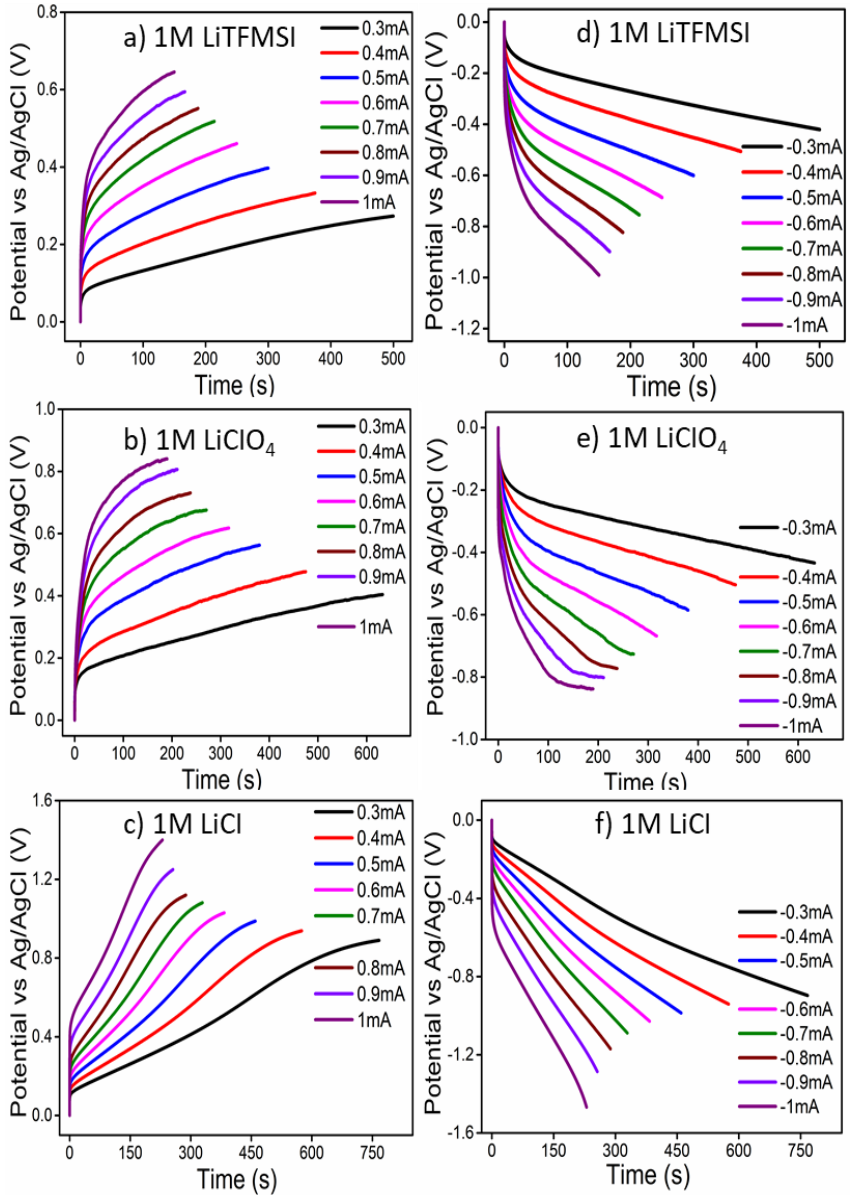

Figure 6.21 *Chronopotentiograms obtained when different constant (a-c) anodic and (d-f) cathodic currents were applied to PPF4 film by passing a constant electrical charge in 1 M solution of different electrolytes*

After the initial potential step for both anodic (Figure 6.21a-c) and cathodic processes (Figure 6.21d-f), when the applied anodic or

cathodic current increase, the potential evolution takes place at higher positive potentials for the anodic process and higher negative potentials for the cathodic process. Figure 6.22a shows that the consumed electrical energy during the electrochemical redox reaction of PPF4 (to attain the same reaction extension) in different electrolytes has a linear dependence with the applied current. Therefore, the consumed electrical energy is an excellent sensor of the locally imposed electrical conditions (the driving current) in all the studied electrolytes and the slope of the curves gives the current sensitivity. The sensitivity of PPF4 film decreases as the size of anions in the electrolyte solution increases and PPF4 shows the highest sensitivity of 155.68 mJ mA^{-1} and -159.44 mJ mA^{-1} for anodic and cathodic processes respectively in 1 M LiCl solution (Figure6.22b). The increase in sensitivity with decrease in the size of anions is related to the easy penetration of small counterions into the polymer matrix.

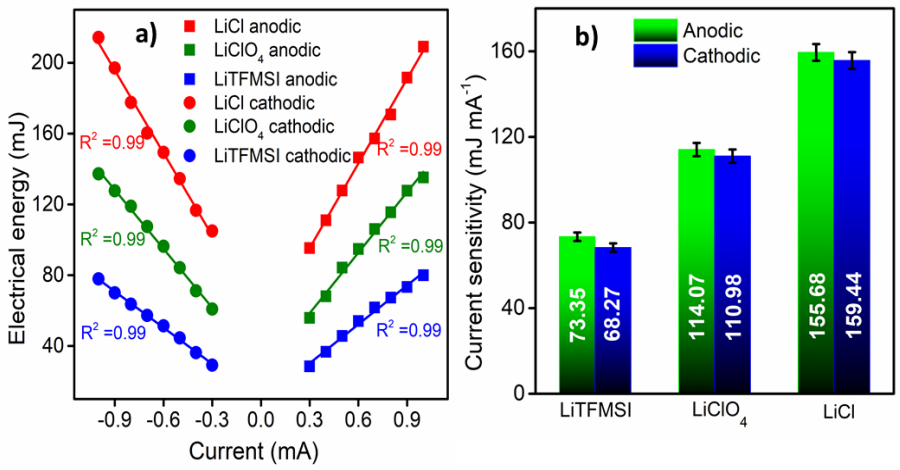

Figure 6.22 *(a) Variation of electrical energy consumed by PPF4 film with the driving current in different electrolytes and (b) Effect of size of anions in the electrolyte solution on the current sensitivity*

6.2.3.2. Effect of size of anions on the concentration sensing characteristics of PPF4

For studying the effect of size of anions in the electrolyte solution on the concentration sensing capability of PPF4 film, the normalized chronopotentiometric responses were recorded at different concentrations of electrolyte ranging from 0.05 M to 1 M at a constant current of ±0.5 mA by keeping all other experimental variables constant. In each electrolyte, the chronopotentiograms were recorded at a constant charge approximately equal to half of their redox charge obtained from the QVs at a scan rate of 2 mV s^{-1}. Figures 6.23a-c and 6.23d-f show the normalized chronopotentiometric responses for the anodic and cathodic processes of PPF4 film respectively in different electrolytes. After the initial potential step, in each electrolyte under similar experimental conditions, the anodic and cathodic potentials evolve at lower values for increasing electrolyte concentrations as expected from the sensing equations 4.19 and 4.20.

Figure 6.24a and 6.24b shows the logarithmic dependence of the consumed electrical energy with the electrolyte concentration for the anodic and cathodic processes respectively in different electrolytes. Therefore, the consumed electrical energy is an excellent sensor of the working chemical condition in all the studied electrolytes and the slope of the curves gives the chemical sensitivity. The sensitivity of PPF4 film is improved by the decrease in the size of anions in the electrolyte solution. The highest sensitivity of -47.91 mJ M^{-1} and -48.83 mJ M^{-1} for anodic and cathodic processes for the PPF4 film is obtained in LiCl solution (Figure6.24c). The increase in sensitivity with decrease in the

size of anions is related to the easy penetration of small counterions to the polymer matrix.

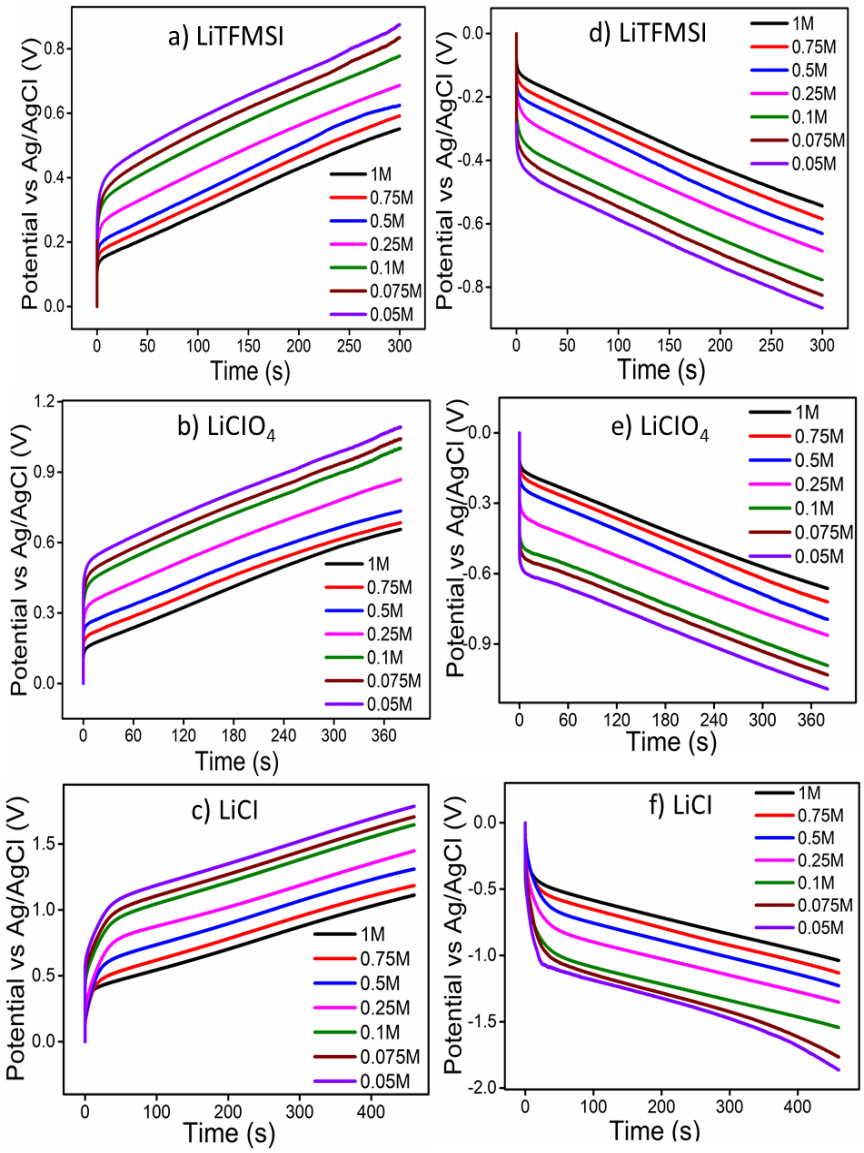

Figure 6.23 *Chronopotentiograms obtained when PPF4 film was subjected to different concentrations of electrolyte by applying (a-c) an anodic current of +0.5 mA and (d-f) a cathodic current of -0.5 mA at a constant electrical charge in different electrolytes*

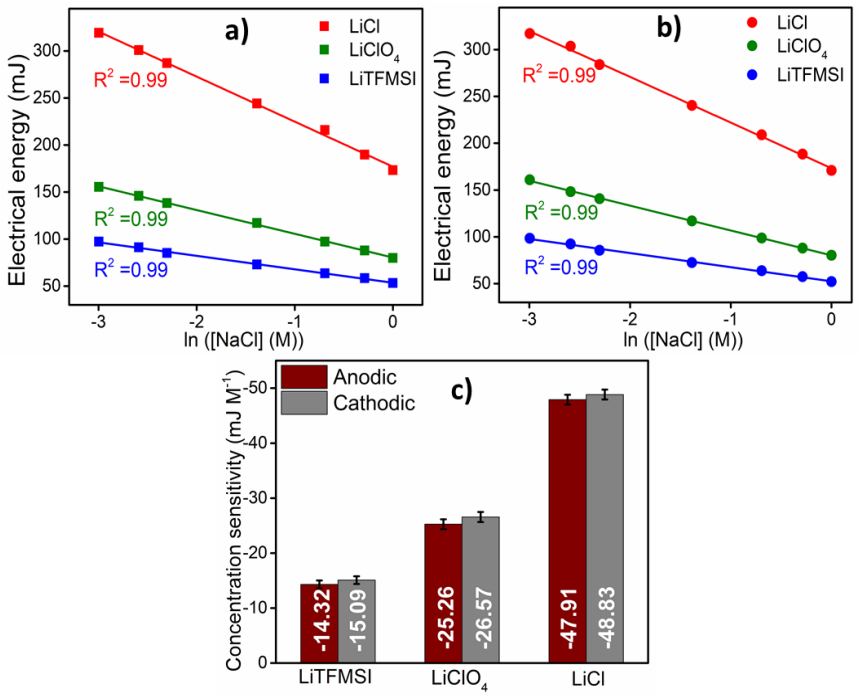

Figure 6.24 *(a) Logarithmic variation of electrical energy consumed by PPF4 film for (a) anodic and (b) cathodic process with the concentration of electrolyte in different electrolytes and (b) Effect of size of anions in the electrolyte solution on the concentration sensitivity*

6.2.3.3. Effect of size of anions on the temperature sensing characteristics of PPF4

For studying the effect of size of anions in the electrolyte solution on the temperature sensing capability of PPF4 film, the normalized chronopotentiometric responses were recorded at different temperatures ranging from 10 ˚C to 50 ˚C under consecutive square current waves of ±0.5 mA in 1 M solution of different electrolytes by keeping all other experimental variables constant (at a constant charge approximately equal to half of their redox charge obtained from the QVs at a scan rate of 2 mV s^{-1}). The obtained stationary chronopotentiometric responses

for the anodic and cathodic processes are depicted in Figure 6.25a-c and 6.25d-f respectively. In each electrolyte, as the temperature increases, the anodic and cathodic potentials evolve at lower values for attaining the same reaction extension [17].

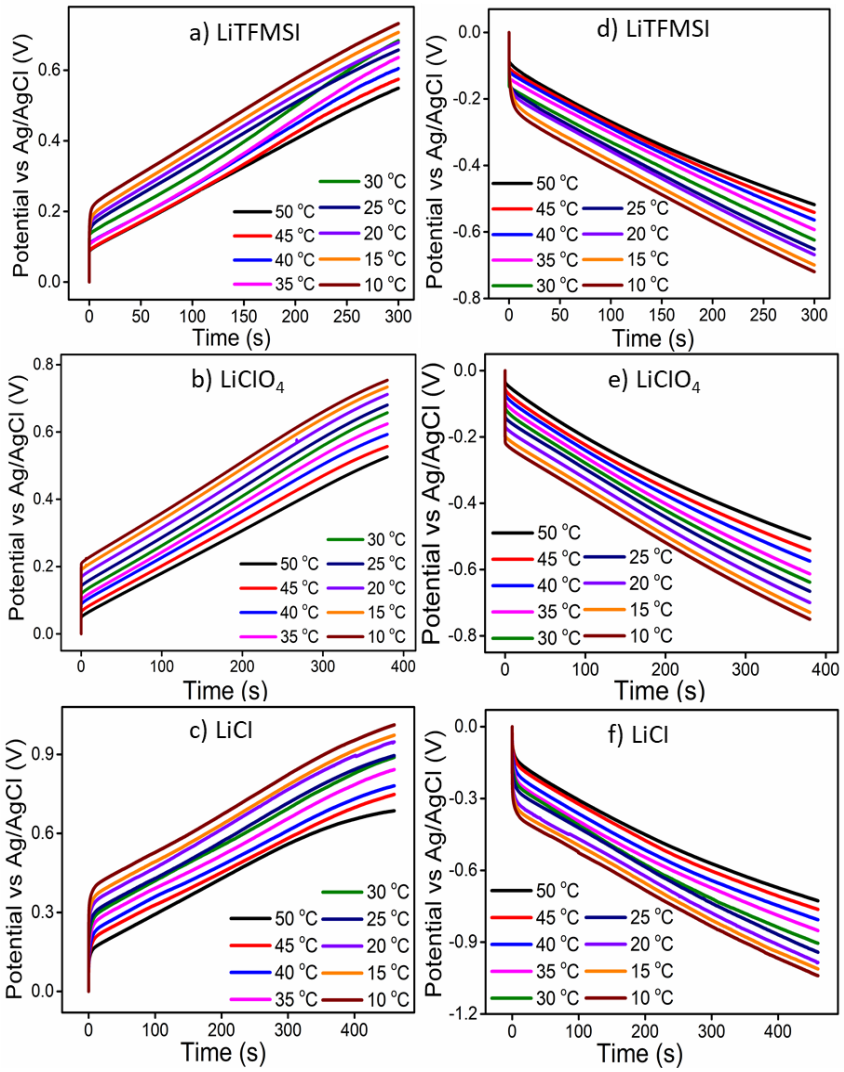

Figure 6.25 *(a-c) Anodic and (d-f) cathodic chronopotentiograms of PPF4 film obtained at different temperatures by applying a constant current of ±0.5 mA in different electrolytes at a constant electrical charge*

The electrical energies consumed during the oxidation and reduction reactions of PPF4 film in the studied electrolytes have a linear relation with the experimental temperature as shown in Figure 6.26a and 6.26b. Thus PPF4 can act as sensors of the working temperature in all the studied electrolytes and the concomitant lines are the calibration lines. Just like current sensitivity and concentration sensitivity , the temperature sensitivity of PPF4 film being the slopes of the curves also increases as the size of anions in the electrolyte decreases and PPF4 in LiCl electrolyte having smaller anions presents the highest sensitivity of -1.48 mJ K^{-1} for the anodic and -1.46 mJ K^{-1} for the cathodic processes respectively (Figure 6.26c).

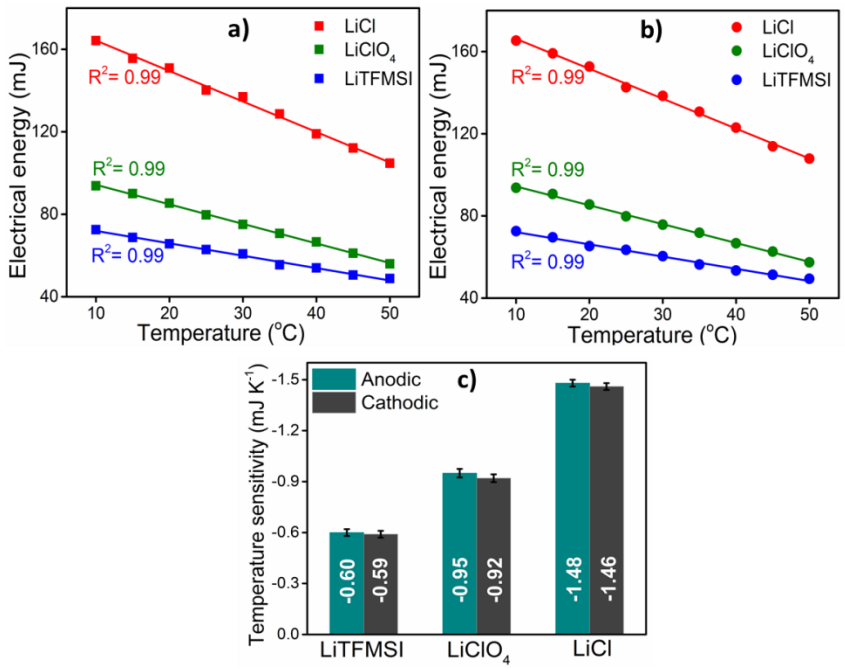

Figure 6.26 *Variation of electrical energy consumed by PPF4 film for (a) anodic and (b) cathodic process with the experimental temperature in different electrolytes and (c) Effect of size of anions in the electrolyte solution on the temperature sensitivity*

6.2.4. The cooperative actuation of multistep molecular motors of polypyrrole senses the working conditions: Voltammetric investigation

6.2.4.1. Cooperative actuation in conducting polymers

As we mentioned earlier in section 1.1.8, the CP chains are considered as electrochemically-driven reversible multi-step molecular motors. The conformational and macroscopic structural changes driving the opening and closing of the polymeric entanglements (a key aspect in biological reactions) can be identified from the electrochemical responses. During the reversible electrochemical reactions, the conformational and structural changes of CPs (through *n* consecutive steps of one electron extraction per step) arises due to the uncoiling and coiling (swelling/shrinking) processes induced by the insertion/expulsion of ions and solvent. It is considered as molecular-level actuation of the polymeric chain [13]. The actuation of the CP chains manifested as the reversible conformational movements. These conformational movements driven by the cooperative actuation of the constitutive chemical machines generates or destroys the free volume required to lodge or expel counterions and solvent. The conformational changes of multi-step sensing motors during the reaction through the cooperative actuation make the coulovoltammetric charge a self-sensor of the working energetic conditions [19, 20]. In this section, we investigated how the various reaction conditions such as chemical, thermal and electrical energetic conditions influence the cooperative actuation of multistep molecular motors of PPy. We further verified that, through the cooperative actuation the consumed charge

can sense their working energetic conditions such as chemical, thermal and electrical conditions.

6.2.4.2. Influence of the chemical condition on the cooperative actuation of multistep molecular motors of Polypyrrole: concentration sensor

The influence of the electrolyte concentration on the redox reactions of PPy was studied by cyclic voltammetry by applying consecutive potential cycles at a scan rate 5 mV s^{-1} between the same potential limits studied earlier under constant thermal and mechanical conditions. The reproducibility of the electroactivity of the PPy/PVA hybrid film was examined in 0.1 M NaCl aqueous solution which is taken as the control solution. This was studied through the following steps:

(a) After stabilizing the CV responses, the PPF4 electrode was placed in the control solution (0.1 M NaCl) and submitted to consecutive potential cycles in order to get stationary voltammetric responses.
(b) After the voltammetric control, the PPF4 electrode was placed in another cell containing a fresh 0.025 M NaCl aqueous solution and submitted to consecutive potential cycles under similar experimental conditions.
(c) The electrode was then placed again in the control solution and cycled until stationary voltammetric responses were obtained.

The steps (b) and (c) were repeated for different electrolyte concentrations that kept ascending from 0.025 M to 1 M and then descending from 1 M to 0.025 M. The voltammetric response from the

control solution i.e., 0.1 M NaCl was recorded in between two consecutive electrolyte concentrations. The procedure is schematically represented in Figure 6.27.

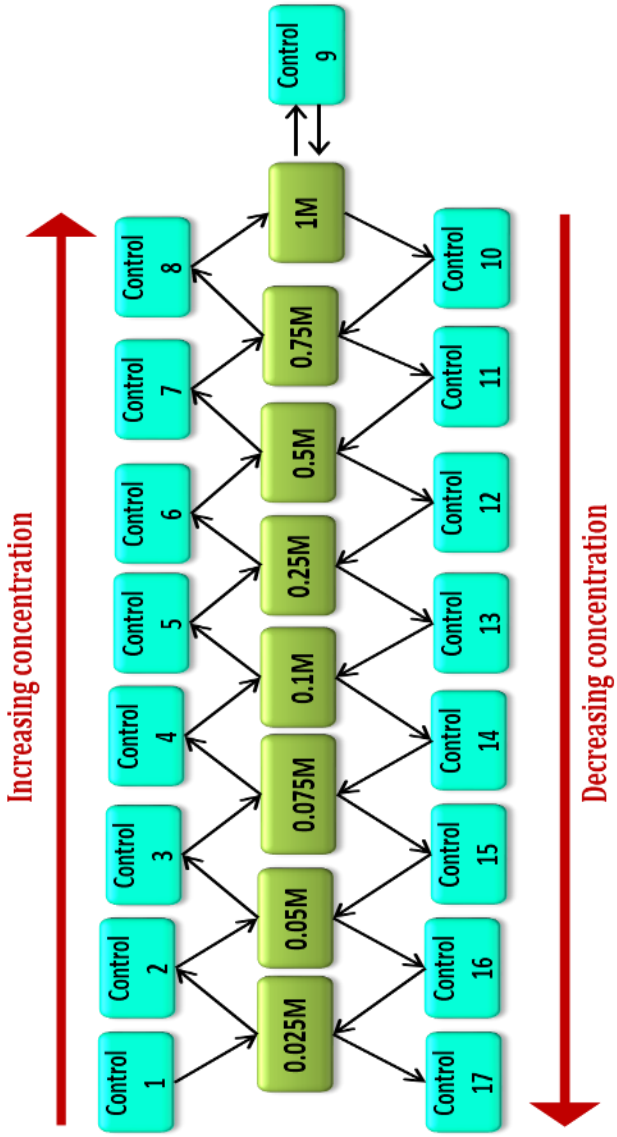

Figure 6.27 *Schematic representation of experimental procedure for studying influence of concentration on the cooperative actuation of molecular motors of PPy*

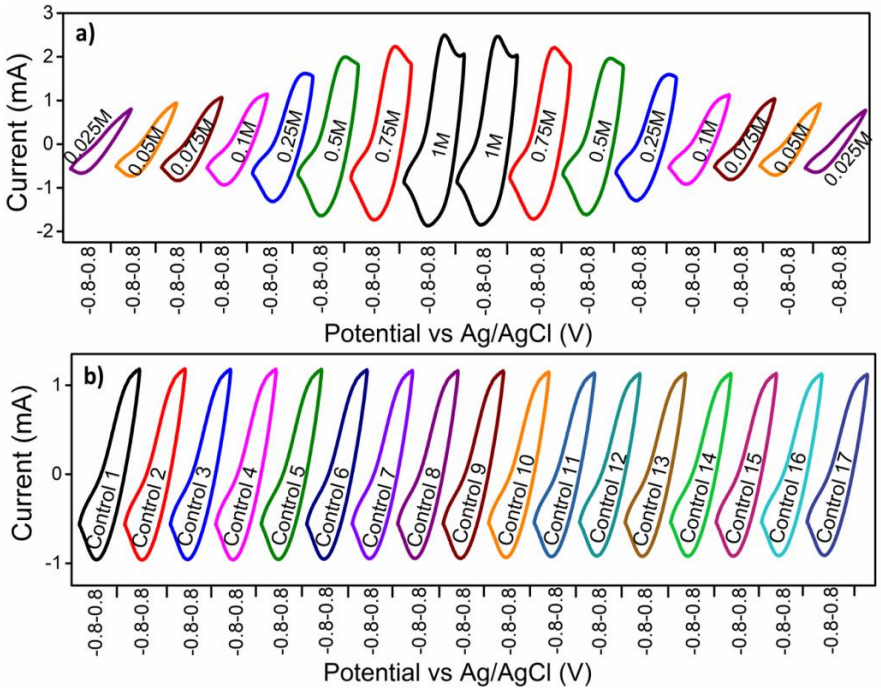

Figure 6.28 *(a) Stationary CV responses of PPF4 in NaCl electrolyte of different concentrations when cycled between −0.8 V and 0.8 V at 5 mV* s^{-1} *and (b) Control CVs obtained from the control solutions in between two consecutive switching of electrolyte concentrations*

The stationary voltammetric responses obtained after three consecutive potential cycles for the PPF4 obtained for different electrolyte concentrations of NaCl are shown in Figure 6.28a. The concentration of the electrolytes are kept ascending from 0.025 M to 1 M and then decending from 1 M to 0.025 M. The peak current increases gradually with an increase in the electrolyte concentration and then decreases with decreasing the electrolyte concentration. From Figure 6.28a, it can be seen that, under the same working energetic conditions, the same concentration of electrolyte gives similar voltammetric responses suggesting the reproducibility of the

electrochemical reaction of the hybrid film. Figure 6.28b presents the CV responses from the control solution recorded in between two consecutive concentrations. The overlapping of the CVs recorded from the voltammetric control (Figure 6.28b) confirms the reproducibility of the process and electrochemical stability of the PPy/PVA hybrid film.

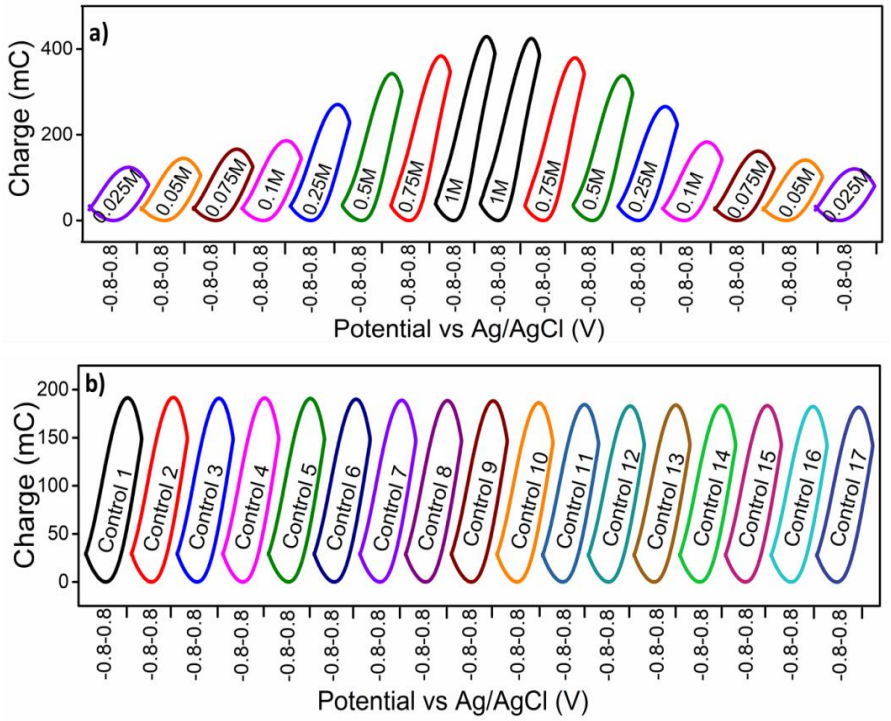

Figure 6.29 *(a) QVs of PPF4 obtained in NaCl electrolyte of different concentrations and (b) QVs obtained from the control solutions in between two consecutive switching of electrolyte concentrations*

The stationary QV responses corresponding to the CVs in Figure 6.28a are presented in Figure 6.29a. The QV responses show a closed loop and a small open fraction in the studied potential range. By adjusting the QV minimum to zero, the redox charge consumed during the reversible reactions increases for increasing the

concentration of the electrolyte and then decreases for decreasing the concentrations. Under the same working energetic conditions, the electrolyte of same concentration gives the same redox charge on repeated switching of the control solution. Figure 6.29b shows the stationary QV responses of the control solution obtained by integrating the CVs in Figure 6.28b. The overlapping of these QVs again ensures that the electroactivity of the hybrid film remains constant during the experiments.

The relative insertion/expulsion of anions and solvent molecules changes with the electrolyte concentration under constant experimental conditions. As mentioned earlier, at a low concentration of electrolyte, the chemical energy available for the reaction 3.1 to extract the electrons from the polymer chain and to drive the conformational movements from the reactant polymeric chains is low and the polymer chains become partially oxidized. When the concentration of the electrolyte increases, the available chemical energy increases and we get a deeper oxidation states at high concentrations under the same thermal, mechanical and electrical conditions. The above described events are summarized in Figure 6.30. From this experiment it is evident that same concentration of electrolyte always produces the same amount of free volume and thus the same number of anions and solvent molecules are inserted. When the electrolyte concentration increases, the redox charge consumed by the reversible reaction driving the conformational movements of the polymer chains also increases. The results prove that for the same concentrations of the electrolytes, the redox charge consumed by the reversible reaction is the same.

For the control solution, each time, we get the same CV and QV that further confirms that the conformational movements due to the cooperative actuation of the polymer chains occur to the same extent under similar experimental conditions irrespective of the direction of the experiment (either increase or decrease of the electrolyte concentration).

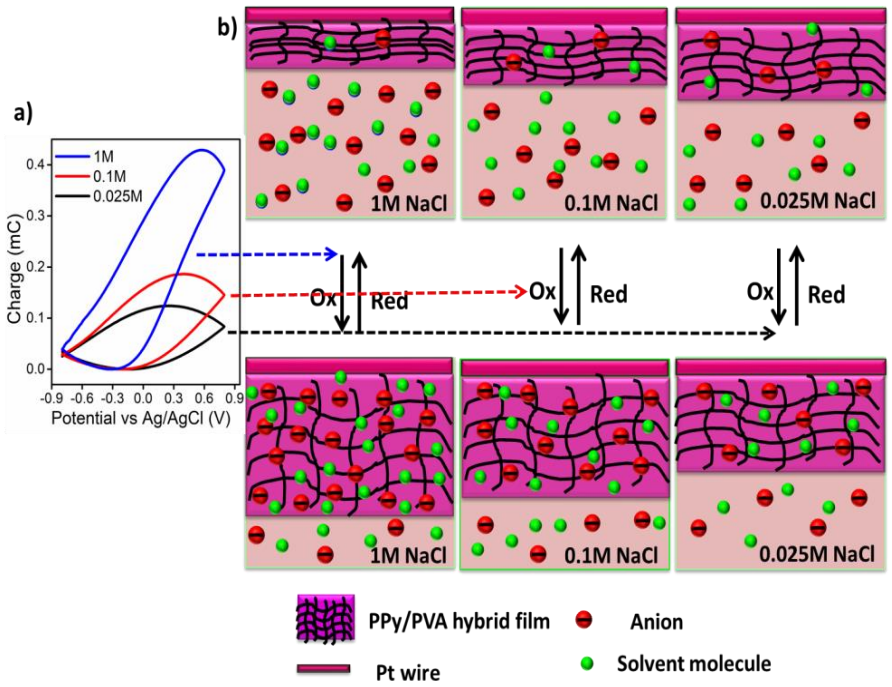

Figure 6.30 *(a) QV responses of PPF4 showing the redox charges in 1 M, 0.1 M, and 0.025 M NaCl aqueous solution and (b) Schematic representation of the extension of the structural changes (swelling/shrinking) by the reversible redox reaction of PPF4 under similar experimental conditions, where Ox means oxidation; Red means reduction*

The variation of redox charge of the hybrid film with the electrolyte concentration is shown in Figure 6.31 for both increasing concentrations and then for the subsequent decreasing concentrations.

Figure 6.31 represents the sensing calibration curve. The slope of the curves (0.351 for increasing concentration and 0.356 for decreasing concentration) represents the sensitivity of the sensor. Thus we can say that any electrochemical device (sensors, supercapacitors, actuators, batteries, etc.) driven by redox reactions of PPy/PVA hybrid film can sense while working, any perturbation of the chemical working energetic conditions, as the natural muscles do.

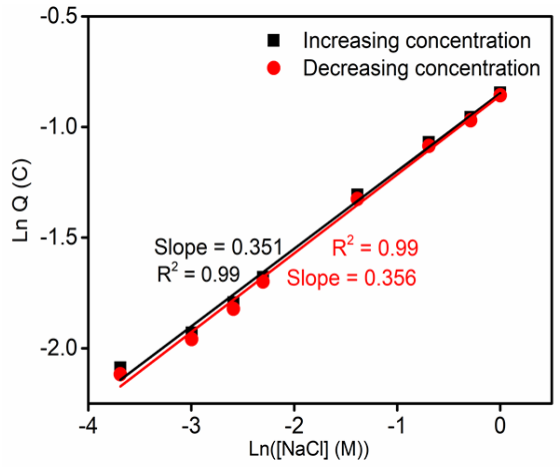

Figure 6.31 *Double logarithmic variation of the electrical charge consumed by the reversible redox reactions of PPF4 with the NaCl concentrations*

6.2.4.3. Effect of number of times of coating on sensing chemical condition of the hybrid films

Figure 6.32a-d represents the stationary voltammetric responses of the hybrid films obtained from electrolytes at different concentrations when it is cycled between −0.8 V and 0.8 V versus Ag/AgCl at 5 mV s^{-1} at room temperature. The peak current increases gradually with an increase in electrolyte concentration for all the hybrid films.

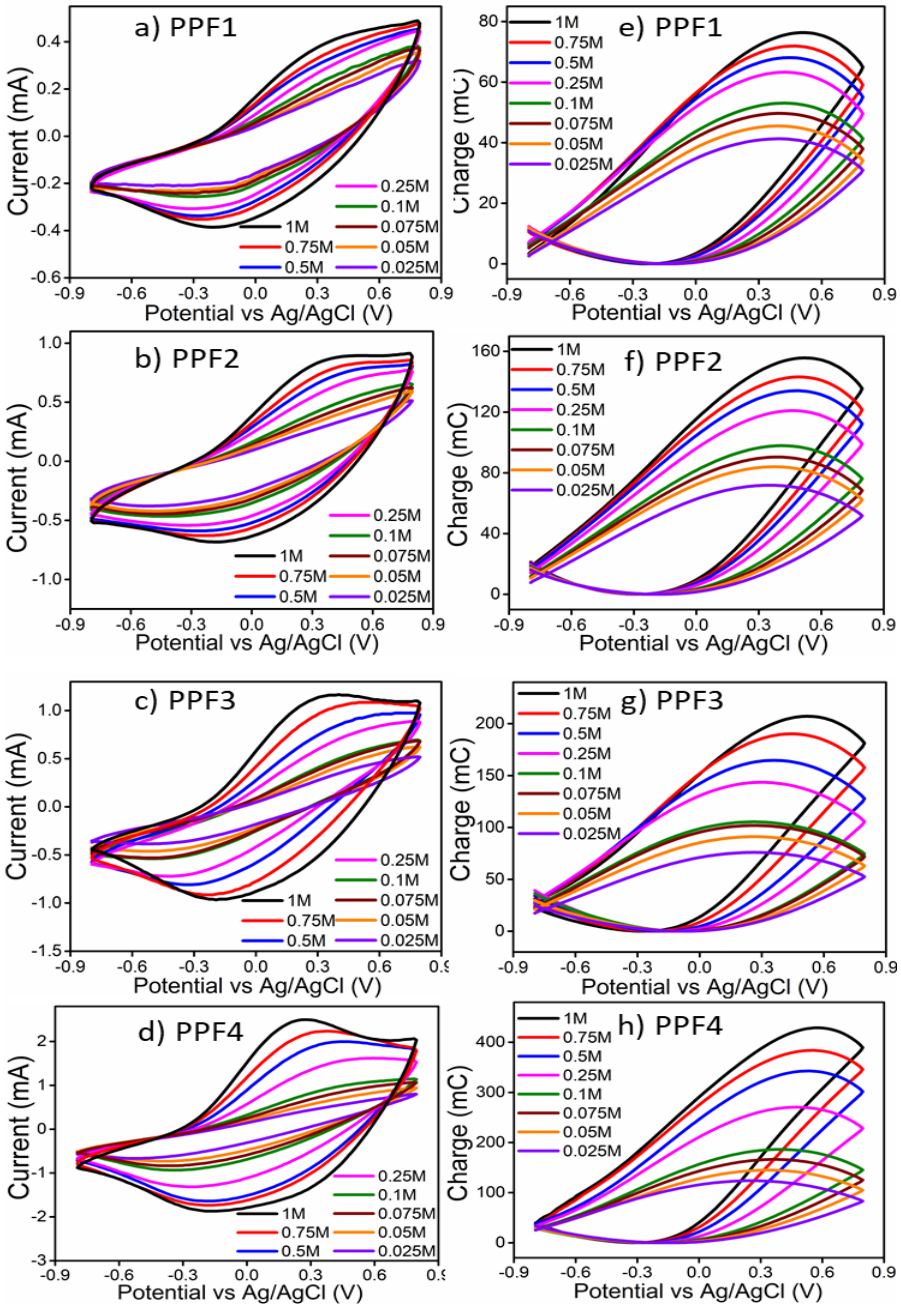

Figure 6.32 *(a-d) Stationary CV responses of PPy/PVA hybrid films obtained in NaCl electrolyte of different concentrations and (e-h) QVs obtained at different electrolyte concentrations*

The CVs in Figure 6.32a-d were integrated and the corresponding QV responses are presented in Figure 6.32e-h. The QV responses show a closed loop and a small open fraction in the investigated potential range for PPF1, PPF2 and PPF3. The sample PPF4 shows only a closed loop in the studied potential range. The redox charge consumed by the reaction of the hybrid films increases with increase in the electrolyte concentration.

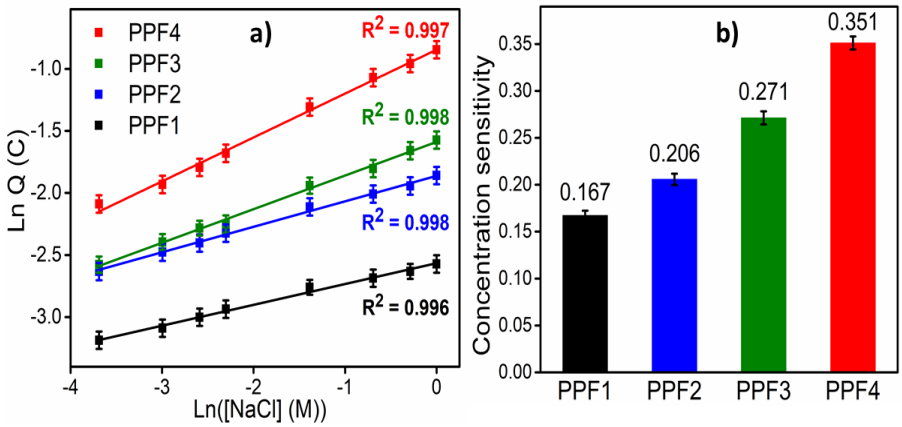

Figure 6.33 *(a) Double logarithmic variation of the consumed electrical charge of PPy/PVA hybrid films with concentration of electrolytes and (b) Effect of number of times of coating of PPy on the concentration sensitivity*

Figure 6.33 shows the double logarithmic variation of the redox charge with the electrolyte concentration. The attained linear relationship indicates that the consumed redox charge of any electrochemical device based on the reversible reactions of PPy/PVA hybrid films can act as a self-sensor of reaction chemical conditions. The chemical sensitivity of the fabricated hybrid films quantified by the slope of the curves is found to increase with an increase in the PPy content, and shows the highest sensitivity of 0.351 for PPF4.

6.2.4.4. Influence of the thermal condition on the cooperative actuation of multistep molecular motors of Polypyrrole: temperature sensor

The influence of temperature (available thermal energy) on the redox charge of the electrochemical reactions of the hybrid film (PPF4) was studied by consecutive potential cycles at different temperatures ranging from 10 ˚C to 50 ˚C under constant chemical (1 M NaCl), physical (from -0.8 V to 0.8 V at 5 mV s^{-1}) and mechanical conditions using a thermostat. The reproducibility of the electrochemical activity of the hybrid film was analyzed using a control solution (1 M NaCl aqueous solution at 25 ˚C) by the following steps:

(a) The PPF4 electrode is dipped in a cell containing the voltammetric control solution (1 M NaCl aqueous solution at 25 ˚C) and records the stationary CV responses.
(b) After the voltammetric control, the hybrid film electrode was dipped in another cell and placed in a thermostat having 1 M NaCl aqueous solution at 10 ˚C and recorded the stationary CV responses under similar conditions.
(c) Then the electrode was placed back in the control solution and submitted to stationary voltammetric cycles.

The procedure (b) and (c) were repeated for various cell temperatures that first gradually increase from 10 ˚C to 50 ˚C and then decrease from 50 ˚C to 10 ˚C. CVs from the control solutions (at 25 ℃) are recorded in between each temperature cycling during increasing and decreasing of the working temperatures.

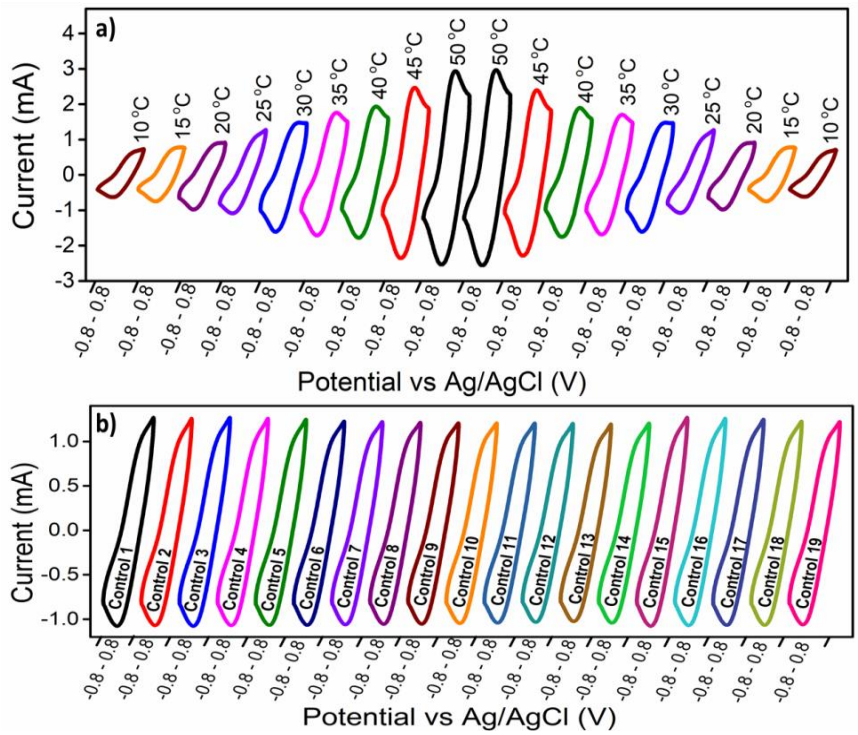

Figure 6.34 *Stationary CV responses of PPF4 recoded at different temperatures when cycled between −0 .8 V and 0.8 V at 5 mV* s^{-1} *in 1 M NaCl aqueous solution and (b) CV responses of the control solution in between two consecutive switching of temperatures*

Figure 6.34a displays the stationary voltammetric response of the PPF4 electrode recorded at different temperatures ranging from 10 ˚C to 50 ˚C under constant experimental conditions. The temperature of the electrolyte kept ascending from 10 ˚C to 50 ˚C and then descending from 50 ˚C to 10 ˚C. The voltammetric responses show that both the anodic and cathodic peak currents increases with the increase of temperature and then decrease with the decrease of temperatures. From Figure 6.34a, it is evident that similar voltammetric responses are attained for experiments of the same temperatures under the same working energetic conditions corroborating the reproducibility

of the redox reaction in hybrid films. The voltammetric response of the control solution (1 M NaCl aqueous solution at 25 ˚C) was recorded between consecutive experiments at two different temperatures (Figure 6.34b). The overlapping of the CVs recorded from the voltammetric control (Figure 6.34b) confirms the reproducibility of the process and electrochemical stability of the PPy/PVA hybrid film.

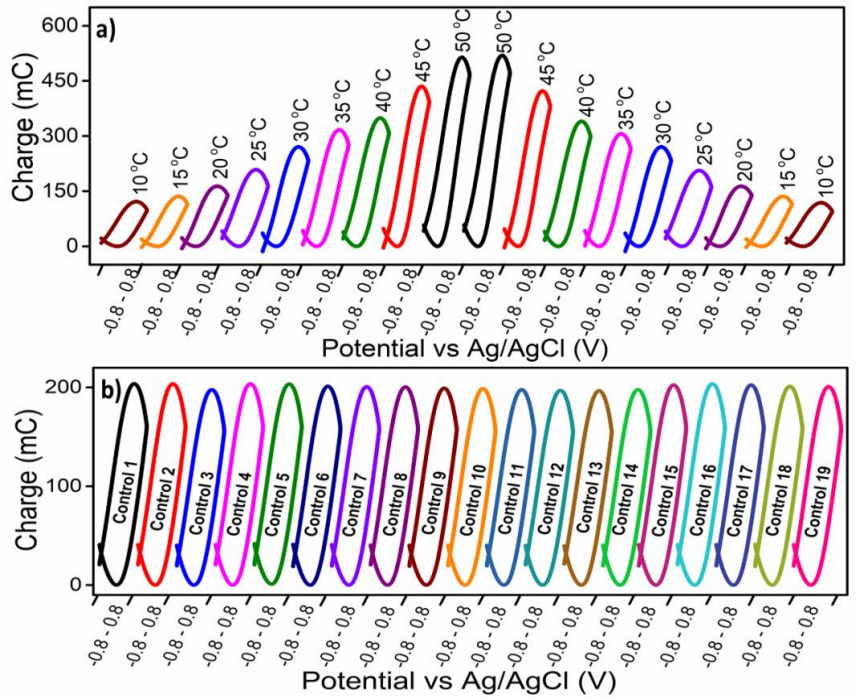

Figure 6.35 (*a) Stationary QVs of PPF4 obtained from different temperature and (b) QVs obtained from the control solutions*

The stationary QV responses corresponding to the CVs in Figure 6.34a are presented in Figure 6.35a. It is observed that all the QVs constitute a closed loop and a small open fraction in the studied potential interval. As the experimental temperature increases, the redox charge consumed during the reversible reactions driving the

conformational movements of the reactive polymeric chain increases under the same chemical, physical and mechanical energetic conditions. Thus we get deeper oxidation/reduction states at higher temperatures. It is interesting to note that a similar redox charge is obtained for the experiments performed at the same temperatures on repeated switching of the control solution under the same working energetic conditions. Figure 6.35b shows the stationary QV responses of the voltammetric control solution. The superimposing of these QVs confirms the reproducibility of the process and electrochemical stability of the PPy/PVA hybrid film.

The lower temperature (low available thermal energy) allows partial conformational movements of the reactive polymeric chains and generates a low amount of free volume to insert the counterions and the solvent molecules with concomitant consumption of low oxidation charge [21]. Thus the polymer chains undergo partial oxidation/reduction at lower temperatures [22, 23]. As the experimental temperature increases, the increased available thermal energy allows faster and longer conformational movements of the polymeric chains with the consumption of increasing redox charges and we get deeper oxidation/reduction states at higher temperatures. The above described events are summarized in Figure 6.36. From Figure 6.35a, it is evident that, as the temperature increases, the redox charge consumed by the reversible electrochemical reaction driving reversible conformational movements of the polymeric chains increases. From this experiment, it is evident that under same temperature, conformational movements due to the cooperative actuation of the polymer chains takes place to equal

extent and produces same amount of free volume and thus same number of anions and solvent molecules are inserted. The results prove that, for the experiments carried out at same temperature, the redox charge consumed by the reversible reaction is the same. For the control solution, each time, we get the same CV and QV that further confirms that the same conformational movements due to the cooperative actuation of the polymeric chains occur to the same extent under similar experimental conditions irrespective of the direction of the experiment (either increase or decrease of temperature).

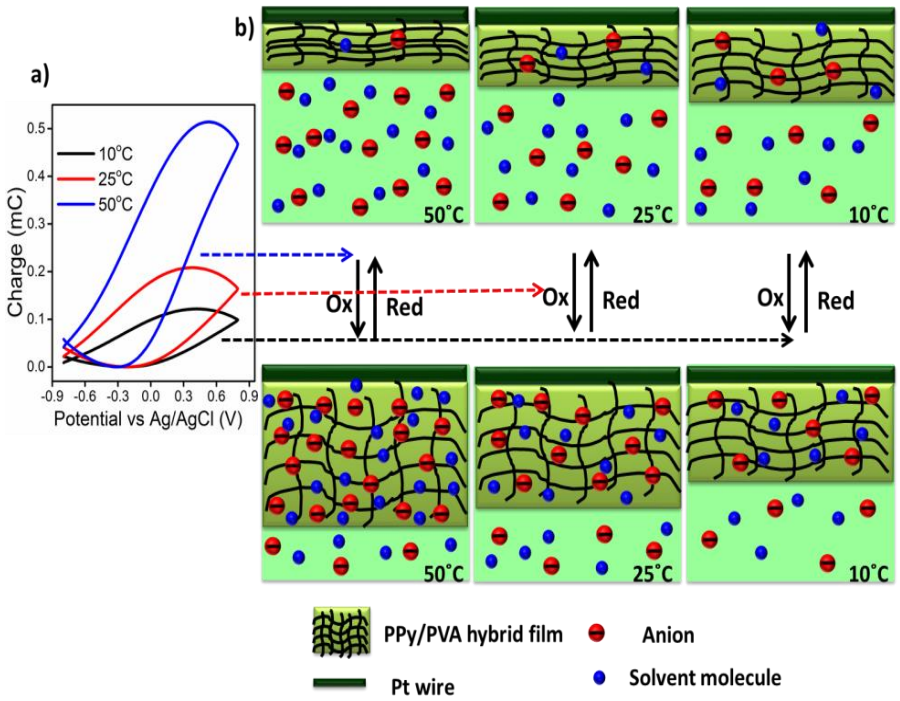

Figure 6.36 *(a) QV responses of PPF4 showing the redox charges at 10 ˚C, 25 ˚C and 50 ˚C and (b) Schematic representation of the extension of the structural changes (swelling/shrinking) by the reversible redox reaction of PPF4 at 10 ˚C, 25 ˚C and 50 ˚C in 1 M NaCl aqueous solution under similar experimental conditions, where Ox means oxidation; Red means reduction*

Figure 6.37 shows the logarithmic variation of the redox charge or extension of the reaction with the inverse of temperature for both increasing and subsequent decreasing of temperatures. By varying the temperature and keeping constant values for all other experimental variables, a good agreement was achieved for the redox charges obtained in experiments carried out in the same temperatures. The slope of the graphs showing the linear dependencies (3411.4 and 3417.6 for increasing and decreasing temperatures respectively) gives the thermal sensitivity of the sensor. Thus for any chemical reaction based on the cooperative actuation of the constitutive PPy polymer chains , the extension of reaction varies, at any instant, as a function of experimental temperature. Translated to molecular motors constituting natural muscles, higher redox charges are consumed by the muscular reactions occurring at higher temperatures.

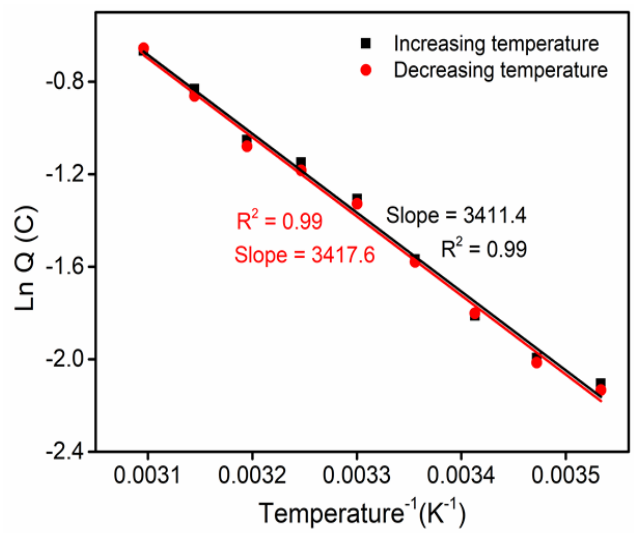

Figure 6.37 *Logarithmic variation of the electrical charge consumed by the reversible redox reactions of the PPF4 with the inverse of temperature*

6.2.4.5. Effect of number of times of coating on sensing thermal condition of the hybrid films

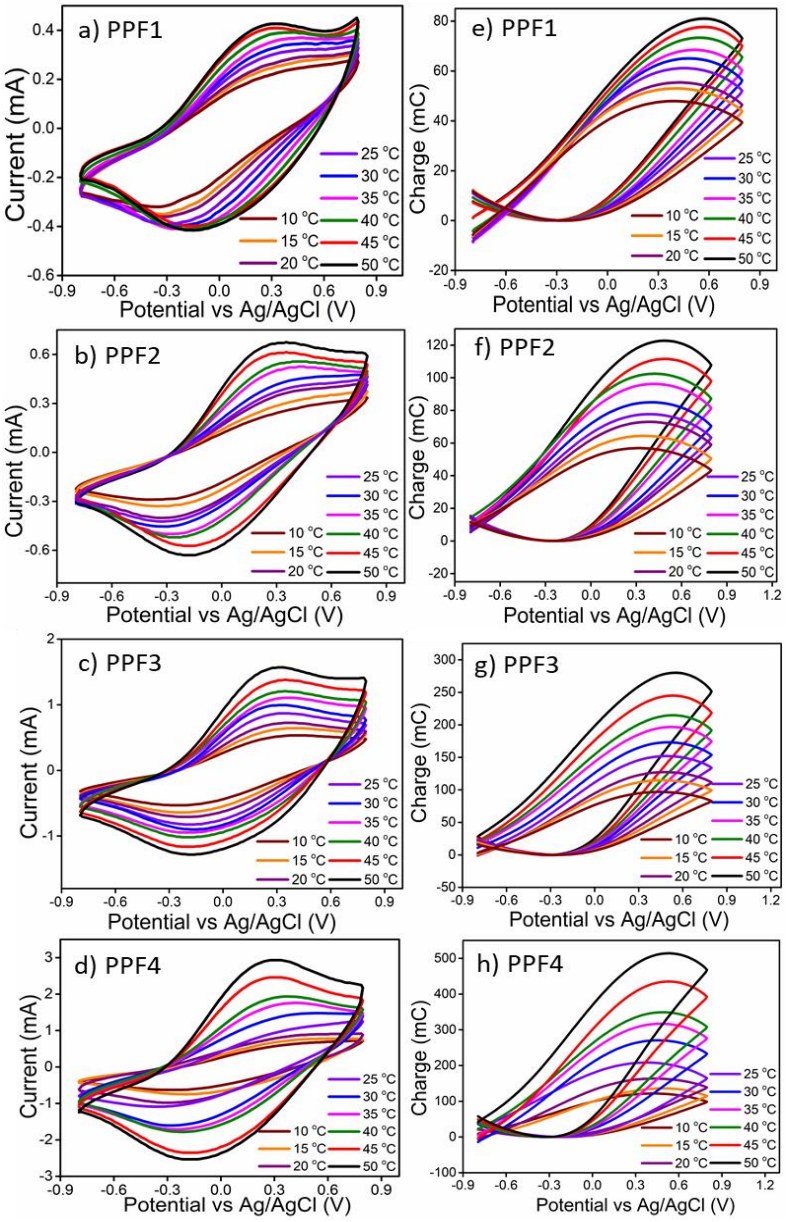

Figure 6.38 *(a-d) Stationary CV responses of PPy/PVA hybrid films at different temperatures and (e-h) QVs obtained at different temperatures*

Figure 6.38a-d shows the stationary voltammetric response of the PPy/PVA hybrid films at different temperatures ranging from 10 ˚C to 50 ˚C when it is cycled between −0.8 V and 0.8 V versus Ag/AgCl at 5 mV s^{-1} in 1 M NaCl aqueous solution. Both the anodic and cathodic peak currents increase with the increase of temperatures. The reason is that deeper oxidation/reduction states are attained at higher temperatures. The stationary QV responses corresponding to the CVs in Figure 6.38a-d are presented in Figure 6.38e-h. It is observed that for all the hybrid films, the QVs constitute a closed loop and a small open fraction in the studied potential interval. For all the samples, the redox charge increases with increase of temperature.

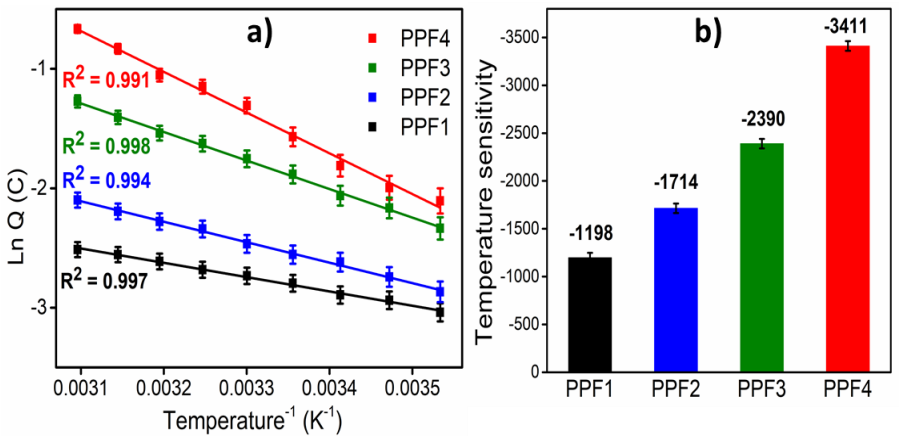

Figure 6.39 *(a) Logarithmic variation of the electrical charge consumed by the reversible redox reactions of the hybrid films with the inverse of temperature and (b) Effect of number of times of coating of PPy on the temperature sensitivity*

Figure 6.39a shows the logarithmic variation of the redox charge with the experimental temperature. The attained linear relationships (R^2 = 0.99) indicates that the consumed redox charge of any

electrochemical device based on the reversible reactions of PPy/PVA hybrid films senses the working thermal condition. The slope of the curves defines the temperature sensitivity of the hybrid films and which is found to increases with increase in number of times of coating, i.e. from PPF1 to PPF4, and PPF4 presents the highest sensitivity of -3411 (Figure 6.39b).

6.2.4.6. Influence of the electrical condition on the cooperative actuation of multistep molecular motors of Polypyrrole

The influence of electrical energetic condition on the redox charge of the electrochemical reactions of the hybrid film (PPF4) was studied by consecutive potential cycles at different scan rates (ranging from 5 to 100 mV s^{-1}) under constant chemical (1 M NaCl), physical (from -0.8 V to 0.8 V), thermal (25 ˚C) and mechanical conditions. The reproducibility of the electrochemical activity of the hybrid film was analyzed by employing a control scan rate (25 mV s^{-1}) through the following steps:

(a) After stabilizing the CV responses, the PPF4 electrode was submitted to potential cycles at a scan rate of 25 mV s^{-1} (control scan rate) in 1 M NaCl solution at room temperature (25 ˚C) and recorded the stationary CV responses.
(b) After applying the control scan rate, the PPF4 electrode was then submitted to a scan rate of 5 mV s^{-1} and recorded the stationary CV responses under similar experimental conditions.
(c) Then the electrode was submitted again to the control scan rate and recorded the CV responses.

The procedure (b) and (c) were repeated for different scan rates which first increase from 5 mV s^{-1} to 100 mV s^{-1} and then decreases from 100 mV s^{-1} to 5 mV s^{-1}. The CVs from the control solution are measured in between two consecutive scan rate cycling during increasing and decreasing of the scan rates.

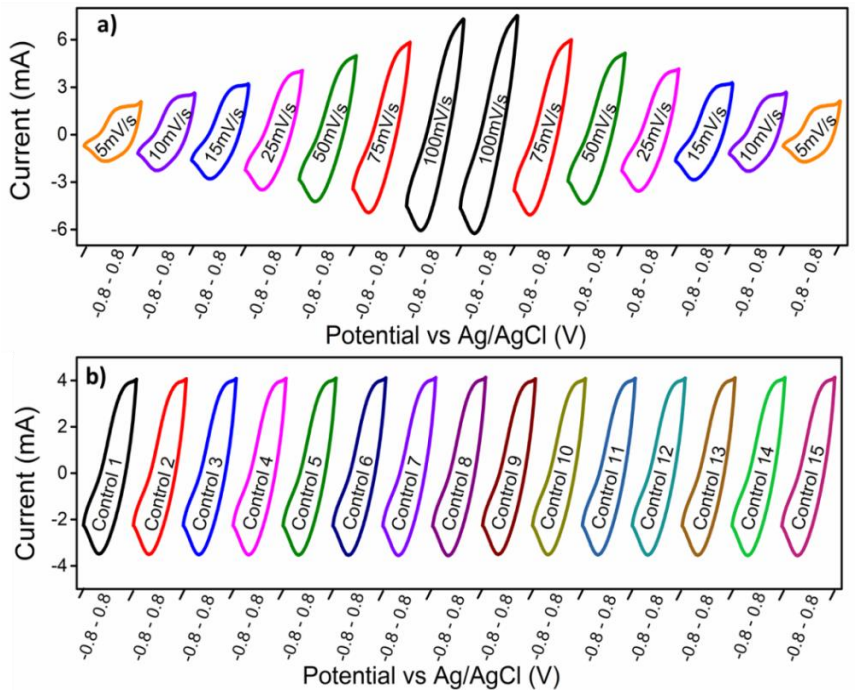

Figure 6.40 *Stationary CV responses of PPF4 at different scan rates in 1 M NaCl aqueous solution and (b) Voltammetric responses of the control scan rate obtained after each increasing or decreasing potential cycling*

Figure 6.40a shows the stationary voltammetric response of the PPF4 at different scan rates (5 mV s^{-1} to 100 mV s^{-1}) under constant experimental conditions. Voltammetric responses illustrate the increase of both the anodic and cathodic peak currents with the increase of scan rate and then decrease with the decrease of scan rate. From

Figure 6.40a, it can be seen that, under the same working energetic conditions, similar voltammetric responses are obtained for the same applied scan rates during the repeated switching of the control solution, suggesting the reproducibility of the electrochemical reaction of the hybrid film. Figure 6.40b presents the voltammetric responses at the control scan rate obtained in between two consecutive scan rates. The overlapping of the CVs in Figure 6.40b confirms the reproducibility of the process and electrochemical stability of the PPy/PVA hybrid film.

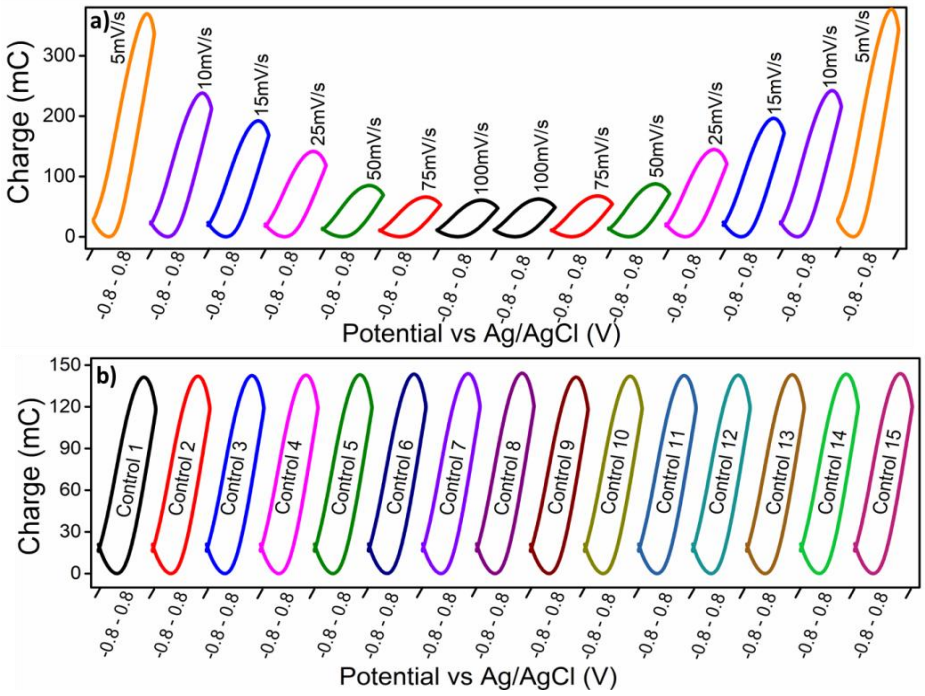

Figure 6.41 (*a) Stationary QVs obtained at different scan rates and (b) Control QVs obtained for the control scan rates*

The stationary QV responses corresponding to the CVs from Figure 6.40a are presented in Figure 6.41a. By adjusting the QV minimum to zero, the redox charge consumed during the reversible

reactions decreases for increasing the scan rate and then increases for decreasing the scan rates. Under the same working energetic conditions, similar redox charges are obtained for the same applied scan rates. Figure 6.41b shows the stationary QV responses at the control scan rate obtained by integrating the CVs in Figure 6.40b. The overlapping of these QVs again ensures that the electroactivity of the hybrid film remains constant during the experiments.

The oxidation and reduction potentials are applied for a larger time interval when the scan rate is low. This promotes deeper conformational changes with the consumption of large redox charges and deeper oxidation/reduction states are attained at lower scan rates. As the scan rate increases, the time taken for the reaction 3.1 to extract the electrons from the polymer chain and to drive the conformational movements of the reactive polymeric chains becomes relatively low. Therefore, the polymer chains undergo partial oxidation/reduction at lower temperatures. The above described events are summarized in Figure 6.42. From this study, it is evident that same scan rate always produces same amount of free volume and thus the same number of anions and solvent molecules are inserted. When we apply the same scan rate during increasing or decreasing mode of scan rate switching, the redox charge consumed by the reversible reaction is found to be the same. For the control scan rate, each time, we get the same CV and QV, which further confirms that the conformational movements occur to the same extent under similar experimental conditions irrespective of the direction of the experiment (either increasing or decreasing of scan rate).

The variation of redox charge during the electrochemical reaction of the hybrid film with the scan rate is shown in Figure 6.43 for both increasing and subsequent decreasing of scan rates. Figure 6.43 represents the sensing calibration curve. The slope of the curves i.e., -0.639 for increasing scan rate and -0.629 for decreasing scan rate represents the sensitivity of the sensor. Thus we can say that any electrochemical device (sensors, supercapacitors, actuators, batteries, etc.) driven by redox reactions of PPy/PVA hybrid film can sense while working, any perturbation of the electrical working energetic conditions.

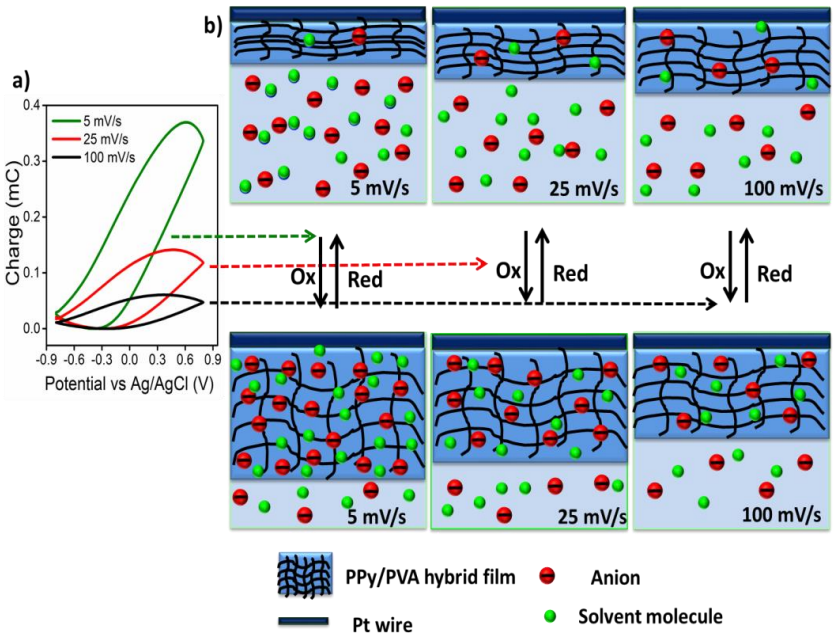

Figure 6.42 *(a) QV responses of PPF4 showing the redox charges at 5 mV s^{-1}, 25 mV s^{-1} and 100 mV s^{-1} and (b) Schematic representation of the extension of the structural changes (swelling/shrinking) by the reversible redox reaction of PPF4 under similar experimental conditions, where Ox means oxidation; Red means reduction*

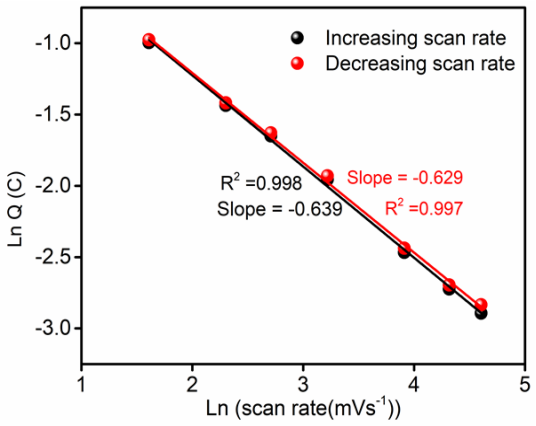

Figure 6.43 *Double-logarithmic variation of the charge consumed by the reversible reactions of PPF4 with the scan rate*

6.2.4.7. Effect of number of times of coating on sensing electrical condition of the hybrid film

The CV responses of all the hybrid films recorded at different scan rates by keeping all other experimental conditions constant are displayed in Figure 6.11a-d and the concomitant QV responses are presented in Figure 6.44a-d. For all the hybrid films, the redox charge consumed during the reversible reactions driving the conformational movements of the reactive polymeric chain decreases with increasing scan rate. Figure 6.45a shows the double logarithmic variation of the consumed charge or extension of the reaction with the scan rate. The experimental results are in good agreement with the sensing equation 4.34. The slope of the curves represents the sensitivity of the sensor and which increases as the number of times of coating increases gradually from PPF1 to PPF4 (Figure 6.45b). The linear fit of the curves corroborates that the consumed charge during the redox reactions of PPy can act as a robust sensor of the imposed electrical

condition (scan rate) under constant thermal, mechanical and chemical conditions.

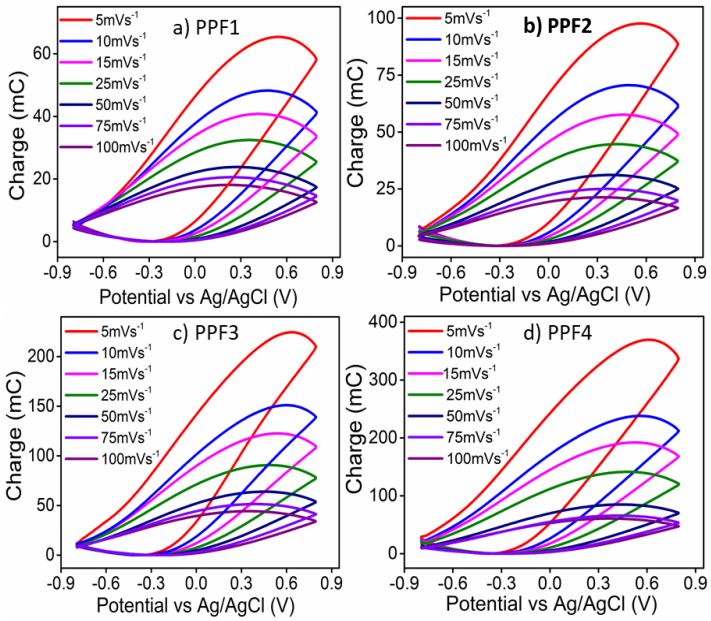

Figure 6.44 *QV responses of PPy/PVA hybrid films obtained at different scan rates*

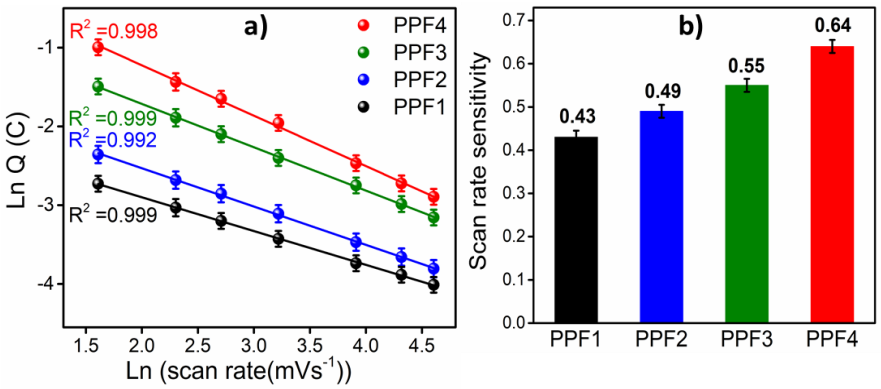

Figure 6.45 *(a) Linear variation showing the double-logarithmic relationship between the charge consumed by the reversible reactions of PPy/PVA hybrid films with the scan rate and (b) Effect of number of times of coating of PPy on sensitivity of the electrical energetic conditions*

6.2.5. Supercapacitive studies

The advantages of all four mechanically stable PPy/PVA hybrid films as active supercapacitor electrodes are explored using GCD, CV and EIS measurements. Figure 6.46a represents the GCD curves of the hybrid films obtained at a current density of 0.5 A g^{-1} in 1 M NaCl aqueous solution within the potential window of -0.8 V to 0.8 V at room temperature. The deviation from linearity exhibited by the GCD profiles reveals the typical pseudocapacitive behavior of the hybrid films. As can be seen in Figure 6.46a, PPF4 displays substantially prolonged charging and discharging time as compared to other electrode materials. The specific capacitance of the hybrid films was calculated from the GCD profile using equation 2.7. Through calculation, the maximum specific capacitances achieved at a current density of 0.5 A g^{-1} for PPF1, PPF2, PPF3 and PPF4 are 116 F g^{-1}, 239 F g^{-1}, 442 F g^{-1} and 594 F g^{-1} respectively. That is, the supercapacitance increases as the number of times of coating or electrical conductivity increases (Figure 6.46b). The charge storage ability of the PPy/PVA hybrid films depends on the transfer of counterions as well as the movement of electrons. The GCD curves of the PPy/PVA hybrid films at different current densities are presented in Figure 6.47a-d. The variation of specific capacitance as a function of specific current is shown in Figure 6.47e. It is observed that, the specific capacitance increases as the current density decreases as expected. This is because, at higher current densities, there is lesser time available for the electrolyte ions to diffuse into active sites and interact with active material and hence only the outer surface

contributes to the specific capacitance. At lower current densities, the ions permeate into the inner surface of the electrode material and utilize both the inner and outer surfaces resulting in higher capacitance values. As the current density increases from 0.5 A g^{-1} to 7 A g^{-1}, 64 % of the capacitance is retained by PPF4 film indicating that the rate capability of the hybrid films is significantly improved as the content of PPy (or conductivity) increases.

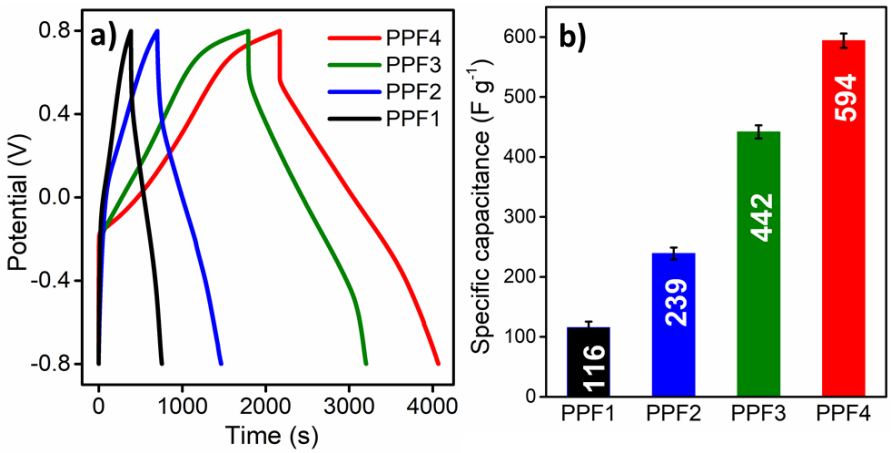

Figure 6.46 *(a) GCD profiles of PPy/PVA hybrid films at a current density of 0.5 A g^{-1} and (b) Specific capacitance of the hybrid films calculated from GCD profiles*

The long-term cycling stability is a key parameter for assessing the performance of a supercapacitor electrode. The cycling stabilities of all the hybrid film electrodes were monitored over 1500 GCD cycles at 2 A g^{-1}.The results are shown in Figure 6.48a. It is well known that CPs possess poor cycling stability as a consequence of the swelling and shrinking (intercalation/deintercalation) of the polymer during repeated cycling. It is worth mentioning that the cycle life is improved as the content of PPy or the number of times of coating increases. It is evident

from Figure 6.48b that, 87.5 % of the initial capacitance is retained by PPF4 electrode after 1500 cycles indicating a good long-term cycle life which is attributed to the strong synergy existing between PPy and PVA.

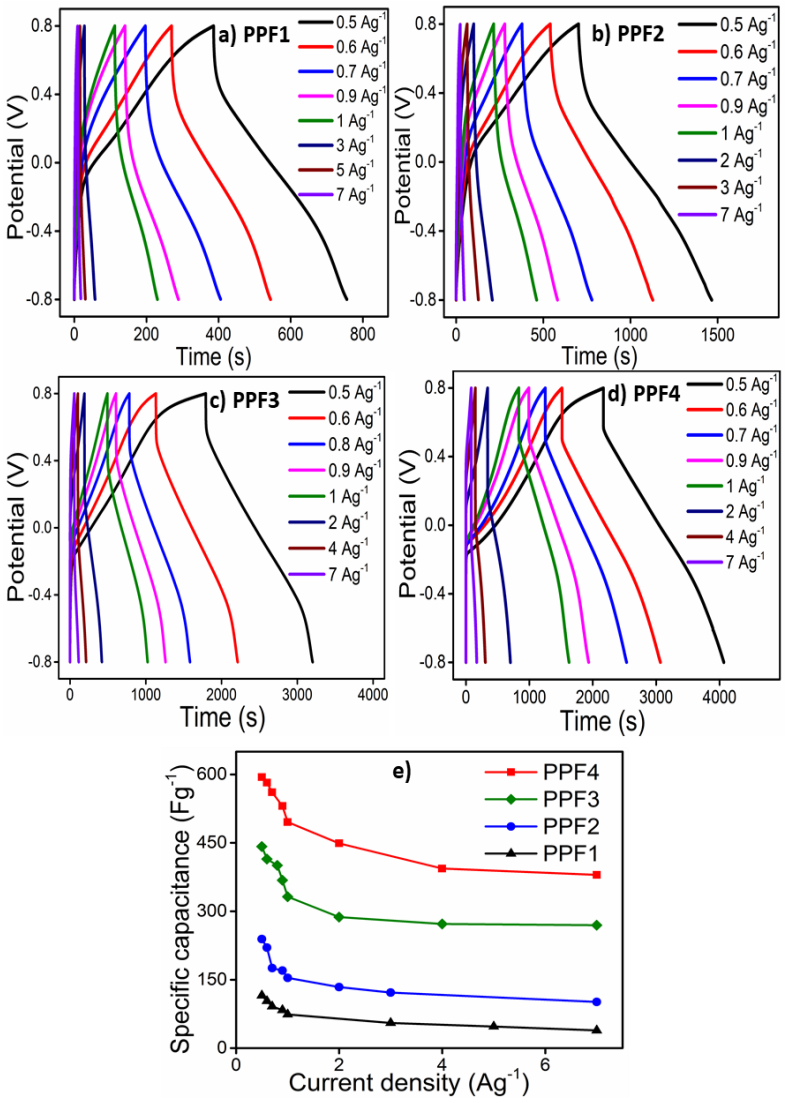

Figure 6.47 *GCD curves of (a) PPF1, (b) PPF2 and (c) PPF3 and (d) PPF4 at different current densities and (e) Specific capacitance of all PPy/PVA hybrid films as a function of current density*

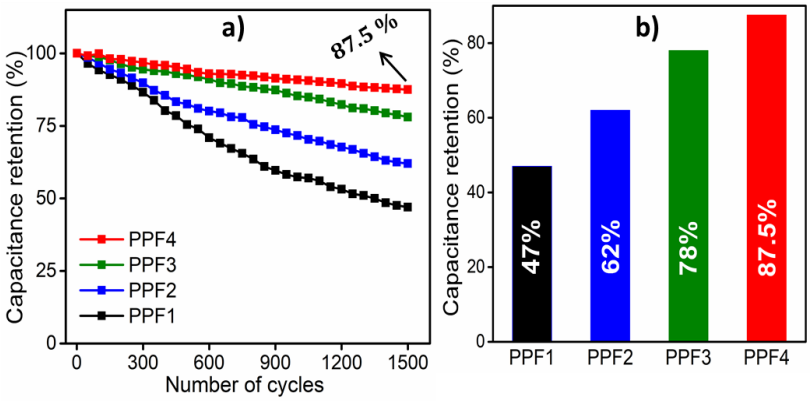

Figure 6.48 *(a) Cycling stability of all PPy/PVA hybrid films and (b) Effect of number of times of coating of PPy on the cycling stability of hybrid films*

The specific capacitance of the hybrid films was further evaluated from CV curves (Figure 6.10) using equation 2.5. The deviation of the CV loops from the rectangular nature and the presence of a pair of redox peaks confirm the faradaic pseudocapacitive dominance prevailing in the hybrid films [24]. It is striking to note that the area encircled by the CV profile is drastically enhanced as the PPy content in the film increases and the capacitance of the hybrid films also increases accordingly. Among the hybrid films, PPF4 showed the largest area with maximum current, revealing that it has the highest specific capacitance and lowest internal resistance. The specific capacitance values of 195 F g^{-1}, 339 F g^{-1}, 479 F g^{-1} and 739 F g^{-1} are obtained at a scan rate of 2 mV s^{-1} for PPF1, PPF2, PPF3 and PPF4 respectively (Figure 6.49a). The variation of specific capacitance with scan rate was studied and is displayed in Figure 6.49b. As the scan rate increases, the specific capacitance decreases. At low scan rates, the longer time allows the complete diffusion of electrolyte ions into the inner active sites of the electrode material and favors the complete

redox transitions. However, at higher scan rates, the electrolyte does not have sufficient time to make use of the inner surface and internal sites of the electrode.

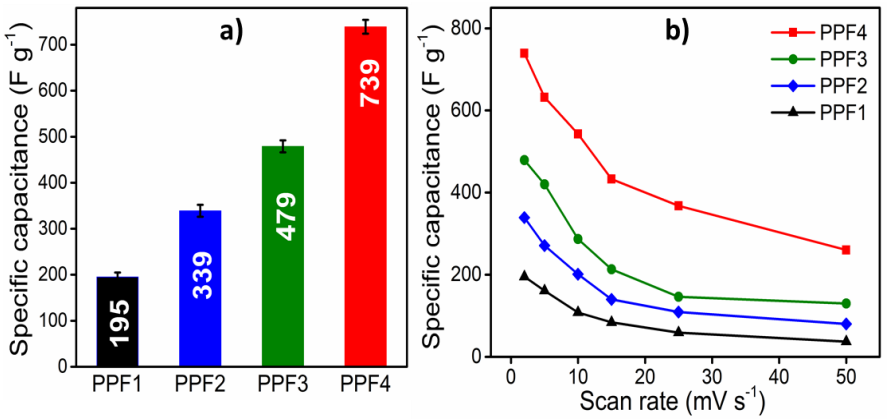

Figure 6.49 *(a) Specific capacitance of the hybrid films obtained from CV and (b) Specific capacitance of all PPy/PVA hybrid films as a function of scan rate*

6.2.5.1. Charge Storage Kinetic Studies

The total capacitance of a material is contributed from both surface capacitive effects and diffusion-controlled faradaic processes [25, 26]. Figure 6.50a demonstrates a linear relationship of log (current) with log (scan rate) at different potentials for PPF4 film and the b-value (explained in section 5.2.4.1) is extracted from the slope of the linear fitting. The calculated b values of PPF4 hybrid film at different potentials are shown in Figure 6.50b. It lies between 0.5 and 1 for different potentials. Thus the electrode is expected to have both pseudocapacitive and EDLC like behaviour. The respective proportion of capacitive (k_1v) and diffusive effects ($k_2v^{1/2}$) are quantified by the Dunn method (Equation 5.3) [27, 28]. Figure 6.50c shows that at a scan

rate of 2 mV s^{-1}, the capacitive (or pseudocapacitive) contribution is 22.4 % while the diffusive contribution is 77.6 %. The percentage of capacitive and diffusive contributions are measured at various scan rates. Figure 6.50d indicates that when the scan rate increases, the capacitive contribution increases and the diffusive contribution decreases. This is because at higher scan rates, the electrolyte does not have sufficient time to reach the internal sites of the electrode material effectively and therefore the surface controlled capacitive effects predominates.

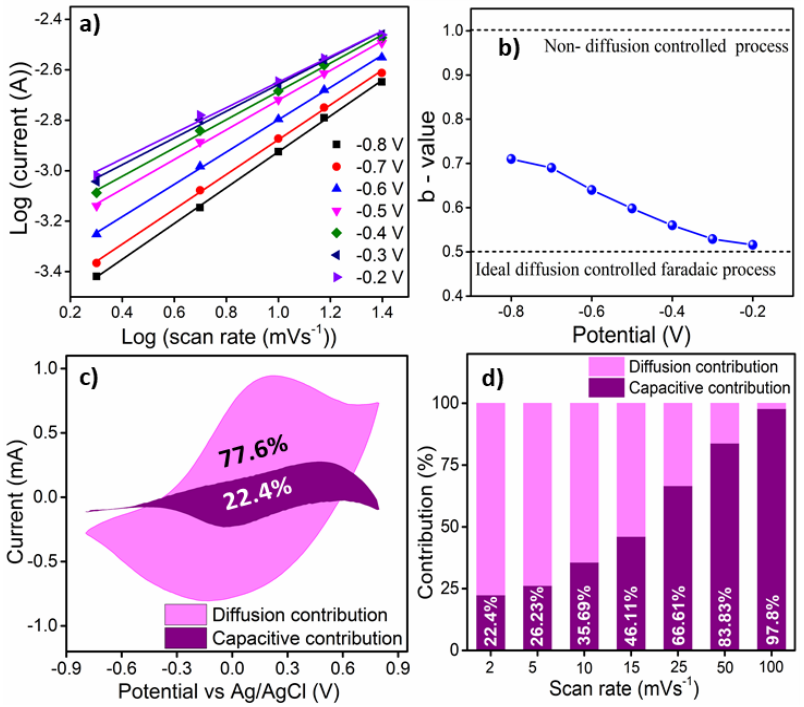

Figure 6.50 *(a) Linear relationship of log (current) versus log (scan rates) at different potentials, (b) The b-values at different potentials, (a) Separation of the pseudocapacitive and diffusion currents of PPF4 at a scan rate of 2 mV s^{-1} and (b) Contribution of capacitance from the surface-controlled pseudocapacitive reaction and diffusion-controlled processes at different scan rates*

6.2.5.2. Electrochemical impedance spectra

As an efficacious test method, EIS measurements were carried out at an open-circuit voltage of 10 mV within a frequency range of 0.1 Hz to 100 kHz in 1 M NaCl aqueous solution using a three electrode cell configuration for evaluating the impedance characteristics of PPy/PVA hybrid films. Their Nyquist plots are presented in Figure 6.51. The inset shows the magnified high-frequency region. The Nyquist plots of all the electrodes consist of two well-separated patterns: a semicircle in the high-frequency region and a nearly straight line in the low-frequency region [29]. From the Nyquist plots, the ESR value (x-intercept of the curve in the high-frequency region) of PPF1, PPF2, PPF3 and PPF4 are 16.69 Ω, 10.53 Ω, 6.89 Ω and 3.9 Ω respectively. Among the hybrid films, PPF4 shows the smallest ESR value suggesting that more number of counterions and solvents can penetrate in and out of the hybrid film. The diameter of the semicircle appeared at high-frequency region, which is related to the charge transfer resistance decreases with an increase in the PPy content indicating its lower resistance behaviour [30]. The straight line in the low-frequency region is associated to the diffusion-limited ion transport process and its slope provides the diffusion resistance. PPF4 exhibited the highest slope and hence has a lower diffusion resistance. In order to better understand all these impedance behaviour, the curves are fitted with an equivalent circuit model (inset of Figure 6.51) by Zman software and the best fitting results are listed in Table 6.4. In the circuit diagram, R_S, R_1 and R_2 signify the solution resistance, charge transfer resistance and diffusion resistance respectively. CPE_1 and CPE_2 are

used to express the constant phase elements. The Y is the CPE parameter and α is the dispersion coefficient. The EIS results are consistent with the CV and GCD results.

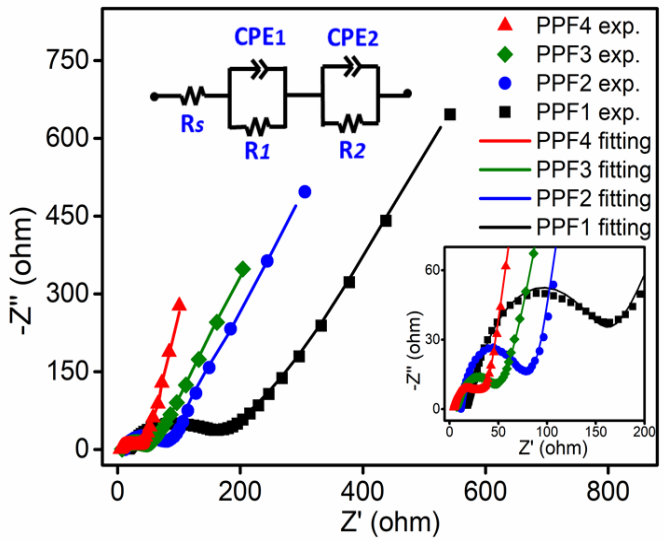

Figure 6.51 *Nyquist plot of PPy/PVA hybrid films (inset: equivalent circuit used to fit the impedance spectra)*

Table 6.4 *Equivalent circuit parameters of EIS of PPy/PVA hybrid films*

Electrode	**PPF1**	**PPF2**	**PPF3**	**PPF4**
R_S (Ω)	16.69	10.53	6.89	3.9
R_1 (Ω)	166.75	69.86	44.99	31.56
R_2 (Ω)	19.19k	18.32k	15.35k	8.72k
CPE_1-Y (S s^{α})	0.00898	0.00644	0.00379	0.000208
CPE_1-α	0.673	0.659	0.703	0.661
CPE_2-Y (S s^{α})	0.000239	0.000067	0.000098	0.000155
CPE_2-α	0.631	0.778	0.669	0.699

6.2.6. All Solid state symmetric device using PPF4 film

To demonstrate the feasibility of PPy/PVA hybrid film as a sensing supercapacitor, a symmetric all solid-state supercapacitor device was fabricated by sandwiching two identical pieces of PPF4 films using PVA/NaCl gel as the electrolyte (detailed procedure of fabrication is given in section 2.2.7). The assembling procedure is simple and effectively avoids the addition of auxiliary materials. The photograph of the solid-state supercapacitor device is shown in Figure 6.52.

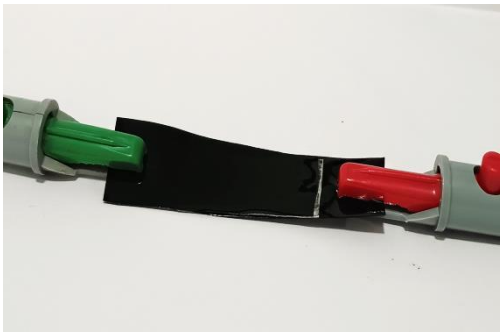

Figure 6.52 *Photograph of solid state symmetric device*

6.2.6.1. Supercapacitive studies of the device

The electrochemical behavior of the device was evaluated through CV, GCD, and EIS analysis in two electrode cell configuration. Figure 6.53a presents the CV curves of the device obtained at different scan rates within the potential window of -0.8 V to 0.8 V. As expected, the specific capacitance values decreased with an increase of the scan rate (Figure 6.53b) due to the inaccessibility of the electrolyte ions to interact with the inner surface of the electrode. The highest specific

capacitance of 364.5 F g^{-1} at a scan rate of 5 mV s^{-1} is obtained for the device from CV measurements. Figure 6.54a shows the GCD curves of the device at different current densities. The specific capacitance values decreases with an increase of the current densities (Figure 6.54b). High electrolyte diffusion occurs at lower current densities due to the better approachability of ions to the inner parts of the electrode. A highest specific capacitance of 241 F g^{-1} was obtained at a current density of 0.5 A g^{-1} from GCD measurements. The long term cycling stability is one of most important characteristics of supercapacitors for the practical applications. The cycle life was assessed by exposing the device to 1500 cycles at a current density of 2 A g^{-1}. The device retains 90 % of its initial specific capacitance after 1500 cycles (Figure 6.55). In Figure 6.55, the inset shows the first and last cycles. The specific capacitance of device is compared with those of various PPy based supercapacitors reported in the literature, which are listed in Table 6.5.

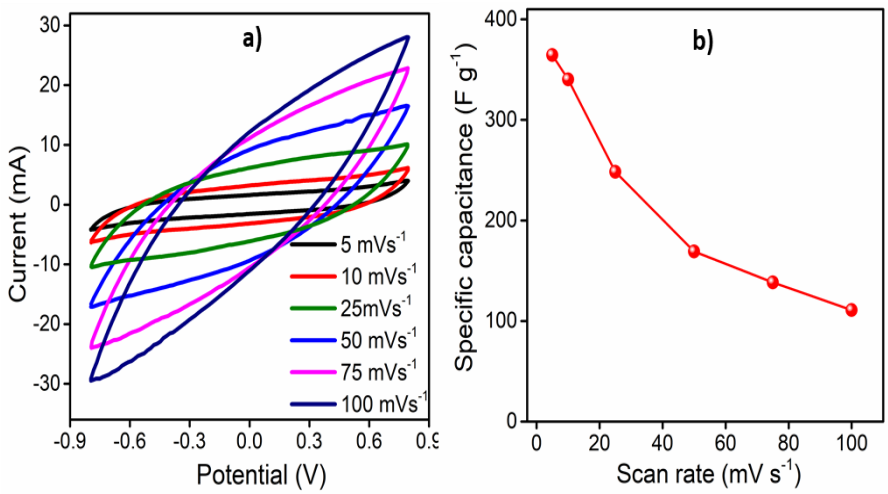

Figure 6.53 *(a) CV curves of PPF4 device at different scan rate and (b) variation of specific capacitance with scan rate*

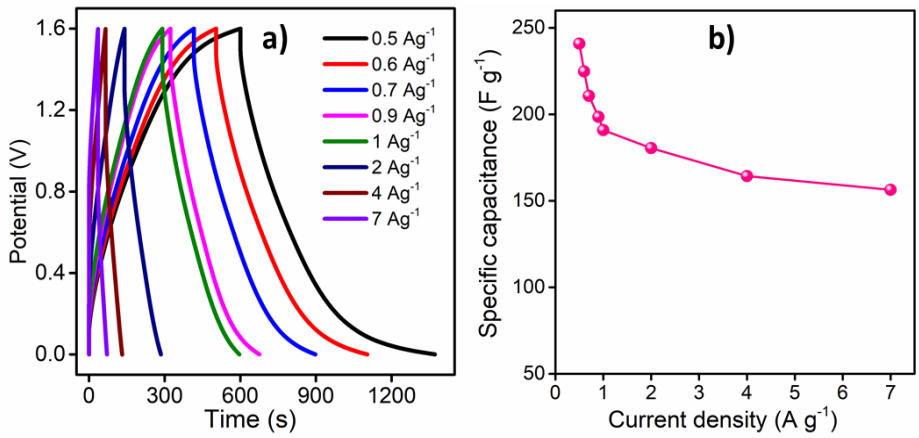

Figure 6.54 *(a) GCD curves of PPF4 device at different current densities and (b) variation of specific capacitance with current density*

Table 6.5 *Capacitive performance of PPy based supercapacitors*

Electrode materials	Specific capacitance ($F\ g^{-1}$)	Energy density ($Wh\ Kg^{-1}$)	Power density ($W\ Kg^{-1}$)	Reference
PPF4	**241 at 0.5 A g^{-1}**	**85.68**	**400.2**	**Present work**
	364.5 at 5 mV s^{-1}			
PPy/MGO	87 at 1A g^{-1}	10	825	[31]
PPy/GO/ZnO	94.6 at 1A g^{-1}	10.65	258.26	[32]
	163.2 at 2 mV s^{-1}			
PPy/Cellulose	255 at 0.25 A g^{-1}	20.4	194	[11]
CNT/PPy-NW	62.5 at 0.25 A g^{-1}	15.1	3000	[33]
PPy/RGO	43.2 at 20 mV s^{-1}	15.8	140	[34]
PPy/MWCNTs	47.1 at 2 mV s^{-1}	10.7	1990	[35]

PPy/Cellulose	200 at 1A g^{-1}	27	900	[36]
PVA/GO/PPy	244.3 at 5 mV s^{-1}	41	1200	[37]
Ag@PPy/Cs	183 at 0.2 A g^{-1}	16.3	322	[38]
CNF/MnO_2/PPy	315 at 25 mV s^{-1}	13.68	485.22	[39]
RGO/CNT/PPy	166 at 25 mV s^{-1}	14.3	6620	[40]
PPy@rGOH-20s	131.8at 1A g^{-1}	46.9	800	[41]
PPy/GO	181 at 5 mV s^{-1}	56.5	1356	[42]

MGO- modified graphite oxide; GO- graphene oxide; ZnO- zinc oxide; CNT- carbon nanotube; PPy-NW- polypyrrole nanowire; RGO- reduced graphene oxide; MWCNT- multiwalled carbon nanotubes; CNF- carbon fiber; MnO_2- manganese oxide; rGOH- reduced graphene oxide hydrogel.

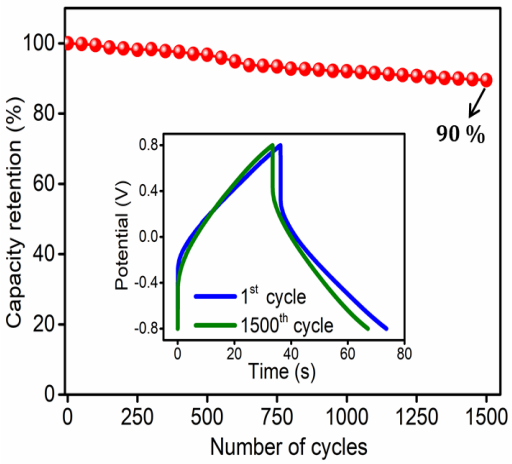

Figure 6.55 *Cycling stability of the device*

For better performance of a supercapacitor, it requires substantially high power density than batteries along with sufficiently high energy density [43, 44]. Figure 6.56 represents the Ragone plot of the fabricated device. The device has a significant energy density of

85.68 Wh kg^{-1} at a power density of 400.2 W kg^{-1}. It retains 65 % of its energy density when the power density reaches 5.6 kW kg^{-1}. From the Ragone plot, it is evident that the results are compatible and superior to the previously reported PPy-based devices [11, 31-34, 45-51], making it a promising electrode material for high performance supercapacitors.

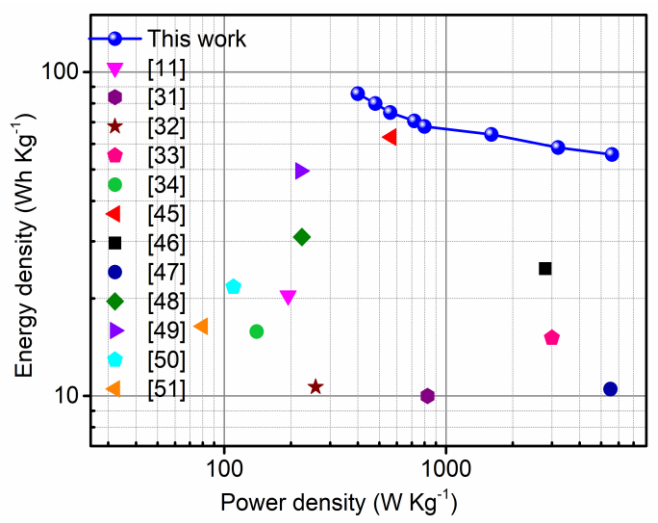

Figure 6.56 *Ragone plot of the device*

The device based on PPF4 film is subjected to EIS measurements to investigate the electrochemical kinetic parameters. Figure 6.57 shows the Nyquist plot of the device at an open-circuit voltage of 10 mV within a frequency range from 0.1 Hz to 100 kHz in 1 M NaCl aqueous solution. It consists of a semicircle in the high frequency region which is related to the charge transfer process and a nearly straight line in the low frequency region which is associated with the diffusion-limited ion transport process [29]. The equivalent circuit obtained by simulating the impedance data using Zman software is showed as an inset in the Figure 6.57 and the electrochemical

parameters are summarized in Table 6.6. The device has an R_S value of 1.92 Ω and R_1 of 12 Ω, suggesting low internal resistance and fast charge transfer compared to the three electrode system. These results suggest that PPF4 hybrid film can be directly used for constructing electrochemical devices.

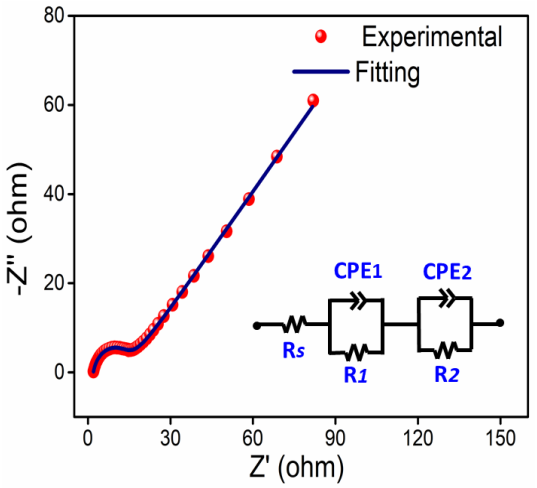

Figure 6.57 *Nyquist plot of the PPF4 device (inset: equivalent circuit used to fit the impedance spectrum)*

Table 6.6 *Equivalent circuit parameters of EIS of the device*

Electrode	PPF4 device
R_S (Ω)	1.92
R_1 (Ω)	12
R_2 (Ω)	468.05
CPE_1-Y (S s^{α})	0.0000836
CPE_1-α	0.857
CPE_2-Y (S s^{α})	0.01175
CPE_2-α	0.506

6.2.6.2. Sensing characteristics of the device

(a) Solid state symmetric device senses working electrical condition

In order to prove the reaction driven sensing capability of the fabricated device, the current sensing capabilities were analyzed in a two electrode mode by applying square current waves of different currents (±0.3 mA to ± 2 mA) in 1 M NaCl while keeping the other experimental variables constant. The normalized chronopotentiometric responses of the device for the anodic (charging) and cathodic (discharging) processes at a constant charge of 210 mC are given in Figure 6.58a and 6.58b respectively.

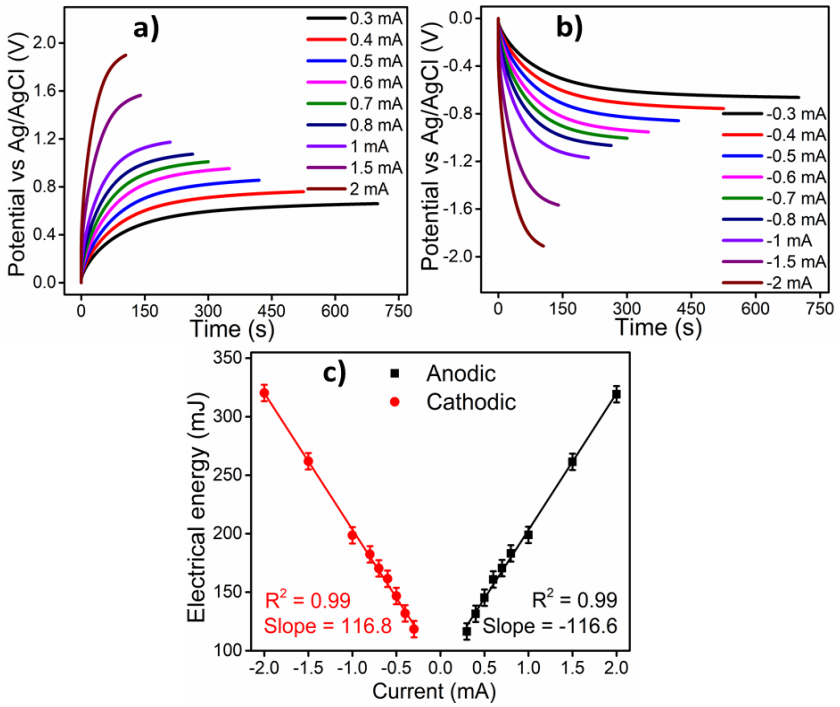

Figure 6.58 *Normalized chronopotentiograms obtained when supercapacitor device was subjected to different (a) anodic and (b) cathodic currents by passing a constant charge of 210 mC and (c) Linear variation of electrical energy consumed by the device as a function of working current*

As the anodic or cathodic current of the device increases, the potential evolution of the device occurs at higher anodic or higher cathodic potentials respectively. The energy consumed by the device during the oxidation and reduction step was plotted as a function of applied current and the result is shown in Figure 6.58c. The excellent linear fit of Figure 6.58c (R^2 =0.99) corroborates that the consumed electrical energy during the electrochemical reactions of the supercapacitor device can sense the driving current i.e., working electrical condition through the same two connecting wires. Thus the supercapacitor acts as a current sensor. The slopes of the line provide the sensitivity of the device towards the applied current: 116.8 mJ mA^{-1} and -116.6 mJ mA^{-1} for the anodic and cathodic processes respectively.

(b) Solid state symmetric device senses working thermal condition

For studying the temperature sensing capabilities, the solid state supercapacitor device was subjected to consecutive square current waves of ±0.5 mA for 420s (at a constant charge of 210 mC for attaining same reaction extension) at different temperatures ranging from 15 ^oC to 50 ^oC using a thermostat while keeping all other experimental variables constant. The resulting stationary and normalized chronopotentiometric responses for the anodic and cathodic processes are shown in Figure 6.59a and 6.59b respectively. As expected the potential of the anodic process decreases with a gradual increase of temperature and for the cathodic processes, a similar, but inverse, behaviour is observed. Figure 6.59c shows a linear increase of electrical energies consumed during the oxidation reduction reactions of the device with the decrease of temperatures. Thus, at any time, the

electrical energy consumed by the device senses the working thermal condition and the concomitant line is the calibration curve. The slope of the curves represents the temperature sensitivity of the fabricated device: -1.91 mJ K^{-1} for the oxidation and -1.89 mJ K^{-1} for the reduction processes. The experimental results are in good agreement with the sensing equations 3.25 and 3.26. This proves that the solid state symmetric supercapacitor can also act as a temperature sensor.

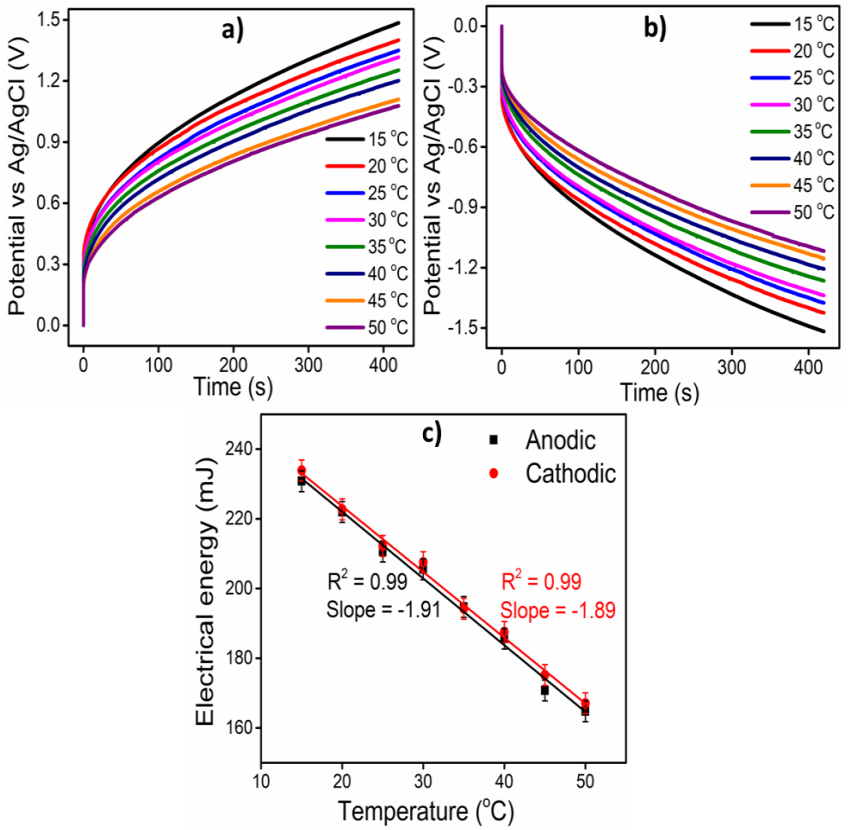

Figure 6.59 *Chronopotentiometric responses obtained at various temperatures when (a) +0.5 mA (anodic) and (b) -0.5 mA (cathodic) currents were applied to the device for 420s and (c) Variation of electrical energy consumed by the device at different temperatures for anodic and cathodic processes*

6.3. Conclusion

A new paradigm of sensing devices (here, sensing supercapacitors) incorporating all the information within two connecting wires is narrated for PPy/PVA hybrid films. Highly mechanically stable and electroactive PPy/PVA hybrid films constituted by macromolecular electrochemical machines of PPy were fabricated using chemical coating of PPy on pre-fabricated PVA films. The as-synthesized PPy/PVA hybrid films were characterized using FTIR spectroscopy, FESEM, electrical conductivity measurement, TGA, UTM analysis and cyclic voltammetry. The hybrid films comprised of grain like morphology of PPy grown on the surface of the PVA film with sufficient porosity enabling the efficient diffusion of ions and solvents through the electrochemical redox reaction. In both dry and wet state, the tensile strength and Young's modulus of the hybrid films are higher than PVA film ,which increases as the number of times of coating increases from PPF1 to PPF4. The hybrid films have sufficient mechanical strength even in the wet state. Therefore, PPy/PVA hybrid films can be used as a stable free standing film for developing various devices capable of working either in dry or wet conditions.

Under galvanostatic conditions, the consumed electrical energy follows a linear relationship with driving current and experimental temperature and follows a logarithmic relationship with electrolyte concentration. The size of anions in the electrolyte solution significantly affects the reaction driven sensing characteristics of PPy/PVA hybrid films. The use of electrolytes with smaller anions

results in greater sensitivity. It is attributed to their easy penetration into the polymer chains during electrochemical reactions. Under potentiodynamic conditions, the extension of the reaction manifested as the consumed electrical charge obtained from the coulovoltammetric responses senses the working electrical, chemical and thermal ambient. The conformational and structural changes under faradaic control that arise due to the cooperative actuation of the constitutive chemical machines of PPy are responsible for this self-sensing property. The sensitivities of the hybrid films with regard to applied current, temperature and electrolyte concentration are found to increase with the increase in the number of times of coating or increase in the PPy content. The fourth coated hybrid film (PPF4) shows best sensitivities. Even though the sensing studies of PPy/PVA hybrid films were done at a charge approximately equal to half of their redox charge, the sensitivities of PPy/PVA hybrid films were found to be better than that of PPy/Cs hybrid films. These results corroborate the excellent electrochemical activity of PPy/PVA hybrid films. The similarity of cooperative actuation of the polymeric chains with biological muscles in simultaneously sensing the working energetic condition suggests the possibility of constructing biomimetic sensing motors using PPy/PVA films in which the driving and sensing signals can be read at any instant of the reaction, through the same two connecting wires.

The specific capacitance of the hybrid films increases as the number of times of coating increases and the PPF4 exhibited the highest specific capacitance of 594 F g^{-1} at 0.5 A g^{-1} and a highest cycling stability of 87.5 % capacitance retention after 1500 cycles. This

suggests that the PPF4 hybrid film can be used as a free standing high-performance electrode material for the next-generation supercapacitors. The charge storage characteristics of PPy/PVA hybrid films are found better than that of PPy/Cs hybrid films. Because of the excellent mechanical stability of PPy/PVA hybrid films, as a proof-of-concept, an all-solid-state symmetric supercapacitor device capable of sensing their surrounding conditions at any reaction moment, without physical separation through the same two connecting wires was fabricated and its charge storage and sensing capabilities were demonstrated. The device showed a large capacitance of 241 F g^{-1} at 0.5 A g^{-1}, high energy density of 85.68 Wh kg^{-1} at a power density of 400.2 W kg^{-1}, and better cycle life of 90 % capacitance retention after 1500 cycles. The sensing ability of the device with regard to working electrical and thermal conditions were evaluated from the charge-discharge responses and proved that the device can act as a current sensor as well as temperature sensor. Thus, one reaction drives, many functions in a single material. Therefore this work open a facile and low-cost strategy to fabricate sensing motors (here, sensing supercapacitors) based on PPy/PVA hybrid films and promote their practical applications in next generation energy storage devices.

6.4. References

1. R. Nagarkar, J. Patel, Acta Sci. Pharm. Sci, 3 (2019) 34-44.
2. H.S. Mansur, C.M. Sadahira, A.N. Souza, A.A. Mansur, Materials Science and Engineering: C, 28 (2008) 539-548.
3. M.I. Baker, S.P. Walsh, Z. Schwartz, B.D. Boyan, Journal of Biomedical Materials Research Part B: Applied Biomaterials, 100 (2012) 1451-1457.
4. S. Muppalaneni, H. Omidian, J. Dev. Drugs, 2 (2013) 1-5.

5. G. Elkomy, S. Mousa, H.A. Mostafa, Arabian Journal of Chemistry, 9 (2016) S1786-S1792.
6. S. Sudhamani, M. Prasad, K.U. Sankar, Food Hydrocolloids, 17 (2003) 245-250.
7. O. Tretinnikov, S. Zagorskaya, Journal of Applied Spectroscopy, 79 (2012) 521-526.
8. S. Gahlot, V. Kulshrestha, G. Agarwal, P.K. Jha, Macromolecular Symposia, Wiley Online Library, 2015, pp. 173-177.
9. F.C. do Nascimento, L.C.V. de Aguiar, L.A.T. Costa, M.T. Fernandes, R.J. Marassi, A.d.S. Gomes, J.A. de Castro, Polymer Bulletin, 78 (2021) 917-929.
10. S.-Y. Lee, D.J. Mohan, I.-A. Kang, G.-H. Doh, S. Lee, S.O. Han, Fibers and Polymers, 10 (2009) 77-82.
11. X. Zhang, J. Zhao, T. Xia, Q. Li, C. Ao, Q. Wang, W. Zhang, C. Lu, Y. Deng, Energy Storage Materials, 31 (2020) 135-145.
12. Y.A. Ismail, J.G. Martínez, A.S. Al Harrasi, S.J. Kim, T.F. Otero, Sensors and Actuators B: chemical, 160 (2011) 1180-1190.
13. T.F. Otero, RSC advances, 11 (2021) 21489-21506.
14. A.J. Bard, L.R. Faulkner, H.S. White, Electrochemical methods: fundamentals and applications, John Wiley & Sons, 2022.
15. Y.A. Ismail, J.G. Martínez, T.F. Otero, Electrochimica Acta, 123 (2014) 501-510.
16. L. Valero, J. Arias-Pardilla, M. Smit, J. Cauich-Rodríguez, T.F. Otero, Polymer international, 59 (2010) 337-342.
17. T.F. Otero, S. Beaumont, Sensors and Actuators B: Chemical, 263 (2018) 493-501.
18. Y.A. Ismail, J.G. Martinez, T.F. Otero, Journal of Electroanalytical Chemistry, 719 (2014) 47-53.
19. T.F. Otero, International Journal of Smart and Nano Materials, 8 (2017) 125-143.
20. T.F. Otero, The Chemical Record, 18 (2018) 788-806.
21. T. Otero, H. Grande, J. Electroanal. Chem., 414 (1996) 171-176.
22. H. Grande, J. Rodríguez, Synth. met., 85 (1997) 1077-1078.
23. T. Otero, H. Grande, J. Rodriguez, J. Electroanal. Chem., 394 (1995) 211-216.
24. X. Zhang, R. Zhang, C. Xiang, Y. Liu, Y. Zou, H. Chu, S. Qiu, F. Xu, L. Sun, Ceramics International, 45 (2019) 13894-13902.
25. L. Liu, Y. Chen, Y. Xie, P. Tao, Q. Li, C. Yan, Advanced Functional Materials, 28 (2018) 1801989.
26. Y. Gong, X.-G. Zeng, T. Luo, Z.-Y. Dai, Y.-Z. Jin, J. Chen, Y. Yi, T. Duan, Y.-J. Tang, Int J Electrochem Sci, 15 (2020) 7508-7519.
27. J. Wang, J. Polleux, J. Lim, B. Dunn, The Journal of Physical Chemistry C, 111 (2007) 14925-14931.

28. V. Augustyn, P. Simon, B. Dunn, Energy & Environmental Science, 7 (2014) 1597-1614.
29. F. Zhang, F. Xiao, Z.H. Dong, W. Shi, Electrochimica Acta, 114 (2013) 125-132.
30. J. Li, Y. Liu, D. Zhan, Y. Zou, F. Xu, L. Sun, C. Xiang, J. Zhang, Journal of Energy Storage, 39 (2021) 102665.
31. H. Feng, B. Wang, L. Tan, N. Chen, N. Wang, B. Chen, Journal of Power Sources, 246 (2014) 621-628.
32. W.K. Chee, H.N. Lim, I. Harrison, K.F. Chong, Z. Zainal, C.H. Ng, N.M. Huang, Electrochimica Acta, 157 (2015) 88-94.
33. H. Fu, Z.-j. Du, W. Zou, H.-q. Li, C. Zhang, Journal of Materials Chemistry A, 1 (2013) 14943-14950.
34. J. Zhu, T. Feng, X. Du, J. Wang, J. Hu, L. Wei, Journal of Power Sources, 346 (2017) 120-127.
35. Y. Su, I. Zhitomirsky, Applied energy, 153 (2015) 48-55.
36. F. Wang, H. Du, Y. Liu, H. Huang, X. Yu, X. Zhu, L. Li, Synthetic Metals, 282 (2021) 116952.
37. D. Wei, J. Zhu, L. Luo, H. Huang, L. Li, X. Yu, Journal of Materials Science, 55 (2020) 11779-11791.
38. J.K. Gan, Y.S. Lim, N.M. Huang, H.N. Lim, RSC advances, 6 (2016) 88925-88933.
39. M.A.A.M. Abdah, N.M.M.A. Edris, S. Kulandaivalu, N.A. Rahman, Y. Sulaiman, International Journal of Hydrogen Energy, 43 (2018) 17328-17337.
40. Y.-J. Peng, T.-H. Wu, C.-T. Hsu, S.-M. Li, M.-G. Chen, C.-C. Hu, Journal of Power Sources, 272 (2014) 970-978.
41. X. Zhang, J. Zhang, Y. Chen, K. Cheng, J. Yan, K. Zhu, K. Ye, G. Wang, L. Zhou, D. Cao, Journal of colloid and interface science, 536 (2019) 291-299.
42. A. Singh, A. Chandra, Journal of Applied Electrochemistry, 43 (2013) 773-782.
43. H. Su, T. Xiong, Q. Tan, F. Yang, P.B. Appadurai, A.A. Afuwape, M.-S. Balogun, Y. Huang, K. Guo, Nanomaterials, 10 (2020) 1141.
44. Y. Fang, X. Chen, C. Yin, L. Cui, Ceramics International, 47 (2021) 24973-24981.
45. A. Aphale, K. Maisuria, M.K. Mahapatra, A. Santiago, P. Singh, P. Patra, Scientific reports, 5 (2015) 14445.
46. S. Hashmi, A. Kumar, S. Tripathi, European Polymer Journal, 41 (2005) 1373-1379.
47. D. Zhang, X. Zhang, Y. Chen, P. Yu, C. Wang, Y. Ma, Journal of Power Sources, 196 (2011) 5990-5996.
48. X. Jian, J.-g. Li, H.-m. Yang, E.-h. Zhang, Z.-h. Liang, Carbon, 114 (2017) 533-543.

49. T. Qian, C. Yu, S. Wu, J. Shen, Journal of Materials Chemistry A, 1 (2013) 6539-6542.
50. M. Hou, M. Xu, Y. Hu, B. Li, Electrochimica Acta, 313 (2019) 245-254.
51. J. Cao, Y. Wang, J. Chen, X. Li, F.C. Walsh, J.-H. Ouyang, D. Jia, Y. Zhou, Journal of Materials Chemistry A, 3 (2015) 14445-14457.

Chapter 7

SUMMARY AND FUTURE OUTLOOK

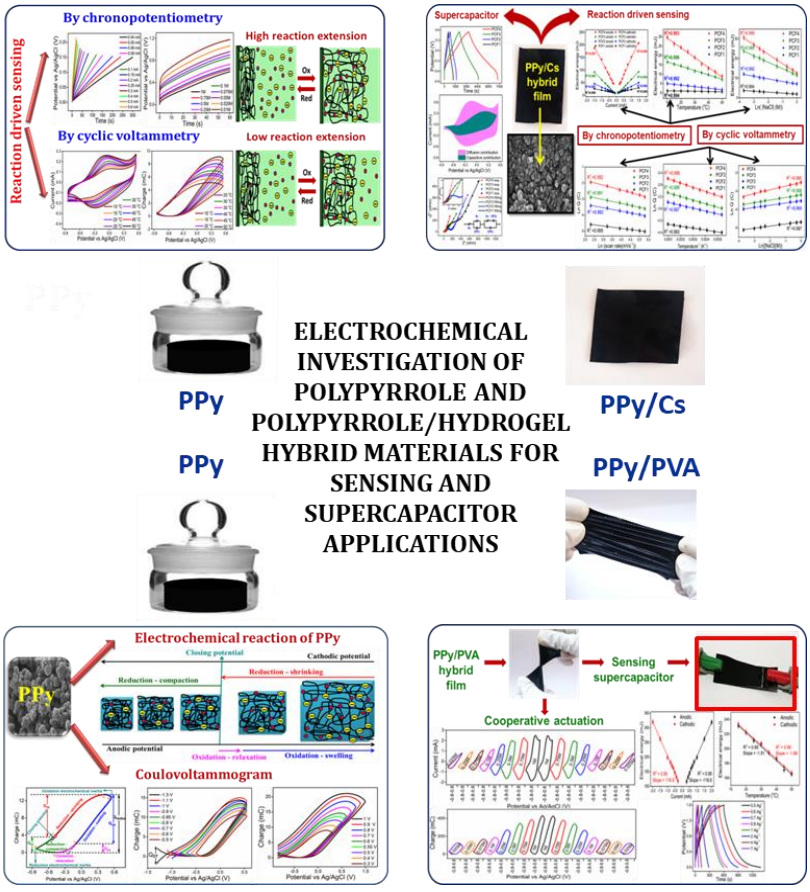

The major findings and highlights of the present work are summarized in this chapter. The biological and technological perspectives of the present study are discussed. The future scopes of the study are briefly outlined, particularly focusing on the development of various biomimetic devices.

7.1. Summary

Polypyrrole has emerged as a prolific candidate for various potential applications as it is endowed with interesting material properties such as tunable electrical conductivity, electrochemical activity over a wide range of pH, ease of synthesis and excellent environmental stability. Though CPs have been exploited thoroughly by the scientific community for various electronic applications due to their tunable electrical conductivity, their composition dependent properties leading to various potential applications have not been studied in detail. Centered on this, the present research explored the composition dependent properties of PPy which can lead to the design of various sensing macromolecular motors.

The thesis is started with the electrochemical studies of PPy by giving an insight to the structural electrochemistry of PPy. The coulovoltammograms are used to gain insight into the structural faradaic processes of PPy and helped in identifying and quantifying reaction-driven conformational changes. The QVs quantified the charge consumed by the reaction and identified four basic reaction-driven structural processes (slope variations): viz. reduction-shrinking, reduction-compaction, oxidation-relaxation and oxidation swelling.

As the extraction of electrons from the polymer chain during oxidation occurs through *n* consecutive steps of one electron extraction per step, the composition of PPy is continuously varying. Consequently, they do not obey the fundamental principles of equilibrium electrochemistry based on Nernst equation and

Le-Chatelier principle. Instead, for such systems the Otero's principle is more pertinent and applicable. Otero's principle states that any physical or chemical perturbation acting on the electrochemical reaction rate should modify the reaction overpotential (electrical energy) to self-adapt to the newly imposed energetic requirements. This principle is the very foundation of the reaction driven sensing characteristics of CPs. To validate this, we have verified the reaction driven sensing characteristics of PPy using two approaches: (1) galvanostatic method, i.e., chronopotentiometry, we proved that the electrical energy can act as the sensing parameter and (2) potentiodynamic method, i.e., cyclic voltammetry, we proved that the electrical charge can act as the sensing parameter. Further, we have proved that the electrochemical reactions of PPy can sense by themselves the electrical, chemical and thermal working ambient. This self-sensing property allows one to suggest that, any device/motor based on the electrochemical reactions of PPy can sense the perturbation of the working energetic conditions at any instant, using the same two connectivities.

The development of multi-sensing electrochemical motors by directly using PPy is limited due to some inherent limitations like poor mechanical strength, brittleness and low processability. To overcome these challenges, we successfully fabricated highly electroactive PPy/hydrogel hybrid films through a facile and low cost method. Two types of hybrid films were fabricated: (1) PPy/Cs hybrid films and (2) PPy/PVA hybrid films. Both the hybrid films were fabricated through an in situ chemical polymerization of pyrrole on pre-fabricated

hydrogel matrix. The hybrid films can go through *n* consecutive fundamental conformational energetic states progressively and reversibly under electrochemical reaction control and can act as multi-step macromolecular motors.

The electroactive PPy/Cs hybrid films constituted by macromolecular electrochemical motors of PPy chains were analysed using different characterization techniques. We have extended the sensing principle to PPy/Cs hybrid films and verified that it can act as a multi-sensing free standing electrode material capable of sensing its surrounding electrical, chemical and thermal conditions using chronopotentiometry and cyclic voltammetry. The sensing equations and sensing parameters of the hybrid films remain the same as that of pure PPy, because PPy is the electroactive material in the hybrid films. Furthermore, we have explored their efficacy as supercapacitor electrodes. Both the reaction driven sensing characteristics and charge storage properties were derived from a single faradaic electrochemical reaction. It is proved that both capacitive behavior and sensing capabilities of the hybrid films increases as the number of times of coating increases.

The PPy/Cs hybrid films have good reaction-driven sensing capabilities as well as charge storage properties. They exhibited reasonable mechanical strength in the dry state and therefore, they can be used for the development of various devices capable of working in dry conditions. It is observed that, their mechanical strength diminishes in the wet state, rendering them unsuitable for applications requiring wet conditions. Our objective to fabricate a mechanically robust,

self sensing device working both in dry and wet conditions, led us to fabricate highly electroactive PPy/PVA hybrid films. These films maintain superior mechanical stability in both wet and dry conditions. Remarkably, they could acted as free-standing highly flexible mechanically stable electrode materials in wet conditions, offering promising potential for the development of sensing devices.

The PPy/PVA hybrid films were characterized using different techniques. The reaction driven sensing characteristics of PPy/PVA hybrid films were studied and proved that they can act as self sensor of working electrical, chemical and thermal conditions. Even though the sensing studies of PPy/PVA hybrid films were carried out at a charge approximately equal to half of their redox charge, the sensitivities of PPy/PVA hybrid films with regard to applied current, temperature and electrolyte concentration were found to be better than that of PPy/Cs hybrid films. These results further confirm the superior electrochemical activity of PPy/PVA hybrid films. The size of anions in the electrolyte solution significantly affects the reaction driven sensing characteristics of PPy/PVA hybrid films. The use of electrolytes with smaller anions resulted in greater sensitivity due to their facile penetration into the polymer chains during electrochemical reactions. The molecular level actuation or cooperative actuation of the CP chains manifested as the reversible conformational movements of the macromolecular motors generates or destroys the free volume required to lodge or expel counterions and solvent. The conformational and structural changes of multi-step macromolecular motors under faradaic control that arise due to the cooperative actuation of the constitutive

polymer chains (chemical machines) make the coulovoltammetric charge a self-sensor of the working energetic conditions.

The charge storage characteristics of PPy/PVA hybrid films were studied and which is found to be better than that of PPy/Cs hybrid films. The remarkable charge storage characteristics of PPy/PVA hybrid films suggested that it can be used as a high-performance electrode material for the next-generation supercapacitors. Transitioning to the practical application, we moved to device fabrication. We have demonstrated the charge storage and sensing characteristics of a self sensing device, i.e. a self sensing all-solid-state symmetric supercapacitor device. Impressively, the device is capable of sensing its electrical and thermal working conditions at any reaction moment, without physical separation through the same two connecting wires. This means that the device can simultaneously function as both current sensor and temperature sensor. Thus, a single reactive chemical device facilitates multiple functions driven by a single faradaic electrochemical reaction without the need for additional connections. Consequently, we have succeeded in contributing to the emergence of a novel paradigm in sensing devices, i.e., sensing supercapacitors incorporating all the information in a couple of connecting wires.

7.2. Biological perspectives

The natural muscles are haptic muscles; that is they can sense by themselves the chemical and physical energetic conditions while actuating. The actin-ATP-myosin chemical motors in natural muscles

sent the signals to the brain through the nervous system to inform the brain about the working chemical conditions or the fatigue state of the muscle. Our findings, particularly those related to different electrolyte concentrations (concentration sensing) can be taken as proof of concept to describe the fatigue state of the muscle after working for a long time. The galvanostatic experiments of PPy and PPy/hydrogel hybrid films conducted at different concentrations reveal that under the same physical and chemical working conditions for the same time period of current flow, an increase in the electrolyte concentration results in lower electrical energy consumption to attain the same reaction extension. Translated to biological muscles: during muscle fatigue, when the concentration of the ATP and oxygen within the sarcomere diminishes, the muscle requires increased energy or effort to facilitate the same amplitude of the muscular movement (reaction extension). The nervous terminal (sensing organ) generates the sensing signal by detecting the changes in the electrochemical (ATP) and chemical (actin and myosin) potentials (sensing parameters) and sent to the brain through the same nervous system.

The results of potentiodynamic experiments of PPy and PPy/hydrogel hybrid films at different concentrations corroborates that the redox charge (reaction extension or amplitude of electrochemical reaction) increases with increasing electrolyte concentration when the reaction is carried out under the same working energetic conditions. Drawing a parallel to biological muscles, under the same brain order or the same energetic conditions, a decrease in the concentration of reactive species like ATP results in diminished amplitude of muscle

movement in response to the same electrical stimulus. In other words the muscular reactions occur in faster or higher amplitude when the concentration of the reactive species is abundant. Thus the experimental results could provide some quantitative perspective for the muscle-fatigue observed in living cells.

The rate of the reaction, driving the cooperative actuation of the polymeric chains, i.e., the conformational movements of the molecular motors constituting the sarcomere of natural muscle increases when the body temperature increases (a phenomenon in line with the Arrhenius description). For PPy and PPy/hydrogel hybrid films, the redox charge (equivalent to reaction extension or amplitude of electrochemical reaction) increases with increasing temperatures when the reaction is carried out under the same working energetic conditions. Translating this to muscles of ectothermic beings, under the same brain command or the same energetic conditions when the body temperature falls, the muscles respond by decreasing the amplitude of muscle movement (extension) generated by the same electrical pulse. Consequently, muscular reactions in ectothermic animals occur in a faster and easier way (or show higher temperature-based efficiency) when they are warmed by exposure to sunlight or a thermal source. These experimental results potentially offer quantitative insights into the muscle-powered movements of ectothermic beings, which can adapt to its thermal environment. Notably, the consumption of lower reaction energies occurs at higher temperatures when the muscular reaction is carried out under constant mechanical energy (running, walking, stomach digestion and so on). Consequently, the energy consumed

(or the efforts taken) by the muscle has to be increased to produce the same muscular action (reaction extension) at decreasing temperatures. Natural muscles, acting as both electro-chemo-mechanical and thermo-mechanical transducers, respond to the reaction energy at various thermal conditions and sent the sensing signals regarding the working thermal (chemical and physical) conditions generated at the muscle/dendrites interface to the brain through sensory neurons. Thus we have proved that PPy based materials can act as model materials to mimic some of the biological functions.

7.3. Technological perspectives

The reversible redox reactions of PPy (reaction 3.1) drive the simultaneous variation of different material properties and functions including conductivity, stored charge, stored conformational energy, stored counterions, porosity, volume, color, wettability, and more. These changes span several orders of magnitude by the same electrochemical reaction (electrochemical switching between oxidized and reduced states). Remarkably, these composition-dependent properties of CPs emulate parallel reactions that occur in biological organs. Translated to technological products working by the reversible redox reactions of PPy i.e., artificial muscles, electron-ion transducers, supercapacitors, full organic batteries, smart windows, drug delivery devices, artificial chemical synapse, etc. our findings corroborates that they can work, simultaneously, as sensors of the surrounding energetic conditions. Within these systems, the driving, (current) storage (charge) and sensing (material potential, reaction energy) signals are present

and, are detected/controlled by the computer at any working instant, through the same two connecting wires. This convergence heralds the emergence of a novel scientific domain: biomimicking, soft, and wet multi sensing systems. We anticipate that, this breakthrough can create immense potential for the inception of sensing motors that can actively respond to their surroundings while working. These devices mimic any biological organ like haptic muscles that work simultaneously as a sensor of the working conditions.

7.4. Future outlook

This research paves the way for the development sensing motors that respond to their surroundings while working. The PPy/PVA hybrid films, which are highly electroactive and mechanically robust, have been fabricated using a simple and facile strategy. This makes them particularly effective for constructing flexible devices. In this thesis, PPy/PVA hybrid films are used to demonstrate a self sensing supercapacitor device capable of sensing its working energetic conditions. Further exploration is necessary for its practical applications.

Our subsequent aim is to develop a sensing actuator device based on PPy/PVA hybrid films. In PPF4, the quantity of PPy is insufficient to generate the force needed for their bending movement. Therefore it is imperative to increase the amount of PPy in the hybrid films. As an initial step toward this goal, for the first time, we innovatively developed a material by electrodepositing PPy on the hydrogel film (PPF4). Here, PPF4 acted as a free standing electrode, on the surface of

which PPy is deposited by electropolymerization, using $LiClO_4$ as electrolyte. About 0.024 g of PPy was deposited on the PPF4 film measuring 1×2 cm^2, which weighed 0.098 g. The electrodeposited film is designated as EPPF4. Subsequent to the electropolymerization, the grain like morphology of PPF4 changes to a cauliflower like morphology in EPPF4 (Figure 7.1a). The FTIR spectra, CV and QV of EPPF4 are shown in Figure 7.1b-d. The peak current and redox charge are enhanced through electrodeposition. Then we have verified its sensing characteristics by both CV and chronopotentiometry. Impressively, EPPF4 acted as current sensor, concentration sensor and temperature sensor (Figure 7.2). The sensing calibration curves confirm that the sensitivity of PPF4 is increased by the electrodeposition of PPy. Therefore it is expected that, the film EPPF4 with high PPy content and high electroactivity will show actuation properties. Further studies are necessary for conforming the same.

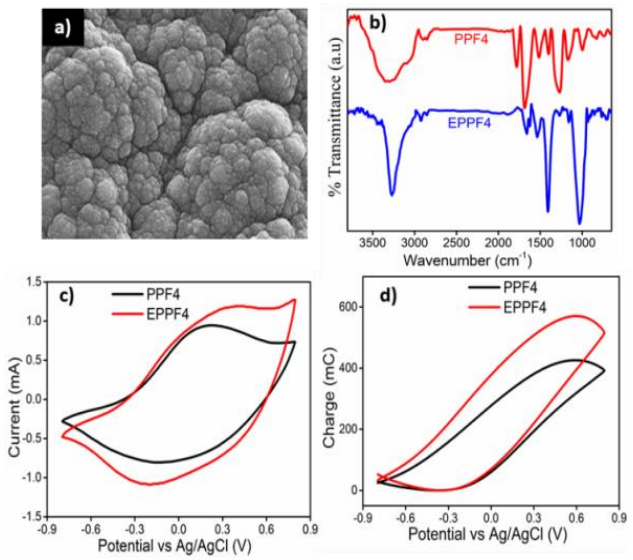

Figure 7.1 *(a) SEM image of EPPF4 film, (b) FTIR spectra, (c) CVs, and (d) QVs of PPF4 and EPPF4*

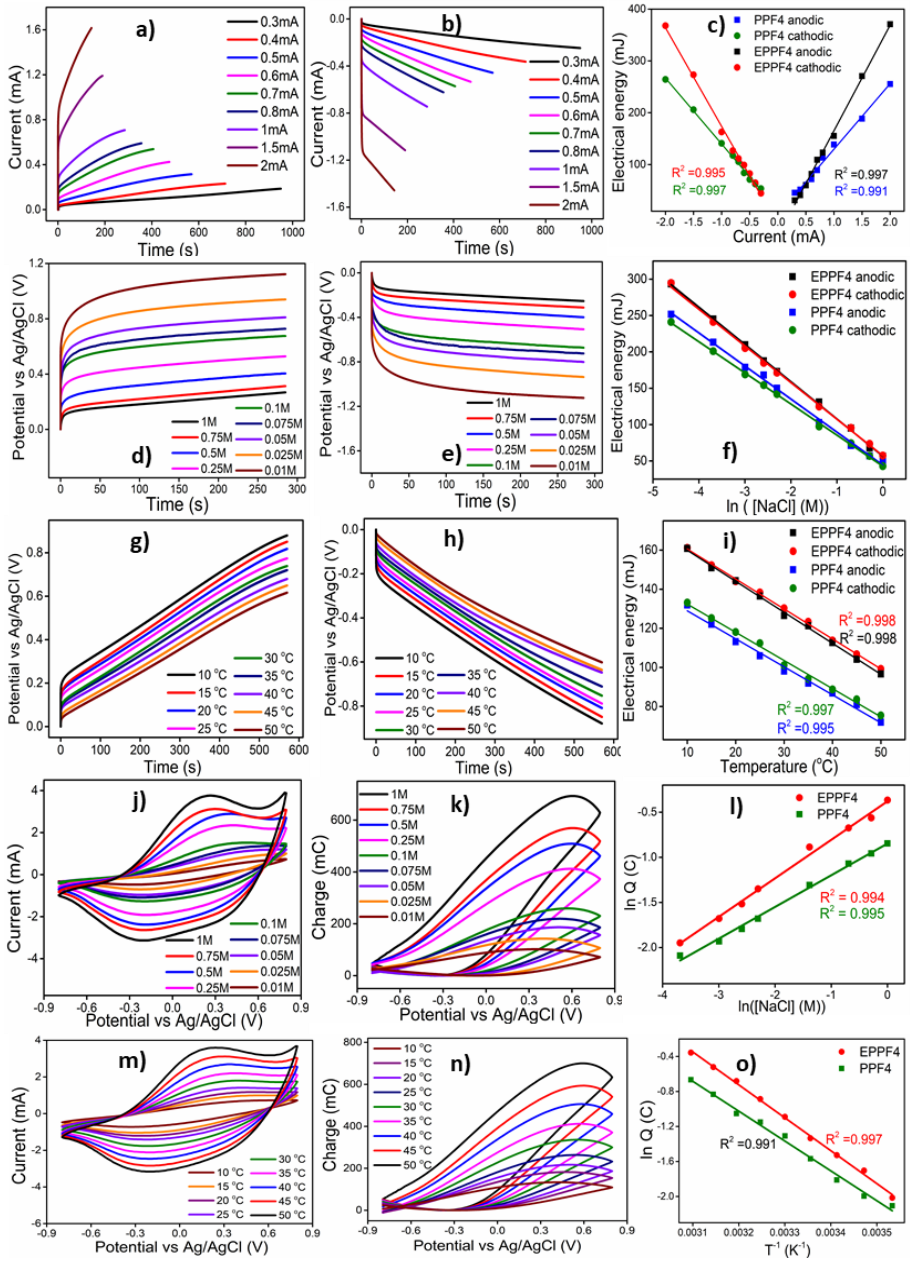

Figure 7.2 *(a-c) Current sensing plots of EPPF4 by chronopotentiometry, (d-f) Concentration sensing plots of EPPF4 by chronopotentiometry, (g-i) Temperature sensing plots of EPPF4 by chronopotentiometry, (j-l) Concentration sensing plots of EPPF4 by CV and (m-o) Temperature sensing plots of EPPF4 by CV*

Like natural muscles, both PPy and PPy/hydrogel hybrid films have the ability to sense their surrounding environment while functioning. As a result, any device harnessing the electrochemical reactions of PPy like actuators, sensors, smart windows, artificial synapse, sensing membranes and more can sense its working conditions without the need for additional connections through the same two connectivities. This discovery holds immense promise for the evolution of biomimetic sensing motors. By harnessing the innate sensing characteristic of PPy and PPy/hydrogel hybrid films, we have the potential to emulate the intricate functionalities of biological organs. The PPy/PVA hybrid films fabricated stand out due to their high mechanical stability, flexibility and pronounced electroactivity. This achievement sets the stage for the development of sophisticated biomimetic systems with self-sensing capabilities and mechanical stability. Potential biomimetic devices based on PPy/PVA hybrid systems for future studies are shown in figure 7.3.

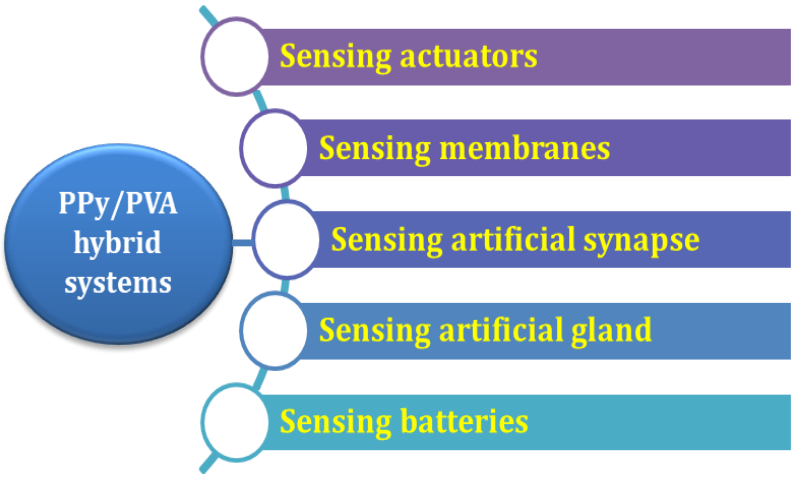

Figure 7.3 *Possible biomimetic devices based on PPy/PVA hybrid films*

The distinctive electrical, electronic and optical properties of polypyrrole paved the way for new horizons in materials research. Polypyrrole/hydrogel hybrid systems heralds a future dominated by smart, intelligent, and multi-functional devices with superior properties.

"Prepare to step into the thrilling era of polypyrrole, a material set to revolutionize sensing motors with its unparalleled capabilities"

LIST OF PUBLICATIONS

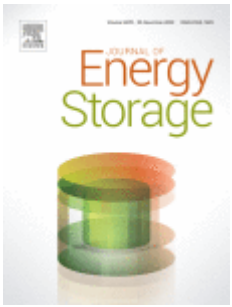	**A. Shabeeba**, L. Rajan**,** M. P. Sidheekha, M. S. Thayyil, Y.A. Ismail, Polypyrrole/hydrogel hybrid films as multi sensing supercapacitor electrodes, *Journal of Energy Storage*, 55 (2022) 105724 https://doi.org/10.1016/j.est.2022.105724
	**A. Shabeeba**, M. P. Sidheekha**,** L. Rajan and Y. A. Ismail, Flexible hybrid film of polypyrrole incorporated chitosan as a biomimetic multistep electrochemical sensor of working temperature: a potentiodynamic study, *RSC advances*, 12 (2022) 31911-31922. https://doi.org/10.1039/D2RA05482E
	**A. Shabeeba** and Y. A. Ismail, Chitosan/ polypyrrole hybrid film as multistep electrochemical sensor: sensing electrical, thermal and chemical working ambient, *Materials Research Bulletin*, 152 (2022) 111817-111830 https://doi.org/10.1016/j.materresbull.2022.111817
	**A. K. Shabeeba**, M. M. Manikandan, M. P. Sidheekha, L. Rajan, Y. A. Ismail, Poly-o-toluidine coated polyvinyl alcohol film: Reaction driven sensing capabilities, *Materials Today: Proceedings*, 51 (2022) 2293-2299. https://doi.org/10.1016/j.matpr.2021.11.403

	L. Rajan, M. P. Sidheekha, **A. Shabeeba** and Y. A. Ismail Reaction energetic condition induced conformational change in polyindole: Polyindole/PVA film as biomimetic sensor of working temperature and electrical energetic condition, *Chemistry an Asian journal, (2023), e202300742.* https://doi.org/10.1002/asia.202300742
	M.P. Sidheekha, **A. Shabeeba**, L. Rajan, M. S. Thayyil, Y. A. Ismail, Conducting polymer/hydrogel hybrid free-standing electrodes for flexible supercapacitors capable of self-sensing working conditions: large-scale fabrication through facile and low-cost route, *Engineered Science*, 2023, 23, 890. https://dx.doi.org/10.30919/es890
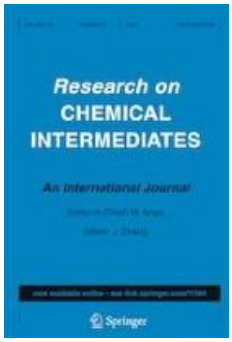	L. Rajan, M. P. Sidheekha, **A. Shabeeba**, S. C. Unnikrishnan and Y. A. Ismail, Reactive sensing capability towards the working electrical and chemical conditions of poly (aniline–co–o-toluidine) copolymers, *Research on Chemical Intermediates,* 48 (2022) 4313-4329 https://doi.org/10.1007/s11164-022-04814-6
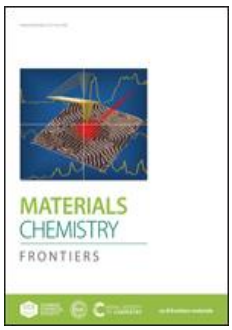	L. Rajan, M. P. Sidheekha, **A. Shabeeba** and Y. A. Ismail, Conducting polymers as bio-mimetic multistep macromolecular sensors of working conditions: polyindole/polyvinyl alcohol hybrid film senses electrical and chemical working ambient, *Materials Chemistry Frontiers*, 6, (2022) 1706-1718 https://doi.org/10.1039/D2QM00322H

	M. P. Sidheekha, K. Nufaira, **A.K. Shabeeba**, L. Rajan, Y. A. Ismail, Characterization of polyanilines synthesized at different pH for electrochemical sensing and supercapacitor applications, *Materials Today: Proceedings*, 51 (2022) 2286-2292. https://doi.org/10.1016/j.matpr.2021.11.40
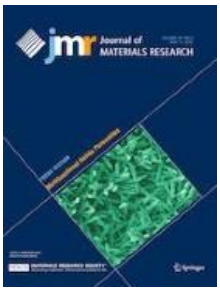	M.P. Sidheekha, G. E. Rajendran, **A. K. Shabeeba** and Y. A. Ismail, Current sensing supercapacitor electrodes based on chitosan/poly-o-toluidine hydrogel composites, *Journal of Materials Research*, 36 (2021) 1914-1926 https://doi.org/10.1557/s43578-021-00241-2

BOOK CHAPTERS

	Y. A. Ismail, **A. Shabeeba,** M. P. Sidheekha, L. Rajan, Electroactive Polymer Actuators, In: Encyclopedia of Polymer Science and Technology, Wiley publishers (2022). https://doi.org/10.1002/0471440264.pst681
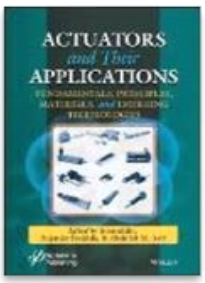	Y. A. Ismail, **A. K Shabeeba,** M. P. Sidheekha, L. Rajan, Conducting polymer/hydrogel systems as soft actuators, Actuators: In: Fundamentals, Principles, Materials and Applications, Wiley-Scrivener publishers, (2020) 211-252 https://doi.org/10.1002/9781119662693.ch9

PRESENTATIONS

1. Poster presentation at the national Seminar 'Frontiers in Chemical Sciences – FCS-2020' organized by the Department of Chemistry, University of Calicut, India during 29-31 January 2020 (***Title: Synthesis and electrochemical characterization of polypyrrole/ hydrogel hybrid film as current sensor***).
2. Oral presentation at the International Conference on 'Advances in material science – ICAMS-2021' jointly organized by Arunai International Research Foundation, Tamilnadu in association with Department of Chemistry ,University of Calicut, India during 11-12 September 2021 (***Title: Poly-o-toluidine coated polyvinyl alcohol film: reaction driven sensing capabilities***).
3. Poster presentation at the international conference 'Frontiers in Chemical Sciences – FCS-2022' organized by the Department of Chemistry, University of Calicut, India during 03-05 March 2022 (***Title: Polypyrrole/hydrogel hybrid film as an electrochemical sensor of working chemical condition***).
4. Poster presentation at the National seminar 'Frontiers in Chemical Sciences – FCS-2023' organized by the Department of Chemistry, University of Calicut, India during 01-03 February **2023** (***Title: Polypyrrole as multistep macromolecular self-sensors of chemical and electrical working ambient***).
5. Oral presentation at the 4th International Symposium on 'New Trends in Applied Chemistry – NTAC-2023' organized by the Department of Chemistry, Sacred Heart College, Thevara, Kochi, India during 07-08 February 2023 (***Title: Macromolecular motors sensing both electrical and thermal working conditions***).